Surface Acoustic Wave Devices on Silicon Substrate using Patterned and Thin Film ZnO

A thesis submitted

for the award of the degree of

DOCTOR OF PHILOSOPHY

by

SAI KRISHNA SANTOSH G

DEPARTMENT OF ELECTRONICS AND ELECTRICAL ENGINEERING

INDIAN INSTITUTE OF TECHNOLOGY GUWAHATI

GUWAHATI -781039, ASSAM, INDIA

FEBRUARY 2016

Certificate

This is to certify that the thesis entitled "**Surface Acoustic Wave Devices on Silicon Substrate using Patterned and Thin Film ZnO**", submitted by Sai Krishna Santosh G (09610201), a research scholar in the Department of Electronics and Electrical Engineering, Indian Institute of Technology Guwahati, for the award of the degree of Doctor of Philosophy, is a record of an original research work carried out by him under our supervision and guidance. The thesis has fulfilled all requirements as per the regulations of the institute and in our opinion has reached the standard needed for submission. The results embodied in this thesis have not been submitted to any other University or Institute for the award of any degree or diploma.

Dated: 12 February 2016

Guwahati.

H Nemade

Dr. Harshal B. Nemade

Professor

Dept. of Electronics and Electrical Engg.

Indian Institute of Technology Guwahati

Guwahati - 781039, Assam, India.

Declaration

This is to certify that the thesis entitled "**Surface Acoustic Wave Devices on Silicon Substrate using Patterned and Thin film ZnO,**" submitted by me to the Indian Institute of Technology Guwahati for the award of the degree of Doctor of Philosophy, is a bonafide record of research work carried out by me under the supervision of Prof. Harshal B. Nemade. Here by I declare that, the contents of this thesis, in full or in parts, have not been submitted to any other Institute or University for the award of any degree or diploma.

Sai Krishna Santosh G

Dated: 12th February 2016

Guwahati

గురుర్బ్రహ్మా గురుర్విష్ణుః గురుర్దేవో మహేశ్వరః |
గురుః సాక్షాత్ పరబ్రహ్మా తస్మై శ్రీ గురవే నమః ||

Guru is verily the representative of Brahma, Vishnu and Shiva. He creates, sustains knowledge and destroys the weeds of ignorance, I salute such a Guru.

To my
Parents Murali Krishna Vara Prasad Rao, Mahalakshmi
&
Wife Roja Venkata Mehar Swathi Mounica

Abstract – Surface acoustic wave (SAW) is a type of wave that propagates on the surface of an elastic material. The concentration of energy of these waves is higher at the surface and decreases exponentially along the depth of the material. In general SAW devices are realized on polished piezoelectric substrates in conjunction with metallic interdigital transducer (IDT) for the transduction of electric energy to acoustic energy and vice versa. Various types of surface waves like Rayleigh wave, shear horizontal wave, Bleustein-Gulyaev-Shimizu (BGS) wave, and Love wave are generated by choosing appropriate crystal cut of the piezoelectric substrate and guiding layers. Electric field generated by the IDT produces strain in the piezoelectric substrate and vice versa. Applying alternating voltage to the IDT results in the generation of SAW in the substrate. The operating frequency of a SAW device depends on the dimensions of IDT structure and acoustic velocity in the substrate.

As technology advances, there is always a need for superior SAW devices with improved stability, high electromechanical coupling coefficient, high frequency of operation, and low acoustic losses. The performance of SAW devices to some extent can be improved by employing piezoelectric and dielectric thin films over SAW devices. It is possible to realize SAW devices on non-piezoelectric substrates using piezoelectric overlay in conjunction with interdigital transducers. SAW devices on non-piezoelectric substrates like silicon, sapphire and diamond have been reported using films of piezoelectric materials like ZnO, CdS, and AlN. The SAW devices made on silicon can be integrated with circuits for lab on chip, signal processing and communication applications.

This thesis mainly focuses on the research work carried out on the realization of SAW devices on silicon substrate using ZnO in the form of either periodically patterned films or thin films. The first major contribution of the thesis is the investigation of transduction of SAW on silicon substrate using periodic patterns of ZnO to achieve SAW devices with high phase velocity and high coupling coefficient suitable to integrate with CMOS and IC circuits on a silicon substrate. The finite element simulations of the proposed SAW devices with patterned-ZnO on silicon are carried out using COMSOL Multiphysics and the results reveal the generation of surface modes having unique property of high coupling coefficient with high phase velocity. The fabrication design parameters are obtained using equivalent circuit model. We fabricated and tested the proposed patterned-ZnO SAW devices on silicon and verified the test results with simulation results of identical SAW devices as fabricated.

The second major contribution of this research work is to realize the proposed structure in the edge reflection (ER) type SAW devices which offer substantially small device area, since the device area on a silicon chip is crucial and minimizing the area of the SAW device would be of high priority in monolithic integration. The simulations of the proposed ER type SAW devices on

silicon are carried out using COMSOL Multiphysics and the device parameters for the fabrication are obtained using equivalent circuit model. We have fabricated the proposed edge reflection type SAW devices on silicon and the testing of the fabricated devices confirms practicability of the proposed devices. In order to demonstrate an application of the proposed devices, we fabricated and tested coupled resonator filters and ladder filters using ER type SAW resonators on silicon substrate for RF signal processing applications.

Acknowledgment

I feel it as a great privilege in expressing my deepest and most sincere gratitude to my thesis supervisor Professor Harshal B. Nemade for his excellent guidance throughout my study. His kindness, dedication, hard work, and attention to detail have been a great inspiration to me. I thank him for the unlimited support, invaluable guidance and utmost patience he has shown to me. He is more than a supervisor for me.

I am thankful to my doctoral committee members Professor R. Bhattacharjee, Professor Roy P. Paily, and Professor Rajiv Tiwari for their precious suggestions and time to improve the quality of my research work. My special thanks to technical staff of EEE Department and centre for Nanotechnology for their support in various tasks. I would like to thank Ministry of Human Resource and Development (MHRD) and Centre for Excellence in Research and Development of Nanoelectronic Theranostic Devices (CENTeD) [DEITY (No-5(9)/2012-NANO, Vol-II)] for providing scholarship.

I am highly thankful to Indian Nanoelectronics User Program (INUP), and Centre for Nano Science and Engineering (CeNSE), IISc., Bangalore, for providing the fabrication facility to carry out my experimental work. I would like to thank all faculty coordinators of INUP, in particular I would like to thank Dr. Sanjiv Srivastav, INUP coordinator for his tremendous help during my stay at IISc, Bangalore. I would like to thank Dr. Prabhakar Rao, Project instructor, sparing his precious time for the execution of my project work. I am very grateful to Mr. K. Sangeeth and Mrs. Smitha Nair for their sincere efforts and precious time to execute my projects. Most importantly I would like give my gratitude to the INUP staff at CeNSE, IISc. Bangalore.

I would like to thank Professor P. K. Giri and Dr. D. Pamu for helping in the deposition of ZnO films in Department of Physics at IIT Guwahati and I would also like to thank Santosh kumar, Mahesh, Anil C, Subbarao, Murali G, and Ravi B for their precious time during the deposition of thin films. I am extremely thankful to Mrs. Leena Nemade for the care shown and support given to me during my stay at IIT Guwahati.

I am very grateful to my friends Surya Prakash, Ramesh, and Soma shekar for their extreme support and caring in every aspect of my stay in IIT Guwahati.

My special thanks to my seniors Dr. Ramakrishnan and Dr. Ashish K. Namdeo for their help and support always. I would like to thank our SAW group members who are always with me, Mandar Maitra, Basudeb Behra, Vivek Lukose, Jitendra Kumar, Sushanta Kundu, and

Shyam Trivedi, for their unconditional care, support, and extreme cooperation during my stay at IIT Guwahati. I would like to thank Gaurav Saxena, Nagesh Kumar, my lab associates Namami Goswami, Ujjwol Barman, and special thanks Krishna Kumar for his support and help.

During these six years at IIT Guwahati I have had several friends that have helped me in several ways, I would like to say a big thank you to all of them for their friendship and support. I would like to extend thanks to all my friends Revathi Prasad, Pavan Kumar, Abhishek, Sangeeth Rao, and Sai Krishna for their continuous encouragement and support.

My deepest gratitude goes to my parents for their unconditional love and support throughout my studies, they are the reasons where I am and what I have accomplished so far. My special thanks to my wife Roja Venkata Mehar Swathi Mounica for their support.

Finally, I believe this research experience will greatly benefit my career in the future.

Sai Krishna Santosh Gollapudi

Contents

Abstract i

Acknowledgement iii

List of Figures xi

List of Tables xxi

List of Acronyms xxiii

List of Symbols xxv

1 Introduction to Surface Acoustic Wave (SAW) Devices 1

1.1 Contribution of the thesis. 2

1.2 Generation of waves in elastic medium. 2

1.3 Surface acoustic wave (SAW) devices 6

1.4 Edge reflection (ER) type SAW devices. 8

1.5 Thin films over SAW devices 9

1.6 SAW devices on non-piezoelectric substrates 10

1.7 Problem definition. 13

1.8 Scope of thesis 14

1.9 Thesis organization 15

2 Modeling and Simulation of Surface Acoustic Wave Devices 17

2.1 Theory of elasticity. 17

2.1.1 Piezoelectricity and constitutive equations. 18

2.1.2 Equation of motion 19

2.1.3 Solution of surface wave in piezoelectric media. 20

2.1.4 Acoustic waves in isotropic media 21

2.2 Modeling of SAW devices. 23

2.2.1 Coupling of modes (COM) model. 23

2.2.2 Discrete source or delta function method. 25

2.2.3 Equivalent circuit model 26

2.2.4 Design parameters. 28

2.3 Finite element method (FEM) 28

2.3.1 Input and output information in FEM. 28

2.3.2 Finite element simulations of SAW devices 29

2.4 ZnO thin film based SAW devices on silicon. 30

2.4.1 Mechanical properties of ZnO 30

2.4.2 3D FE simulations of IDT/ZnO/Si configured one-port SAW resonator. 31

2.4.3 Effect of aperture length on operating frequency and admittance 35

2.4.4 Effect of mesh density on resonance frequency. 36

2.4.5 ZnO/Si layered configurations 37

2.4.6 2D FE simulations of ZnO/Si configured SAW resonator 38

2.4.7 Results of ZnO/Si SAW resonator. 38

2.4.8 2D simulation of ZnO/IDT/Si SAW delay line 42

2.4.9 Results of thin film ZnO/IDT/Si SAW delay line 42

2.4.10 Observations. 44

2.5 Summary 44

3 Design and Simulation of Patterned-ZnO/Si SAW Devices 45

3.1 Patterned-ZnO/Si structure – Theory and operation. 46

3.2 3D FE simulation of one port SAW resonator with patterned-ZnO on silicon 49

3.2.1 Structure of one port SAW resonator on silicon with periodically patterned ZnO 49

3.2.2 Simulation methodology. 50

3.2.3 Results of 3D simulations one port SAW resonator. 50

3.2.4 Conclusion based on 3D simulations. 52

3.2.5 Surface modes generated due to transverse bulk waves in ZnO pattern 53

3.2.6 Surface modes generated due to longitudinal bulk waves in ZnO pattern 54

3.2.7 Observations from 3D and 2D simulation results 55

3.3 Addition of a buffer layer in patterned-ZnO/Si structure 57

3.3.1 Patterned-ZnO/SiO_2*/Si structure* 57

3.3.2 ZnO-patterned/AlN/Si structure. 62

3.3.3 Observations from the study of inclusion of buffer layer (SiO_2 *and* 65

AlN) . . . .

3.4 2D simulation of SAW delay line on silicon using periodically patterned ZnO 66

3.4.1 Simulation methodology 66

3.4.2 Results of 2D SAW delay line with patterned structure 67

3.5 Design of proposed patterned-ZnO/Si SAW devices using equivalent circuit model 69

3.5.1 Calculation of IDT parameters for proposed SAW devices on silicon 71

3.6 Summary 73

4 Fabrication of Patterned-ZnO/Si SAW Devices 75

4.1 Fabrication of SAW devices on Si using UV lithography process 75

4.1.1 Design of SAW devices on silicon 75

4.1.2 Fabrication of SAW devices on silicon 77

4.1.3 Notable observations from the fabrication process 88

4.2 Fabrication of SAW devices on Si using e–beam lithography process. . 89

4.3 Summary 92

5 Testing and Fabricated Patterned-ZnO/Si SAW Devices 93

5.1 S parameters of fabricated SAW devices on silicon substrate 93

5.2 S parameters of one port SAW resonator. 95

5.2.1 Simulation of one port SAW resonator as fabricated 96

5.3 S parameters of two port SAW resonator fabricated on silicon substrate 100

5.3.1 Simulation of one port SAW resonator on silicon substrate as fabricated 101

5.3.2 S parameters of two port SAW resonator fabricated on silicon substrate with oxide layer 102

5.3.3 Compensation network to match impedance 104

5.4 The study of effect of misalignment of patterned-ZnO structure 107

5.5 The study of effect of width of patterned-ZnO structure 108

5.6 Calculation of K^2 using delay line configurations 110

5.7 S parameters of SAW devices fabricated through e-beam lithography process 111

5.7.1 One port SAW resonators 111

5.7.2 Simulation of fabricated SAW device using e-beam lithography process 112

5.7.3 Two port SAW resonators 114

5.8 Summary 116

6 Edge Reflection Surface Acoustic Wave Devices on Silicon 119

6.1 Introduction 120

6.2 Love wave based SAW devices on silicon using ZnO films 121

6.3 Proposed edge reflection (ER) type SAW devices on silicon using ZnO films 122

6.4 Finite element simulations of ER type SAW devices on silicon 123

6.4.1 Simulation methodology 124

6.4.2 Results of ER type one port ZnO/Si SAW resonator 125

6.5 Effect of buffer layers in ER type SAW devices on silicon 129

6.5.1 Effect of SiO_2 buffer layer on ZnO/Si structure 130

6.5.2 Effect of AlN buffer layer on ZnO/Si structure 132

6.5.3 Frequency dependent analysis 135

6.5.4 Observations 137

6.6 ER type SAW device on silicon periodically using patterned-ZnO film 139

6.6.1 Simulation methodology 140

6.6.2 Results of ER SAW one-port resonator with patterned-ZnO 141

6.6.3 Effect of heavy metals on SAW characteristics 142

6.6.4 Effect of buffer layers in ER type patterned-ZnO/Si structure on SAW characteristics 144

6.6.5 Observations 146

6.7 Applications of ER type SAW resonator 146

6.7.1 Longitudinally coupled resonator filter (LCR) 146

6.7.2 Transversely coupled resonator filter (TCR) 147

6.7.3 Ladder filters 148

6.8 Design of ER type SAW devices on silicon using equivalent circuit model 149

6.9 Summary 150

7 Fabrication of Edge Reflection Type SAW Devices on Silicon 153

7.1 Fabrication of edge reflection type SAW devices on silicon 153

7.1.1. Design of edge reflection type SAW devices 153

7.1.2 Fabrication process 154

7.2 Summary 162

8 Testing of Fabricated ER type SAW Devices on Silicon 163

8.1 S parameters of ER type ZnO/Si one port SAW resonator 163

8.1.1 Testing of ER type one port SAW resonator using compensation network 165

8.1.2 FE Simulation of ER type ZnO/Si one port SAW resonator 165

8.2 S parameters of ER type ZnO/Si two port SAW devices 166

8.3 S parameters of ER type SAW devices with pattern-ZnO 167

8.4 Summary 168

9 Conclusion and Future work 169

A Material Constants of ZnO, AlN, SiO_2, and Si 171

B Absorbing Boundary Conditions 173

Bibliography 175

List of Publications 181

List of Figures

1.1 Schematic of elastic wave propagation in perturbed medium, (a) longitudinal or compressional wave, (b) shear or transverse wave, (c), Rayleigh wave, and (d) Love wave, adapted from *www.aeic.alaska.edu.* 3

1.2 (a) Excitation of surface acoustic waves over piezoelectric substrates using interdigital transducer (IDT) and (b) Top view of an IDT. 4

1.3 Various methods employed to excite SAW over non-piezoelectric materials. (a) Point excitation, (b) mode conversion using wedge, (c) and (d) piezoelectric film transducers, adapted from White *et al.* [6]. 5

1.4 Mutual conversion of bulk and surface waves at periodic irregularities in a substrate, adapted from White *et al*. [6]. 5

1.5 Schematic of SAW devices fabricated on piezoelectric substrate with metal IDT. (a) one-port resonator with reflector gratings, (b) one-port SAW resonator with large number of IDT fingers, (c) two-port SAW resonator, and (d) SAW delay line device with absorbers. 7

1.6 Schematics of Edge reflection type SAW devices (a) one port and (b) two port SAW resonators. 8

1.7 Methods of generation and detection of SAW over non-piezoelectric substrates reported by (a) thin film SAW device on silicon substrate with ZnO thin film for the generation and propagation of surface waves, Kino *et al.* [20] and (b) SAW device on silicon substrate using ZnO thin film transducer for the excitation of SAW that propagates in silicon Hickernell *et al.* [21]. 11

2.1 Particles position in equilibrium and deformed states of solid body. Note: The deformation of the solid is shown in broken lines [38]. 17

2.2 Coordinates of an IDT [3] 24

2.3 Mason equivalent circuit of one period of IDT analyzed by Smith *et al.* [6] 26

2.4 Equivalent circuit for entire IDT, made up with *N* pairs of IDT finger with acoustic ports in cascade and electrical ports in parallel. 27

2.5 Overall equivalent circuit of an IDT. 27

2.6 Illustration showing a solid body discretized into finite number of elements. 29

2.7 Orientation of ZnO wurtzite structure in (0001) basal plane. 31

2.8 3D Geometry of the periodic section used for the simulation. 32

2.9 Displacement profiles of Rayleigh mode generated in IDT/ZnO/Si SAW resonator having YZ oriented ZnO, (a) x–displacement, (b) y–displacement, and (c) z–displacement, displacements are in µm. 34

2.10 Displacement profiles of Love wave generated in IDT/ZnO/Si SAW resonator having XY oriented ZnO, (a) x–displacement, (b) y–displacement, and (c) z–displacement. *Displacement scale in µm*. 34

2.11 Normalized harmonic admittance plots obtained from frequency dependent analysis, (a) characteristics of Rayleigh mode generated in IDT/ZnO/Si SAW resonator having YZ oriented ZnO and (b) love wave characteristics with XY oriented ZnO. 35

2.12 Normalized harmonic admittance plots obtained from frequency dependent analysis, (a) characteristics of Rayleigh mode generated in IDT/ZnO/Si SAW resonator having YZ oriented ZnO and (b) love wave characteristics with XY oriented ZnO. 36

2.13 Meshed 3D Geometry of the periodic section used for the simulation. 37

2.14 The possible four layered configurations adapted from Kino [20]. 38

2.15 2D Geometry of the periodic section used for the simulation. 38

2.16 The phase velocity and electromechanical coupling coefficients dispersion characteristics of four ZnO/Si configurations. 39

2.17 The variation of phase velocities of 0^{th}, 1^{st}, 2^{nd}, and 3^{rd} Rayleigh modes with respect to ZnO film thickness ratio in conventional ZnO/Si structure. 41

2.18 (a) Normalized admittance and (b) normalized displacement characteristics of Rayleigh surface modes generated in conventional ZnO/IDT/Si configured SAW resonator at h/λ = 0.3. 41

2.19 (a) Total displacement, (b) x-displacement, (c) y-displacement profiles of fundamental Rayleigh mode, and (d) total displacement profile, (e) x-displacement, (c) y-displacement profiles of first higher order Rayleigh modes generated in the ZnO/IDT/Si structure at h/λ = 0.3, *displacement scale in µm.* 42

2.20 2D schematic of ZnO/IDT/Si SAW delay line 42

2.21 (a) y-displacement profile of ZnO/IDT/Si SAW delay line at 27.7 ns with color legend in Armstrong's (A°), (b) particle's y-displacement on ZnO surface near input IDT, (c) y-displacement of a particle on the ZnO surface at top of IDT, and (d) output voltage obtained with respect to time. 44

3.1 (a) Three dimensional schematic of the proposed one-port SAW resonator on silicon with periodically patterned ZnO disposed in the spaces of IDT fingers and reflector gratings, (b) 3D schematic of one port SAW resonator with IDT consisting of a large number of electrode fingers with ZnO pattern in the spaces of IDT. 46

3.2 Pictorial representation of mutual conversion of SAW and BAW at periodic structures (a) conversion of SAW incident at the periodic structure into BAW, and (b) conversion of BAW incident at the periodic structure into SAW. 47

3.3 3D schematic of mutual conversion of BAW and SAW in the proposed periodically patterned-ZnO/Si structure. (a) BAW to SAW conversion, and (b) SAW to BAW conversion. 48

3.4 Geometries used in FE simulations of the proposed one port SAW resonator, (a) schematic of the cross-sectional view of the device, (b) 3D geometry of half periodic section, and (c) 2D geometry of half periodic section with anti-periodic boundaries along x, assuming $n \rightarrow \infty$, and a perfectly matched layer (PML) at the bottom, and (d) meshed half periodic section of patterned-ZnO/Si. 49

3.5 Harmonic admittance (HA) and normalized displacement plots of SAW modes generated in the patterned-ZnO/Si structure at h/λ of 0.19. Total of five surface modes are observed, out of which both SH modes are insignificant and only two VP modes are dominant. 51

3.6 The normalized x and y displacement profiles of vertically polarized SAW modes generated in the patterned-ZnO/Si structure at h/λ of 0.19. The displacements are normalized, as in Figure 3.5, with respect to the maximum displacement in silicon. U_{T0_x}, U_{T0_y} and U_{T1_x}, U_{T1_y} are the x, y displacements of surface modes generated by the fundamental transverse bulk mode (a, b) and first higher order transverse bulk mode (c, d) excited in ZnO pattern. (e) U_{L0_x} and (f) U_{L0_y} are the x, y displacements of surface mode excited due to mode conversion of the fundamental longitudinal mode in ZnO. 51

3.7 The phase velocity and coupling coefficient dispersion curves of vertically polarized modes generated in silicon by the transverse bulk waves excited in ZnO pattern. 54

3.8 The phase velocity and coupling coefficient dispersion curves of vertically polarized modes generated in silicon by longitudinal bulk waves excited in patterned ZnO. 55

3.9 TCD dispersion characteristics of surface modes generated conventional ZnO/IDT/Si and VP_T modes in patterned-ZnO/Si structure. 56

3.10 2D Geometry of the proposed device with SiO_2 layer used for the simulation with periodic boundary conductions. 58

3.11 The phase velocity and K^2 dispersion curves of vertically polarized modes generated in patterned-ZnO/0.2μm-SiO_2/Si structure due to transverse bulk waves excited in ZnO pattern. 58

3.12 Phase velocity and coupling coefficient characteristics of patterned-ZnO/SiO_2/Si structure with SiO_2 thicknesses of 0.8 μm, 1.6 μm, and 2.4 μm. 59

3.13 The phase velocity and K^2 dispersion curves of vertically polarized modes generated in patterned-ZnO/SiO_2/Si structure due to transverse bulk waves excited in ZnO pattern obtained with the parametric sweep of SiO_2 thickness (h_{SiO_2}/λ) for a constant ZnO height of 1.6 μm (0.2λ) which has shown high K^2. 60

3.14 The TCD dispersion characteristics of first three VP_T surface modes generated in the patterned-ZnO/SiO_2/Si structure with respect to ZnO and SiO2 thicknesses. 63

3.15 2D Geometry of the periodic section of proposed device with AlN buffer layer for the simulation. 63

3.16 The phase velocity and K^2 dispersion curves with respect to height of ZnO in patterned-ZnO/ 4μm-AlN/Si structure. 64

3.17 The phase velocity and K^2 dispersion curves of vertically polarized modes generated by transverse bulk waves in patterned-1.6μm-ZnO/AlN/Si structure. 65

3.18 2D schematic of the SAW delay line device on silicon with periodically patterned ZnO in the spaces of IDT. 67

3.19 Structure of mesh used in the simulation of the SAW delay line device with triangular elements with minimum element size of $\lambda/10^3$ at ZnO-silicon interface and having growth rate of 1.09 reaching to a maximum element size of $\lambda/8$. 67

3.20 (a) y-displacement profile of patterned-ZnO/IDT/Si SAW delay line at 27.7 ns, color legend displacement units are in μm, (b) transient y-displacement profile of a particle at input IDT-silicon interface, (c) transient y-displacement profile of a particle at output IDT-silicon interface, (d) output voltage obtained at output IDT with respect to time, and (e) magnified view of output IDT with deformation shows SAW in silicon been converted to first higher order transverse BAW in ZnO blocks. 69

3.21 y-displacement profile of patterned-ZnO/IDT/2μm-SiO_2/Si SAW delay line at 34.16 ns. Addition of SiO_2 buffer layer has reduced the acoustic radiation into bulk and increased acoustic energy concentration near the surface as compared to the results shown in Fig. 3.18 (a) for patterned-ZnO/IDT/Si SAW delay line. 70

3.22 Equivalent circuit model of the proposed ZnO-patterned structure on silicon with oxide layer. 71

4.1 (a) Mask layout using CleWin software, (b) schematic of one port SAW resonator, (c) schematic of and two port SAW resonator, (d) magnified view of device showing the dimensions of IDT, and (e) schematic of the delay line devices with open and metalized propagation paths. 78

4.2 Optical microscopic images of (a) IDT structure on mask plate 1 and (b) ZnO pattern on mask plate 2. 79

4.3 Process flow employed for the fabrication of periodically patterned-ZnO/SiO_2/Si SAW devices. 81

4.4 Microscopic view of IDT pattern developed after UV lithography process using MF-26A developer. 82

4.5 Microscopic image of IDT structure showing electrodes and bus bar, obtained after lift-off process. 82

4.6 (a) XRD analysis of ZnO film on silicon substrate annealed at different temperatures and (b) FESEM image of ZnO thin film deposited on silicon substrate without oxide layer after annealing at 650°C. 83

4.7 (a) Microscopic image of photoresist pattern on test sample after ZnO etching process using dilute HF solution and (b) its FESEM image showing undercut as the cause of washing away of photoresist. 84

4.8 Microscopic images of the device after the development of HM, (a) before removal of photoresist and (b) after removal of photoresist showing HM. 86

4.9 (a) Illustration of conventional flow of etchant over the device, the cross-section along the aperture is depicted and (b) experimental setup for patterning of ZnO film using magnetic stirrer. 87

4.10 SEM image depicts the SiO_2 hard mask over the ZnO pattern. 87

4.11 FESEM images of patterned ZnO film on test samples using dilute acetic acid of concentration (a) 0.1M, (b) 0.2M, (c) 0.3M. (d) Shows the ZnO pattern obtained on actual device using 0.2M acetic acid with convectional flow of 1.6 m/s. 89

4.12 SEM images of (a) one port SAW resonator and (b) magnified view of IDT structure. 91

4.13 (a) SEM image and (b) magnified view of the IDT structure of one port SAW resonator after ZnO patterning. 92

5.1 Experimental setup used for the determination of S parameters of fabricated SAW devices (a) RF probe station with network analyzer and (b) RF probes. 93

5.2 Layout showing the distribution and arrangement of SAW devices on processed 2” wafers. Shaded devices are the delay lines with metalized propagation path. 94

5.3 Characteristics of one port SAW resonator 75P-55L (a) magnitude plot of S11 parameter and (b) Smith chart. 95

5.4 Magnitude and phase plots of S11 parameter measured for 75P-55L SAW one port resonator and the modes are identified by the corresponding localized peaks in magnitude plot. 95

5.5 (a) The 2D geometry of fabricated proposed one port SAW resonator with SiO2 layer and (b) S11 characteristics obtained from FE simulations. 96

5.6 (a) The 2D geometry of fabricated proposed SAW resonator with SiO_2 layer without shift in ZnO pattern (b) S11 characteristics obtained from FE simulations. 98

5.7 Magnitude and phase plots of measured S parameters of a fabricated two port SAW resonator labeled 65P-60L-0.5 on plain silicon wafer without an oxide layer. The resonance modes are identified by the zero crossings in the phase plots of S12. 100

5.8 (a) The 2D geometry of fabricated proposed SAW resonator on silicon substrate with ZnO pattern shift of 0.5 μm (b) S11 characteristics obtained from FE simulations. 101

5.9 The snapshot of measured S parameter characteristics of a two port SAW resonator labeled 45P-50L-0.5 fabricated on silicon wafer with 1.73 μm thick oxide film. 103

5.10 Magnitude and phase plots of S11, S12, S22, and S21 characteristics of fabricated two port SAW resonator labeled 45P-50L-0.5 having an oxide layer of 1.73 μm. The resonance modes are identified by the zero crossings in S12 phase plot. 104

5.11 The S11 characteristics of 45P-50L-0.5 SAW device with matching network. 105

5.12 (a) Cross sectional view of a section one port SAW resonator and (b) frequency characteristics with respect to misalignment shift of ZnO pattern. 107

5.13 Admittance characteristics of proposed structure at different values of misalignment. 108

5.14 (a) The 2D geometry used for parametric sweep of ZnO width, *y*-displacement profile of surface modes generated in the structure at (b) $2b/\lambda$ = 0.25, and (c) $2b/\lambda$ = 0.5. 109

5.15 Frequency variation with respect to base width of ZnO pattern on the proposed structure. 109

5.16 S21 characteristics of (a) free surface delay line and (b) metalized surface delay line. 111

5.17 (a) Magnitude of S11 parameter obtained from network analyzer and (b) S11 characteristics showing magnitude and phase parameters plotted from the exported data. 112

5.18 The 2D geometry of fabricated proposed SAW resonator on silicon substrate with 278nm thick oxide layer using *e*-beam lithography. 112

5.19 (a) The XRD pattern of ZnO film deposited at room temperature and (b) XRD pattern of ZnO sample annealed at 650 °C. 115

5.20 Magnitudes of S11, S12, S22, and phase plots of S12 characteristics of a fabricated two port SAW resonator having 65 pairs of electrode and 60 wavelength aperture length on silicon substrate with 200 nm oxide layer. The modes are identified by the corresponding localized peaks in S11, S22 characteristics and phase zero crossing of S12, S21. 115

6.1 3D schematics of (a) conventional one port SAW resonator with reflector gratings and (b) edge reflection type SAW resonator with edge electrodes. 120

6.2 (a) Schematic of proposed ER type SAW resonator using a diced section of silicon substrate and (b) schematic of proposed ER type SAW resonator developed using micro machined vertical grooves for bulk manufacturing. 123

6.3 (a) Cross sectional view of the proposed ER type SAW device and (b) 3D geometry with periodic boundaries along aperture used to obtain phase 124 velocity and coupling coefficient dispersion characteristics as well as admittance characteristics, and (c) meshed ER type SAW resonator of 1λ.

Note: IDT position is varied according to the device configuration.

6.4 Phase velocity dispersion characteristics of Love modes generated in the ZnO/Si structure. 125

6.5 The coupling coefficient characteristics of various Love modes generated in all possible configurations of ZnO/Si structure. 126

6.6 Characteristics of L_0 mode generated in the 0.8μm-ZnO/IDT/Si structure at h/λ of 0.10. (a) Total displacement, (b) Harmonic admittance, (c) surface displacement profiles and (d) particle displacement plots along *x*, *y*, *z* with respect to the depth of the substrate. 127

6.7 Characteristics of L_0 mode generated in the IDT/2.2μm-ZnO/Si structure at h/λ of 0.275 (a) Total displacement, (b) Harmonic admittance, (c) surface displacement profiles and (d) particle displacement plots along *x*, *y*, *z* with respect to the depth of the substrate. 128

6.8 Cross sectional view of one periodic section of the proposed ER type SAW device with buffer layers. (a) ZnO/IDT/SiO_2/Si, (b) IDT/ZnO/SiO_2/Si, (c) ZnO/IDT/AlN/Si, and (d) IDT/ZnO/AlN/Si. 129

6.9 Dispersion characteristics of Love modes generated in the ZnO/IDT/SiO_2/Si structure. 131

6.10 K^2 dispersion characteristics of Love modes generated in the IDT/ZnO/SiO_2/Si structure, (a) with respect to SiO_2 film thickness, constant ZnO thickness and (b) with respect to ZnO film thickness, constant SiO_2 film thickness. 131

6.11 Phase velocity and K^2 dispersion characteristics of Love modes generated in the IDT/ZnO/AlN/Si structure. (a) and (b) with respect to AlN thickness, constant ZnO film thickness, (c) and (d) with respect to ZnO thickness, constant AlN film thickness. 133

6.12 Phase velocity and K^2 dispersion curves of Love modes generated in the IDT/ZnO/AlN/Si structure. (a) and (b) dispersion charactersitics with respect to AlN, a fixed ZnO film thickness, (c) and (d) with respect to ZnO thickness, fixed AlN film thickness. 134

6.13 (a) 1.1μm-ZnO/IDT/2μm-SiO_2/Si, (b) IDT/2.2μm-ZnO/2μm-SiO_2/Si, (c) 0.8μm-ZnO/IDT/4μm-AlN/Si, and (d) IDT/1.1μm-ZnO/4μm-AlN/Si. 136

6.14 Proposed ER type SAW resonator on silicon substrate using periodically patterned ZnO film and vertically etched grooves for total reflection of generated Love waves. 139

6.15 (a) Cross sectional view of the proposed ER type SAW device with periodically patterned-ZnO on silicon and (b) 3D geometry with periodic boundaries along 140 aperture used to obtain phase velocity and coupling coefficient dispersion characteristics as well as admittance characteristics.

6.16 Phase velocity dispersion characteristics of Love wave generated in the patterned-ZnO/IDT/Si structure. 141

6.17 (a) Harmonic admittance characteristics of Love wave generated in the patterned-ZnO/IDT/Si structure and (b) the displacement profile of generated surface mode at resonance frequency. 142

6.18 (a) Displacement distribution of SH-SAW generated in silicon with IDT of various metals and (b) the displacement profile of generated surface mode in silicon with gold electrodes. 143

6.19 Admittance characteristics of Love mode generated in the ER type 2μm-patterned-ZnO/Si SAW resonator with (a) copper IDT, (b) palladium IDT, (c) tungsten IDT and (d) gold IDT. 143

6.20 Phase velocity dispersion characteristics of Love wave generated in the 4μm-patterned-ZnO/IDT/SiO_2/Si structure. 145

6.21 (a) Harmonic admittance characteristics of Love mode generated in the 2μm-patterned-ZnO/IDT/1.8μm-SiO_2/Si structure and (b) displacement profile of Love mode generated by TSM mode excited in ZnO pattern. 145

6.22 Schematics of resonator filter configurations using ER type SAW resonators, (a) two port resonator filter, (b) longitudinal coupled resonator filter, (c) ladder filter, and (d) block diagram of arrangement of series (S) and parallel (P) resonators in a typical ladder filter. 147

6.23 (a) Equivalent circuit of IDT and (b) typical characteristics of an L-section. 148

7.1 (a) Optical microscopic images of IDT structure on mask plate and (b) magnified view of IDT. 154

7.2 Fabrication Process flow of ER type SAW devices on silicon with grooves developed at the last. 155

7.3 Fabrication Process flow of ER type SAW devices on silicon with grooves developed first IDT 156

7.4 Fabrication Process flow of ER type SAW devices on silicon with grooves developed after IDT. 157

7.5 Microscopic images of vertical grooves developed in silicon substrate and (b) developed IDT photoresist pattern developed using MF-26A solution. 158

7.6 Microscopic images of developed IDT structure after the development of mircomachined grooves. 158

7.7 (a) Developed IDT structure of a two port resonator and (b) magnified view of IDT structure. 159

7.8 (a) Developed groove structure and (b) removal of unwanted metallic regions. 160

7.9 (a) Microscopic image of ER device after RIE process (b) ER type device after DRIE process showing the vertically developed groove. 161

8.1 Layout showing the distribution and arrangement of proposed ER type SAW devices on the mask plate and on silicon wafers. 164

8.2 (a) Magnitude of S11 parameter of a one port ER type SAW resonator 100P-50L and (b) re plotted schematic of S11 characteristics. 164

8.3 Measured S11 parameters showing the magnitude and phase plots of 100P-50L one port ER type SAW resonator with compensation network indicating resonance frequency of about 260 MHz. 165

8.4 (a) One wavelength of ER type one port SAW device with periodic boundaries along the aperture and (b) S11 characteristics showing resonance frequency at about 269 MHz. 166

8.5 (a) Microscopic image of TCR filter after fabrication showing the washed away ZnO film at the edges and (b) FESEM image showing steps formed in ZnO film due to the presence of IDT underneath. 167

List of Tables

1.1 List of selected reports on implementation of thin films over traditional SAW devices. 10

1.2 List of selected reports of SAW devices on non-piezoelectric substrates. 13

2.1 Phase velocity and coupling coefficient of ZnO/Si layered configuration with different orientations of ZnO. 33

2.2 Variation in resonant frequency with change in aperture (W). 35

2.3 Variation of device resonant frequency with respect to change in mesh density. 37

2.4 Dimensions of one port SAW resonator obtained using equivalent circuit model. 40

3.1 Characteristics of surface modes generated in the proposed structure and conventional ZnO/Si layered structure at high coupling coefficient. 56

3.2 The notable observations from phase velocity and K^2 characteristics given in Fig. 3.10, Fig. 3.11, and Fig. 3.12. 60

3.3 Calculated IDT dimensions using equivalent circuit model. 72

4.1 Dimensions used for the fabrication of one-port saw resonators. 76

4.2 Dimensions used for the fabrication of two-port saw resonators. 76

4.3 Dimensions used for the fabrication of SAW delay line devices. 76

4.4 RF sputtering conditions of gold and chromium metal deposition. 82

4.5 RF sputtering deposition parameters used for ZnO thin films. 83

4.6 Trial runs carried out for ZnO patterning using different types of photoresists. 85

4.7 Details of test runs carried out on ZnO patterning. 88

4.8 Dimensions of proposed SAW devices using e-beam lithography. 90

4.9 ZnO deposition conditions for RF sputtering. 92

5.1 Comparison of measured results and simulated results of fabricated 75P-55L device. 97

5.2 Measured S11 parameters of fabricated one port SAW resonators. 99

5.3 Resonance and anti-resonance frequencies for surface modes and corresponding effective coupling coefficients (K_{eff}^2) using S21 characteristics of 65P-60L-0.5 two port SAW resonator. 100

5.4 Comparison of measured S11 results and simulated results for 65P-60L-0.5 two port SAW resonator. 102

5.5	Resonance and anti-resonance frequencies for surface modes and corresponding effective coupling coefficient values of two port SAW resonator 45P-50L-0.5 fabricated on silicon substrate with oxide layer.	103
5.6	Measured S12 parameters of fabricated two port SAW resonators.	106
5.7	Measured Q factor for various surface modes generated in the fabricated two port SAW resonators.	107
5.8	Comparison of tested and simulated results of *e*-beam SAW one port resonator device	114
5.9	Measured S11 parameters of one port SAW resonators fabricated using *e*-beam lithography.	114
5.10	Measured S12 parameters of fabricated two port SAW resonators using *e*-beam lithography.	116
6.1	List of selected reports on Love wave based ZnO thin film SAW devices.	122
6.2	Notable observations from the phase velocity and K^2 dispersion characteristics of all four possible configurations.	127
6.3	Notable observations of ZnO/IDT/SiO_2/Si and IDT/ZnO/SiO_2/Si configurations with constant oxide thickness of 2 µm.	132
6.4	Notable observations of ZnO/IDT/AlN/Si and IDT/ZnO/AlN/Si configurations with constant oxide thickness of 4 µm.	134
6.5	Phase velocity, series resonance, parallel resonance, total displacement, and bandwidth of ER type SAW devices with buffer layers.	136
6.6	Optimal parameters of ZnO and buffer layers suitable for fabrication.	138
6.7	Admittance characteristics of surface wave in silicon with IDT of various metals.	144
6.8	Calculated IDT dimensions of ER type SAW devices on silicon using equivalent circuit model.	149
8.1	Measured S12 parameters of fabricated two port ER SAW resonator filters with ZnO film.	166
8.2	Measured S12 parameters of fabricated two port ER SAW resonators using patterned-ZnO film.	167

List of Acronyms

AlN	Aluminium Nitride
APM	Acoustic Plate Mode
BAW	Bulk Acoustic Wave
BGS	Bleustein–Gulyaev-Shimizu
CdS	Cadmium Sulfide
CMOS	Complementary Metal-Oxide Semiconductor
COM	Coupling of Mode
DC	Direct Current
DI	De-ionized
DOF	Degrees of Freedom
ER	Edge Reflection
FEM	Finite Element Method
FESEM	Field Emission Scanning Electron Microscope
FPM	Flexural Plate Mode
GSG	Ground-Source-Ground
HF	Hydro-Fluoric Acid
IC	Integrated Circuit
IDT	Interdigital Transducer
M	Metal
MEMS	Microelectromechanical Systems
MR	Metallization Ratio
NCD	Nano Crystalline Diamond
PDE	Partial Differential Equation

RF	Radio Frequency
RFID	Radio Frequency Identification
S	Scattering
SAW	Surface Acoustic Wave
SEM	Scanning Electron Microsope
SH	Shear Horizontal
TCF	Temperature coefficient of frequency
TOSM	Through Open Short Matched
TSM	Thickness Shear Mode
UV	Ultraviolet
VP	Vertically Polarized
XRD	X-Ray Diffraction

List of Symbols

p	IDT finger pitch
v	SAW phase velocity
v	SAW phase velocity in substrate
λ	SAW wavelength
f	Operating frequency
N	Number of electrodes in reflector gratings
r_s	Reflection coefficient of one electrode
L_p	Penetration depth
L_g	Distance between IDT and reflector grating
L_c	Distance between two IDTs
d	Center-to-center distance between input and output IDT
W	Aperture of IDT
A_n	Amplitude of impluse
L	Length of resonator plinth
ω	Angular frequency
a_0	Amplitude of step response
K_R	Electromechanical coupling coefficient of Rayleigh wave
C_1	Capacitance per pair of IDT fingers and per unit length
P_R	Mean power density of transported by the wave
$\|U\|$	Amplitude of applied input signal
C_s	Electrode capacitance per electrode (static)
j	Imaginary unit
E_n	Electric potential equivalent to F_n (n stands for number of electrodes)
I_n	Equivalent electric current

ϕ	Turns ratio of an acoustic-to-electric circuit transformer
C_T	Total capacitance of IDT
G_a	Radiation conductance
B_a	Susceptance
α	Transduction coefficient
ε	Permittivity
R_f	Thin film resistance in one transduction unit
C_f	Interdigital capacitance in one transduction period
k	Reflection coefficient per one electrode in the reflector grating
F_n	Acoustic terminal force(*n* stands for number of electrodes)
P_{11} and P_{22}	Reflections coefficients of IDT in P-Matrix
P_{12} and P_{21}	Transmission coefficients of IDT in P-Matrix
P_{13} and P_{23}	Excitation coefficients of IDT in P-Matrix
P_{31} and P_{32}	Current generated by the wave arriving at acoustic ports of IDT
P_{33}	Admittance of IDT in P-matrix
S	Strain
T	Stress
V_{in}	Input electric potential to IDT
V	Scalar electric potential
$\mathbf{u}$	SAW particle displacement
u'_i	Particle velocity of SAW along i direction
$T_{ij(mech)}$	Stress due to mechanical strain
$T_{ij(elec)}$	Stress due to electric field
ε_{ij}	Permittivity tensor of dielectric medium

c_{ijkl}^{E}	Stiffness tensor for constant electric field
S_{jk}	Strain components
ε_{ij}^{s}	Permittivity tensor for constant stress
E_j	Electric field vector
ρ	Material density
δ	Edge length
B	Magnetic field
E	Electric field
X, Y, and Z	Crystal lattice direction
k and β	Wave number of the surface wave
U_{left}, and V_{left}	Displacements and potentials at left side of boundaries
U_{right} and V_{right}	Displacements and potentials at right side of boundaries
f_{sc-}	Lower edge frequency called as resonance frequency
f_{sc+}	Upper edge frequency called as antiresonance frequency
Γ_L	Denotes left side boundary of the SAW resonator geometry
Γ_R	Denotes right side boundary of the SAW resonator geometry
d	IDT electrode width
η	Normalized frequency
f_r	Resonance frequency
Q	Quality factor at resonance frequency
Δf	Bandwidth at half of the peak-conductance
γ	Capacitance ratio
f_a	Anti-resonance frequency
B_L, B_R and B_B	Critical damping at the edge of the transmitter, receiver,

and bottom of the substrate

$|\kappa_p|$ Absolute value of the reflection coefficient per period

K^2_{eff} Effective electromechanical coupling coefficient

P_B Total power generated by IDT in the form of bulk wave

s Slowness of BAW

h_s Depth of the piezo-substrate

h_h Thickness of holding substrate

h_a Air gap between NCIDT and piezo-substrate

α_p Transaction coefficient per period of fingers

γ_p Attenuation per period of IDT fingers

G_r Conductance at resonance frequency

v_f Free surface SAW phase velocity of the device

v_m Metallized surface SAW phase velocity of the device

S_{11} Scattering parameter (return loss)

K^2 Electromechanical coupling coefficient

I Cross-section moment of inertia

i_n Current equivalent to particle velocity for a single pair of electrode of IDT

x_i Co-ordinate axis (i = 1, 2, 3)

ξ Damping ratio

ς Piezoelectric constant used in mason equivalent circuit

Z_o Acoustic impedence

$\mathbf{Z}$ Rayleigh damping matrix

x_i Co-ordinate axis (i = 1, 2, 3)

φ_a Phase offset of the gratings of IDT

φ_t Phase offset in the potential

V_{in} Input voltage to IDT

V_o Output voltage from IDT

A_{dM} Mass proportional damping parameter

B_{dk} Stiffness proportional damping parameter

S12 Scattering parameter (insertion loss)

Γ Reflection coefficient of grating structure

VP_T Vertical polarized surface modes generated in the substrate by the transverse bulk wave in ZnO pattern

VP_L Vertical polarized surface modes generated in the substrate by the longitudinal bulk wave in ZnO pattern xxx

Chapter 1

Introduction to Surface Acoustic Wave Devices

There has been tremendous growth in the micro electromechanical systems (MEMS) industry and subsequent increase in demand for high quality components. Surface acoustic wave (SAW) devices form an important part of MEMS family. The SAW devices are widely used as resonators, correlators and delay lines for signal processing and sensing applications in the area of electronic and telecommunications industry [1]. A SAW is an acoustic wave traveling along the surface of a material exhibiting linear elasticity. The concentration of energy of these waves is higher at the surface and decreases exponentially along the depth of the substrate. SAW devices provide geometrical freedom near the surface for modification, amplification and physical interaction with the generated SAW along its propagation path, which permits SAW devices for wide range of applications. Conventionally, SAW devices are realized on polished piezoelectric substrate in conjunction with an interdigital transducer (IDT) as the transduction element for the excitation of various types of surface waves like Rayleigh wave, Shear horizontal wave, Bleustein–Gulyaev-Shimizu (BGS) wave, and Love wave, owing to piezoelectric nature of the substrate. In piezoelectric materials electric field is produced when mechanically strained and vice versa. The frequency characteristics of SAW devices depend on the IDT structure and material properties of the substrate.

SAW devices have unique advantages of realizing real time signal processing in compact devices without using external power supply. As the acoustic velocity of surface wave is about 10^{-5} times that of electromagnetic waves, it allows a significant reduction in size of the device [1]. SAW devices are one of the major components in many communication systems such as satellite receivers, remote control units, keyless entry system, radio frequency identification (RFID), television sets, and mobile phones. SAW devices are also used in micro actuators such as SAW nano-stepping motors and SAW micro-pumps. As technology advances, there is always a need for superior SAW devices with improved stability, high electromechanical coupling coefficient, high frequency of operation, and low losses. The performance of SAW devices can be improved by employing piezoelectric and dielectric thin films over SAW devices. It is possible to realize SAW devices on non-piezoelectric substrates using piezoelectric overlay in conjunction with interdigital transducers. SAW devices on non-piezoelectric substrates like silicon, sapphire and diamond have been reported using films of piezoelectric materials like ZnO, CdS, and AlN. Hence SAW devices made on silicon can be integrated with circuits for lab on chip and wireless applications [2]. Onboard antennas can be integrated within SAW devices and employed in sensors for remote and inaccessible locations.

1.1 Contributions of the thesis

This thesis mainly focuses on the research work carried out on the realization of novel class of SAW devices on silicon substrate using piezoelectric zinc oxide (ZnO) thin films and periodically patterned ZnO films. The first contribution of the thesis is the improvement in device parameters of the reported thin film SAW devices on silicon by introducing periodic patterns in the piezoelectric film. The investigation and simulations of the proposed SAW devices with patterned-ZnO on silicon, carried out using COMSOL, reveal generation of surface modes with high coupling coefficient and high phase velocity. We fabricated the proposed patterned-ZnO SAW devices on silicon and verified the simulation results. The second contribution of the thesis is the development of novel edge reflection (ER) type SAW devices realized on silicon using ZnO films as well as periodically patterned-ZnO films. The simulations of the proposed ER type SAW devices on silicon are carried out using COMSOL and the device parameters for fabrication are designed using equivalent circuit model. We fabricated the proposed edge reflection type SAW devices on silicon and the testing of the fabricated devices confirms practicability of the proposed devices. In order to demonstrate an application of the proposed devices, we fabricated and tested coupled resonator filters and ladder filters using ER type SAW resonators in silicon for RF signal processing applications.

1.2 Generation of waves in elastic medium

An elastic or acoustic wave generated in a solid material implicate changes in relative position of the particles, expressed in terms of *strains*. The change in position also specifies the displacement of particle from the equilibrium state and the displacement is generally a function of position. In the presence of strains, internal forces are generated in the material as the particles tend to return to their equilibrium state or unstrained state. The forces are expressed in terms of *stresses* and the propagation of acoustic wave involves stresses and strains. For example, a localized displacement, such as a hammer blow on a material will cause strains which in turn generate stress, the stresses generate further strains at distant points and the disturbance propagates away from the excitation source in the form of acoustic waves [3]. From the perspective of concentration of energy, elastic waves are classified into bulk waves and surface waves [4]. Bulk waves propagate into the medium whereas surface waves propagate along the surface of the medium. Bulk waves are classified mainly into longitudinal and transverse waves. Longitudinal waves are type of waves that involve compression and rarefaction having particle displacement along the direction of wave propagation as shown in Fig. 1.1(a). The other type of bulk wave is transverse wave or shear wave, where the particle displacement is perpendicular to the direction of propagation as shown in Fig. 1.1(b) [4].

Surface waves are elastic waves propagating along the surface of a semi-infinite solid (bounded medium). There are two main types of surface waves, viz. Rayleigh waves and Love waves. Rayleigh waves were first identified by Lord Rayleigh in 1885. The particles of Rayleigh wave near the surface possess elliptically motion along the sagittal plane with anti-clockwise motion, whereas particles within a wavelength depth of material have clockwise direction of motion, shown in Fig. 1.1(c) [5]. In case of Love waves, the particle displacements are in plane of the surface and transverse to the direction of wave propagation, as shown in Fig. 1.1(d). In general, Love waves are generated along a guiding layer over a substrate with acoustic velocity higher than the guiding layer and most of the energy is confined to the guiding layer [3].

In general, elastic waves are excited in a solid depending on the nature of material and interaction with the type of excitation like mechanical, thermal, electrical and magnetic. For the generation of elastic waves the materials in which normally the stress varies linearly with the applied excitation are suitable, e.g. piezoelectric and piezo-magnetic materials. Normally, piezo-magnetic materials have applications limited to low frequencies (below 1 MHz), and piezoelectric materials are suitable for applications with high operating frequencies. In this thesis we consider devices using piezoelectric materials.

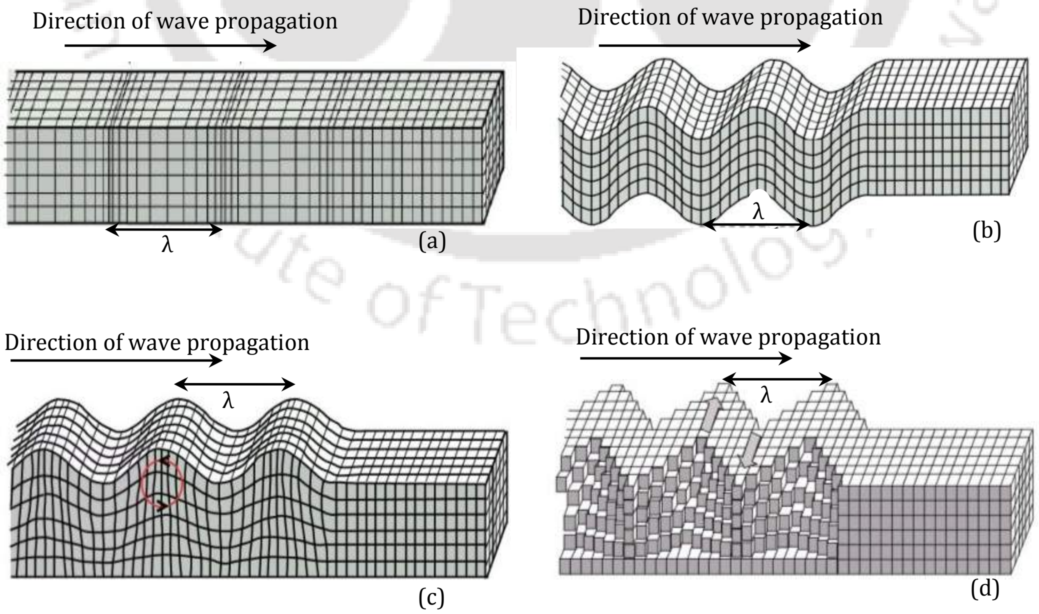

Fig. 1.1. Schematic of elastic wave propagation in perturbed medium, (a) longitudinal or compressional wave, (b) shear or transverse wave, (c), Rayleigh wave, and (d) Love wave, adapted from *www.aeic.alaska.edu.*

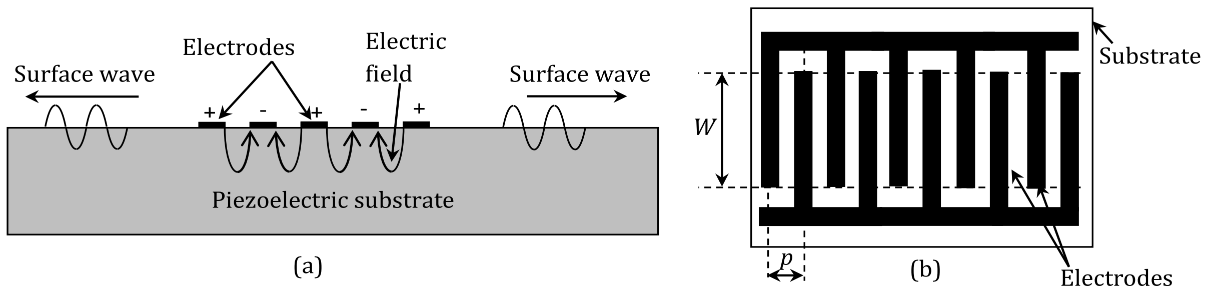

Fig. 1.2. (a) Excitation of surface acoustic waves over piezoelectric substrates using interdigital transducer (IDT) and (b) Top view of an IDT structure on a piezoelectric substrate.

Elastic waves are generated in piezoelectric substrate by means of electrical excitation using a transducer. So far 14 types of elastic waves have been discovered [6], however the thesis mostly deals with two types of surface acoustic waves (Rayleigh and Love) and two types of bulk acoustic waves (longitudinal and transverse) as depicted in Fig. 1.1. The propagation characteristics of generated surface and bulk waves in a medium are determined by the substrate properties, dimensions, and orientation of transducer [1].

Fig. 1.2(a) shows interdigital transducer (IDT) commonly used for the generation and detection of surface acoustic waves on a piezoelectric substrate and Fig. 1.2(b) depicts the top view of IDT structure. An IDT consists of comb shaped metallic electrodes with large number of interleaved fingers, and voltage applied to the electrodes cause spatial periodic fringing field at the surface of the substrate causing strain field due to piezoelectric coupling and the stress developed with the strain leads to generation of SAW in both left and right sides of each finger pair. The waves add constructively and reach maximum if the adjacent fingers are spaced at half wavelength of the SAW. The frequency of operation of the IDT is given by

$$f = v/\lambda \tag{1.1}$$

$$\lambda = 2p \tag{1.2}$$

where v is the phase velocity of SAW which is constant for a material, λ is acoustic wavelength, and p is the pitch of the IDT as shown in Fig. 1.2(b).

In general, elastic waves are generated in non-piezoelectric substrates by means of a piezoelectric transducer with mode conversion between bulk acoustic waves (BAW) and surface acoustic waves. Fig. 1.3 shows the most common ways of generating surface waves on non-piezoelectric materials [6]. Fig. 1.3(a) shows a simple method for the excitation of surface wave, employed in studying the acoustic properties of material using a point contact excitation of surface waves over non-piezoelectric materials, where a pointed piezoelectric crystal is used as the transduction element. The bulk wave transducers with wedge-shaped mode converters are commonly used to launch surface waves for non-destructive testing of materials as depicted

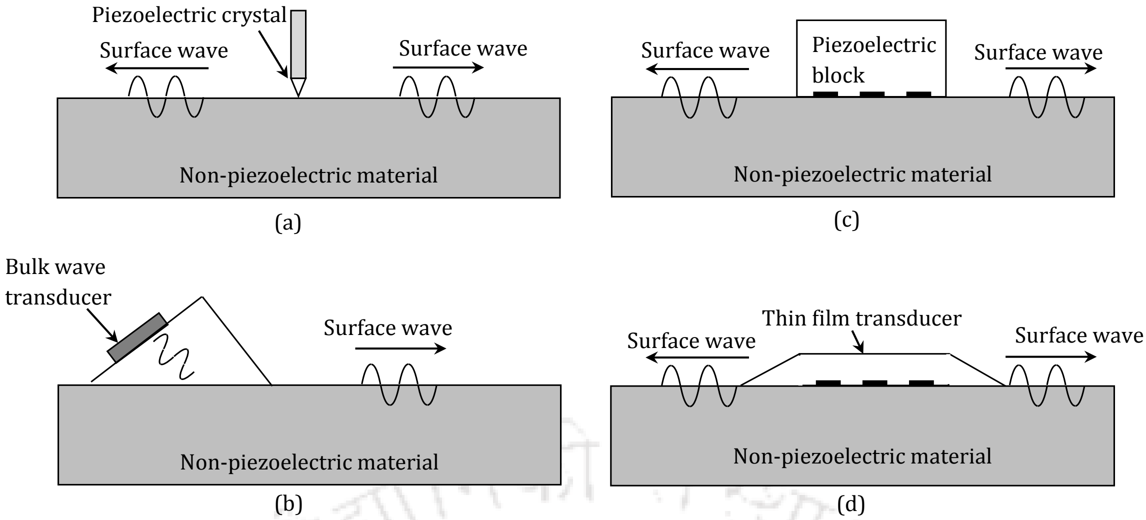

Fig. 1.3. Various methods employed to excite SAW over non-piezoelectric materials. (a) Point excitation, (b) mode conversion using wedge, (c) and (d) piezoelectric film transducers, adapted from White *et al.* [6].

in Fig. 1.3(b). The transducer comprises of a wedge shaped piezoelectric medium with electrode, physically in contact with substrate. By applying an electric signal generates a bulk wave that is converted into a unidirectional surface acoustic wave at the wedge-material interface and the wave propagates along the surface of the material. Fig. 1.3(c) and (d) shows the transduction phenomenon of surface acoustic waves on non-piezoelectric materials using piezoelectric thin film in conjunction with a transducer. The stresses generated in the piezoelectric film are induced into the material resulting in propagation of surface wave along the surface of the non-piezoelectric medium. The conversion efficiency of the transducer depends on the quality and dimensions of the film.

In general, mutual mode conversion between surface wave and bulk wave is observed at periodic irregularities and periodic structures or grooves in solids as shown in Fig. 1.4. The periodic structures can be formed by gratings, grooves etched in a substrate or by depositing strips over the substrate. The grating structure couples SAW and bulk acoustic waves (BAWs), and the coupling is exploited to generated SAW by the incident BAW as shown in Fig. 1.4(a). The

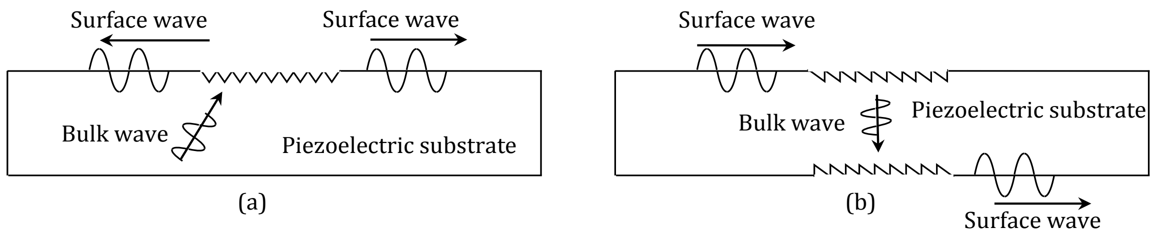

Fig. 1.4. Mutual conversion of bulk and surface waves at periodic irregularities in a substrate, adapted from White *et al*. [6].

incident BAW can be transformed into Rayleigh or shear horizontal SAW depending on the material properties and type of BAW incident at the periodic structure [7], [8]. Fig. 1.4(b), shows a device for double mode conversion where the incident surface wave at a periodic grating is converted into BAW that propagates through the substrate and is converted back to surface wave at the bottom surface of the substrate using another periodic grating [6].

1.3 Surface acoustic wave (SAW) devices

The principle of generation of SAW on piezoelectric substrates described in previous section is used to design SAW devices. SAW devices are usually fabricated on polished single crystal piezoelectric substrates such as lithium niobate, lithium tantalate, quartz and langasite. SAW devices are also realized on various non-piezoelectric materials like silicon, diamond, sapphire, and silicon dioxide using piezoelectric thin films like ZnO and AlN in conjunction with IDT. In general, SAW devices are operated in two configurations: resonator and delay line as shown in Fig. 1.5 [1]. The metallic IDTs employed in SAW devices are fabricated on piezoelectric substrate using well-established lithography techniques used in semiconductor industry.

Fig. 1.5 shows common configurations of SAW devices. In SAW resonators, SAW propagates within a resonant cavity such that the wave is reflected back to the generating IDT by the reflector gratings. The resonator devices are mainly of two types: one port resonator and two port resonator. A one port resonator comprises of a pair of reflector gratings that are fabricated on the either side of the bidirectional IDT. The reflector gratings act as mirrors to confine the generated surface wave between them by forming standing wave pattern, the arrangement of IDT and grating structures are shown in Fig. 1.5(a) [3]. Sharp resonance can be observed by the IDT when the device is designed so that the dimensions of IDT and reflectors are similar [1].

The reflectors could be made of shorted metal strips or grooves. At the Bragg frequency, such that the periodicity of reflector electrodes equals half the wavelength, reflections from individual strips have the same phase so they add coherently, as in a single electrode of an IDT. Surface waves are completely reflected from the gratings when $N|r_s|\sim 1$, where N is the number of electrodes and r_s is the reflection coefficient of each electrode. Typically, $|r_s|$ is in range of 1–3%, which is proportional to electromechanical coupling coefficient and value of N is about 100 or more [1]. Considering practical aspect of device, the length of grating structure must be greater than the penetration depth (L_p) which is the distance that the surface wave propagates into the grating structure. A one port SAW resonator can also be made by using large number of IDT fingers without reflectors as shown in Fig. 1.5(b). In this device, multiple reflections within the IDT lead to formation of standing waves and the device resonates at a particular frequency and the bandwidth of the device depends on the number of IDT finger pairs. A two-port SAW resonator consists of a set of IDTs arranged in between two reflectors gratings as shown in the Fig. 1.5(c). Two port resonators are used as a controlling element for a high stability oscillator [1]. One IDT act as transmitter and the other as receiving IDT, these two port resonators are widely used in design of high stability oscillators. The band width of a two port resonator is proportional to the number of fingers in IDT, L_c, and L_g. Where L_c is the distance between IDT's and L_g is the distances between the reflector grating and IDT structure.

Fig. 1.5(d) shows the schematic of a delay line SAW device, as the term delay corresponding to the distance between the IDTs centers (d). The device consists of transmitting IDT and receiving IDT, absorbers are placed at the end of the IDT structure to avoid unwanted reflections form edges of substrate or any other spurious acoustic reflections. Effectively, both transducers are

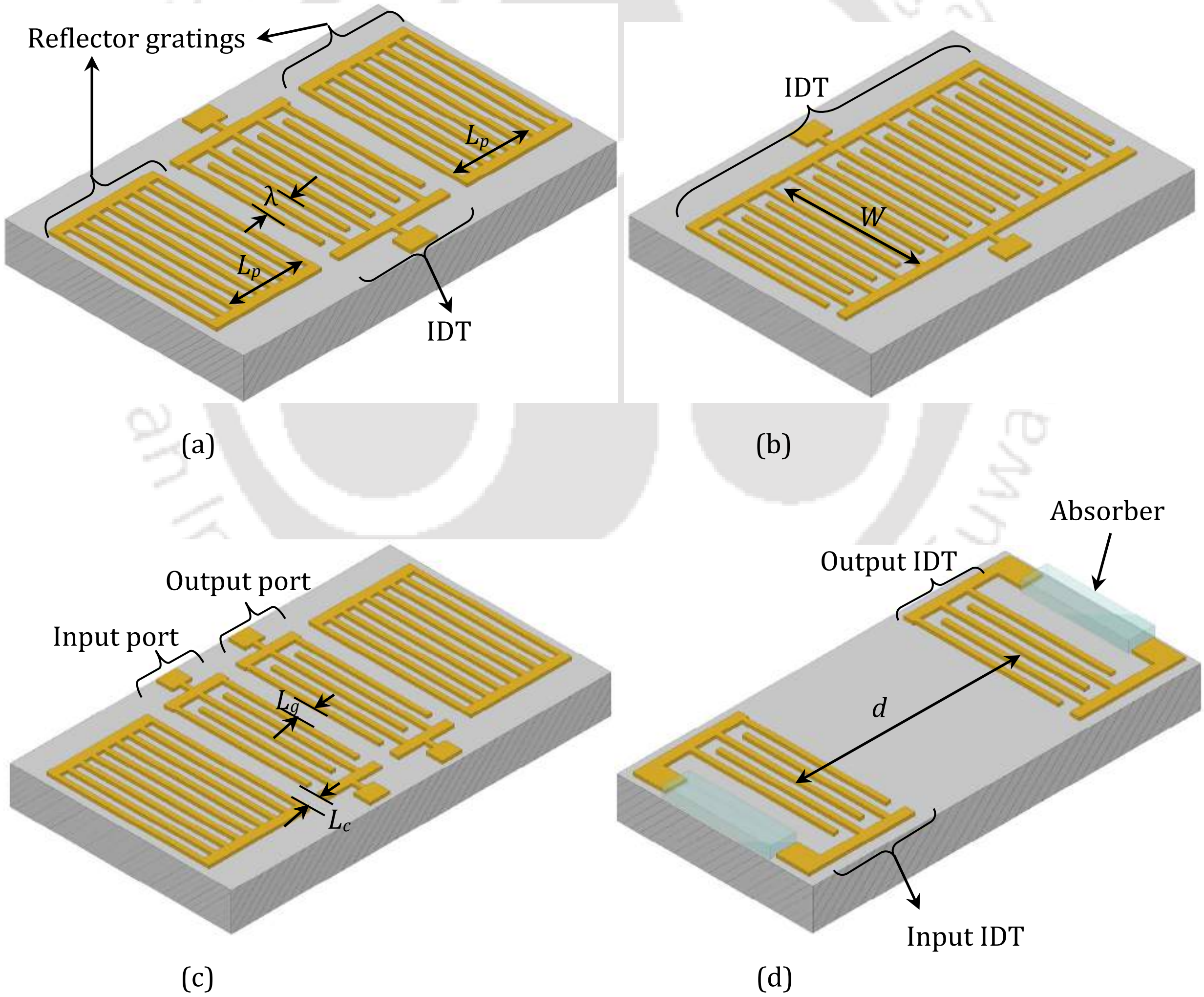

Fig. 1.5. Schematic of SAW devices fabricated on piezoelectric substrate with metal IDT. (a) one-port resonator with reflector gratings, (b) one-port SAW resonator with large number of IDT fingers, (c) two-port SAW resonator, and (d) SAW delay line device with absorbers.

maintained at a similar pitch corresponding to SAW wavelength. Hence, the response is strongest at this frequency and weak at other frequencies, so that the device can also act as band pass filter. Delay lines are widely used for sensing applications.

1.4 Edge reflection (ER) type SAW devices

In general, surface waves reflect from a free surface perpendicular to the propagation direction, in case of Ryleigh SAW mode conversion occurs whereas in case of SH-type waves like BGS and Love wave are totally reflected from the surface without mode conversion. Suzuki *et al.* in 1976 [9], first reported the realization of resonators on a piezoelectric substrate with free parallel edges using the property of total reflection of shear horizontal type waves. Further, Kadota *et al.* in 2002 [10] reported several edge reflection type SAW devices fabricated on single crystal piezoelectric substrates like 41° Y–X lithium niobate, 64° Y–X lithium niobate, and 128° Y–X lithium tantalate. The schematic of edge reflection type one port and two port SAW resonators on piezoelectric substrate are shown in Fig. 1.6. The IDT for ER types SAW devices consists of a pair of λ/8 electrodes positioned at the edges and λ/4 electrodes between the two edge electrodes. The generated surface waves propagates perpendicular to the aperture of IDT and totally reflect back at the free edges to add in phase with the generated wave to form standing wave pattern between the two free edges of the device. Fig. 1.6(b), shows the two port resonator configuration of the ER type SAW device, the resonant frequency depends on the dimensions of the IDT and the device characteristics are substantially depends on the overall length of device and positioning of the edge electrode.

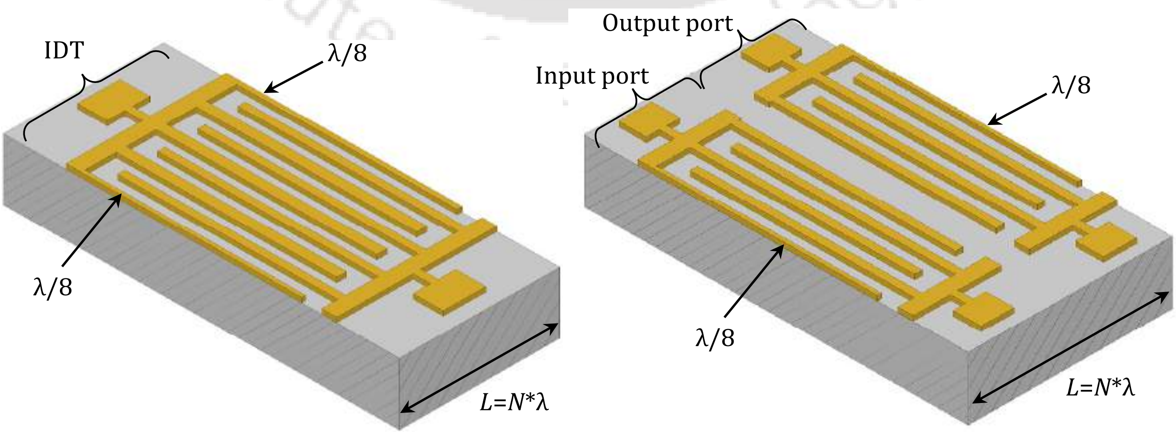

(a) (b)

Fig. 1.6. Schematics of Edge reflection type SAW devices (a) one port and (b) two port SAW resonators.

1.5 Thin films over SAW devices

Recent trend in electronics is towards device miniaturization and high performance. In general SAW devices are fabricated over single crystal piezoelectric substrates and its frequency of operation is determined by the IDT structure. The higher the frequency of operation, the lower is the dimension of IDT, for a given substrate material. Therefore the maximum frequency of operation is limited by the minimum possible feature size of the lithography technique. Substrates with high acoustic velocity can be employed for the fabrication of high frequency SAW devices. However materials like diamond and sapphire that exhibit high acoustic velocity are non-piezoelectric in nature. To improve the performance of SAW devices, not only in terms phase velocity but also temperature coefficient, insertion loss and coupling coefficient, thin films are employed in SAW devices. There are several reports in the literature on thin film SAW devices employing piezoelectric and dielectric films. Dielectric films are employed for customization of SAW characteristics, electrical and chemical passivation, improve the coupling efficiency and temperature characteristics of the device. SiO_2 films are used for temperature stability, whereas thin films like diamond and SiC (silicon carbide) are used for improving phase velocity and silicon nitride films are used for chemical passivation. ZnO thin film over quartz and glass substrates are very popular and commercially used in television filters [11]. Thin films over SAW devices are used for sensing applications and dielectric films like SiO_2 and Si_3N_4 are used for temperature stability and surface passivation [12-13], whereas films like nano-porous ZnO and polymers are used in bio-sensing applications [14-15]. ZnO films over SAW devices are also widely used for ultraviolet (UV) sensors [16]. The metal films and patterned metal films are used to influence the direction of wave propagation, velocity, and propagation loss. Piezoelectric films have been used in SAW devices to improve the device performance in terms of coupling coefficient and temperature stability. Piezoelectric films on amorphous and non-piezoelectric materials are used to realize SAW devices, where transduction of surface waves is carried out by an IDT [3]. In particular, substrates like silicon, diamond, and sapphire with films of piezoelectric materials like ZnO and AlN are used for high frequency devices with low insertion loss characteristics that have additional advantage of possible integration with microelectronic circuitry. Relevant literature on thin films implemented over traditional SAW devices are tabulated in Table 1.1.

Thin films are widely used on SAW devices in sensing applications and for the customization of the following SAW device parameters.

Phase velocity (v): Phase velocity of SAW propagating on the substrate, and frequency of operation is directly proportional to it.

Electromechanical coupling coefficient (K^2): Efficiency of electrical to mechanical energy conversion and vice versa.

Temperature coefficient of frequency (TCF): Change in device operating frequency with respect to change in temperature, and defines the stability of device with respect to temperature.

Insertion loss (IL): Attenuation of a signal due to its conversion and propagation in a device, typically expressed in dB.

Table 1.1 List of selected reports on implementation of thin films over traditional SAW devices.

SI. No	Layered structure	Type of surface wave	Application	Reference and year
1.	$Si_3N_4/LiNbO_3$	Rayleigh wave	Low loss devices with frequency tuning and passivation	Jacqueline *et al.* [12] 1995
2.	$SiO_2/LiNbO_3$	Rayleigh wave	High frequency and temperature stable wide band filters	Yamanouchi *et al.* [13] 1995
3.	$SiO_2/LiTaO_3$	Love wave	Low loss wide band filters	Yamanouchi *et al.* [13] 1995
4.	$ZnO/LiTaO_3$	Love wave	Liquid sensors	Powell *et al.* [17] 2002
5.	ZnO/Quartz	Love wave	Low loss IF SAW filters	Kadota *et al.* [18] 2003
6.	ZnO/ 36° YX $LiTaO_3$	Shear wave	NO_2 sensor	Ippolito *et al.* [16] 2003
7.	ZnO nano-rod/ 64° YX $LiNbO_3$	Shear wave	CO sensor	Sadek *et al.* [14] 2006
8.	ZnO/Quartz	Love wave	Gas sensors with high K^2 and high temperature stability	Moreira *et al.* [11] 2008
9.	$SiO_2/LiNbO_3$	Rayleigh wave	High K^2 and high temperature stability	Nakai *et al.* [19] 2008

1.6 SAW devices on non-piezoelectric substrates

To realize SAW devices on non-piezoelectric substrates, films of piezoelectric materials like ZnO, AlN, and CdS are employed in conjunction with interdigital transducers. Substrates like silicon, diamond and sapphire are chosen based on the application and requirement. In 1973, Kino *et al.* [20], posted a method for the excitation of surface wave on non-piezoelectric substrates by depositing a thin piezoelectric film over the transducer as shown in Fig. 1.7(a). Electrical excitation to IDT causes acoustic stress in the piezoelectric film, which induces the stress in non-piezoelectric substrate resulting in launching of surface wave. An identical transducer is used for acoustic to electric conversion. In 1976, Hickernell [21] published a fabrication methodology

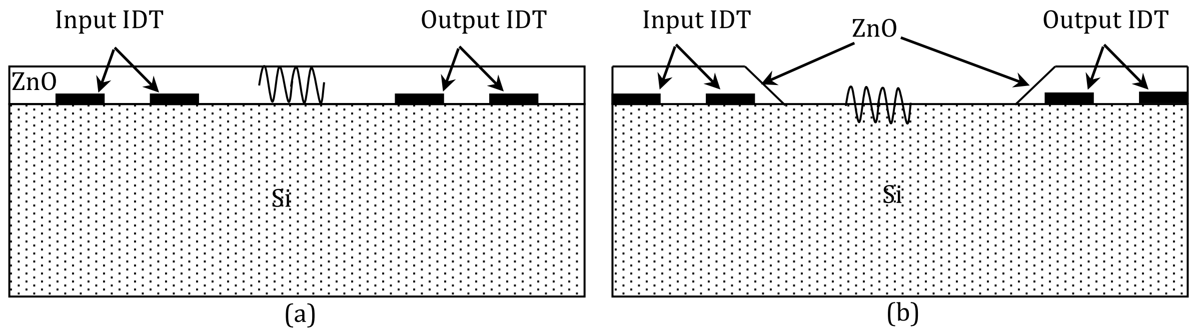

Fig. 1.7. Methods of generation and detection of SAW over non-piezoelectric substrates reported by (a) thin film SAW device on silicon substrate with ZnO thin film for the generation and propagation of surface waves, Kino *et al.* [20] and (b) SAW device on silicon substrate using ZnO thin film transducer for the excitation of SAW that propagates in silicon Hickernell *et al.* [21].

of ZnO thin film transducers to excite surface waves on non-piezoelectric substrates as shown in Fig. 1.7(b) and studied the effects of ZnO film properties and deposition conditions. The device performance substantially depends on the quality ZnO film as well as its surface roughness. ZnO quality is determined by the percentage of defects which can be reduced by precise control of substrate temperature, working pressure and percentage of oxygen. Because of high acoustic velocity in diamond and sapphire, ZnO or AlN thin film on diamond or sapphire results in SAW devices with high frequency of operation. Uehara *et al.* demonstrated a SAW filter with 5 GHz band and 0.1% coupling coefficient using AlN film over sapphire substrate [18]. Using diamond thin films, high frequency devices are implement over silicon substrate, where surface wave transduction is carried out with the help of ZnO thin films. The phase velocity, coupling coefficient, and temperature coefficient of frequency (TCF) characteristics of Rayleigh waves and other higher order modes generated in the ZnO/Diamond/Si structure, and also the change in surface wave characteristics with respect to the thickness of diamond layer has been reported by Nakahata *et al* [22]. Another high frequency SAW device using bi-layered structure of AlN/nano crystalline diamond (NCD) on silicon with operating frequency of 11.3 GHz has been reported by Ali *et al.* [23].

Integration of SAW filters (ZnO/SiO_2/Si structure) with transistor circuits made on the same Si substrate is first reported by Visser *et al.* [24] in 1989. He reported the monolithic integration of SAW device and its fabrication process flow and also demonstrated the SAW filter applications in wireless communication systems. In 1994 Vellekoop *et al.* [25], reported a liquid sensors using acoustic plate modes generated in IDT/ZnO/M/SiO_2/Si structure interfaced with transistor circuitry on a single silicon substrate and sensing is carried out by realizing an oscillator circuit with SAW device in the feedback path. Subsequent research on the integration of SAW devices with Si technology is reported by the group of Nordin, and Tigili [26-28]. In 2005 Tigli *et al.*, demonstrated the fabrication of delay lines on silicon integrated monolithically with CMOS circuit for chemical and bio-sensing applications. In 2007, Nordin *et at.* Reported the design of fabrication of $ZnO/SiO_2/Al/Si$ configured two port SAW resonators with CMOS circuits on silicon [29]. A consolidated list of reports on implementation of SAW devices on silicon substrate using piezoelectric thin films is given in Table 1.2. It presents various configurations of thin film SAW devices on non-piezoelectric substrates reported in last four decades.

Table 1.2 List of selected reports of SAW devices on non-piezoelectric substrates

SI. No	Layered structure	Type of surface wave	Application	Reference and year
1.	ZnO/Si, $LiNbO_3/Al_2O_3$, ZnO/Al_2O_3, ZnO/SiO_2	Rayleigh wave	Demonstration of excitation of surface waves on non-piezoelectric substrates	G. S. Kino *et al.*[20] 1973
2.	ZnO/Si	Rayleigh wave	Thin film transducers on non-piezoelectric substrates	Hickernell *et al.* [21] 1976
3.	$ZnO/SiO_2/Si$	Rayleigh wave	Amplification of Rayleigh waves	J. H. Visser *et al.* [24] 1989
4.	$ZnO/SiO_2/Si$	Rayleigh wave	SAW filters on silicon with electronic circuitry	J. H. Visser *et al.* [31] 1989
5.	ZnO/Si	Lamb wave	SAW monolithic micro sensors	Vellekoop *et al.* [25] 1994
6.	ZnO/Diamond/Si, $LiNbO_3$/Diamond/Si, SiO_2/ZnO/Diamond	Rayleigh wave	High frequency devices	Nakahata *et al.* [22] 1995
7.	AlN/ Al_2O_3	Rayleigh wave	5 GHz band SAW filter	Uehara *et al.* [32] 2004
8.	ZnO/Si	Rayleigh wave and love wave	SAW-CMOS chemical sensor	Tigli *et al.* [26] 2005
9.	$ZnO/SiO_2/Si$	Love wave	High frequency devices	Krishnamurthy *et al.* [33] 2006
10.	ZnO/SiO_2/Metal/Si	Rayleigh wave	CMOS–SAW resonators	Nordin *et al.* [26] 2007
11.	$LiNbO_3$/Si	Rayleigh wave and Love wave	High frequency devices	Pastureaud *et al.* [34] 2007
12.	AlN/ZnO/Diamond	Waveguiding layer acoustic wave	Package less SAW devices	Laurent *et al.* [35] 2010
13.	ZnO/Si, AlN/Si	Plate waves	High coupling coefficient devices	Anisimkin *et al.* [36] 2011
14.	ZnO/Si	Plate waves	UV sensors	Phan *et al.* [37] 2011
15.	AlN/NCD/Si	-	High frequency SAW devices	Ali B *et al.* [23] 2012

In 2005 Tigli *et al.* [26], published the fabrication and characterization of SAW resonators with CMOS circuits for cancer biomarker sensing. They realized the fabrication of SAW device with CMOS process, where initial metal layers and oxide layers are carried out and IDTs are patterned along with the final metal layer of CMOS process and ZnO is deposited all over the substrate, another lithography process is carried out to opening the contact pads for characterization.

1.7 Problem definition

SAW devices are normally fabricated on piezoelectric substrates and therefore are difficult to integrate with circuits made on silicon substrate. For example, SAW filters are widely used in intermediate frequency section of radio receivers, however the SAW devices have to be separately packaged and externally connected with the chip containing the most of the receiver circuitry. Therefore the researchers mostly in last decade have attempted monolithic fabrication of SAW devices on silicon substrate. SAW devices can be realized on non-piezoelectric substrates using piezoelectric films in conjunction with IDT for various applications. However, the reported SAW devices using piezoelectric films exhibit tradeoff between electromechanical coupling coefficient and phase velocity. The performance of thin film SAW devices significantly depends on the quality of the piezoelectric film usually deposited by RF sputtering, and it is difficult to maintain the quality of the film and reproduce the devices in mass production.

The aim of the research work reported in the thesis is to develop SAW devices feasible to fabricate monolithically on silicon substrate using CMOS processes and providing high phase velocity and high coupling coefficient while reducing the dependency on the quality of the piezoelectric film deposition. Consequently we thought of changing the principle of SAW transduction used in the reported devices. It can be achieved by periodically patterning the piezoelectric film, so that the patterned structure resonates and the bulk mode generated in the structure induces surface wave in silicon by mode conversion. Since the piezoelectric film is patterned, the surface wave is confined to propagate in silicon which has high acoustic velocity. In addition, the quality of piezoelectric film has little effect on the surface wave propagation as the wave is not travelling in the film. The resonance frequency of bulk mode in the patterned piezoelectric structure mainly depends on the thickness of the film which can be accurately controlled during the deposition process.

The second major objective of this research work is to realize the proposed structure in the edge reflection type SAW devices which offer substantially small device area, since the device area on a silicon chip is crucial and minimizing the area of the SAW device would be of high priority in monolithic integration.

1.8 Scope of the thesis

The thesis presents a research work on the development of SAW devices on silicon substrate using piezoelectric ZnO films and periodically patterned ZnO films, and their application for resonators and RF filters. The theoretical and practical study of the proposed SAW devices on non-piezoelectric substrates has not been reported in literature to the best of author's knowledge. The major contributions of the thesis are as follows.

- Study of mutual mode conversion of bulk waves and surface waves at periodically patterned ZnO structures on silicon substrate.
- Modeling and simulation of SAW resonator and delay line on silicon substrate using the proposed periodically patterned ZnO structure to obtain the phase velocity and electromechanical coupling coefficient dispersion characteristics.
- Modeling and simulation of conventional thin film SAW resonator and delay line on silicon substrate and comparison of their performance with the proposed devices.
- Process steps suggested for the fabrication of the proposed patterned-ZnO SAW devices on silicon using UV lithography for low frequency devices (up to 1 GHz) and using E-beam lithography for high frequency devices (beyond 1 GHz).
- Fabrication of large number of one port resonators, two port resonators and delay lines using the proposed patterned-ZnO structure on silicon.
- Testing of the fabricated devices and obtaining their S-parameter characteristics using network analyzer and RF probe station.
- Determination of phase velocity and electromechanical coupling coefficient of the fabricated devices using test results.
- Simulation of edge reflection type SAW devices on silicon substrate, with and without SiO_2 layer, using ZnO films and using periodically patterned-ZnO films.
- Process steps suggested for bulk fabrication of edge reflection type SAW devices on silicon using ZnO films and using periodically patterned-ZnO films.
- Fabrication of large number of edge reflection type SAW devices (one port resonators, two port resonators) on silicon substrate using ZnO films and using periodically patterned-ZnO films.

- Fabrication of edge reflection type SAW ladder filters on silicon substrate using ZnO films and using periodically patterned-ZnO films.
- Testing of the fabricated edge reflection type devices and obtaining their S-parameter characteristics using network analyzer and RF probe station.

1.9 Thesis organization

The thesis has been organized into 9 chapters and their contents are briefly outlined as follows.

In chapter 1, we give a brief introduction of elastic waves, methods of generation of elastic waves, classification of elastic waves, surface acoustic waves, generation of SAW by an IDT, SAW device configurations, thin film SAW devices, edge reflection type SAW devices on piezoelectric substrates, a brief literature over thin film SAW devices on silicon substrate, problem definition and the scope of the thesis.

In chapter 2, we present various modeling and simulation techniques of SAW device such as equivalent circuit method, coupling of modes (COM) model, impulse response method, and finite element (FE) simulations using COMSOL Multiphysics. We performed mesh optimization for the simulation of thin film SAW devices on silicon substrate and calculated the phase velocity. In latter part of the chapter presents the mechanical properties of piezoelectric ZnO, orientation of ZnO on COMSOL Multiphysiscs, simulation of conventional ZnO film based SAW devices on silicon substrate, study of phase velocity and electromechanical coupling coefficient dispersion characteristics of various ZnO/Si device configurations and simulation of ZnO/Si SAW delay line using COMSOL Multiphysics.

Chapter 3 presents the proposed periodically patterned-ZnO thin film SAW devices on silicon substrate. In this chapter we discuss the theory of generation of surface waves on silicon using periodically patterned-ZnO and its theory of operation. Initially 3D simulations with eigenmode and frequency dependent studies are carried out to study the displacement and admittance characteristics of surface modes generated in the structure. The simulation results of proposed SAW device are compared with the simulation results of conventional ZnO/Si thin film SAW devices on silicon. Further simulation study is carried out on the proposed patterned-ZnO/Si SAW resonator with the inclusion of buffer layer like SiO_2 and AlN, the phase velocity and coupling coefficient characteristics are obtained using eigenmode analysis. The fabrication design parameters of proposed patterned-ZnO/Si SAW devices are designed using equivalent circuit model.

Chapter 4 demonstrates the fabrication of patterned-ZnO/Si and patterned-ZnO/SiO_2/Si SAW devices using UV lithography and *e*-beam lithography processes. The fabrication process steps of development of IDT pattern on silicon substrate, ZnO thin film deposition parameters using RF sputtering, and various chemical recipes used in ZnO etching process are presented.

In chapter 5, we present the testing of fabricated SAW devices using network analyzer and RF probe station. The device characteristics are studied using S parameters and FE simulations are carried out with dimensions of the device observed by FESEM analysis to identify the surface modes generated in the structure. The experimental results and simulation results are compared and further study is carried out on the effect of practical deviations on the device operating frequency.

In Chapter 6, we present the simulation of edge reflection type SAW devices on silicon substrate, one of the major contribution of the thesis. The background theory of Love wave and its property of complete edge reflection at free edges and literature on conventional edge reflection type devices are presented. FE simulations of ER type SAW devices on silicon and the effect of buffer layers in proposed ER type SAW devices are presented. The dispersion characteristics of ER SAW devices with patterned-ZnO film and the effect of buffer layer are discussed. The design of ER type SAW devices on silicon using equivalent circuit model and the background theory of coupled resonators and ladder filters are detailed in this chapter.

Chapter 7 discusses the various fabrication process steps suitable for the fabrication of the proposed ER type SAW devices on silicon substrate with ZnO film and patterned-ZnO film via UV lithography process. The micromachining processes employed in the development of vertical grooves are reported.

In chapter 8, we present the details of the measured S parameters of ER type SAW devices, obtained using network analyzer and RF probe station. FE simulations are carried out to study the effect of practical deviations on operating frequency of the device.

Chapter 9 lists the conclusion of the research work and recommendation for the future work.

Chapter 2

Modeling and Simulation of Surface Acoustic Wave Devices

The background of SAW devices and implementation of thin film SAW devices on silicon substrate are discussed in the previous chapter. This chapter of the thesis discuss the basics of piezoelectricity, modeling of SAW devices, mechanical properties of ZnO, finite element (FE) simulations of thin film SAW devices, and the orientation of ZnO in COMSOL Multiphysics. The piezoelectric nature of ZnO is discussed in brief and the phase velocity and electromechanical coupling coefficient (K^2) dispersion characteristics of surface waves generated in the layered structure (ZnO/Si) are testified. Design of conventional thin film SAW devices on silicon using the equivalent circuit model and dispersion characteristics obtained from FE simulations and simulation of ZnO/Si SAW delay line devices are reported.

2.1 Theory of elasticity

A solid subjected to external forces gets deformed and returns to its original form when the forces are removed, the body is said to be elastic. Various types of forces like, mechanical, thermal, electrical and magnetic can be employed for the generation of elastic waves in an elastic medium, however it is more suitable to choose materials in which the stress varies linearly with applied electric field. Elasticity of a solid is concerned with the internal forces within the solid and its particle displacement from equilibrium position [38]. The forces are expressed as stress T, while the displacements are expressed in terms of strain S. The particle is an elementary region of a material much larger than the inter-atomic distance and much smaller than any characteristic elastic dimensions such as wavelength. Assume the equilibrium state of solid with a particle located at point $\mathbf{x} = (x_1, x_2, x_3)$ and is displaced by an amount $\mathbf{u} = (u_1, u_2, u_3)$ under the application of external force. Where, the components u_1, u_2 and u_3 are the general displacement components along coordinates x_1, x_2 and x_3, respectively. Thus the particle has been displaced to a new position $\mathbf{x}+\mathbf{u}$ as shown in Fig. 2.1. If $\mathbf{u}$ is independent of $\mathbf{x}$ there will be no internal force, since this simply shows a displacement of a material as a whole, and also

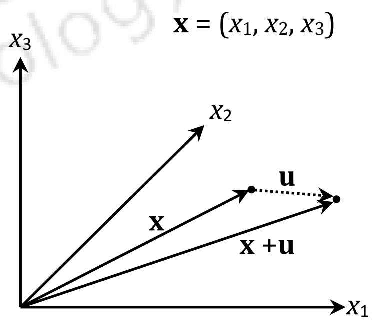

Fig. 2.1. Particle position in equilibrium and deformed states of solid body. Note: The deformation of the solid is shown in broken lines [38].

there will be no force if the material is rotated. The strain at each point can thus be defined as

$$S_{ij}(x_1, x_2, x_3) = \frac{1}{2}\left(\frac{\partial u_i}{\partial x_j} + \frac{\partial u_j}{\partial x_i}\right);\; i, j = 1,2,3. \tag{2.1}$$

Thus the strain is related to the internal forces. The strain is a second rank tensor and symmetrical as $S_{ij} = S_{ji}$. The stress T is defined as internal stress in the material *i.e.* force per unit area. The second-rank stress tensor is defined as T_{ij} (x_1, x_2, x_3) and is symmetric, $T_{ij} = T_{ji}$. According to Hooke's law, each components of stress is given by the linear combination of the strain components and is expressed as

$$T_{ij(mech)} = \sum_k \sum_l c_{ijkl} S_{kl}, \qquad i, j, k, l = 1, 2, 3. \tag{2.2}$$

where, C_{ijkl} is the fourth-rank stiffness tensor. These elements are the physical properties of the materials under consideration [3].

2.1.1 Piezoelectricity and constitutive equations

Piezoelectricity is a phenomenon which couples the elastic stress and strain to the electric field and displacement that occurs only in anisotropic materials, whose internal lattice structure lacks a center of symmetry [38]. The stress, $T_{ij\,(elec)}$ produced by the piezoelectric effect is given by

$$T_{ij(elec)} = \sum_k e_{kij} E_k, \qquad i, j, k, l = 1, 2, 3. \tag{2.3}$$

where, electric field $E_k = -\partial V/\partial x_k$, Total stress T_{ij} is the sum of stresses due to the electric field E_k and mechanical strain and can be expressed as [3], [38-40]

$$T_{ij} = \sum_k \sum_l c^E_{ijkl} S_{kl} - \sum_k e_{kij} E_k = \sum_k \sum_l c^E_{ijkl} S_{kl} + \sum_k e_{kij} \frac{\partial V}{\partial x_k} \tag{2.4}$$

When an electric field is applied to the dielectric medium, the electric displacement can be expressed by electric field and permittivity tensor ε_{ij} of the dielectric medium. In case of piezoelectric material, the additional electric field displacement caused by the strain is developed due to piezoelectric effect. The total electric displacement D_i can then be given as

$$D_i = \sum_j \varepsilon^s_{ij} E_j + \sum_j \sum_k e_{ijk} S_{jk} \tag{2.5}$$

where, C^E_{ijkl} is the stiffness tensor for constant electric field (N/m²), S_{jk} is the strain components, e_{ijk} is the piezoelectric tensor relating elastic to electric fields (C/m²), ε^S_{ij} is the permittivity tensor for constant stress (F/m), and E_j is the electric field vector (V/m) [38].

2.1.2 Equation of motion

If the stress and strain are functions of time and position then the above equations can be expressed in the terms of equation of motion using Newton's laws [38]. Theoretically, the electric field distribution can be found by solving the equations of Newton and Maxwell simultaneously. For an elementary cube centered at **X'** = (x'_1, x'_2, x'_3) with edge length of δ, density ρ, and the mass $\rho\delta^3$, the total force in terms of stress along x_i direction is given by

$$\delta^3\left[\sum_j \frac{\partial T_{ij}}{\partial x_j}\right]_{\mathrm{X}'} \tag{2.6}$$

$$\rho\frac{\partial^2 u_i}{\partial t^2} = \sum_j \frac{\partial T_{ij}}{\partial x_j}, \qquad i, j = 1,2,3. \tag{2.7}$$

In case of piezoelectric medium elastic waves travel much slowly than the electromagnetic waves. Hence the magnetic field due to these waves is negligible and electric field can be expressed using quasi static approximation. Thus Maxwell equation can be approximated as

$$\mathrm{curl}\,E = -\frac{\partial \mathbf{B}}{\partial t} = 0, \quad \mathbf{E} = -\mathrm{grad}\,V \tag{2.8}$$

where, **B** is the magnetic field, **E** is the electric field derived from the scalar electric potential V [3].

$$E_i = -\frac{\partial V}{\partial x_i} \tag{2.9}$$

From equations (2.1), (2.9) and (2.4) the equation of motion for piezoelectric material can be expressed as [3]

$$\rho\frac{\partial^2 u_i}{\partial t^2} = \sum_j\sum_k\left\{e_{kij}\frac{\partial^2 V}{\partial x_j \partial x_k} + \sum_l c^E_{ijkl}\frac{\partial^2 u_k}{\partial x_j \partial x_l}\right\} \tag{2.10}$$

In addition, the material is taken to be an insulator there are no free charges. Thus div D = 0. From equation (2.5)

$$\sum_i \sum_j \left\{ \varepsilon_{ij}^S \frac{\partial^2 V}{\partial x_i \partial x_j} - \sum_k e_{ijk} \frac{\partial^2 u_j}{\partial x_i \partial x_k} \right\} = 0 \tag{2.11}$$

The degrees of freedom (dependent variables) are the global displacements u_1, u_2, and u_3 in the global x_1, x_2, and x_3 directions, respectively, and the electric potential V can be obtained by solving the equations (2.10) and (2.11) using appropriate boundary conditions [38].

2.1.3 Solution of surface wave in piezoelectric media

The detailed procedure for finding the solution of surface waves in isotropic and anisotropic materials is explained in [38]. In this section, boundary conditions and solutions of surface waves are briefly elaborated. The boundary conditions at the surface should be satisfied in order to determine the phase, velocity and amplitude of the waves. The appropriate boundary conditions should be applied in order to determine the phase velocity and amplitude of the wave [38]. In general, two cases are considered; the first case is called as free surface case where the space above the surface of piezoelectric material is a vacuum and no conductor is present, so that there are no free charges. The second case is called as metalized case where the surface of piezoelectric material is covered with thin metal layer with infinite conductivity and short the horizontal components of the electric field **E**. These two cases give different surface wave velocity and measure the coupling between wave and electrical perturbation at the surface. For free surface case, if the wave number of the surface wave is β then the potential in vacuum $(x_3 \geq 0)$ using Laplace's equation can be expressed as

$$V = V_0 e^{(-|\beta| x_3)} e^{j(\omega t - \beta x_1)} \tag{2.12}$$

where, V_0 is a constant. For metalized surface case the potential at x_3 = 0 is zero. The mechanical boundary conditions at the surface of the substrate is stress-free condition as expressed in equation below

$$T_{13} = T_{23} = T_{33} = 0 \text{ at } x_3 = 0 \tag{2.13}$$

The electrical boundary is imposed by Maxwell's equation, the normal component of **D** being continuous across the air/substrate interface (at x_3 = 0). To find the surface wave solutions, we first consider the partial waves in which the displacements and potential, denoted by **u'** and V', take the form

$$\mathbf{u}' = \mathbf{u}'_0 \exp(j\tau x_3)\exp[j(\omega t - K_0 x_1)], \quad (2.14)$$

$$V' = V'_0 \exp(j\tau x_3)\exp[j(\omega t - K_0 x_1)] \quad (2.15)$$

where K_0 is the wavenumber of the surface wave, assumed to be real. These expressions are substituted to equation (2.10) and (2.11). Then these equations are solved for τ numerically, giving eight solutions for the same. Accordingly for every solution of τ, relative solutions of $\mathbf{u}'$ and V' are obtained. There are four values of τ in general denoted by τ_1 , τ_2 τ_3 ,and τ_4 . The partial waves are therefore,

$$\mathbf{u}'_i = \mathbf{u}'_{0i} \exp(j\tau_i x_3)\exp[j(\omega t - K_0 x_1)], \quad (2.16)$$

$$V'_i = V'_{0i} \exp(j\tau_i x_3)\exp[j(\omega t - K_0 x_1)], \; i = 1,2,3,4 \quad (2.17)$$

In the half-space it is assumed that the solutions is a linear sum of these partial waves, so that

$$\mathbf{u} = \sum_{i=1}^{4} A_i \mathbf{u}'_i \quad (2.18)$$

$$V = \sum_{i=1}^{4} A_i V'_i \quad (2.19)$$

The coefficients A_i are to be such that the solution satisfies the electrical and mechanical boundary conditions. These conditions give a determinant which must be zero for a valid solution for a right choice of K_0. The velocity than can be determined by ω/K_0 and displacement and potential are given by equation (2.18) and (2.19).

2.1.4 Acoustic waves in isotropic media

In an isotropic material the stiffness tensor c_{ijkl} is given by [3]

$$c_{ijkl} = \lambda\delta_{ij}\delta_{kl} + \mu(\delta_{ik}\delta_{jl}+\delta_{il}\delta_{jk}) \quad (2.20)$$

Where, the Kronecker delta is defined by δ_{ij} = 1 for $i=j$ and δ_{ij} = 0 for $i\neq j$. The constants λ and μ are known as Lamé constants and in practice these are always positive. μ is also called rigidity. Substituting c_{ijkl} into (2.2) and the stress is written in form of

$$T_{ij} = \lambda\delta_{ij}\Delta + 2\mu S_{ij} \tag{2.21}$$

$$\Delta = \sum_i S_{ii} = \sum_i \frac{\partial u_i}{\partial x_i} \tag{2.22}$$

The equation of motion (2.7) rewritten as

$$\rho\frac{\partial^2 u_j}{\partial t^2} = (\lambda+\mu)\frac{\partial\Delta}{\partial x_j} + \mu\nabla^2 u_j \tag{2.23}$$

Where $\nabla^2 = \sum_i \frac{\partial^2}{\partial x_i^2}$

Considering an infinite isotropic medium supporting plane waves, with frequency ω and the displacement **u** can be given by

$$\mathbf{u} = \mathbf{u}_0 \exp\,[j(\omega t - \mathbf{k.x}\,)] \tag{2.24}$$

The wave vector **k** = (k_1, k_2, k_3), gives the direction of propagation. Wave fronts are solutions of **k.x** = constant, and they are perpendicular to **k**. The phase velocity of the wave is $V=\omega/|\mathbf{k}|$. From eq (2.24), $\partial u/\partial x_j = -jk_j\mathbf{u}$, and substituting into eq (2.23) and we obtain

$$\omega^2\rho u_j = (\lambda+\mu)\ (\mathbf{k.u})\ kj+\mu|\mathbf{k}|^2 u_j,\ j = 1,2,3, \tag{2.25}$$

where $|\mathbf{k}|^2 = k_1^2 + k_2^2 + k_3^2$, substituting for u_j in eq (2.25), and results in vector form, gives

$$\omega^2\rho\mathbf{u}_0 = (\lambda+\mu)\ (\mathbf{k.u}_0)\ \mathbf{k}+\mu|\mathbf{k}|^2\ \mathbf{u}_0 \tag{2.26}$$

Here, there are two terms parallel to $\mathbf{u}_0$ and the other term is parallel to **k**, with the latter including the scalar product $\mathbf{k.u}_0$.Therefore two cases are to be considered, firstly if $\mathbf{u}_0$ is perpendicular to **k** and the scalar product is zero, and the remaining terms in the equation are parallel. Secondly, if $\mathbf{u}_0$ is not perpendicular to **k** the scalar product is non-zero. Hence, for non-trivial solutions we must have $\mathbf{u}_0$ parallel to **k**. These two cases give shear wave and longitudinal wave solutions respectively.

Considering shear wave case, $\mathbf{u}_0$ is perpendicular to $\mathbf{k}$ gives shear waves and wave vector denoted by **kt** given by $|\mathbf{k}_t|^2 = \omega^2\rho/\mu$ and the phase velocity of shear waves is denoted by V_t, equal to $\omega/|\mathbf{k}_t|$, and then transvers wave

$$V_t = \sqrt{\mu/\rho} \tag{2.27}$$

For longitudinal wave, $\mathbf{u}_0$ is parallel to $\mathbf{k}$ then $\mathbf{k} = \pm\mathbf{u}_0\ (|\mathbf{k}|/|\mathbf{u}_0|)$, using this relation we find $(\mathbf{k}.\mathbf{u}_0)\mathbf{k} = \mathbf{u}_0|\mathbf{k}|^2$, and substituting in eq (2.26) gives $|\mathbf{k}_l|^2 = \omega^2\rho/(\lambda+2\mu)$, and then longitudinal phase velocity is given by

$$V_l = \sqrt{(\lambda + 2\mu)/\rho} \tag{2.28}$$

2.2 Modeling of SAW devices

In order to fabricate SAW devices, the device performance and its dimensions are to be estimated for the optimum performance of SAW device. SAW devices can be modeled by theoretical models or computer aided based simulations. Several theoretical methods are developed by various researchers to study the performance of SAW transducers and estimate various device characteristics such as admittance, bandwidth, coupling coefficient, and impedance parameters. Theoretical models such as the equivalent circuit model, coupling of mode (COM) method, delta function model, impulse response method, and piezoelectric permittivity method are reported for the estimation of SAW device performance and IDT designing [3], [38], [39], and [40].

2.2.1 Coupling of mode (COM) model

COM model is widely used in designing of SAW devices, this method is based on local analysis of way of two coupled waves evolve when propagating in both directions opposite to each other. This section gives brief description about COM model. The COM model comprises of differential equations governing SAW mode amplitudes $R(x, \omega)$, $S(x, \omega)$ in either side of IDT and the current due to the flow of charges $I(x, \omega)$(see Fig. 2.2).

$$\begin{aligned}
\frac{dR(x)}{dx} &= -jk_E R(x) + j\kappa_R e^{-j2k_0x} S(x) + j\alpha_R V e^{-jk_0x} \\
\frac{dS(x)}{dx} &= -jk_E S(x) + j\kappa_s e^{+j2k_0x} R(x) - j\alpha_S V e^{+jk_0x} \\
\frac{dI(x)}{dx} &= +j2\alpha_S R(x) e^{+j2k_0x} + j2\alpha_R S(x) e^{-jk_0x} - j\left(\frac{3\omega C_F/\lambda}{3 + j\omega R_F C_F}\right)_S V
\end{aligned} \tag{2.29}$$

where, V is the voltage across the IDT electrodes, $k_0 = 2\pi/\lambda$ is transducer synchronous wave number, and

$$\begin{aligned}
\kappa_E &= +\frac{\omega}{v} - \left(\frac{2\alpha_R^2 \omega R_f^2 C_f^2 \lambda}{9+(\omega R_f C_f)^2} \right) - j\left[\gamma + \left(\frac{6\alpha^2 R_f \lambda}{9+(\omega R_f C_f)^2} \right) \right] \\
\alpha_R &= \frac{3\alpha e^{+j\phi_T}}{3+j\omega C_f R_f} \\
\alpha_S &= \frac{3\alpha e^{-j\phi_T}}{3+j\omega C_f R_f} \\
\kappa_R &= +\kappa_i e^{+j\phi_B} + \frac{2j\alpha^2 R_f \lambda e^{-2j\phi_T}}{3+j\omega C_f R_f} \\
\kappa_S &= +\kappa_i e^{-j\phi_B} + \frac{2j\alpha^2 R_f \lambda e^{+2j\phi_T}}{3+j\omega C_f R_f}
\end{aligned} \tag{2.30}$$

In the above equations $\phi_T = \pi$ and $\phi_B = \pi/2$ are phase offsets of the grating and the potential respectively, and $\omega = 2\pi f$ is the angular frequency. The COM parameters are as follows, v phase velocity of SAW, α transduction coefficient, R_f thin film resistance in one transduction unit, C_f interdigital capacitance in one transduction period, κ the reflection parameter, γ propagation loss per unit length. The suffix R and S represent the values for the corresponding direction of wave propagation shown in Fig. 2.2. These parameters can be computed through computer simulation such as FEM or using experimental analysis of a test structure. The COM equations can be represented in P matrix form. The acoustic ports are treated as scattering port and electric port as admittance port and

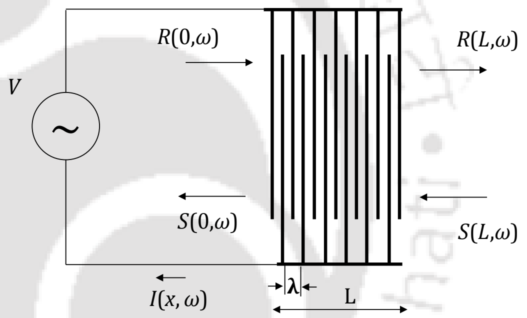

Fig. 2.2. Coordinates of an IDT [3].

$$\begin{bmatrix} S(0) \\ R(L) \\ I \end{bmatrix} = \begin{bmatrix} P_{11} & P_{12} & P_{13} \\ P_{21} & P_{22} & P_{23} \\ P_{31} & P_{32} & P_{33} \end{bmatrix} \begin{bmatrix} R(0) \\ S(L) \\ V \end{bmatrix} \tag{2.31}$$

where,

$$P_{11} = \frac{+jK_S \sin(DL)}{D\cos(DL) + j\Delta \sin(DL)}$$

$$P_{12} = \frac{D}{D\cos(DL) + j\Delta \sin(DL)} e^{-jK_0 L}$$

$$P_{13} = P_{31} + jL\frac{\sin(DL/2)}{DL/2} \times \frac{\alpha_S D\cos(DL/2) + j(K_S\alpha_R + \Delta\alpha_S)\sin(DL/2)}{D\cos(DL) + j\Delta \sin(DL)}$$

$$P_{22} = \frac{+jK_R \sin(DL)}{D\cos(DL) + j\Delta \sin(DL)} e^{-j2K_0 L}$$

$$P_{23} = P_{32} + jL\frac{\sin(DL/2)}{DL/2} \times \frac{\alpha_R D\cos(DL/2) + j(K_R\alpha_S + \Delta\alpha_R)\sin(DL/2)}{D\cos(DL) + j\Delta \sin(DL)}$$

$$P_{33} = +j2\left(\frac{K_S\alpha_R^2 + K_R\alpha_S^2 + 2\Delta\alpha_R\alpha_S}{D^3}\right) \times DL - \frac{D\sin(DL) + j\Delta(1-\cos(DL))}{D\cos(DL) + j\Delta \sin(DL)}$$

$$-2\left(\frac{K_S\alpha_R^2 + K_R\alpha_S^2 + 2\Delta\alpha_R\alpha_S}{D^3}\right) \times \left(\frac{1-\cos(DL)}{D\cos(DL) + j\Delta \sin(DL)}\right) \times j\left(\frac{3\omega C_f L/\lambda}{3 + j\omega R_f C_f}\right)$$

$$\Delta = K_E - K_0$$

$$D = \sqrt{\Delta^2 - K_R K_S}$$

P_{11} and P_{22} are the reflection coefficients, and P_{12} and P_{21} are the transmission coefficients. The remaining terms P_{13} and P_{23} correspond to the excitation coefficients of the IDT and the term P_{33} clearly represents the admittance of the structure relating the current flowing in the electrode (*i*) and the drive voltage (*V*). P_{31} and P_{32} terms represent the current generated by the waves arriving at the acoustic ports. Admittance or P_{33} can be calculated from simulations and it is the most useful parameter in the device design.

2.2.2 Discrete source or delta function method

The discrete source method or delta function method is one of the earliest and simplest methods which explain the shape of the IDT frequency response [39]. It does not consider energy, capacitance, and electromechanical coupling coefficient of the material used in the device. The discrete source model is derived from the examination of spatial distribution of charge density or electric field at the surface of piezoelectric substrate. This method associates either two charge spikes of the same sign to each IDT finger or two electric field spikes of the same sign to each interval between adjacent IDT fingers [39]. The amplitude of each delta function is proportional to the corresponding aperture W of the IDT and sign depends on the polarity of the charge density or electric field.

2.2.3 Equivalent circuit model

The mason equivalent circuit model for surface wave transducers is well explained by smith *et al*. [38]. An IDT with N number of pairs can be modeled using a periodic section of IDT can be represented by an equivalent electromechanical circuit. The equivalent circuit model of one period of IDT is shown in Fig. 2.3. It consists of three ports, viz. two acoustic ports and one electric port. The electrical equivalent of the two acoustic ports is represented as SAW transmission line and third port is represented as electric port where the electric potential is applied and sensed. In this model, θ is expressed as $2\pi f/f_0$, where f is the frequency of the applied input potential and f_0 is the resonance frequency and is the periodic section transit angle. R_0 is the electrical equivalent to Z_0 or mechanical impedance given by

$$R_0 = \frac{Z_0}{\phi^2} \tag{2.32}$$

where, $\phi = \varsigma C_s/2$ is the turns ratio of an acoustic-to-electric circuit transformer, C_s is the static electrode capacitance of one periodic section, and ς is a piezoelectric constant.

In this model, the acoustic forces are converted into electric potentials as $E_n = F_n/\theta$ and SAW velocities are converted into equivalent electric currents $I_n = v_n'\,\theta$. These transformations allow the mechanical characteristic admittance (similar to the transmission line characteristic impedance expressed in ohms) to be expressed as an equivalent transmission line characteristic admittance as,

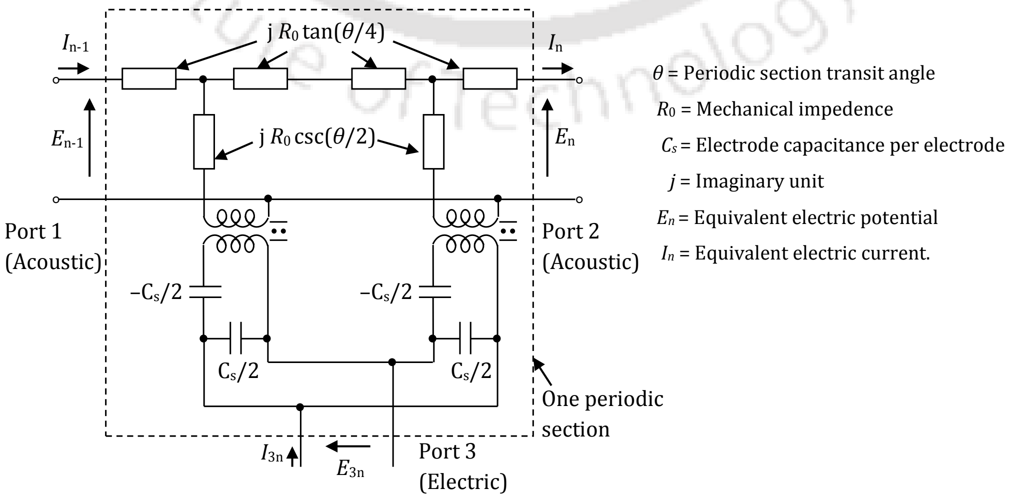

Fig. 2.3. Mason equivalent circuit of one period of IDT analyzed by Smith *et al.* [6]

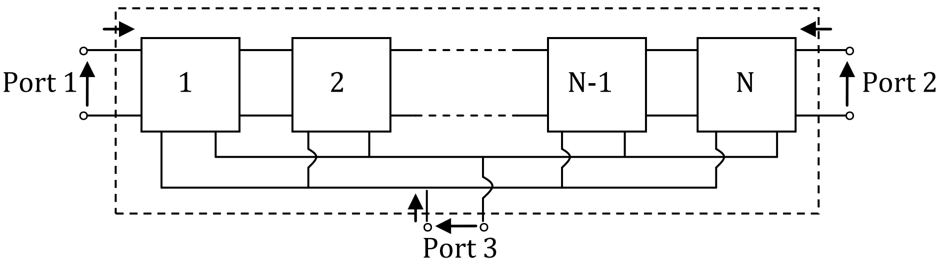

Fig. 2.4. Equivalent circuit for entire IDT, made up with N pairs of IDT finger with acoustic ports in cascade and electrical ports in parallel.

$$G_0 = 1/R_0 = (\omega C_s K^2)/2\pi \tag{2.33}$$

where, K^2 represents electromechanical coupling coefficient and its values can be approximated by $-2\Delta v/v$, where, Δv is the change in SAW velocity when the piezoelectric surface is electrically shorted by a thin metal film [41]. The entire IDT can be realized by connecting acoustic ports in series and electrical ports in parallel as shown in Fig. 2.4.

If the generator IDT and receiver IDT of the SAW device are completely matched, the Y parameters of the 3-port network using the equivalent circuit of a period of an IDT can be expressed as

$$\begin{bmatrix} I_1 \\ I_2 \\ I_3 \end{bmatrix} = \begin{bmatrix} -jG_0 \cot N\theta & jG_0 \csc N\theta & -jG_0 \tan(\theta/4) \\ jG_0 \csc N\theta & -jG_0 \cot N\theta & jG_0 \tan(\theta/4) \\ -jG_0 \tan(\theta/4) & jG_0 \tan(\theta/4) & j\omega C_T + 4jNG_0 \tan(\theta/4) \end{bmatrix} \begin{bmatrix} E_1 \\ E_2 \\ E_3 \end{bmatrix}$$

where, $C_T = NC_s$ (total capacitance of IDT) [24].

The overall equivalent circuit of an IDT is shown in Fig. 2.5 [38], [39]. The input admittance can be expressed as

$$Y(f) = G_a(f) + B_a(f) + j\omega C_T \tag{2.34}$$

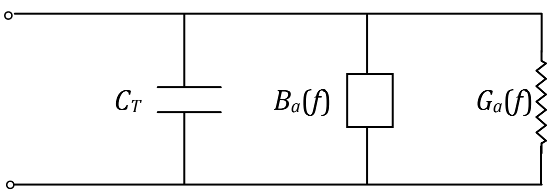

Fig. 2.5. Overall equivalent circuit of an IDT.

where, $G_a(f)$ is the radiation conductance and $B_a(f)$ is the susceptance given as

$$G_a(f) \approx 8N^2 G_0 \left|\frac{Sin\,X}{X}\right|^2 \tag{2.35}$$

$$B_a(f) \approx 8N^2 G_0 \left|\frac{Sin\,(2X) - 2X}{2X^2}\right|^2 \tag{2.36}$$

where, $X = N\pi(f - f_0)/f_0$. The radiation susceptance is a reactive parameter that goes to zero at the resonance frequency. Conductance at resonant frequency f_0 is given by

$$G_a(f_0) \approx 8NK^2 C_t f_0 \tag{2.37}$$

Where N is number of transducer pairs in the IDT structure and f_0 is the operating frequency. In the above described models for designing the IDT of a SAW device, the second order effects such as electrode resistance, electrode discontinuities, and propagation losses are neglected.

2.2.4 Device design parameters

In design of SAW devices, certain parameters are very crucial in the performance of device and also the design IDT to match with source impedance (50 Ω). As defined in the above equivalent circuit model, the electromechanical coupling coefficient (K^2) which depends on the material for transduction of SAW, frequency of operation is determined by the wavelength of IDT structure and acoustic velocity of the substrate, using these two parameters the admittance of IDT is designed for 50 Ω at operating frequency.

2.3 Finite element method (FEM)

The finite element method (FEM) is a numerical technique for solving differential equations or integral equations used in almost every discipline of engineering particularly in the areas of stress/strain analysis of solid structures, heat conduction analysis and fluid dynamics. The propagation of SAW governed by differential equations given in equations (2.10) and (2.11) must be solved along with complexities in geometry of device, materials used in the device, and proper boundary conditions. This section gives some basic procedures and techniques used in finite element method formulations. The detailed descriptions can be found in [42] and [43].

2.3.1. Input and output information in FEM

In FEM, the following input information about the structure that to be analyzed is given.

1. The geometry of the structure to be solved.
2. Coordinate systems according to the geometry in 3D or 2D.
3. Properties of the materials used in the model.

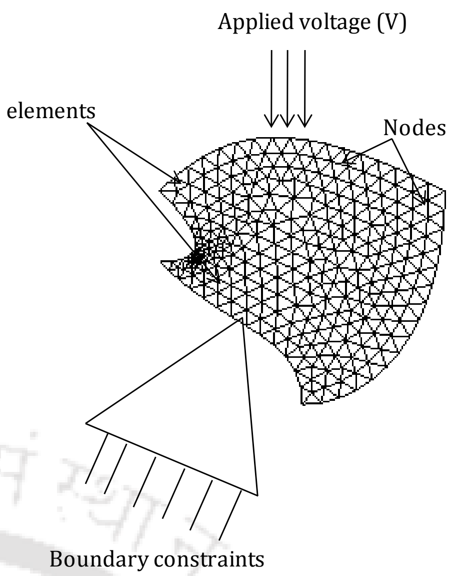

Fig. 2.6. Illustration showing a solid body discretized into finite number of elements.

For example, in SAW devices material properties of the piezoelectric substrate such as elasticity matrix, piezoelectric constant, permittivity constant, and density are to be furnished and for IDT electrodes an isotropic material properties such as Young's modulus, density, Poisson ratio, etc. are to be provided. Boundary conditions at the boundaries of the structure are to be provided. For example in case of stress/strain analysis for piezoelectric material, the boundary conditions can be displacement constraints and electric boundary conditions such as electric potential, electric displacement, charge etc.

Further the geometry domains are to be divided into smaller domains called elements which are connected at specific points called nodes as shown in Fig. 2.6. The elements created in the geometry can be in the shape of triangular, quadrilateral, tetrahedral, or brick depending on the dimensionality. The output information in case of stress/strain analysis in piezoelectric material involves nodal and elemental information, the solution to the primary unknown quantities, the displacements in all directions, and voltage are determined at nodes. These unknowns are called as degrees of freedom (DOF).

In this thesis, the simulations and analysis of SAW devices are carried out by FEM using piezoelectric module of COMSOL Multiphysics software. The software has well developed solvers, graphical user interface (GUI) and post-processing capabilities. More details of the software can be found in the user guide of the software [43].

2.3.2 Finite element simulation of SAW devices

Simulations of conventional SAW devices using FEM have been reported by many researchers. Some of them are given below. Lerch *et al.* [44] presented an FEM scheme to calculate Eigen modes, and dynamic response to mechanical and electrical excitations of 2D and 3D piezoelectric transducer for any geometry. Rahman *et al.* [45] performed FEM simulation to study SAW based quantum devices. Atashbar *et al.* [46] simulated the mass loading effect of palladium sensing film in the presence of hydrogen gas. Wu *et al.* [47] used Taguchi method on FEM results and established robust design processes for SAW sensors based on the mass loading principle. Ippolito *et al*. [48] performed the FEM based analysis of acoustic waves propagating on layered SAW devices. In most of the earlier works, the number of DOF to solve is large due to the large size of the SAW structures considered in the model. In order to solve DOF for an entire SAW device, it requires high computing facility and large computation time. Thus a valid approximation and simplified model are required to perform FE simulation of SAW devices. In this chapter, the conventional SAW devices such as one port SAW resonators and SAW delay line devices are simulated to verify the mass loading effects, electrical loading effects, bulk acoustic wave (BAW) generation, and other secondary effects due to the presence of metallic IDT on the piezo-substrate using COMSOL Multiphysics.

2.4 ZnO thin film based SAW devices on silicon

To design SAW devices on silicon, it is very essential to study the elastic properties and surface modes generated by the piezoelectric thin films. Piezoelectric films like ZnO, AlN and CdS are commonly used materials to improve the performance of conventional piezoelectric substrate SAW devices and also in the implementation of SAW devices on silicon substrate, as discussed in chapter 1. In this thesis we consider ZnO as the piezoelectric material for the transduction of surface on silicon substrate, due to its high coupling coefficient in comparison with other materials like AlN, $LiNbO_3$ and CdS. ZnO is a unique material that exhibit both semiconductor and piezoelectric properties based on its crystal orientation. Piezoelectric ZnO films are have been used for many years for the bulk wave generation [3]. ZnO/Glass IF SAW filters with frequencies around 40 MHz, are widely used in television sets. Piezoelectric ZnO films on semiconducting substrate like silicon and gallium arsenide provides the possibility of integration of SAW devices with electronic circuits. The crystal structure and piezoelectric orientations of ZnO are as follows.

2.4.1 Mechanical properties of ZnO

ZnO is anisotropic material exhibits both semiconductor and piezoelectric properties based on the orientation of the deposited film [49]. The wurtzite structure of ZnO crystal is shown in Fig. 2.7, where three unit cells form a hexagonal structure with six fold symmetry and the orientations of ZnO that exhibits piezoelectric properties are mentioned. In general the mechanical properties of a material involves various concepts like stiffness, piezoelectric

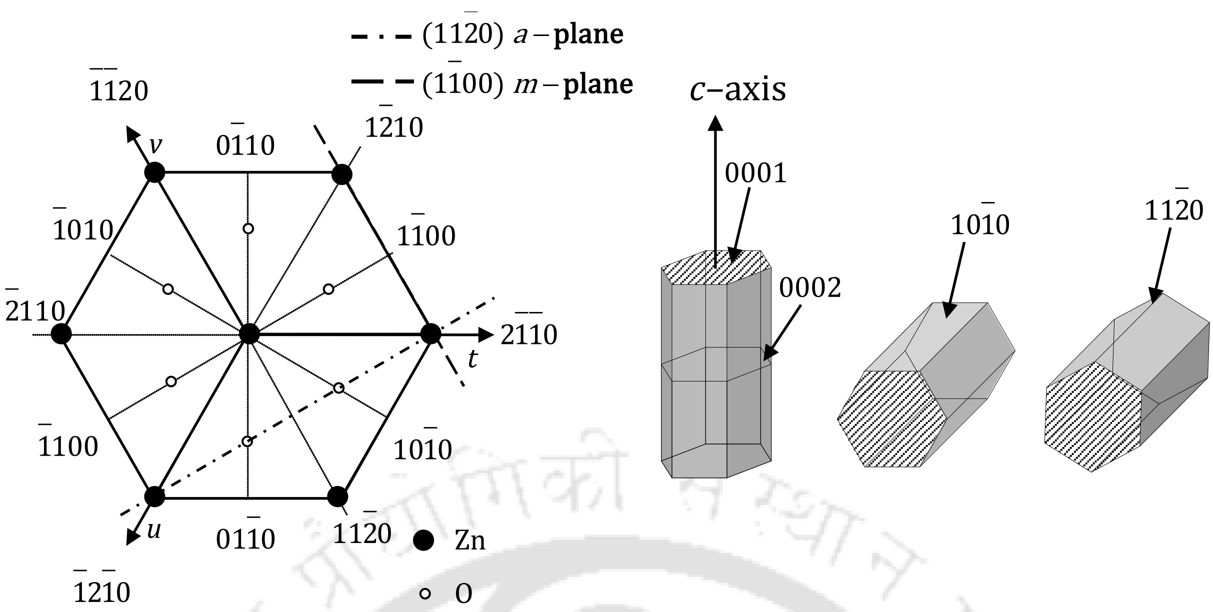

constants, Young's and bulk modulus. Since stiffness tensor is symmetric consisting of 21 independent elastic constants forming 6x6 matrix, due to the symmetric of hexagonal crystal nature of ZnO, there remain only 5 independent elastic constants: C_{11}, C_{12}, C_{13}, C_{33}, and C_{44}. Elastic constants C_{11} and C_{33} corresponds to longitudinal modes along directions, whereas C_{44} and C_{66} relates to transverse modes propagating in [1000] and [0001] directions. The material constants of ZnO are given in Appendix A. The orientation of sputtered ZnO film is determined by using X-ray diffraction and the grain size of the film is determined by AFM (Atomic force microscope). Both Rayleigh and Love waves can be excited along the ZnO film, based on the orientation and arrangement of the IDT structure [33], [49-51]. In general (002) and (100) oriented ZnO thin films are used for SAW devices and in the orientation representation [*tuvw*] *v* is neglected. Here we consider (002) oriented ZnO films on silicon for design of SAW devices which are modeled using finite element simulations and equivalent circuit method.

2.4.2 3D FE simulations of IDT/ZnO/Si configured one-port SAW resonator

FE simulations of similar thin film SAW devices on silicon have been reported by the following researchers. Tigili *et al.* [27] presented the FE simulations of SAW delay line on silicon and time dependent analysis to study the characteristics of surface waves generated in the structure. Laurent *et al.* [35] and Gao *et al.* [52] presented the wave guiding characteristics of surface waves in bi-layered and multilayered structures. R. Ro *et al.* [53] performed FE simulations on diamond based SAW device to obtain the SAW reflection characteristics. S. wu *et al.* [54] reported the phase velocity and coupling coefficient characteristics of surface modes generated in ZnO/Si layered configuration. In order to solve complete device it requires high computation facility and consumes time, so valid approximation and simplified model is considered to perform FE simulations of thin film SAW devices using COMSOL Multiphysics.

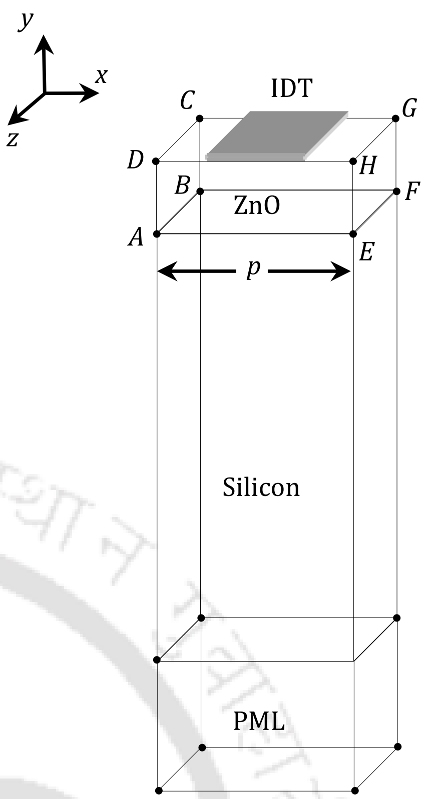

3D geometry with *piezoelectric devices* physics module is used for the simulations. Since, ZnO is anisotropic material the elastic constants vary according to orientation of film. The elastic constants of (002) oriented ZnO are obtained from the literature [22], [35], still the orientation has to be in coordinate with COMSOL axis to obtained accurate phase velocity and coupling coefficient results. To obtain proper alignment of ZnO, we carried out 3D FE simulations of one port SAW resonator with IDT/ZnO/Si configuration with different COMSOL axis orientations. Similar to the conventional SAW resonators, thin films devices are modeled using periodic boundary conditions [27], [35]. The model employed in 3D simulations with boundary conditions is depicted in Fig. 2.8. As IDT exhibit periodic nature, one period of IDT is considered for all the four layered configurations and eigenmode analysis is performed for various thicknesses of ZnO. The structure composed of (002) oriented ZnO layer and (001) silicon substrate of 10λ thickness and a perfectly matched layer (PML) below the silicon to absorb unwanted acoustic reflections from bottom surface. Material constants of (002) ZnO, Al and Si are summarized in Appendix A and electrical conductivity 2×10^{-3} S/m is considered in simulations.

The short circuit boundary conditions are applied to the electrodes for the calculation of reflection coefficient of a pair of shorted reflection gratings. The phase velocity (v), reflection coefficient (k), and electromechanical coupling coefficient (K^2) are calculated using the following expressions [53], [55] and [56].

$$v = f.\lambda \tag{2.38}$$

$$K^2 = 2 * (v_f - v_m)/v_f \tag{2.39}$$

$$k = \pi \left(\frac{f_a - f_r}{f_a + f_r} \right) \tag{2.40}$$

Where, f is the operating frequency, ν_f and ν_m are the free surface and metalized surface velocities. To calculate metalized surface velocity, a thin metal film is included at the IDT position and the thickness of metal film is preferable small, so that mass loading effect due to the film is negligible. f_a and f_r are the anti-resonance and resonance frequencies, respectively and are obtained from the parametric sweep of eigenmode analysis, where the parameter is the ZnO film thickness. The phase velocity and coupling coefficient obtained from FE simulations are tabulated in Table 2.1 and the values are in good agreement with the values reported by G. S. Kino *et at.*[20] and Sean wu *et al.* [54].

The simulation concludes that the *c*–axis of ZnO coincides with *z*-axis of COMSOL. In general the shear coupling along *c*–axis of ZnO is zero [49], and also observed form the YZ oriented ZnO simulation. From the reported and obtained values, YZ orientation generates Rayleigh wave and Love wave is generated in ZX orientation, which is observed from 3D simulations. Displacement profiles of the Rayleigh and Love waves generated in IDT/ZnO/Si layered structure are depicted in Fig. 2.9 and Fig. 2.10 respectively. From the eigenmode analysis, we obtain the frequencies of all surface wave modes generated in the structure and to know the dominant mode generated. In case of two orientations XY and YZ we observed both Rayleigh and love waves in the structure, from the K^2 values we can conclude that Rayleigh waves are generated in YZ orientation and love wave in XY. To avoid further discrepancies, we performed frequency dependent analysis over both the orientations. In frequency dependent analysis, 1V electrical boundary conditions are applied to the IDT and frequency sweep is carried over the frequency range of both Rayleigh and Love surface waves observed in eigenmode analysis, to obtain the harmonic admittance characteristics and the results are shown in Fig. 2.11.

Table 2.1. Phase velocity and coupling coefficient of ZnO/Si layered configuration with different orientations of ZnO.

Orientation of ZnO	Phase velocity (m/s)		K^2 (%)	
	Rayleigh wave	Love wave	Rayleigh wave	Love wave
X propagation Y normal	3373.02	3311.26	0	5.1
Y propagation Z normal	3393	3357.45	0.49	0
Z propagation X normal	3397.38	3317.02	4.7	0

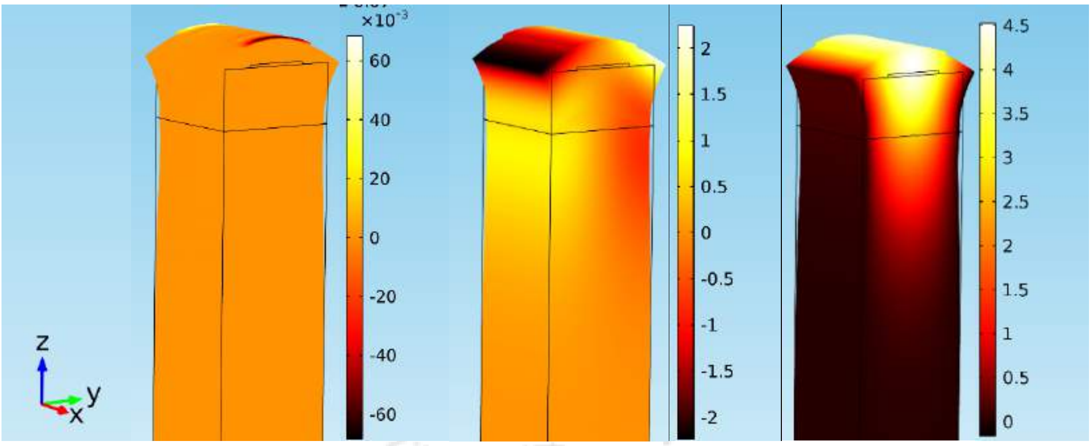

(a) (b) (c)

Fig. 2.9. Displacement profiles of Rayleigh mode generated in IDT/ZnO/Si SAW resonator having YZ oriented ZnO, (a) x–displacement, (b) y–displacement, and (c) z–displacement, *Displacements are in μm*.

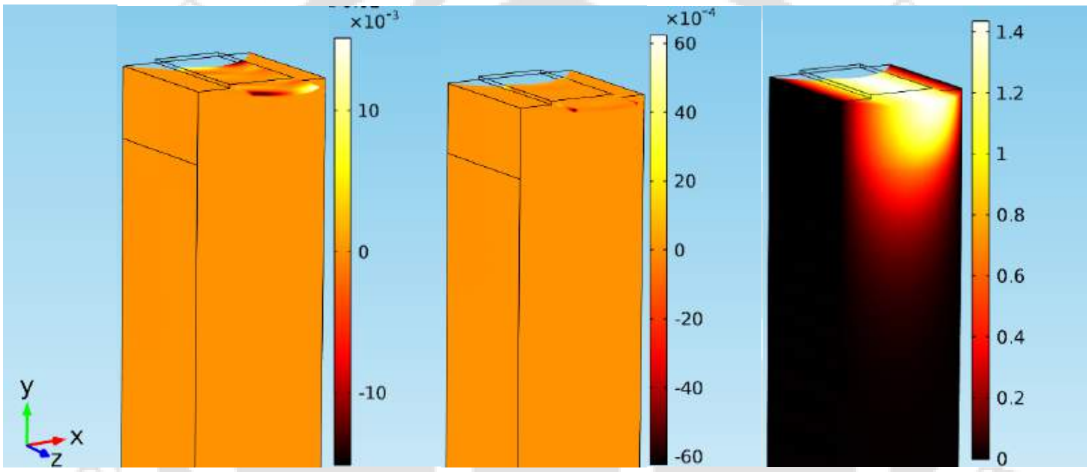

(a) (b) (c)

Fig. 2.10. Displacement profiles of Love wave generated in IDT/ZnO/Si SAW resonator having XY oriented ZnO, (a) x–displacement, (b) y–displacement, and (c) z–displacement. *Displacement scale in μm*.

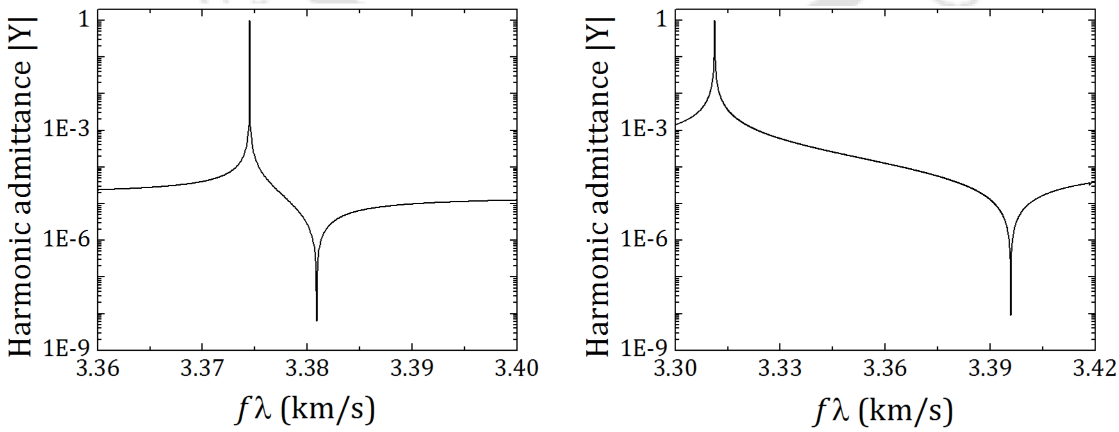

(a) (b)

Fig. 2.11. Normalized harmonic admittance plots obtained from frequency dependent analysis, (a) characteristics of Rayleigh mode generated in IDT/ZnO/Si SAW resonator having YZ oriented ZnO film and (b) love wave characteristics with XY oriented ZnO film.

From the harmonic admittance plots, we observed that the bandwidth of Rayleigh wave is lower than love wave device, which is in agreement with the K^2 values, as K^2 is directly proportional to bandwidth of the device.

2.4.3 Effect of aperture length on operating frequency and admittance characteristics

Further, the eigenmode analysis is carried out on 3D model to study the change in resonant frequencies with various lengths of aperture (W). For this study, we consider 8 μm wavelength and 0.25λ thickness of ZnO film with IDT on top of it. Mechanical and electrical boundaries conditions are applied to geometry as discussed in the previous section. From the eigenmode parametric analysis the resonance frequencies of Rayleigh and love waves generated in the structure for an aperture of 1 μm to 40 μm is tabulated in Table 2.2. It can be seen that the frequency variations are within ±0.05 MHz and after 4λ length of aperture the Rayleigh wave frequency is constant and love wave is almost constant at 5λ.

The harmonic analysis of 3D model SAW resonator is performed for various values of W (1 μm and 2 μm) to study the effect of aperture length on the admittance characteristics. The admittance and displacement characteristics for aperture widths 1 μm and 2 μm are shown in Fig. 2.12. Fig. 2.12 (a) shows the admittance plots of first Rayleigh wave generated in the IDT/ZnO/Si configuration and Fig. 2.12 (b) shows the characteristics of Love wave generated in the structure.

Table 2.2 Variation in resonant frequency with change in aperture (W)

Aperture (μm)	Rayleigh wave (MHz)	Love wave (MHz)
1	421.7761	413.9217
2	421.7882	413.9311
4	421.8007	413.9434
8	421.8031	413.9455
12	421.8039	413.9463
16	421.8043	413.9466
24	421.8047	413.9470
32	421.8049	413.9472
40	421.8051	413.9474

It is to be noted that the eigenmode and frequency analysis for Rayleigh and Love waves in the structure are simulated with YZ and XY orientations respectively.

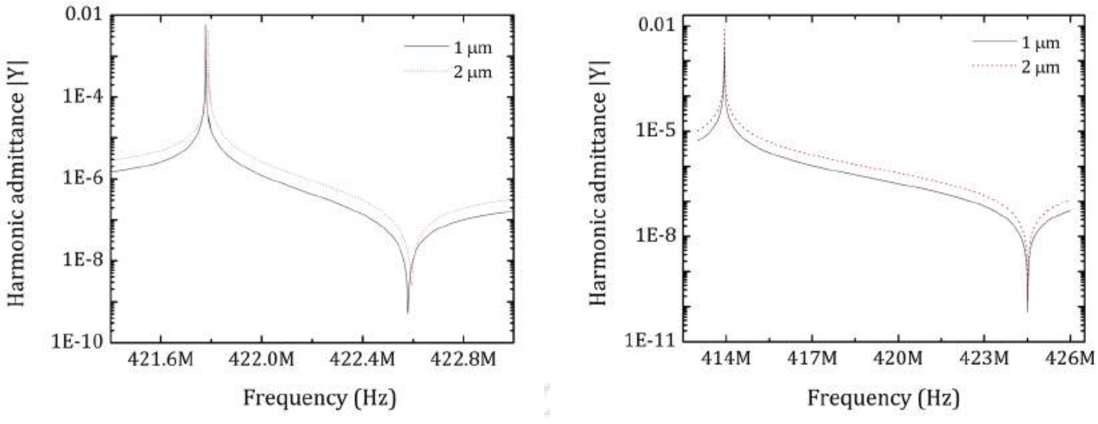

(a) (b)

Fig. 2.12. Harmonic admittance plots obtained from frequency dependent analysis with respect to aperture length, (a) characteristics of Rayleigh mode generated in IDT/ZnO/Si SAW resonator having YZ oriented ZnO and (b) love wave characteristics with XY oriented ZnO.

It is observed that the magnitude of the admittance value is proportional to the length of the aperture. Thus the minimum aperture length is sufficient to simulate a SAW resonator to study its displacement and admittance characteristics.

2.4.4 Effect of mesh density on resonance frequency

Further, the eigenmode analysis is carried out on 3D model to study the effect of mesh density on the resonance frequency of the Rayleigh surface mode generated in the ZnO/Si layered structure. SAW wavelength 8 μm, 0.25λ thickness of ZnO film on top of silicon substrate of 10λ depth, aperture length of 1λ and half periodic section with periodic boundary conditions is consider for eigenmode analysis. The meshed structure of 3D geometry used in the simulation is shown in Fig. 2.13. Parametric sweep of maximum element size per wavelength is carried out with a fixed mesh parameters, element growth rate of 1.05, minimum element size of 2 nm, resolution of narrow regions 0.95. The obtained resonance frequency of Rayleigh wave with respect to number of mesh elements are listed in Table 2.3. From the results it is observed that a mesh density of 32 elements per wavelength gives a relative error

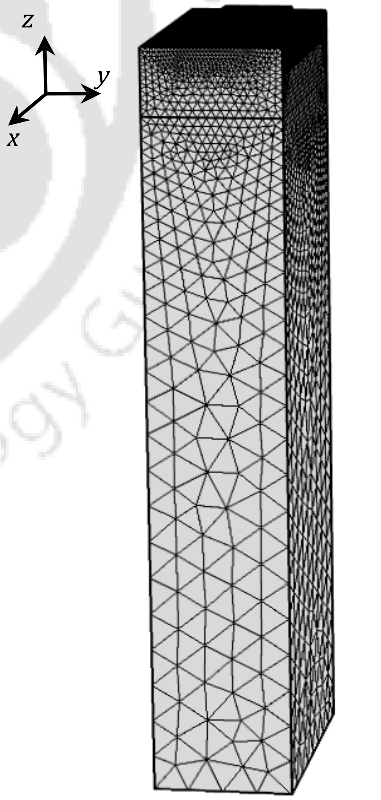

Fig. 2.13. Meshed 3D Geometry of the periodic section used for the simulation.

of 1e-4% in the resonance frequency, which is insignificant compared with the operating frequency obtained at 48 elements per λ which is maximum possible meshing density with the available computational resources. Hence we have used 32 elements per λ for all the simulations.

Table 2.3 Variation of device resonant frequency with respect to change in mesh density.

Number of mesh elements per λ	Rayleigh wave (MHz)	Velocity (km/s)
8	421.786223	3.374289784
12	421.7957166	3.374365733
16	421.8030323	3.374424258
20	421.8030584	3.374424467
24	421.8030923	3.374424738
28	421.8031154	3.374424923
32	421.8031241	3.374424993
36	421.8031377	3.374425102
40	421.8031439	3.374425151
44	421.8031479	3.374425183
48	421.8031481	3.374425185

2.4.5 ZnO/Si layered configurations

The possible layered configurations of ZnO/Si structure are shown in Fig. 2.14 [20], [21]. Since, phase velocity and coupling coefficient are important factors of SAW device to operate with appreciable efficiency and K^2 is greatly varied by the position of IDT and inclusion of thin metal films. In Fig. 2.14(a), (b) are commonly used configurations, whereas in case of (c) and (d), metal films are employed for customization of K^2 and electrical passivation from external electric fields also to reduce the elector magnetic feed through (EMF) the silicon substrate. The phase velocity and coupling coefficient dispersion curves with respect to ZnO thickness is obtained using FEM based simulations. Hence, we

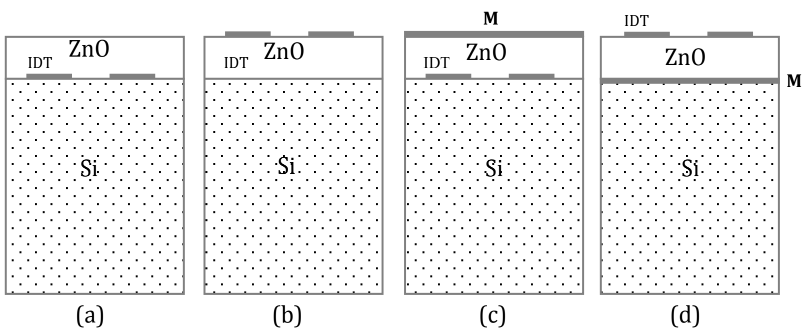

Fig. 2.14. The possible four layered configurations adapted from Kino [20].

simulated the 2D modeled SAW resonator structure with one period of IDT, from this point we considered simulations only on Rayleigh wave based SAW devices on silicon using YZ oriented ZnO and love wave based devices on silicon substrate using XY oriented ZnO are described and detailed in chapter 6.

2.4.6 2D FE simulations of ZnO/Si configured SAW resonator

Since, we are considering devices based on Rayleigh wave and it propagates in sagittal plane of x_1x_2 with zero displacements in x_3 direction. To save computational time, we considered 2D simulations to obtain the phase velocity and K^2 dispersion characteristics of SAW resonators on silicon. The 2D model used in simulations is shown in Fig. 2.15. Periodic boundary conditions are applied to left and right edges of the structure. Eigenmode analysis is carried out to obtain dispersion curves for all four configurations described above. The dispersion characteristics of first Rayleigh wave generated in the four configurations are shown in Fig. 2.16.

2.4.7 Results of ZnO/Si SAW resonator

The phase velocity in the layered structure ranges in between the surface wave velocity of substrate and the surface wave velocity of bulk ZnO, which is surface wave velocity in (100) silicon (4921 m/s) and in ZnO (2507 m/s) [54]. The phase velocity dispersion is higher in case of large acoustic impedance difference between piezoelectric thin film and substrate [3]. At smaller thicknesses of ZnO film the surface wave exhibits the properties of substrate with high phase velocity and as the thickness increase the phase velocity tend to reach the velocity bulk ZnO. From the K^2 characteristics, we observed that the position of IDT and inclusion of metal layers affects the values significantly. From Fig. 2.16, M/ZnO/IDT/Si configuration exhibits relative high K^2 of 4.5% at h/λ = 0.4, which requires a thick ZnO film and also compatibility and characterization difficulties arises due to presence of metal layer above ZnO. Relative high K^2 of 1.5% at h/λ = 0.1 with phase velocity of 4252 m/s is exhibited by IDT/ZnO/Si configuration. Relative high K^2 of 3% at h/λ = 0.32 with phase velocity of 3248 m/s is observed from ZnO/IDT/Si configuration.

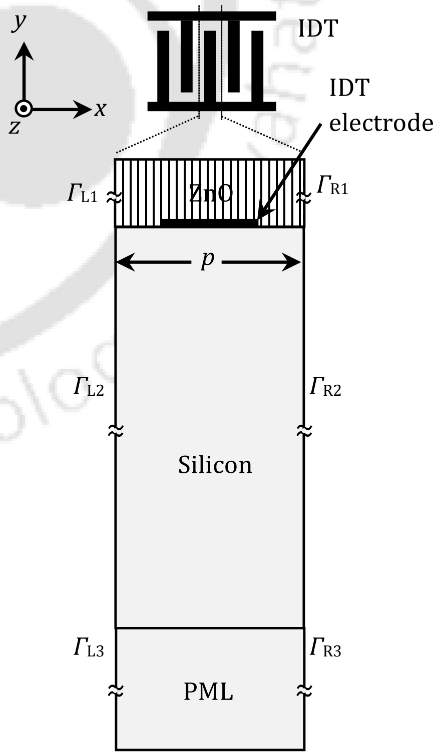

Fig. 2.15. 2D Geometry of the periodic section used for the simulation.

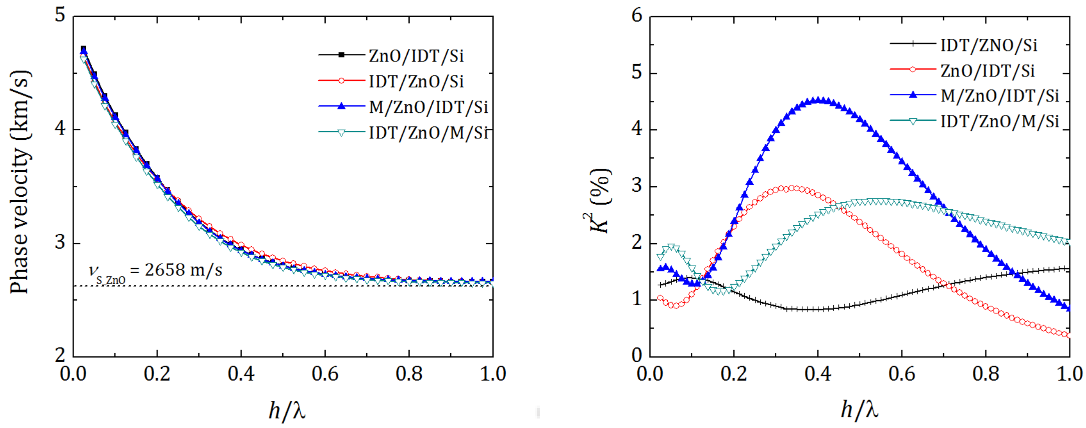

Fig. 2.16. The phase velocity and electromechanical coupling coefficient dispersion characteristics of four ZnO/Si configurations.

IDT/ZnO/M/Si configuration exhibits relative maximum K^2 of 2.75% at h/λ = 0.5 with low phase velocity of 2668 m/s.

The IDT is designed with an admittance of 0.02 mho at center frequency. The center frequency can be obtained using eigenmode analysis or frequency dependent analysis. One port SAW resonator is designed using equivalent circuit model for all the configurations, the number of finger pairs in IDT and resonance frequency, coupling coefficient, and ZnO thicknesses are summarized in Table 2.4. The thicknesses of ZnO are considered to obtain high frequency of operation with K^2 at that h/λ.

$$k = j|0.5 * K^2| * \left(\frac{\pi}{2}\right) * \left((-cos\Delta) + \left(\frac{P_{0.5}(cos\Delta)}{P_{-0.5}(cos\Delta)}\right)\right) \tag{2.41}$$

where $\Delta = n\pi$, $P_{0.5}(\cos \Delta)$= 1.5061 and $P_{-0.5}(\cos \Delta)$= 1.3280 are the Legendre polynomials adapted from Nordin [26].

Total reflectivity of grating is given by

$$|\Gamma| = \tanh N|k| \tag{2.42}$$

Where N is number of reflector gratings, using the reflectivity k the penetration length of the generated surface wave is calculate using

$$L_p = \lambda/|4r| \tag{2.43}$$

Table 2.4 Dimensions of one port SAW resonator obtained using equivalent circuit model.

Configuration	ZnO (μm)	K^2 (%)	f_0 (MHz)	N_t	k (per one finger)	N
(a) IDT/ZnO/Si	0.8	1.392	508.6653	81	0.0028	348
(b) IDT/ZnO/M/Si	0.4	1.95	549.2043	66	0.0016	608
(c) ZnO/IDT/Si	2.6	2.95	389.3882	63	0.011	88
(d) M/ZnO/IDT/Si	0.4	1.53	556.3627	74	0.01	0.01

Further, we carried out eigenmode analysis to study the generation of higher order modes in ZnO/IDT/Si structure, as it exhibit high coupling coefficient at smaller thickness of ZnO compared with other configurations as well as small device size. The phase velocity and coupling coefficient dispersion of curves of first four modes generated in the ZnO/IDT/Si layered structure are shown in Fig. 2.17. From (a) we observe the maximum velocity attained by the modes generated is near to shear bulk wave velocity of silicon which is 5653 m/s and as the thickness of ZnO increases the phase velocity tends to SAW velocity of bulk ZnO. In case of layered structures the maximum phase velocity attain by higher order modes is the shear bulk velocity of the substrate [3], [47]. From Fig. 2.17(b), we observe the 0th Rayleigh mode exhibits relative maximum coupling coefficient at h/λ = 0.3. 1st higher order Rayleigh wave is observed at h/λ = 0.2 having phase velocity of 5285 m/s with K^2 = 0.92% which is the relative maximum exhibited by 1st mode. 2nd mode starts at h/λ = 0.55 with phase velocity of 5328 m/s with a K^2 value of 0.27% and reaches a relative maximum value of 0.33% with a phase velocity of 5275 m/s. Mode 3 starts from h/λ = 0.875 with phase velocity of 5317 m/s and K^2 value of 0.29%. As mode 0 exhibiting maximum coupling coefficient, we carried out the harmonic analysis to obtain total displacement and harmonic admittance characteristics of modes generated in ZnO/IDT/Si one port SAW resonator structure. The obtained frequency dependent results are shown in Fig. 2.18 and the surface displacement profiles of two modes generated in the structure are show in Fig. 2.19.

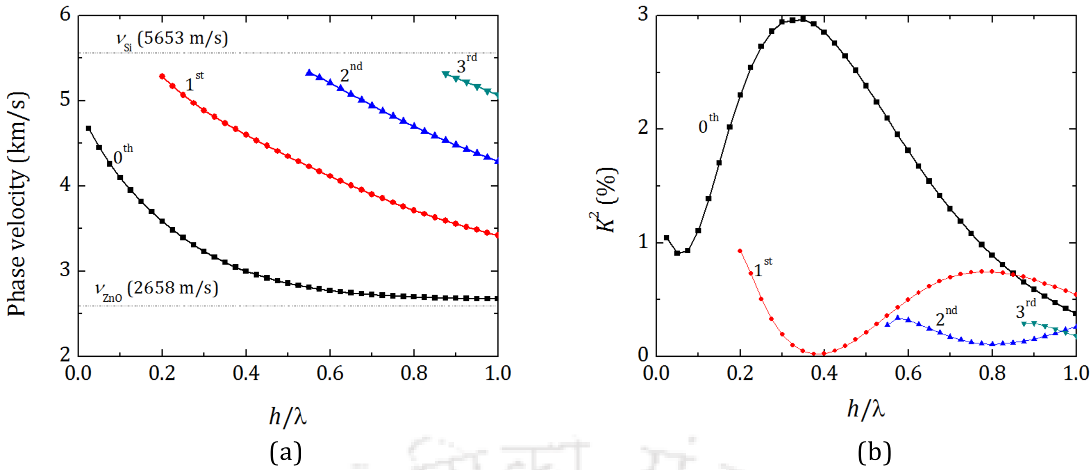

Fig. 2.17. The variation of phase velocities of 0th, 1st, 2nd, and 3rd Rayleigh modes with respect to ZnO film thickness ratio in conventional ZnO/Si structure.

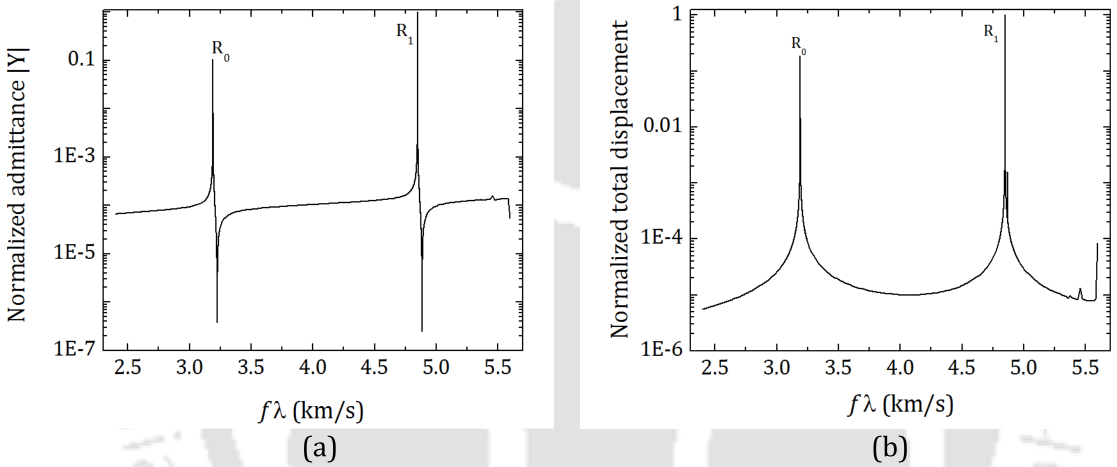

Fig. 2.18. (a) Normalized admittance and (b) normalized displacement characteristics of Rayleigh surface modes generated in conventional ZnO/IDT/Si configured SAW resonator at $h/\lambda = 0.3$.

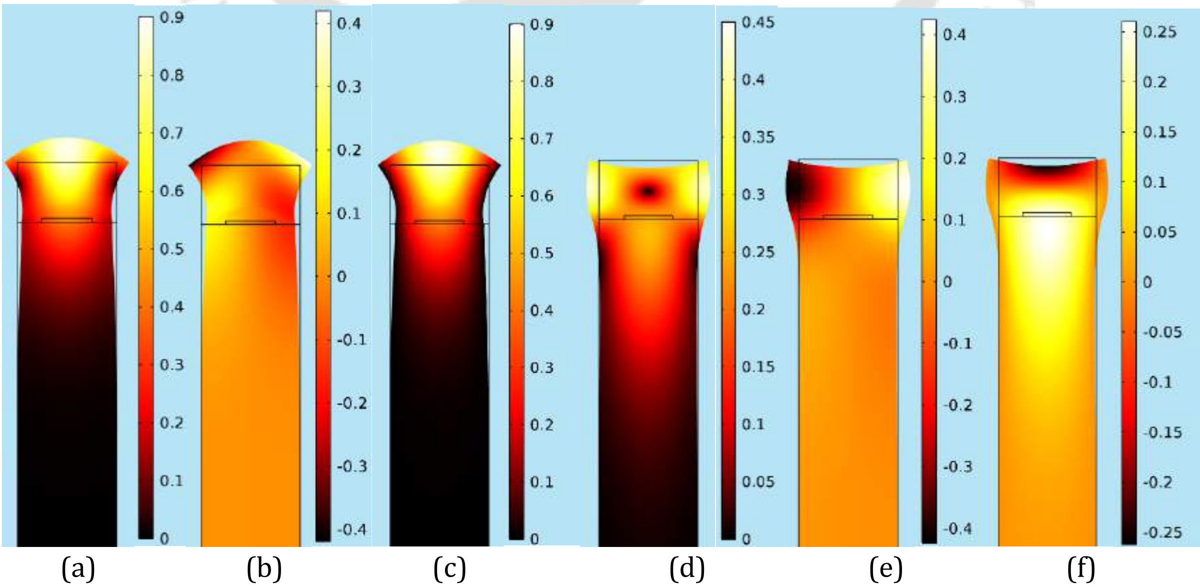

Fig. 2.19. (a) Total displacement, (b) *x*-displacement, (c) *y*-displacement profiles of fundamental Rayleigh mode, and (d) total displacement profile, (e) *x*-displacement, (c) *y*-displacement profiles of first higher order Rayleigh modes generated in the ZnO/IDT/Si structure at $h/\lambda = 0.3$, *displacement scale in µm.*

2.4.8 2D simulation of ZnO/IDT/Si SAW delay line

A few literature has been reported on the FE simulation of thin film SAW device on silicon using ZnO film and many researchers reported the simulation of conventional piezoelectric substrate based SAW delay lines [46], [57], and [58]. In this section, ZnO/IDT/Si structure SAW delay is simulated to compare the simulation results with the proposed SAW delay line on silicon described in the next chapter. A delay line with 4λ distance between the centers of input and output IDT’s. The dimensions used in the simulation are as follows: pitch of 4 μm, metallization ratio of 0.5, and thickness of IDT electrodes 0.1 μm and substrate depth of 5λ. The 2D schematic of ZnO/IDT/Si SAW delay line with subdomain conditions are shown in Fig. 2.20. Fixed boundary condition is applied to bottom boundaries of the geometry and rest all boundaries are assumed stress free. Rayleigh damping boundary conditions are applied to absorb medium, which is extend to one wavelength on the both sides of the delay line to absorb the unwanted reflections form the edges of the device. The electrical boundary conditions are as follows: the alternate fingers of input port are grounded and a 1V sinusoidal driven voltage of its resonance frequency (367.9581 MHz) of is given to remaining electrodes [59]. Meshing is optimized in such way that extreme fine meshing is obtained at active surface region of structure and fine mesh into the substrate. The transient analysis is carried out using the direct solver available in COMSOL multiphysics for 30 ns with a time interval of 1 ps. The displacements and potential at the receiver electrode are recorded at every step.

2.4.9 Results of thin film ZnO/IDT/Si SAW delay line

Fig. 2.20(a) shows the *y*-displacement profile in SAW delay line at time 27.7 ns from the instant of application of input. The output potential and *y*-displacement of particle on the ZnO surface at input and output IDT’s are shown in Fig. 2.21 (b, c, and d). Due to the applied electric potential the surface waves are launched along the surface of ZnO film and the

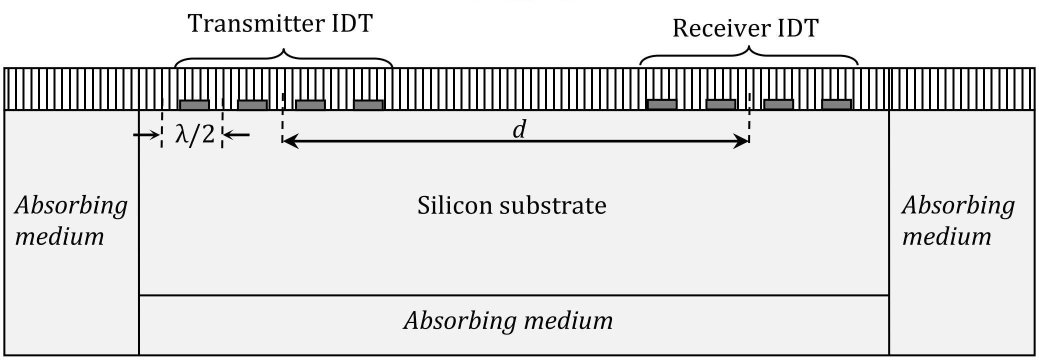

Fig. 2.20. 2D schematic of ZnO/IDT/Si SAW delay line.

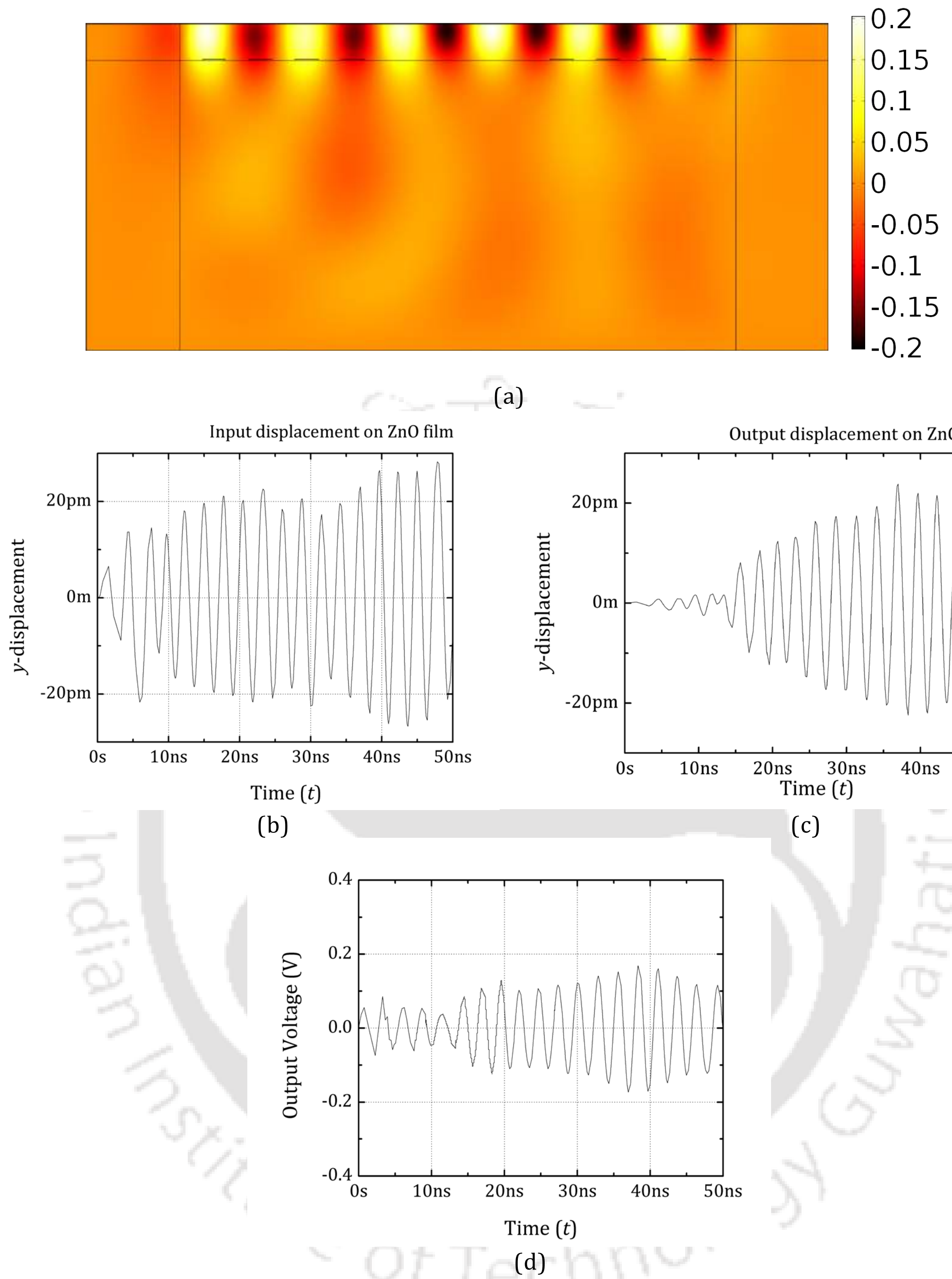

Fig. 2.21. (a) *y*-displacement profile of ZnO/IDT/Si SAW delay line at 27.7 ns with color legend in Armstrong's (A°), (b) particle's y-displacement on ZnO surface near input IDT, (c) *y*-displacement of a particle on the ZnO surface at top of IDT, and (d) output voltage obtained with respect to time.

particle displacements are obtained on the ZnO surface at the center position of IDT. The output electrical potential of 0.18 V is obtained at the receiver IDT electrodes. In SAW delay line, delay time is one of the important parameter and is estimated from the envelopes of the *y*-particle displacement at input and output transducers, also the phase velocity of the surface wave can be calculated. From the output displacement envelope, velocity is equal to the inverse of difference between two nodes or anti-nodes, the nodes at 20.38 ns and 23.098 ns are considered to calculate the velocity and is equal to 3679.17 m/s. From the y-displacement plots we observed that the relative maximum y-displacement at input IDT is 28 pm and at the output IDT it is 22 pm.

2.4.10 Observations

Phase velocity and K^2 characteristics are very crucial in design of SAW devices using equivalent circuit model, phase velocity defines the frequency of operation with respect λ and K^2 defines dimension of reflector grating as the reflectivity of an electrode finger is proportional to coupling coefficient. Simulation of ZnO/Si one port SAW resonator configurations are carried out so that the results will be used for the design of resonator for fabrication. In case of thin film SAW devices on silicon they exhibit tradeoff between phase velocity and coupling coefficient and also reproducing same quality ZnO is very difficult for mass production.

2.5 Summary

In this chapter, a brief introduction on basics of elasticity, piezoelectric constitutive equations, modeling of SAW devices using equivalent circuit model, thin films SAW devices, mechanical properties of ZnO and its orientation, various layered configurations of ZnO/Si structure, and FE simulations of conventional SAW devices and thin film SAW devices.

In summary, FE simulations of ZnO/Si one port SAW resonator configurations are performed using FE based software, COMSOL Multiphysics. 3D simulations of ZnO/Si structure with periodic boundary conditions is simulated to study orientation of ZnO and the surface modes generated in the structure. Harmonic admittance characteristics are obtained from frequency dependent analysis to identify the dominant surface mode generated in the structure. Eigenmode analysis is carried out to obtain the phase velocity and coupling coefficient dispersion characteristics of all four possible configurations. The effect of position of IDT and metal layer on the coupling coefficient characteristics are examined. Since ZnO/IDT/Si configuration exhibits high K^2, the dispersion characteristics of higher order modes generated in the ZnO/IDT/Si structure are studied. The obtained simulation results are in good agreement with the values reported in literature. The method used in the FE simulations can be further extended to study the proposed SAW devices on silicon. It is shown that using COMSOL and equivalent circuit model, IDT can be designed for SAW device fabrication. From the simulation study of conventional thin film ZnO/Si SAW devices we observe a tradeoff between phase velocity and coupling coefficient. Also reproducing same quality ZnO film using RF sputtering is very difficult for mass production.

Chapter 3

Design and Simulation of Patterned-ZnO/Si SAW Devices

Chapter 2 has discussed modelling of SAW devices and simulation of conventional thin film SAW devices on silicon covering four possible layered configurations of conventional ZnO/Si structure. This chapter presents the proposed SAW devices on silicon using periodically patterned ZnO films and their simulation to investigate their performance vis-à-vis conventional thin film SAW devices simulated in chapter 2.

The major drawbacks of conventional thin film SAW devices on silicon are as follows. The reported SAW devices using piezoelectric films exhibit tradeoff between electromechanical coupling coefficient and phase velocity. The performance of the thin film SAW devices significantly depends on the quality of the piezoelectric film usually deposited by RF sputtering, and it is difficult to maintain the quality of the film and reproduce the devices in mass production.

However, the proposed conception is based on an alternative method of transduction of surface waves by mode conversion of bulk waves possible with periodically patterned piezoelectric film on a non-piezoelectric substrate. The patterned structure resonates and the bulk mode generated in the structure induces surface wave in silicon due to mode conversion. Since the piezoelectric film is patterned, the surface wave is confined to propagate in silicon which has high acoustic velocity. In addition, the quality of piezoelectric film has little effect on the surface wave propagation as the wave is not travelling in the film. The resonance frequencies of bulk modes excited in the patterned piezoelectric structure mainly depend on the film thickness which can be accurately controlled during the deposition process.

In this thesis, we propose two distinct types of SAW devices realized on silicon:

1. SAW devices with patterned-ZnO/IDT/Si structure, covered in chapters 3, 4, and 5.

2. Edge reflection type SAW devices on silicon, covered in chapters 6, 7, and 8.

This chapter discusses the first type of proposed SAW devices on silicon using periodically patterned ZnO film and phenomenon of mutual mode conversion between bulk waves and surface waves at periodic structures, FE simulations of proposed patterned structure on silicon to study the phase velocity and coupling coefficient characteristics. The dispersion

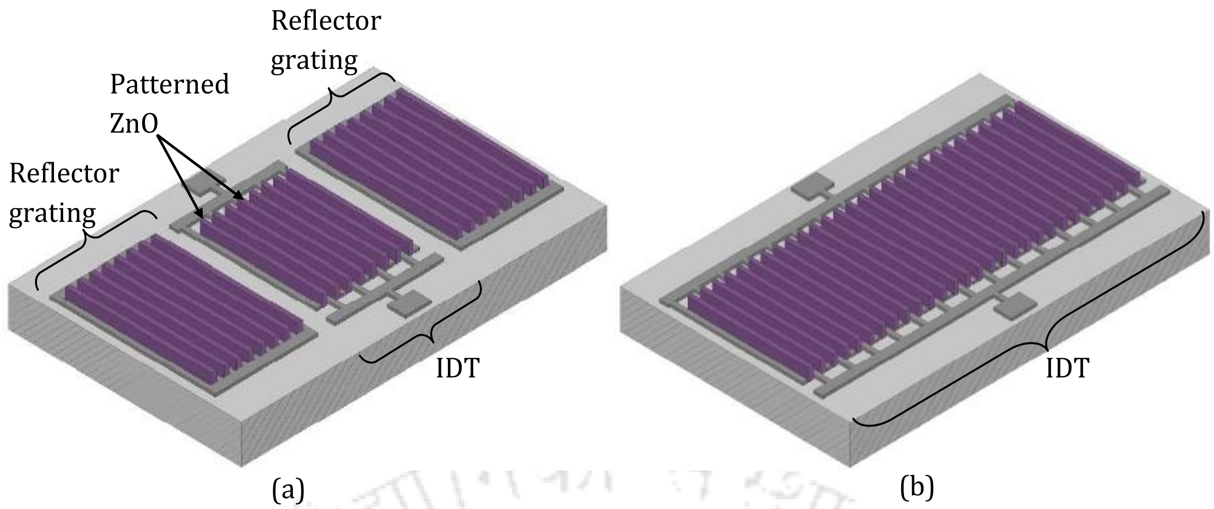

Fig. 3.1. (a) Three dimensional schematic of the proposed one-port SAW resonator on silicon with periodically patterned ZnO disposed in the spaces of IDT fingers and reflector gratings, (b) 3D schematic of one port SAW resonator with IDT consisting of a large number of electrode fingers with ZnO pattern in the spaces of IDT.

characteristics of various surface modes generated at the surface of silicon substrate are included. Inclusion of buffer layers like SiO_2 and AlN films to reduce the acoustic impedance mismatch and its effect on dispersion characteristics is investigated. Design methodology using equivalent circuit model for the fabrication of the proposed SAW devices with periodically patterned ZnO is discussed.

The schematic of the proposed SAW device on silicon using periodically patterned ZnO thin film is shown in Fig. 3.1. The device comprises of plain (100) oriented *p*–type silicon substrate with periodically patterned ZnO thin film disposed in between the spaces of electrodes of the IDT structure. In this thesis, the *c*-axis (002) of ZnO film is oriented perpendicular the surface of the substrate in all the devices.

3.1 Patterned-ZnO/Si structure – Theory and operation

The transduction mechanism in the proposed patterned-ZnO/Si structure is based on the mode conversion between bulk waves and surface waves. In general, there exists a mutual conversion between surface acoustic waves and bulk acoustic waves (BAW) at the interface of periodic structures or irregularities on a substrate [6], [7]. The SAW incident at the interface of the periodic structures and substrate as depicted in Fig. 3.2(a) is transformed into BAW [6]. Similarly the BAW incident at the interface of periodic structures and substrate is transformed into longitudinal or transversely polarized surface waves, as

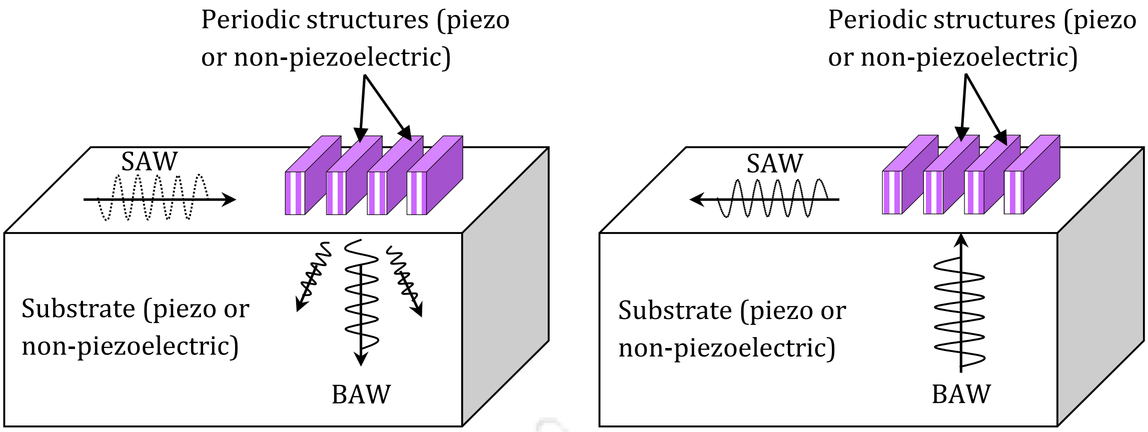

Fig. 3.2. Pictorial representation of mutual conversion of SAW and BAW at periodic structures (a) conversion of SAW incident at the periodic structure into BAW, and (b) conversion of BAW incident

depicted in Fig. 3.2(b) [6]. The finite element simulation of mutual conversion of SAW and BAW in piezoelectric media is reported by darsnic *et al.* [7]. Pleesky *et al.* [8] reported the micro acoustic resonators for the generation of film bulk modes on non-piezoelectric substrates like silicon and sapphire. They reported the simulation of BAW resonators excited by the electrodes placed on the top and bottom of AlN micro grating, and the device showed features of SAW transducer and FBAR (Film bulk acoustic wave resonator).

In the current study, we propose periodically patterned film of *c*-axis oriented (002) ZnO disposed in the spaces of IDT on silicon substrate to implement SAW resonators and delay lines on silicon. The patterned ZnO structure resembles periodically placed bulk acoustic wave resonators excited laterally using IDT structure, as depicted in Fig. 3.3(a). The RF signal applied to the IDT electrodes generates electric field that cuts through the patterned-ZnO structure and induces stress-strain resulting into the generation of bulk acoustic wave in ZnO along the *c*-axis. In each ZnO block, the generated BAW is reflected from the top and bottom surfaces of the ZnO block, and at particular excitation frequency, standing waves are formed causing resonance. BAW excited in ZnO pattern acoustically couples to the silicon substrate resulting in generation of surface wave along the surface of silicon substrate. Fig. 3.3(b) illustrates the conversion of surface waves to bulk waves at the periodic ZnO structure. The generated surface acoustic wave can be longitudinal or transverse depending on the orientation of ZnO pattern and the type of mode generated in ZnO pattern [7].

The acoustic power transmission and reflection coefficients [7] of acoustic waves with normal incidence at the interface of ZnO pattern and silicon are given by

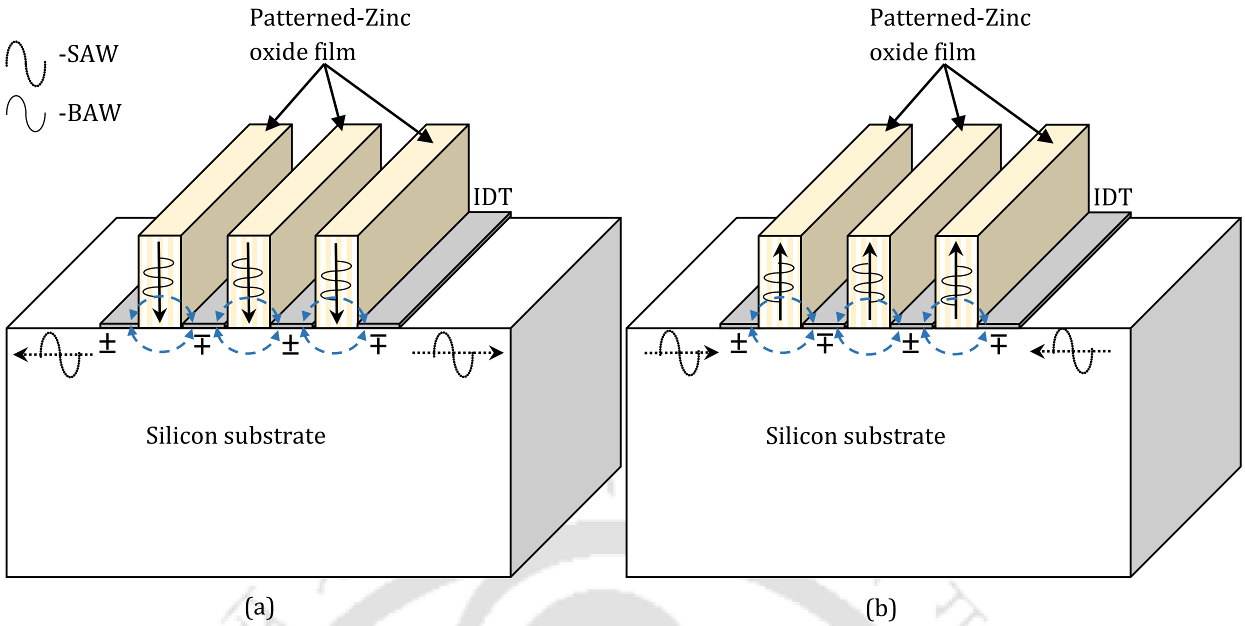

Fig. 3.3. 3D schematic of mutual conversion of BAW and SAW in the proposed periodically patterned-ZnO/Si structure. (a) BAW to SAW conversion, and (b) SAW to BAW conversion.

$$\boldsymbol{T} = \frac{4Z_{Si}Z_{ZnO}}{(Z_{ZnO} + Z_{Si})^2}\ ; \quad \boldsymbol{R} = \left(\frac{Z_{ZnO} - Z_{Si}}{Z_{ZnO} + Z_{Si}}\right)^2 \tag{3.1}$$

where Z_{ZnO} and Z_{Si} are the acoustic impedances of ZnO and silicon respectively. Since the acoustic impedance ZnO is about 5500 times greater than of air, *R* is very close to 1, and 100% reflection in assumed from top boundary of ZnO block.

The energy flux of BAW generated in ZnO and two SAWs generated in opposite directions along the silicon surface are given by [7]

$$P_{BAW} = \rho_{ZnO}\, v_{BAW}\, \omega^2\, N\, |A_{BAW}|^2; \quad P_{SAW} = 2\, \rho_{Si}\, v_{SAW}{}^2\, \omega^2\, |A_{SAW}|^2\, \frac{\boldsymbol{T}}{\alpha} \tag{3.2}$$

where *N* is the number of ZnO blocks, *A* is the amplitude of acoustic wave, and α is the decay factor.

The theoretical or experimental study of SAW devices with the proposed patterned structure on silicon substrates, to the best of author's knowledge, has not been reported in literature. The thesis investigates the patterned ZnO/Si structure by carrying out rigorous simulations , fabrication and testing of devices, and the results show that the SAW devices on silicon with the proposed configuration exhibit high phase velocity with high coupling coefficient and can be integrated within IC and CMOS circuitry to realize monolithic systems with the unique qualities.

The simulations of proposed SAW devices with periodically patterned-ZnO/Si structure are carried out using COMSOL Multiphysics. The following sections include the phase velocity and electromechanical coupling coefficient characteristics of the proposed structure and the results of comparison with the conventional ZnO/Si SAW devices. Further, simulations are carried out to study the effect of addition of buffer layers like SiO_2 and AlN films on the device characteristics.

3.2 3D FE simulation of one port SAW resonator with patterned-ZnO on silicon

This section presents the simulation of the proposed SAW resonator on silicon having large number of IDT fingers with periodically patterned-ZnO film in COMSOL Multiphysics. The simulation results are compared with the results given in Section 2.4.6 for an identical ZnO/IDT/Si conventional thin film one port SAW resonator on silicon.

3.2.1. Structure of one port SAW resonator on silicon with periodically patterned ZnO

The structure of one port SAW resonator with proposed patterned-ZnO structure is shown in Fig. 3.4. It consists of a silicon substrate with IDT containing a large number of fingers

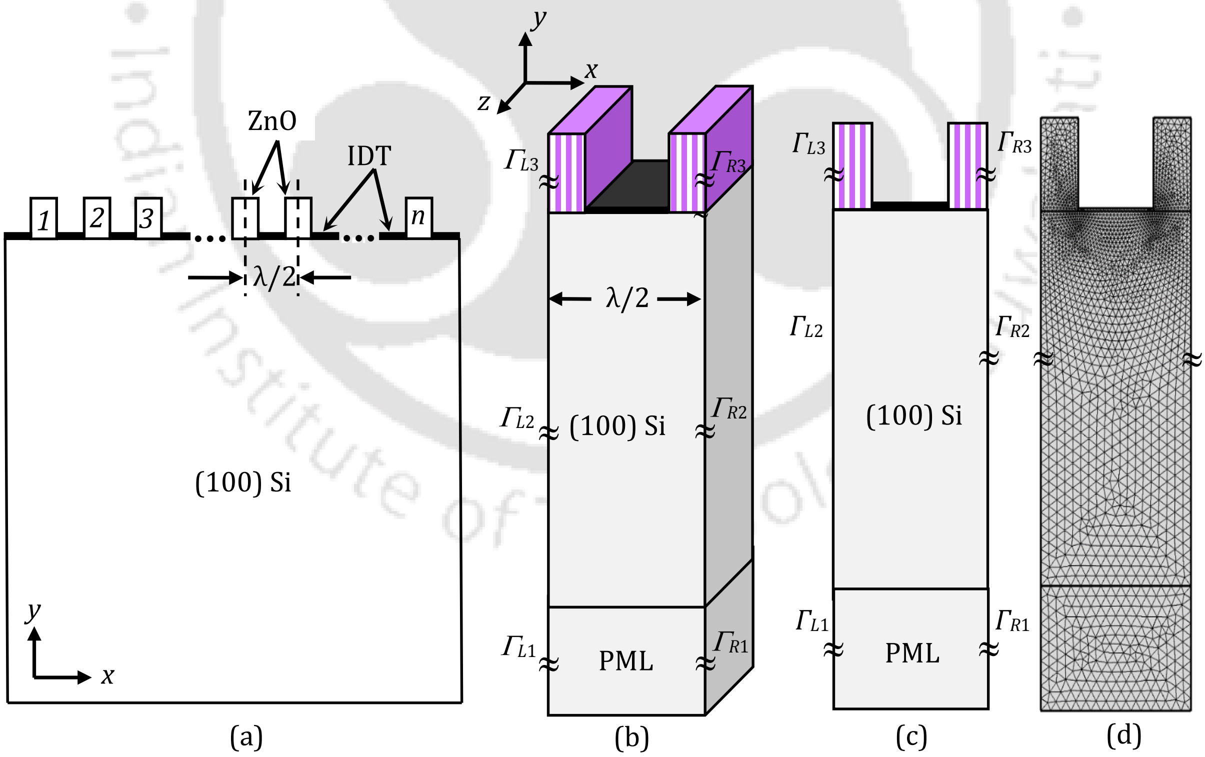

Fig. 3.4. Geometries used in FE simulations of the proposed one port SAW resonator, (a) schematic of the cross-sectional view of the device, (b) 3D geometry of half periodic section, and (c) 2D geometry of half periodic section with anti-periodic boundaries along *x*, assuming $n \to \infty$, and a perfectly matched layer (PML) at the bottom, and (d) meshed half periodic section of patterned-ZnO/Si.

and ZnO blocks are deposited in between the IDT fingers. The dimensions of the device are identical to the conventional thin film SAW resonator simulated in Chapter 2, Section 2.4.6, and the same simulation process is followed.

3.2.2 Simulation methodology

The proposed one port SAW resonator with infinite number of IDT fingers on a (001) silicon substrate is considered in the FE simulation. Owing to the periodic nature of the structure, half period of the structure with anti-periodic boundary conditions is used to model the proposed one port SAW resonator [35]. The three dimensional (3D) and the corresponding two dimensional (2D) geometries for one period of the structure are depicted in Fig. 3.4(b) and (c).

Uniform IDT with metallization ratio of 0.5 is considered over (100) silicon substrate and overlaid ZnO is patterned along the aperture of IDT to fill the spaces between IDT fingers, as shown in Fig. 3.4(b). The (002) oriented ZnO with *c*-axis along the sagittal plane is chosen due to its high electromechanical coupling for the bulk waves propagating along *c*-axis [46]. Perfectly matched layer (PML) is considered at the bottom of the silicon substrate as an absorbing boundary to eliminate unwanted reflections from the bottom surface and fixed boundary condition is applied to the bottom surface of PML. We consider finger width of 2 μm and thickness of 100 nm with pitch 4 μm, and the material properties of ZnO, silicon, and aluminum used in the simulation are adapted from [35] and the conductivity of silicon substrate 2.3e5 is considered [76].

The structure is meshed using triangular elements with minimum element size of $\lambda/10^4$ with growth rate of 1.05 reaching to maximum element size of $\lambda/20$. The meshed structure is shown in Fig. 3.4(d). A potential of 1 V is applied to the IDT and harmonic admittance of the proposed structure is obtained using frequency dependent analysis. In the simulations, the effect of mechanical properties of aluminum and silicon are taken into account. We consider rectangular ZnO pattern in the simulation because of its high reflectivity and high coupling coefficient compared with triangular or trapezoidal shapes [60] and practically viable. The process of fabricating rectangular pattern of ZnO is described in chapter 4.

3.2.3 Results of 3D simulation of one port SAW resonator

Initially, 3D model is considered to obtain the harmonic admittance (HA) and normalized displacement characteristics of surface modes generated in the proposed structure (Fig. 3.4) at h/λ= 0.19, at which we have observed high electromechanical coupling coefficient as well as high phase velocity in the dispersion characteristics (presented in section 3.2.5).

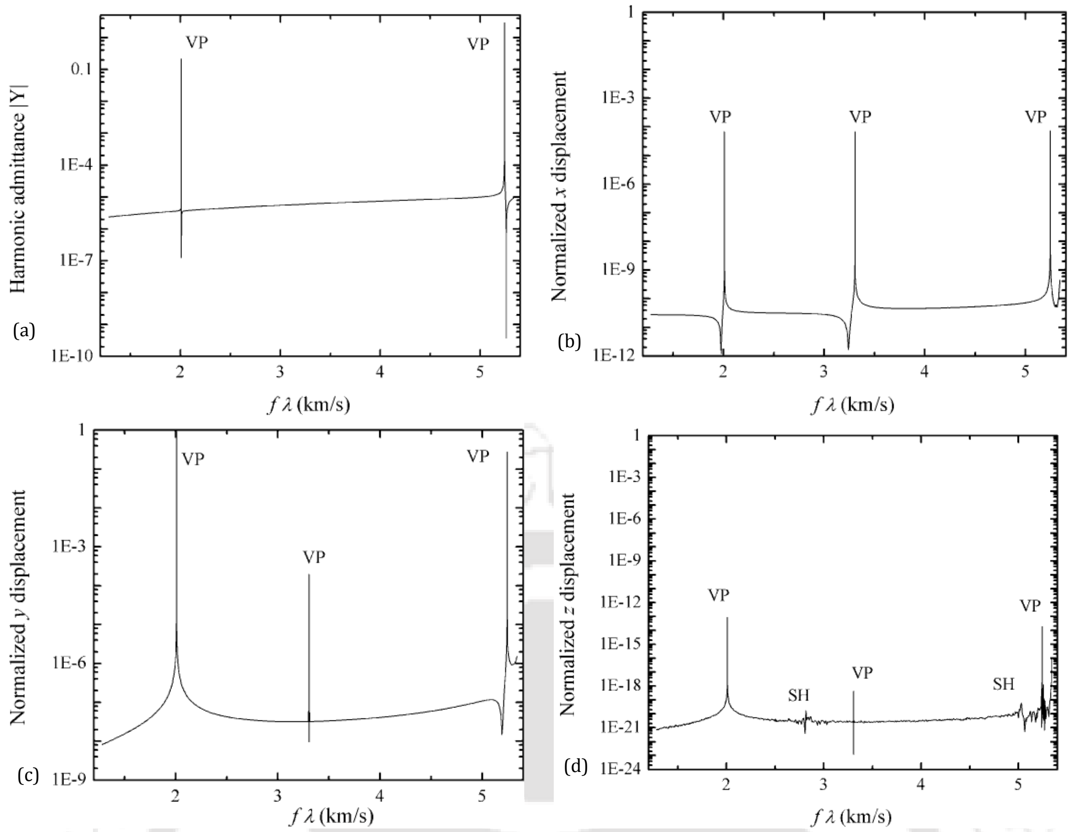

Fig. 3.5. Harmonic admittance (HA) and normalized displacement plots of SAW modes generated in the patterned-ZnO/Si structure at h/λ of 0.19. Total of five surface modes are observed, out of which both SH modes are insignificant and only two VP modes are dominant.

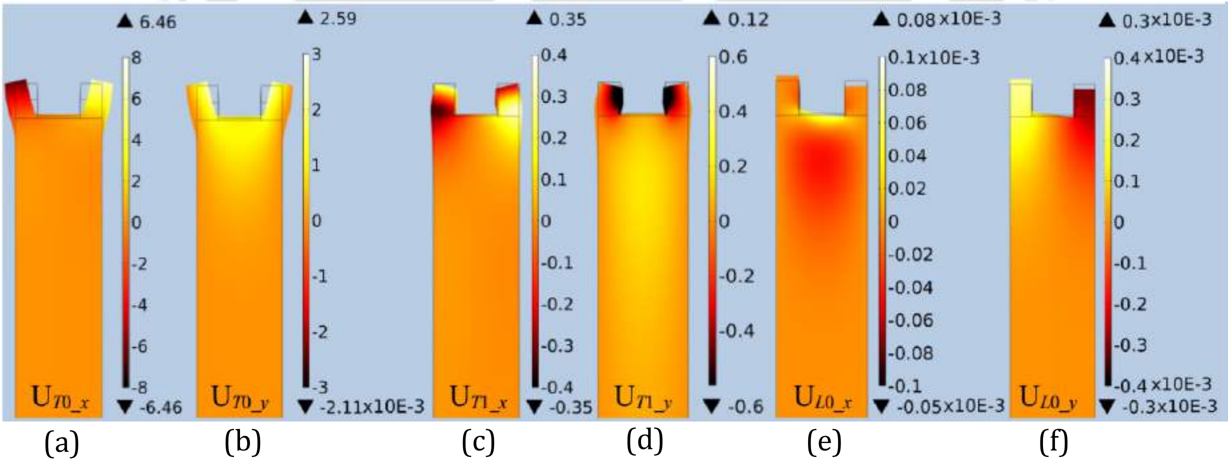

Fig. 3.6. The normalized *x* and *y* displacement profiles of vertically polarized SAW modes generated in the patterned-ZnO/Si structure at h/λ of 0.19. The displacements are normalized, as in Figure 3.5, with respect to the maximum displacement in silicon. U_{T0_x}, U_{T0_y} and U_{T1_x}, U_{T1_y} are the *x*, *y* displacements of surface modes generated by the fundamental transverse bulk mode (a, b) and first higher order transverse bulk mode (c, d) excited in ZnO pattern. (e) U_{L0_x} and (f) U_{L0_y} are the *x*, *y* displacements of surface mode excited due to mode conversion of the fundamental longitudinal mode in ZnO.

From the normalized displacement plots in Fig. 3.5(b, c, d), total five surface modes are observed, however the HA plot and the magnitudes in the displacement plots reveal that only two modes are dominant. The surface modes with predominant displacement along *y* are considered as vertically polarized (VP) modes and the modes with predominant displacement along *z* are consider to be shear horizontally polarized (SH) modes, whereas *x* is the direction of propagation of the generated surface modes. Here polarization of a wave refers to the direction of particle displacement. From the normalized displacement plots in Fig. 3.5, we observe that the displacements for SH surface modes are insignificant compared to the displacements of VP modes, which confirms the insignificant existence of shear polarized modes in the proposed periodically patterned-ZnO structure, as the shear horizontal coupling is minimal along *c*-axis in ZnO [49]. The *x* and *y* displacement profiles of the first three vertically polarized surface modes generated in the structure are shown in Fig. 3.6. Fig. 3.6(a–d) show the generation of surface modes in silicon due to the mode conversion of transverse bulk waves excited in the ZnO pattern and Fig. 3.6(e–f) show the generation of surface modes in silicon by the coupling of longitudinal bulk waves excited in ZnO pattern. However, the magnitudes of *y*-displacement in Fig. 3.6 indicate that the surface modes generated by the mode conversion of transverse bulk waves in ZnO are greater compared with that generated by the mode conversion of longitudinal bulk waves in ZnO. The fact can also be verified from Fig. 3.5.

The dominant normal component at ZnO-silicon interface is due to the acoustic coupling of BAW generated in ZnO pattern and the displacement profile resembles Rayleigh waves. Plessky *et.al*, reported similar result with periodic structure of bulk acoustic wave resonators formed by patterning AlN film on silicon with IDT located on the top the patterned AlN [8]. In the proposed patterned-ZnO/Si structure, as the cross-fields in ZnO structure are dominant compared to inline fields (along *c*-axis), the transverse BAW is dominant over longitudinal BAW in ZnO pattern, and the dominant surface modes observed in HA plot from Fig. 3.5 are excited by the transverse BAW in ZnO. The VP surface modes generated in silicon by transverse and longitudinal bulk waves in ZnO are referred as VP_T and VP_L respectively. The phase velocity and K^2 characteristics of the surface modes generated in the proposed device with respect to ZnO height to wavelength ratio are discussed in the next section.

3.2.4 Conclusion based on 3D simulations

The surface modes generated in silicon substrate are due to the acoustic coupling of transverse and longitudinal bulk modes generated in the patterned ZnO structure. The displacement and harmonic admittance plots show that the vertical polarized surface modes generated by transverse BAW are dominant compared to VP surface modes generated by the longitudinal BAW and shear horizontal surface waves generated in the structure. Since the generation and propagation of VP_T and VP_L modes are in the sagittal plane of the structure, 2D simulations are adequate to obtain the dispersion characteristics of the proposed devices. Hence, the rest of the simulations in this chapter are carried out in 2D.

3.2.5 Surface modes generated due to transverse bulk waves in ZnO pattern

Eigenmode analysis is carried out using 2D geometry shown in Fig. 3.3(c) with ZnO height as parametric sweep to obtain the phase velocity and coupling coefficient dispersion characteristics of surface modes generated in the proposed structure. From Eigenmode analysis, the frequency of the generated surface mode is obtained and its phase velocity (v) is calculated using $v = f\,\lambda$, where λ is the wavelength of IDT. As discussed in the previous section, the generated modes are vertically polarized and 2D simulations are adequate to obtain the dispersion curves. The electromechanical coupling coefficient (K^2) of the proposed structure is calculated using

$$K^2 = \left(\frac{v_f - v_m}{v_f}\right) \tag{3.3}$$

where, v_f and v_m are the SAW phase velocities obtained when the interface boundary between ZnO and silicon containing IDT is electrically free and shorted, respectively.

The dispersion characteristics of the first five surface modes generated in silicon due to the acoustic coupling of transverse bulk waves excited in ZnO pattern are plotted in Fig. 3.7, where h is the height of ZnO pattern and λ is the wavelength of IDT structure. From the phase velocity dispersive curves in Fig. 3.7(a), we observe that with the increase in the height of ZnO pattern, the phase velocity of generated SAW decreases rapidly due to the decrease in the frequency of bulk mode in ZnO structure. The first higher order transverse mode in ZnO results in the generation of VP_{T1} in the structure at h/λ = 0.185, with SAW phase velocity of 5305 m/s. The second higher mode in ZnO starts at h/λ = 0.275 resulting in VP_{T2} with SAW phase velocity of 5335 m/s. As the height of ZnO increases, higher order transverse modes excited in ZnO result in additional VP modes in silicon. VP_{T3} and VP_{T4} modes are generated at h/λ = 0.59 and h/λ = 0.775 with SAW phase velocities of 5332 m/s and 5328 m/s respectively. The plot also shows that the higher cutoff at the point where phase velocity equals the shear bulk velocity in silicon (5653 m/s).

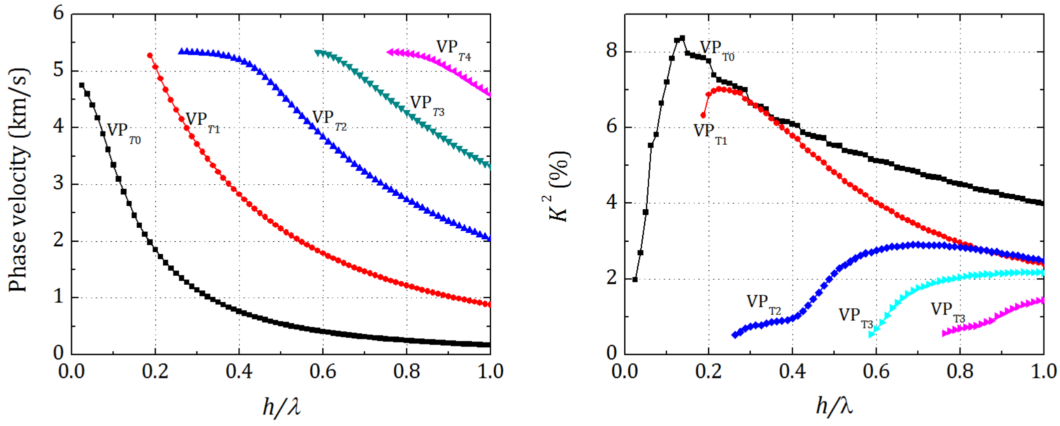

Fig. 3.7. The phase velocity and coupling coefficient dispersion curves of vertically polarized modes generated in silicon by the transverse bulk waves excited in ZnO pattern.

The K^2 dispersion curves of the first five vertically polarized modes generated in the structure are shown in the Fig. 3.7(b). For VP_{T0}, the coupling coefficient K^2 starts at 2% at h/λ = 0.025 with SAW phase velocity of 4747 m/s and reaches a relative maximum of 8.37% at h/λ = 0.13 with SAW phase velocity of 2656 m/s and reduces gradually and reaches 4% at h/λ = 1. For VP_{T1}, K^2 starts from 5.9% at h/λ = 0.185 with phase velocity 5305 m/s and reaches a relative maximum value of 7% at h/λ = 0.225 with phase velocity 4672 m/s and then decreases gradually and reaches 2.4% at h/λ = 1 with phase velocity of 876 m/s. For VP_{T2}, K^2 starts from 0.59% at h/λ = 0.275 with phase velocity of 5335 m/s and reaches a relative maximum of 3% at h/λ = 0.7 with phase velocity of 3218 m/s, as the ZnO height increases the K^2 decreases and reaches a value of 2.48% at h/λ = 1 with phase velocity 2044 m/s. For VP_{T3}, K^2 starts from 0.52% at h/λ = 0.59 with phase velocity of 5333 m/s and reaches a value of 2.16% at h/λ = 1 with phase velocity of 3320 m/s. For VP_{T4} the K^2 starts from 0.56% at h/λ = 0.775 with phase velocity 5328 m/s and it reaches a value of 1.49% at h/λ = 1 with phase velocity of 4586 m/s.

3.2.6 Surface modes generated due to longitudinal bulk waves in ZnO pattern

The SAW phase velocity dispersion characteristics of the first three modes generated by longitudinal bulk waves along ZnO pattern on silicon are shown in Fig. 3.8(a). The SAW phase velocity of generated modes depends on the longitudinal mode excited in ZnO structure. The phase velocity of VP_{L0} is 4767 m/s at h/λ = 0.025 and decreases with increase in ZnO height, VP_{L1} starts at h/λ = 0.425 with phase velocity 5319 m/s and decreases with increase in ZnO height. The VP_{L2} mode starts at h/λ = 0.9 with SAW phase velocity of 5331 m/s. Since the acoustic velocity of longitudinal wave in ZnO is greater than the acoustic velocity of transverse bulk wave, the longitudinal modes are found at larger heights of ZnO.

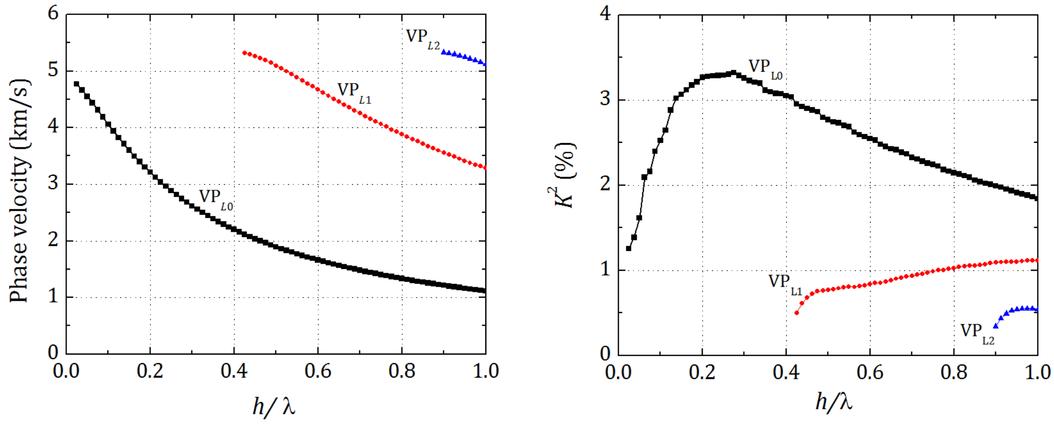

Fig. 3.8. The phase velocity and coupling coefficient dispersion curves of vertically polarized modes generated in silicon by longitudinal bulk waves excited in patterned ZnO.

The K^2 dispersion curves of first three vertically polarized surface modes generated by longitudinal waves in ZnO are shown in the Fig. 3.8(b). For VP_{L0} K^2 starts from 1.25% at h/λ = 0.025 with phase velocity of 4767 m/s and reaches a relative maximum of 3.3% at h/λ = 0.26 with phase velocity of 2815 m/s and decreases gradually with the increase in ZnO height. For VP_{L1} K^2 starts from 0.5% at h/λ = 0.425 with phase velocity of 5319 m/s and saturates at 1.1% at h/λ = 1 with phase velocity of 3282 m/s. VP_{L2} starts with K^2 of 0.34% at h/λ = 0.9 with phase velocity of 5332 m/s and reaches 0.54% at h/λ = 1 with phase velocity of 5121 m/s. For the generated SAW modes, the phase velocities at the point where K^2 reaches the relative maximum are summarized in Table 3.1. The surface waves generated by the transverse waves in ZnO exhibits high coupling coefficient up to 8.37% compared with conventional layered configuration ZnO/Si which has maximum K^2 of 3.3% [20]. VP_{T1} exhibits encouraging result of high phase velocity of 5272 m/s with high coupling coefficient of 6.4% at h/λ = 0.19. Therefore using these values and the equivalent circuit model, IDTs are designed and fabricated to have 50 Ω load impedance for one-port and two-port resonators and delay lines, as described in section 3.5.

3.2.7 Temperature coefficient of frequency

The temperature coefficient of frequency (TCF) is investigated for patterned-ZnO/Si structure and ZnO/IDT/Si conventional structure and the results shown in Fig. 3.9. The TCF calculation is as follows [20, 77]

$$\text{TCF}=\frac{(v_{35}-v_{15})}{20*v_{25}}$$

Where v_{15}, v_{25}, and v_{35} represents the phase velocity of surface waves in the structure at temperatures 15°C, 25°C, and 35 °C respectively. The phase velocities are obtained having electrically short circuit condition of electrodes.

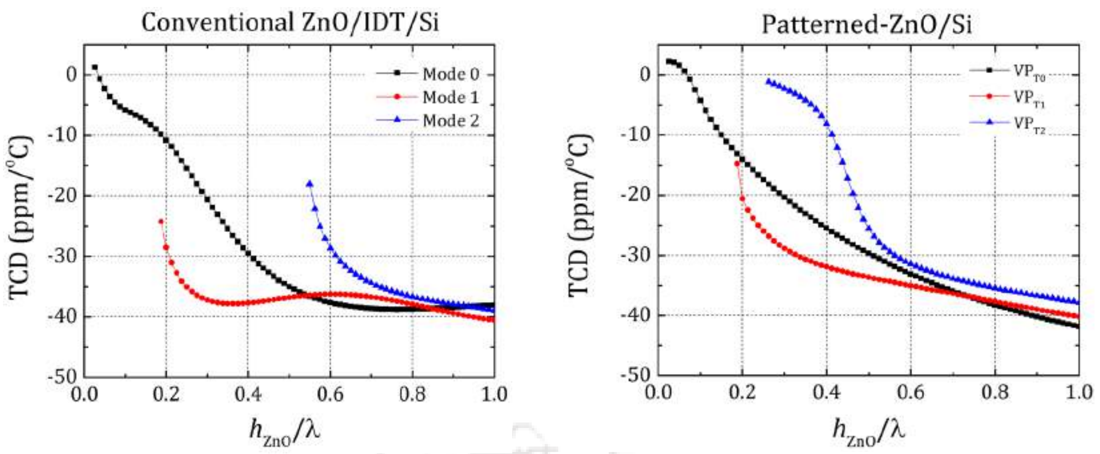

Fig. 3.9. TCD dispersion characteristics of surface modes generated conventional ZnO/IDT/Si and VP_T modes in patterned-ZnO/Si structure.

3.2.8 Observations from 3D and 2D simulation results

1. In ZnO, the shear coupling along *c*-axis is negligible and with the application of electric field only longitudinal bulk wave are excited and their acoustic coupling with silicon substrate results in the generation of surface waves in the silicon substrate.
2. Two types of bulk modes are observed in ZnO pattern and the transverse bulk wave exhibits high displacements compared to longitudinal bulk wave, due to the dominant cross-field generated across the ZnO pattern.
3. The above fact is verified with the admittance characteristics which show two dominant admittance peaks corresponding to the surface modes generated by the transverse bulk waves excited in the ZnO pattern and one insignificant admittance peak corresponding to the surface mode generated by the longitudinal bulk wave excited in the ZnO pattern.
4. VP_{T0} at h/λ = 0.13 exhibits maximum coupling coefficient of 8.37% which is 2.5 times higher than the maximum coupling coefficient in conventional SAW devices fabricated with ZnO film on silicon substrate.
5. VP_{T1} exhibits unique property of high phase velocity of 5272 m/s with high coupling coefficient of 6.4% at h/λ = 0.19.
6. From the phase velocity dispersion curves, we observe that the surface modes generated by the ZnO pattern are highly dispersive with respect to height of ZnO. In general, highly dispersive devices exhibit higher sensitivity, hence high sensitivity sensors can be realized on silicon using the proposed periodically patterned-ZnO film.

7. From the TCF characteristics VP_{T0} exhibit zero TCF at h/λ = 0.06 with phase velocity of 5272 m/s and coupling coefficient of 6%.

Table 3.1 Characteristics of surface modes generated in the proposed structure and conventional ZnO/Si layered structure at high coupling coefficient.

Configuration/ Mode	K^2 (%)	SAW phase velocity (m/s)	h/λ	TCF (ppm/℃)
Patterned-ZnO/Si structure (Transverse mode in ZnO)				
VP_{T0}	6	4400	0.06	0
	8.37	2656	0.13	-9
VP_{T1}	6.4	5272	0.19	-14.7
	7	**4672**	**0.225**	**-23.8**
VP_{T2}	0.59	5326	0.26	-1.1
	3	5008	0.65	-32.8
VP_{T3}	2.3	3880	0.87	-34.7
VP_{T4}	1.49	4586	1	-32.4
Patterned-ZnO/Si structure (Longitudinal mode in ZnO)				
VP_{L0}	3.3	2887	0.25	-10.2
VP_{L1}	1.1	3282	1	-35.6
VP_{L2}	0.54	5121	1	-29.6
Conventional ZnO/Si layered structure				
ZnO/IDT/Si (Mode 0)	0.9	4619	0.04	0
	3	3231	0.30 [20]	-20.6
IDT/ZnO/Si (Mode 1)	3.37	5258	0.28 [54]	-41

3.3 Addition of a buffer layer in patterned-ZnO/Si structure

We employed a buffer layer of SiO_2, a material easy to grow on silicon, in between ZnO pattern and silicon substrate, and the results of FE simulations show that the required thickness of ZnO for a given operating frequency of the SAW device is reduced nearly by 50% and velocity dispersion with respect to ZnO thickness is also reduced. The reduction in ZnO thickness is beneficial for the following reasons, SiO_2 layer on silicon has shown to improve the quality of ZnO film [61]. In addition, inclusion of buffer layer reduces the practical limitations in ZnO deposition process, like thickness of ZnO, radial non-uniformity in ZnO film thickness and deviation from the targeted thickness due to uncertainty in deposition parameters (e.g. temperature, working pressure, and fluctuations in RF source) make it difficult to reproduce the film with the same quality and uniformity for bulk manufacturing. In addition, the inclusion of buffer layers provides better wave guiding of generated surface waves and in turn decreases the propagation losses and radiation of acoustic energy in to the bulk of silicon substrate.

3.3.1 Patterned-ZnO/SiO₂/Si structure

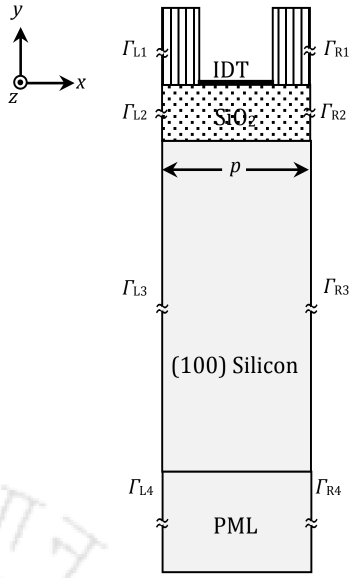

Fig. 3.10. 2D Geometry of the proposed device with SiO_2 layer used for the simulation with periodic boundary conductions.

To obtain the dispersion characteristics of proposed patterned-ZnO/Si structure with the inclusion of oxide buffer layer, 2D FE simulations are performed over a periodic structure of one port resonator and 2D geometry of the structure is shown in Fig. 3.10. The dimensions of IDT are the same as described in Section 3.2.1, and the simulation methodology is as described in Section 3.2.2, except SiO_2 buffer layer is added in the structure. In the simulations, oxide layer is considered as a non-piezoelectric material and the material parameters like density, Young's modulus, and dielectric constants are adapted from Nakahata *et al.* [22] and the details of elastic constants are included in Appendix A. Eigenmode analysis is performed on the 2D structure for various thicknesses of oxide film ranging from 0.2 μm to 2.4 μm with the parametric sweep of ZnO height in the range of 0.1λ–1λ. The phase velocity and K^2 dispersion curves of VP surface modes generated by the mode conversion of transverse bulk waves in the patterned-ZnO/0.2μm-SiO_2/Si structure are shown in Fig. 3.11. From the dispersion curves we observe that the phase velocities are slightly reduced after inclusion of oxide layer and a significant decrease in K^2 value of VP_{T0} from 8.4 % to 4.4 % is observed, however very small reduction in K^2 values of other VP modes generated in the structure is observed. Interestingly, the surface mode VP_{T2} exhibits slight non-dispersive characteristics within h/λ range of 0.25–0.36 with K^2 values ranging between 0.76%–0.86%

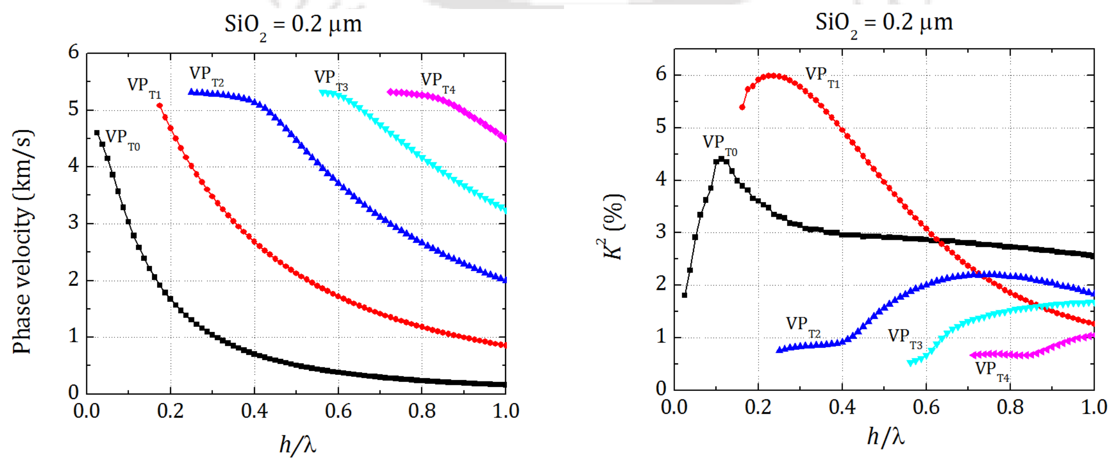

Fig. 3.11. The phase velocity and K^2 dispersion curves of vertically polarized modes generated in patterned-ZnO/0.2μm-SiO_2/Si structure due to transverse bulk waves excited in ZnO pattern.

and phase velocity ranging between 5313 m/s–5224 m/s. Further simulations are carried out with various thicknesses (0.8 μm, 1.6 μm, and 2.4 μm) of SiO_2 film and their dispersion characteristics are shown in Fig. 3.12. From the dispersion characteristics of surface modes, it is observed that the phase velocity and coupling coefficient values decrease gradually with increase in the oxide thickness. At oxide thickness of 0.8 μm (0.1λ), the second higher order mode VP_{T2} exhibits an exciting characteristics of almost constant phase velocity over

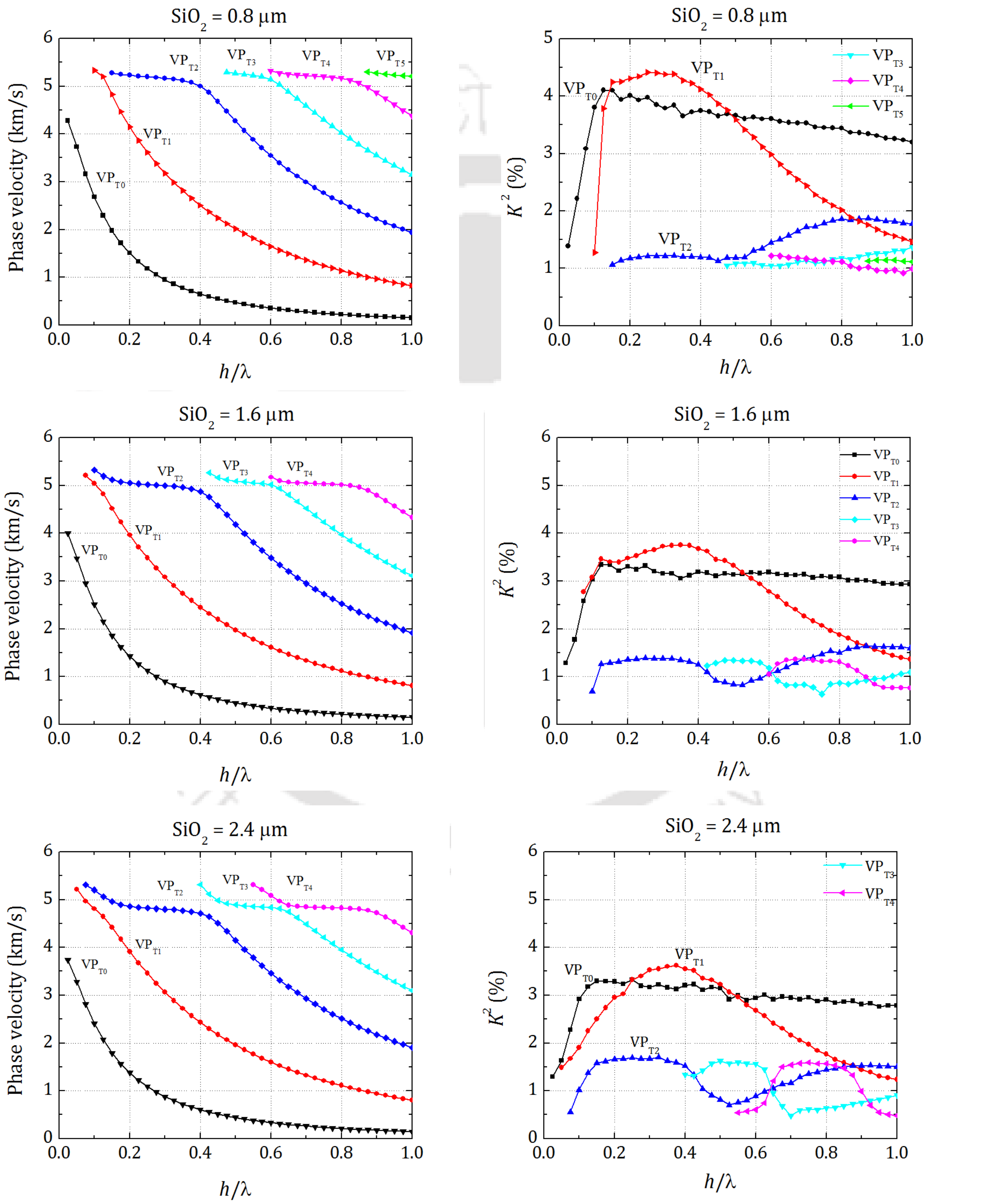

Fig. 3.12. Phase velocity and coupling coefficient characteristics of patterned-ZnO/SiO_2/Si structure with SiO_2 thicknesses of 0.8 μm, 1.6 μm, and 2.4 μm.

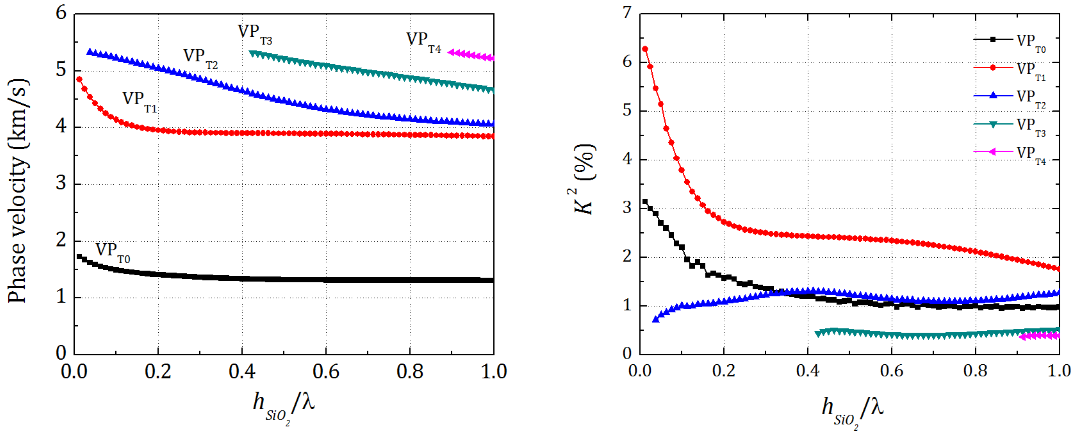

Fig. 3.13. The phase velocity and K^2 dispersion curves of VP modes generated in patterned-ZnO/SiO_2/Si structure due to transverse bulk waves excited in ZnO pattern obtained with the parametric sweep of SiO_2 thickness (h_{SiO_2}/λ) for a constant ZnO height of 1.6 μm (0.2λ) which has shown high K^2.

a wide range of h/λ (0.2–0.4) with reasonably high coupling coefficient. Other higher order modes generated in the structure exhibit similar characteristics at higher thicknesses of ZnO, which is difficult to obtain in practice. Further eigenmode analysis is carried out on the proposed structure with parametric sweep of SiO_2 thickness for a constant ZnO height of 0.2λ which has shown high K^2. The obtained phase velocity and coupling coefficient characteristics of the surface modes are shown in Fig. 3.13. The characteristics of all the surface modes generated in the structure and notable observations in phase velocity and coupling coefficient values are listed in Table 3.2. From the dispersion characteristics obtained with respect to the thickness of oxide layer shown in Fig. 3.13, we observe that the phase velocities of surface modes VP_{T0} and VP_{T1} are independent of SiO_2 film thickness after h_{SiO_2}/λ = 0.2, at which both the surface modes exhibit non-dispersive nature, as the energy is substantially concentrated within the guiding layer. The phase velocity of other surface modes reduces gradually with increase in thickness of SiO_2 film and reaches the surface wave velocity of bulk SiO_2. From the K^2 dispersion curves shown in Fig. 3.13, we observe that K^2 decreases gradually with increase in the thickness of oxide layer and for VP_{T0} and VP_{T1} the K^2 values are saturated to 1% and 2.5% respectively beyond h_{SiO_2}/λ = 0.5. In case of VP_{T2} the K^2 values starts at 0.76% and increases up to 1.4% at h_{SiO_2}/λ = 0.4 and reaches to a value 1.2% at h_{SiO_2}/λ = 1. VP_{T3} and VP_{T4} modes exhibit very low coupling coefficient but high phase velocities. However, the addition of SiO_2 buffer layer has resulted in lower K^2 value due to the large difference in acoustic impedances between ZnO (15.53 M Rayl) and SiO_2 layer (8.28 M Rayl) than between ZnO and silicon (13.6 M Rayl). To improve K^2, we replace the SiO_2 buffer layer with a layer of AlN, as its acoustic impedance is (18.32 M Rayl) close to ZnO and it is also a piezoelectric material having higher acoustic velocity (5620 m/s) than silicon substrate (4921 m/s).

Table 3.2 The notable observations from phase velocity and K^2 characteristics given in Fig. 3.10, Fig. 3.11, and Fig. 3.12.

Device configuration	Surface mode	h/λ	Phase velocity (m/s)	K^2 (%)	TCF (ppm/°C)	Comments
Patterned-ZnO/IDT/0.2 µm-SiO_2/Si (Fig. 3.10)	VP_{T0}	0.11	2789	4.6	-7.67	Maximum K^2 value.
	VP_{T0}	0.037	4630	2.3	0	Zero temperature coefficient.
	VP_{T0}	1	160	2.56	-41.5	Low phase velocity is due the reduction in mode frequency of ZnO with increase in height.
	VP_{T1}	0.162	5078	5.4	-15.4	Beginning of mode and shows high K^2 and high phase velocity.
	VP_{T1}	0.22	4873	6	-24	Maximum K^2 value.
	VP_{T1}	1	851	1.26	-43.9	Low phase velocity is due the reduction in mode frequency of ZnO with increase in height.
	VP_{T2}	0.25–0.36	5313–5224	0.8	-4.3 to -9.6	**Non-dispersive region, where ΔV is very small, and small variations in K^2 and TCF.**
Patterned-ZnO/IDT/ 0.8µm-SiO_2/Si (Fig. 3.11)	VP_{T0}	0.125	2294	4.1	-7.31	Maximum K^2 value.
	VP_{T0}	1	152	1.3	-37.1	Low phase velocity is due the reduction in mode frequency of ZnO with increase in height.
	VP_{T1}	0.1	5329	1.27	-2.12	Beginning of mode and low TCF.
	VP_{T1}	0.15	4829	4.24	-10.2	High K^2 and good phase velocity.
	VP_{T1}	0.25	3613	4.4	-18	Maximum K^2 value.
	VP_{T1}	1	1937	0.7	-41.2	Low phase velocity is due the reduction in mode frequency of ZnO with increase in height.
	VP_{T2}	0.15	5276	1	-2.21	Beginning of higher order mode.
	VP_{T2}	0.2–0.4	5228–5002	1.2	**-3.4 to -11**	**Non-dispersive region, where ΔV is very small, and constant K^2.**
	VP_{T2}	1	3148	1.7	-38.5	Lower phase velocity is due the reduction in mode frequency of ZnO with increase in height.

	VP_{T0}	0.125	2153	3.3	-6.54	Maximum K^2 value.
	VP_{T0}	1	147	1.84	-35.1	Low phase velocity is due the reduction in mode frequency of ZnO with increase in height.
	VP_{T1}	0.07	5207	2.8	-2	Beginning of surface mode.
	VP_{T1}	0.12	4822	3.46	-5	High K^2 and good phase velocity.
Patterned-ZnO/IDT/1.6 μm-SiO_2/Si (Fig. 3.11)	VP_{T1}	0.25	3483	3.61	-18	Maximum K^2 value.
	VP_{T1}	1	812	1.36	-41	Low phase velocity is due the reduction in mode frequency of ZnO with increase in height.
	VP_{T2}	0.1	5322	0.69	-0.5	Beginning of surface mode and low TCF.
	VP_{T2}	0.12–0.3	5192–4993	1.26	**-2 to -5**	**Non-dispersive region, change in phase velocity is very small, and constant K^2.**
	VP_{T2}	1	1914	1.6	-38.4	Lower phase velocity is due the reduction in mode frequency of ZnO with increase in height.
	VP_{T0}	0.025	3831	1.3	-0.1	Low TCF.
	VP_{T0}	0.15	1793	3.3	-7.3	Maximum K^2 value.
	VP_{T0}	1	145	2.78	-34.1	Low phase velocity is due the reduction in mode frequency of ZnO with increase in height.
	VP_{T1}	0.05	5214	1.49	0	Zero TCF and high phase velocity.
Patterned-ZnO/IDT/2.4 μm-SiO_2/Si (Fig. 3.11)	VP_{T1}	0.375	4749	3.62	-26.6	High K^2 and good phase velocity.
	VP_{T1}	1	805	1.23	-41.2	Low phase velocity is due the reduction in mode frequency of ZnO with increase in height.
	VP_{T2}	0.1	5307	0.56	0	Beginning of VP_{T2} mode and zero TCF.
	VP_{T2}	0.15–0.4	4960–4713	1.58	**-3.6 to -8.56**	**Non-dispersive region, where Δv is very small, and constant K^2.**
	VP_{T2}	1	1903	1.5	-38.5	Low phase velocity is due the reduction in mode frequency of ZnO with increase in height.
	VP_{T0}	0.01	1726	3.13	-15.3	Maximum K^2 value.
	VP_{T0}	0.41	1320	1	-9.4	Phase velocity is saturated at 1320 m/s as well as K^2 at 1%.
Patterned-1.6μm-ZnO/IDT/SiO_2/Si (Fig. 3.12)	VP_{T1}	0.01	4851	6.28	-15.8	Beginning of mode, high K^2 and good phase velocity.
	VP_{T1}	0.3	3900	2.5	-13.1	Both phase velocity and K^2 saturates at 3900 m/s and 2.5%.
	VP_{T2}	0.03	5320	0.7	-2.8	Exhibits relative maximum velocity and low coupling coefficient.
	VP_{T2}	1	4058	1.2	-6.2	The phase velocity decreases linearly and reached 4058 m/s with a K^2 value of 1.2.

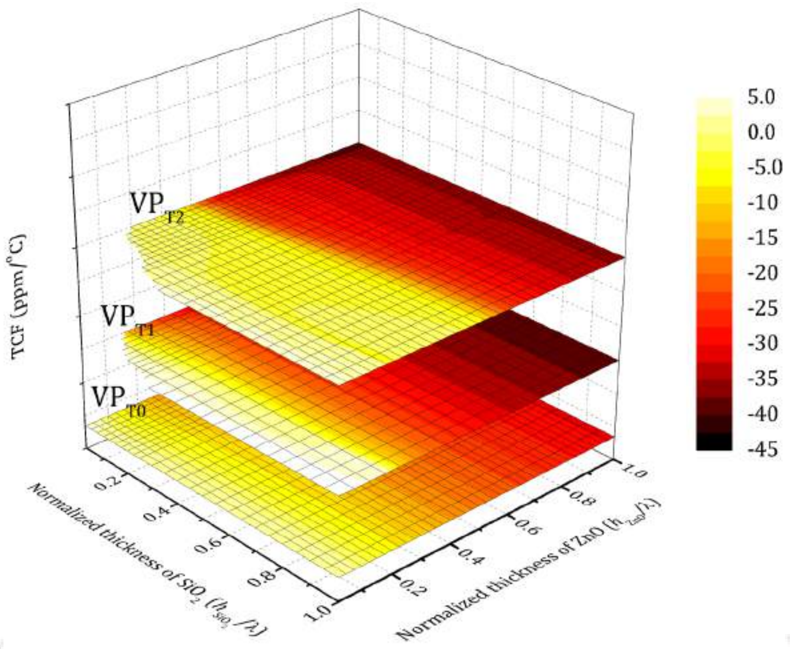

Fig. 3.14. The TCF dispersion characteristics of first three VP_T surface modes generated in the patterned-$ZnO/SiO_2/Si$ structure as a function of ZnO and SiO_2 thicknesses.

3.3.2 ZnO-patterned/AlN/Si structure

As discussed above, we employ aluminum nitride (AlN) as a buffer layer in the proposed structure because its acoustic impedance is close to ZnO and it is a piezoelectric material widely used to implement SAW devices on silicon for high frequency applications. However, the coupling coefficient of AlN is low [2] compared to ZnO and also requires reactive sputtering for film deposition.

To the study the effect of addition of buffer layer of AlN film in the proposed structure, 2D FE simulations are carried on the patterned-ZnO/AlN/Si structure to obtain the phase velocity and coupling coefficient dispersion characteristics with respect to ZnO height. The simulations described in the previous section are repeated with AlN as the buffer layer instead of SiO_2. For initially study, we assumed λ/4 thickness of AlN, at which the AlN/Si structure exhibits non-dispersive nature with maximum phase velocity that can be attained with silicon substrate [2] and 2D geometry used for the eigenmode analysis is shown in Fig. 3.15.

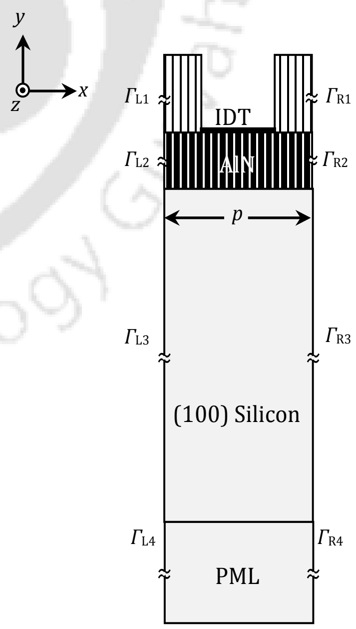

Fig. 3.15. 2D Geometry of the periodic section of proposed device with AlN buffer layer for the simulation.

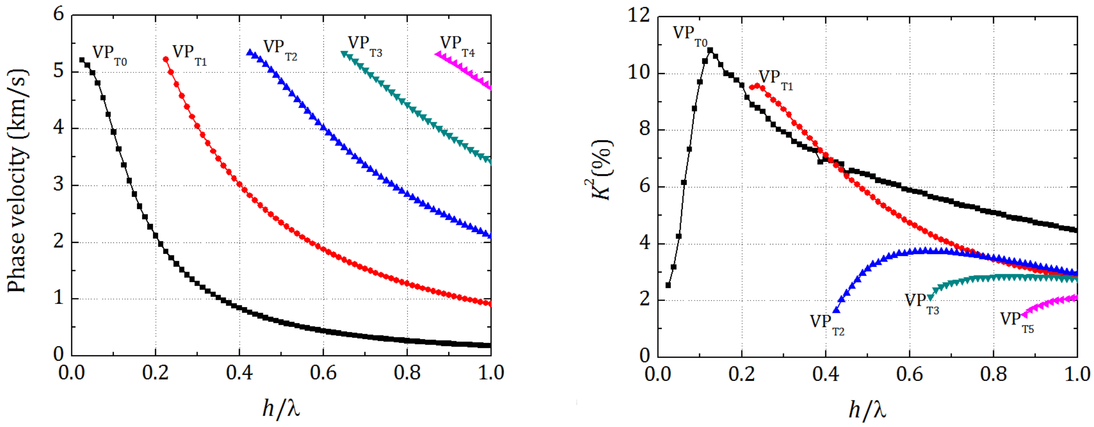

Fig. 3.16. The phase velocity and K^2 dispersion curves with respect to height of ZnO in patterned-ZnO/ 4µm-AlN/Si structure.

The geometry comprises of thin film of AlN deposited over the silicon substrate and IDT structure patterned over it, followed by the deposition and patterning of ZnO film. In these simulations, we assume that the ZnO is located exactly in the spaces of IDT. The phase velocity and K^2 dispersion curves are obtained using eigenmode analysis and results are shown in Fig. 3.16. From the characteristics, we observe that the patterned-ZnO/AlN/Si structure exhibits high coupling coefficient values compared to conventional thin film AlN/Si structure and the resultant phase velocity depends on the frequency of bulk modes generated in the ZnO pattern. With increase in height of ZnO, the phase velocity of generated SAW decreases rapidly due to the decrease in frequency of bulk modes excited in ZnO structure. As the height of ZnO increases the VP_{T0} surface mode tends to reach the frequency of ZnO structure.

The higher order transverse mode in ZnO results in generation of VP_{T1} in the structure at $h/\lambda = 0.225$, with SAW phase velocity of 5223 m/s. The second higher mode in ZnO starts at $h/\lambda = 0.425$ resulting in VP_{T2} with SAW phase velocity of 5336 m/s. As the height of ZnO increases, higher order transverse modes generated in ZnO result in corresponding VP modes. VP_{T3} and VP_{T4}modes are generated at $h/\lambda = 0.65$ and $h/\lambda = 0.875$ with SAW phase velocities of 5335 m/s and 5316 m/s respectively. The maximum phase velocity of VP modes generated in the structure is equal to shear bulk velocity in silicon (5653 m/s).

The K^2 dispersion curves of the first five vertically polarized modes generated in the structure are shown in the Fig. 3.16. For VP_{T0}, the coupling coefficient K^2 starts at 2.5% at $h/\lambda = 0.025$ with SAW phase velocity of 5212 m/s and reaches a relative maximum of 10.8% at $h/\lambda = 0.125$ with SAW phase velocity of 3359 m/s and reduces gradually and reaches 4.4% at $h/\lambda = 1$. For VP_{T1}, K^2 starts from 9.5% at $h/\lambda = 0.225$ with phase velocity 5223 m/s

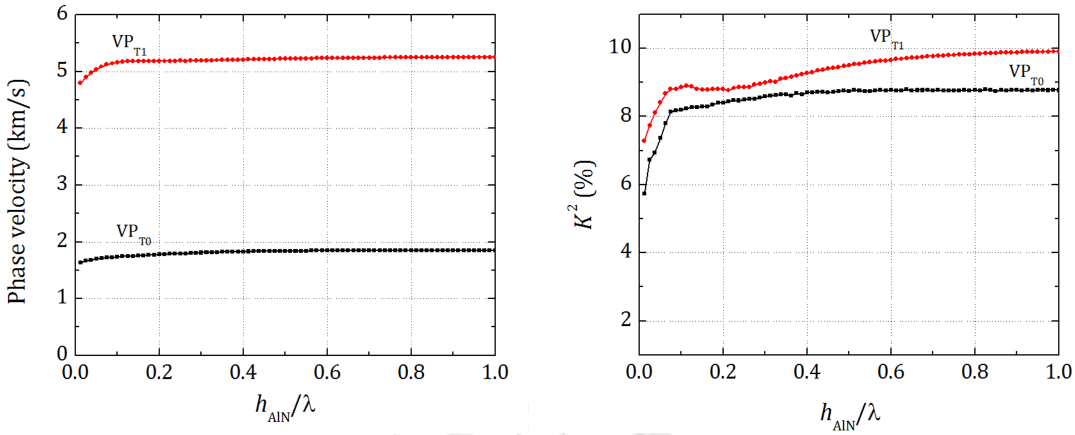

Fig. 3.17. The phase velocity and K^2 dispersion curves of vertically polarized modes generated by transverse bulk waves in patterned-1.6μm-ZnO/AlN/Si structure.

and reaches a relative maximum value of 9.56% at h/λ = 0.24 with phase velocity 4996 m/s and then decreases gradually and reaches 2.8% at h/λ = 1 with phase velocity of 909 m/s. For VP_{T2}, K^2 starts from 1.63% at h/λ = 0.425 with phase velocity of 5336 m/s and reaches a relative maximum of 3.7% at h/λ = 0.6 with phase velocity of 4016 m/s and reaches a value of 2.94% at h/λ = 1 with phase velocity 2110 m/s. For VP_{T3}, K^2 starts from 2.13% at h/λ = 0.65 with phase velocity of 5335 m/s and reaches a value of 2.76% at h/λ = 1 with phase velocity of 3422 m/s. For VP_{T4} the K^2 starts from 1.5% at h/λ = 0.875 with phase velocity 5316 m/s and at h/λ = 1 it reaches a value of 2.1% with phase velocity of 4718 m/s. In general, the K^2 values are slightly higher than pattern-ZnO/Si structure, because the AlN buffer layer is piezoelectric in nature as well as it exhibits higher acoustic velocity than silicon.

Further we carried out FE simulations on proposed structure with fixed ZnO height and varying the AlN thickness to study the phase velocity and coupling coefficient characteristics. We consider IDT wavelength of 8 μm and ZnO height of 0.225λ, where the device exhibits high phase velocity and high coupling coefficient. The obtained characteristics are shown in Fig. 3.17. From the dispersion curves, we observe that two transverse modes (VP_{T0} and VP_{T1}) are generated in the structure and their phase velocities saturate at 1800 m/s and 5180 m/s respectively as AlN thickness increases. The K^2 of VP_{T0} starts from 5.7% and reaches to 8.7% at h/λ = 1 and VP_{T1} starts from 8.67% at h/λ = 0.0125 and reaches 9.9% at h/λ = 1. From the above simulations, we can conclude that the phase velocity of the surface modes generated in the proposed structure depends on the modes excited in the ZnO pattern and its resonant frequency. As the patterned structures exhibit high resonant frequencies, buffer layers with high acoustic velocity are recommended in order to obtain high coupling and high phase velocity.

3.3.3 Observations from the study of inclusion of buffer layer (SiO_2 and AlN)

The results and observations from the FE simulations of proposed patterned-ZnO/Si SAW devices with the addition of buffer layer are summarized as follows:

1. The dispersion characteristics of patterned-ZnO/SiO_2/Si show a reduction in coupling coefficient values compared with patterned-ZnO/Si, due to the large acoustic impedance difference between ZnO block and SiO_2.
2. A wide non-dispersive region is observed in the range of 0.2–0.4 of h/λ for patterned-ZnO/0.8μm-SiO_2/Si structure with an acceptable coupling coefficient range of 0.8%–0.86%. The drawback of low coupling coefficient can be overcome by using IDT with large number of finger pairs.
3. The dispersion characteristics of patterned-ZnO/AlN/Si show a substantial increase in coupling coefficient values, viz. VP_{T0} exhibits a maximum value of 10.8% at h/λ = 0.125 with SAW phase velocity of 3359 m/s and VP_{T1} exhibits a high K^2 value of 9.5% at h/λ = 0.225 with high phase velocity of 5223 m/s.
4. The results show that the inclusion of AlN buffer layer improves the coupling coefficient significantly compared with SiO_2 layer. So, buffer layers with high acoustic velocity are recommended in order to obtain high coupling and high phase velocity.
5. Assuming the maximum thickness of 4 μm achievable in ZnO film deposition using RF sputtering, the SAW device with maximum λ of 16 μm can be fabricated with patterned-4μm-ZnO/0.8μm-AlN/Si structure with unique property of high phase velocity and high coupling coefficient.
6. The phase velocity characteristics are predominantly depend on the dimensions of ZnO pattern rather than the thickness of buffer layer (SiO_2 and AlN).

3.4. 2D simulation of SAW delay line on silicon using periodically patterned ZnO

SAW resonator configuration with periodically patterned-ZnO on silicon substrate is demonstrated in section 3.2. In this section, we employ the proposed patterned-ZnO structure to realize, another popular SAW device, i.e. delay line device on silicon substrate. 2D finite element simulations are performed on delay line configuration with patterned ZnO structures in the spaces of IDT. From the phase velocity and K^2 dispersion characteristics, dimensions of IDT and ZnO pattern are chosen to obtain a surface mode with high phase velocity and high coupling coefficient. The simulation results of SAW delay line with

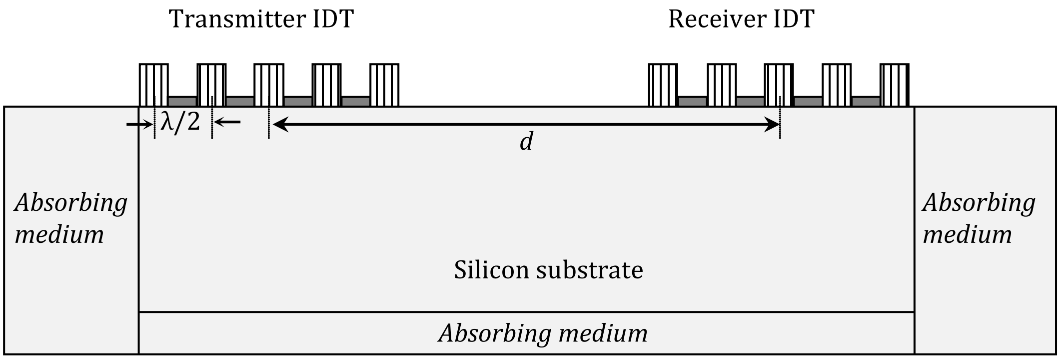

Fig. 3.18. 2D schematic of the SAW delay line device on silicon with periodically patterned ZnO in the spaces of IDT.

patterned-ZnO structure is compared with the conventional ZnO thin film SAW delay line on silicon substrate (Section 2.4.7).

3.4.1. Simulation methodology

A delay line with 4λ center to center distance between input and output IDTs having ZnO blocks in the spaces of the IDT fingers is consider for simulation. The dimensions of delay line are as follows: pitch of 4 μm (λ = 8 μm), metallization ratio of 0.5, and thickness of IDT electrodes 0.1 μm and substrate depth of 5λ. The ZnO height is chosen 1.6 μm (h/λ = 0.2) which has high K^2 and phase velocity as observed in Table 3.1. Absorbing boundary conditions are used on either ends of the device to suppress the unwanted reflections from the boundaries. The 2D schematic of patterned-ZnO/IDT/Si SAW delay line structure is shown in Fig. 3.18. Fixed boundary condition is applied to the bottom boundaries of the geometry and rest all boundaries are given stress free boundary condition. Rayleigh damping boundary conditions are applied to the absorbing subdomain to absorb the generated SAW and the reflections form the edges of the device. The electrical boundary

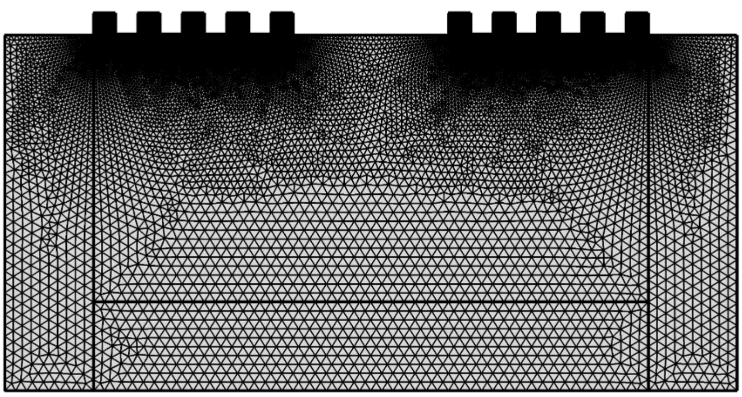

Fig. 3.19. Structure of mesh used in the simulation of the SAW delay line device with triangular elements with minimum element size of λ/10³ at ZnO-silicon interface and having growth rate of 1.09 reaching to a maximum element size of λ/8.

conditions are as follows: alternate fingers of input port are grounded and a 1 V sinusoidal driven voltage of the device resonance frequency is given to the remaining fingers [59]. From the eigenmode analysis the resonance frequency is 611.4774 MHz. Structure of the mesh used in the simulation (Fig. 3.19) consists of triangular elements with minimum element size of $\lambda/10^3$ at ZnO-silicon interface and having growth rate of 1.09 reaching to a maximum element size of $\lambda/8$. The transient analysis is carried out using the '*Generalized-alpha*' solver available in COMSOL multiphysics for duration of 50 ns with a time interval of 1 ps.

3.4.2. Results of 2D SAW delay line with patterned-ZnO structure

The surface displacement profile of delay line structure at time 12.28 ns is shown in Fig. 3.20(a). The transient *y*-displacements of particles at the center of IDT-silicon interface at input and output IDTs are shown in Fig. 3.20(b) and (c) respectively. The output voltage of 0.1 V is observed at the receiver IDT in Fig. 3.20(d). In SAW delay line, delay time is one of the important parameters and is estimated from the time difference between the first peak of waveforms in Fig. 3.20(b) and (c). The delay observed is about 3 ns. Assuming SAW velocity in silicon 4921 m/s [54] the calculated delay is 3.25 ns. However, the input and output displacements are low in comparison with the conventional ZnO/Si delay line and is due to considerable radiation of acoustic energy into the bulk of the silicon substrate in case of patterned-ZnO structure. This acoustic radiation can be reduced by employing a guiding layer [3], e.g. thin film of SiO_2 or AlN. Fig. 3.20 shows the *y*-displacement surface profiles of SAW delay with patterned-2μm-ZnO/2μm-SiO_2/Si structure. The inclusion of SiO_2 buffer layer has reduced the acoustic radiation into bulk and increased acoustic energy concentration near the surface as compared to the displacement profile of patterned-ZnO/IDT/Si SAW delay line shown in Fig. 3.20(a). However, the input and output displacements are low in comparison with the conventional ZnO/Si delay line and is due to considerable radiation of acoustic energy into the bulk of the silicon substrate in case of patterned-ZnO structure. This acoustic radiation can be reduced by employing a guiding layer [3], e.g. thin film of SiO_2 or AlN. Fig. 3.20 shows the *y*-displacement surface profiles of SAW delay with patterned-2μm-ZnO/2μm-SiO_2/Si structure. The inclusion of SiO_2 buffer layer has reduced the acoustic radiation into bulk and increased acoustic energy concentration near the surface as compared to the displacement profile of patterned-ZnO/IDT/Si SAW delay line shown in Fig. 3.21(a).

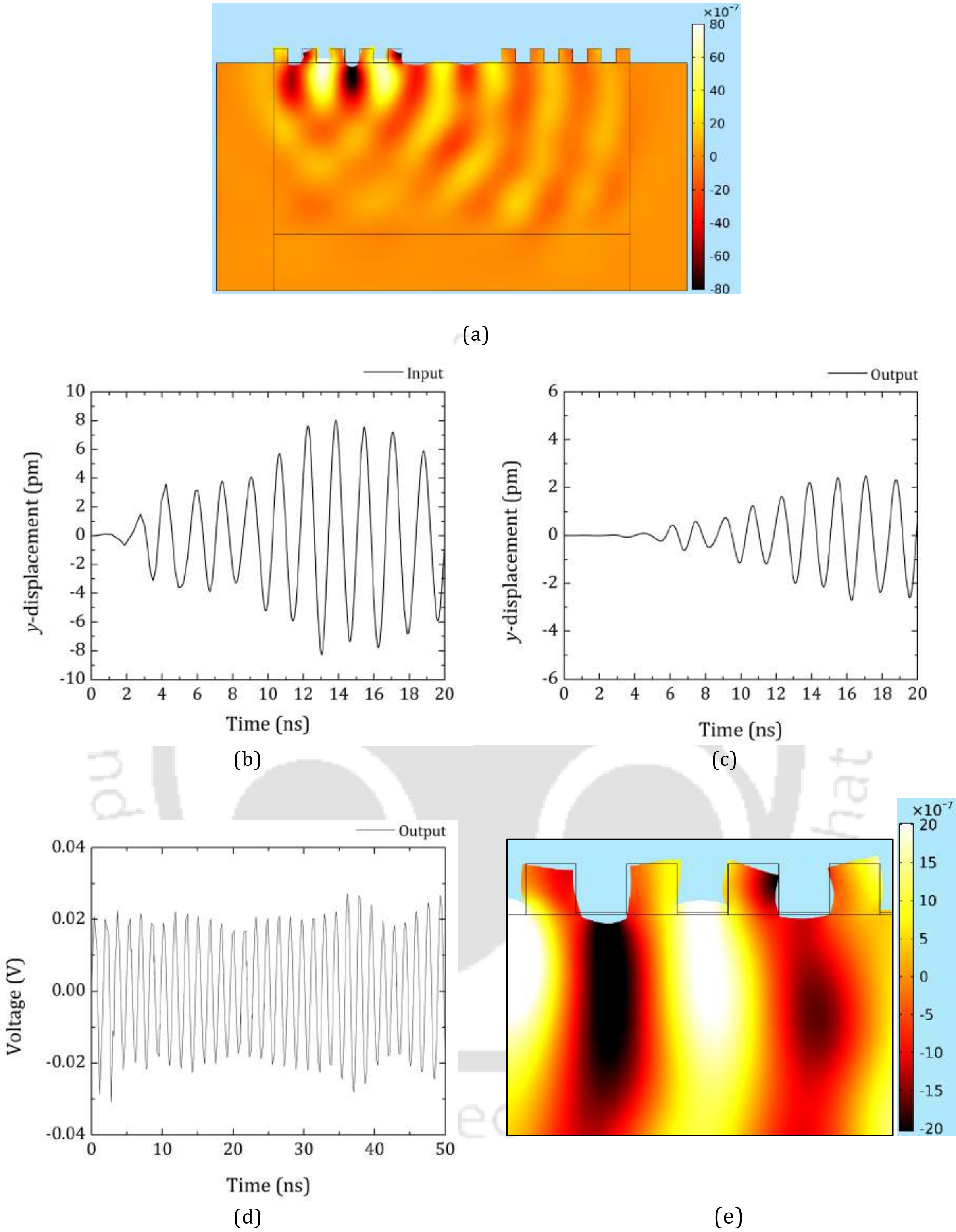

Fig. 3.20. (a) y-displacement profile of patterned-ZnO/IDT/Si SAW delay line at 27.7 ns, color legend displacement units are in μm, (b) transient y-displacement profile of a particle at input IDT-silicon interface, (c) transient y-displacement profile of a particle at output IDT-silicon interface, (d) output voltage obtained at output IDT with respect to time, and (e) magnified view of output IDT with deformation shows SAW in silicon been converted to first higher order transverse BAW in ZnO

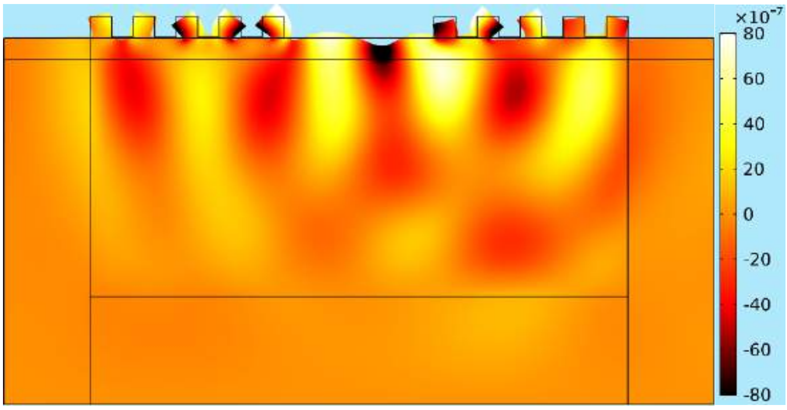

Fig. 3.21. *y*-displacement profile of patterned-ZnO/IDT/2μm-SiO_2/Si SAW delay line at 34.16 ns. Addition of SiO_2 buffer layer has reduced the acoustic radiation into bulk and increased acoustic energy concentration near the surface as compared to the results shown in Fig. 3.18 (a) for patterned-ZnO/IDT/Si SAW delay line.

3.5 Design of proposed patterned-ZnO/Si SAW devices using equivalent circuit model

The equivalent circuit model of a section of proposed periodically patterned-ZnO SAW devices on silicon with oxide buffer layer is shown in Fig. 3.22. The equivalent circuit has been modeled based on the equivalent circuit models of SAW devices reported by Nordin [29], Thompson [5], and Venema [62]. The equivalent circuit model of a conventional SAW device has been discussed in Chapter 2. The acoustic wave propagation is modeled by a series RLC circuit in parallel with a parasitic capacitor (C_0), and R_x, L_x, C_x, define the radiation resistance, motional inductance and motional capacitance respectively. C_{ox} exists due to the presence of oxide layer in the structure and is formed between source electrode and ground electrode. The oxide capacitance C_{ox} is given by

$$C_{ox} = W\varepsilon_{ox}N_P \tag{3.4}$$

where W is the aperture length of the IDT, ε_{ox} is the permittivity of oxide layer and N_P is the number of finger pairs in the IDT.

The total transducer capacitance (C_T) for the proposed structure with an oxide film is given by

$$C_T = W\varepsilon_{ZnO}(2N_P - 1) + C_{ox} \tag{3.5}$$

where ε_{ZnO} is the permittivity of ZnO and is equal to 135 pF/m [26], and $W\varepsilon_{ZnO}(2N_P - 1)$ is equivalent to transducer capacitance without oxide layer.

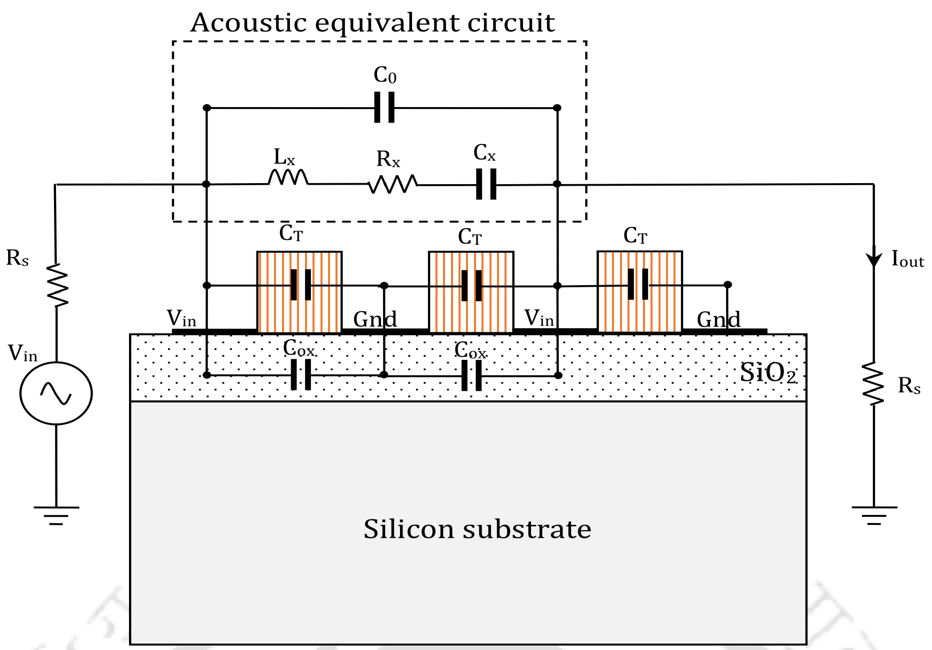

Fig. 3.22. Equivalent circuit model of the proposed ZnO-patterned structure on silicon with oxide layer.

A sinusoidal input V_{in} is applied to IDT results in excitation of bulk waves inside the ZnO pattern and the bulk waves are mode converted into surface waves that propagate along the silicon substrate. When the acoustic waves are incident at the output IDT with patterned-ZnO structure, the surface waves are converted back to bulk waves in ZnO and a portion is radiated into the bulk of silicon. The BAW excited in ZnO pattern will induce an alternating current I_{out} in the load connected to the output IDT. The ratio of I_{out}/V_{in} is known as forward admittance and real part of admittance (G_a) is known as radiation conductance [29] and is approximated as

$$G_a = 8 f_r K^2 C_T N_P \tag{3.6}$$

where K^2 is the electromechanical coupling coefficient and f_r is the resonance frequency of the device obtained from the FE simulations.

The conductance of device is given by

$$G_s(f_r) = G_a \left(\frac{1 + 2\Gamma Cos(4\pi\delta) + \Gamma^2}{1 - \Gamma^2} \right) \tag{3.7}$$

where Γ is reflection coefficient of the reflector grating structure and δ is given by $\delta = L_g + L_p + \frac{N_P \lambda}{2}$ [29] where L_g is the distance between IDT and grating structure, L_p is the penetration depth of acoustic wave along the grating, and N_p is the number of finger pairs in IDT structure. The acoustic equivalent circuit parameters are obtained as follows [29]

$$\text{Acoustic resistance Rx} = 1/G_s(f_r) \tag{3.8}$$

$$\text{Inductance Lx} = \frac{L+2L_p}{G_a v} \cdot \frac{\Gamma^2}{1+2\Gamma Cos(4\pi\delta)+\Gamma^2} \tag{3.9}$$

$$\text{Acoustic capacitance Cx} = \frac{1}{4\pi^2 f_r^2 L_x} \tag{3.10}$$

$$\text{Feed through capacitance Cf} = \frac{W\varepsilon}{L_c} \tag{3.11}$$

Using the equations (3.5 and 3.6), the number of finger pairs and the aperture length of IDT are chosen in such a way that the impedance of IDT at the operating frequency matches with the source impedance and load impedance, normally 50 Ω. The following section describes the design of SAW devices with patterned-ZnO structure on silicon.

3.5.1 Calculation of IDT parameters for proposed SAW devices on silicon

The IDT parameters for one port SAW resonators, two port SAW resonators, and SAW delay lines are calculated using above mentioned equivalent circuit model and used for device fabrication. The above mentioned equations are written in MATLAB to obtain the IDT dimensions with desired 50 Ω impedance.

From Table 3.1, it is noticed that h/λ = 0.19 exhibits high K^2 and high phase velocity for patterned-ZnO/Si structure. Hence, for the fabrication of proposed devices, the ZnO film thickness of 3.04 μm chosen for an IDT wavelength of 16 μm. In the phase velocity and K^2 characteristics, at h/λ = 0.19, VP_{T1} mode exhibits K^2 value of 6.4% and phase velocity of 5072 m/s which corresponds to the device operating frequency of 317 MHz. Substituting the values of K^2 and operating frequency in equation (3.6), aperture (W) and number of finger pairs (N_P) are calculated. In general, to reduce the diffraction effects of the generated surface waves, it is advisable to have aperture length greater than 50λ [5]. Accordingly the aperture length is decided and the respective number of finger pairs is calculated. The penetration depth of the generated surface modes is estimated by calculating reflection coefficient k, which is reflectivity of surface wave for one electrode finger in the grating structure and is given by [29]

$$k = j|0.5\,K^2|\frac{\pi}{2}\left((-\cos\Delta) + \left(\frac{P_{0.5}\,(\cos\Delta)}{P_{-0.5}\,(-\cos\Delta)}\right)\right) \tag{3.12}$$

where $\Delta = n\pi$ and n is metallization ratio.

In this design n of 0.5 is considered, Legendre polynomials $P_{0.5}(\cos\Delta) = 1.5061$ and $P_{-0.5}(-\cos\Delta) = 1.328$ are adapted from Nordin [29].

The total reflectivity of the grating structure is given by (3.10) and ideally should be ~1.

$$\Gamma = \tanh(Nk) \tag{3.13}$$

Using the reflection coefficient, the penetration depth L_p is calculated using the following formula

$$L_p = \lambda/(4|k|) \tag{3.14}$$

Using the above mentioned equations, with K^2 value of 6.4% and operating frequency 317 MHz the calculated IDT parameters are as follows

From (3.12) reflection coefficient of an electrode in the grating structure k = 0.057

Minimum number of electrodes in reflector grating (N) required to ensure complete reflection of SAW at the grating structure is calculated using (3.13), and Γ = 0.99 is assumed and the number of electrodes in grating structure N = 48.

From (3.14) calculated penetration depth L_p = 70.17 μm.

Table 3.3 Calculated IDT dimensions using equivalent circuit model.

Sr. No.	Aperture length (W)	Number of finger pairs (N)
1	55 λ	65
2	60 λ	63
3	65 λ	60
4	75 λ	58

3.6 Summary

This chapter discusses the theory and operation of the proposed periodically patterned-ZnO SAW devices on silicon substrate and mutual conversion of BAW and SAW at the interface of periodic structure and substrate. Eigenmode analysis and frequency dependent analysis are performed on 3D and 2D geometries of the proposed patterned-ZnO/Si structure to obtain the phase velocity and K^2 characteristics of surface modes generated in the structure. Results reveal the generation of vertically polarized surface modes in silicon substrate owing to the acoustic coupling of bulk waves excited in the ZnO pattern. The displacement plots from frequency dependent analysis show two types of surface modes in silicon, VP surface modes generated by transverse and longitudinal BAWs in ZnO blocks and SH modes which are insignificant compared to the VP modes. The admittance characteristics show VP modes generated by transverse BAW more dominant than the VP modes generated by longitudinal BAW in ZnO blocks, since the electric field across ZnO pattern is stronger than in-line field in proposed structure and insignificant shear coupling along the *c*-axis of ZnO. Results show that the VP surface mode generated by transverse BAW excited in ZnO pattern exhibits high phase velocity and high coupling coefficient.

SiO_2 buffer layer is employed to reduce the thickness of ZnO required to generate surface modes with high phase velocity and high coupling coefficient. FE simulations are performed to obtain the phase velocity and K^2 dispersion characteristics with respect to ZnO height and SiO_2 film thickness. Results disclose that the required ZnO height is reduced appreciably, however the addition of SiO_2 buffer layer has resulted in lower K^2 values due to the large difference in acoustic impedances between ZnO and SiO_2 layer than between ZnO and silicon. Interestingly in patterned-ZnO/0.8μm-SiO_2/Si structure, the surface mode (VP_{T2}) generated by second higher order transverse BAW in ZnO exhibits a non-dispersive nature over a wide range of ZnO thickness variations during deposition (h/λ = 0.2-0.4). The drawback of low K^2 can be overcome by employing IDT structure with large number of finger pairs.

By replacing SiO_2 with AlN for the buffer layer the K^2 values are improved, as acoustic impedance of AlN is close to ZnO, in addition, phase velocity is increased due to higher acoustic velocity in AlN than in silicon substrate. The dispersion characteristics of patterned-ZnO/AlN/Si show a substantial increase in coupling coefficient values, viz. VP_{T0} exhibits a maximum value of 10.8% at h/λ = 0.125 with SAW phase velocity of 3359 m/s and VP_{T1} exhibits a high K^2 value of 9.5% at h/λ = 0.225 with high phase velocity of 5223 m/s. The results show that the inclusion of AlN buffer layer improves the coupling coefficient significantly compared with SiO_2 buffer layer. Hence, buffer layers with high acoustic velocity are recommended in order to obtain high coupling and high phase velocity. The phase velocity characteristics have been found to depend predominantly on the dimensions of ZnO pattern rather than the thickness of the buffer layer (SiO_2 and AlN).

SAW delay line device with patterned-ZnO is simulated and the displacement plots have verified mutual conversion of BAW and SAW at the patterned-ZnO-Si interface. Equivalent circuit model is employed to design the proposed SAW devices with patterned-ZnO on silicon for micro-fabrication of the devices discussed in the next chapter.

Chapter 4

Fabrication of Patterned-ZnO/Si SAW Devices

The chapter presents micro-fabrication process of the proposed SAW devices on silicon substrate with patterned-ZnO structure. Conventionally, SAW devices are fabricated on piezoelectric substrates by disposing the metallic IDT pattern using UV lithography or *e*-beam lithography process. Commonly, UV lithography process is widely used for bulk manufacturing of SAW devices, whereas *e*-beam lithography process is preferred in the fabrication of high frequency SAW devices [63]. In this research work, we fabricated the proposed patterned-ZnO SAW devices on silicon substrate using both the UV lithography and *e*-beam lithography processes, at Indian Institute of Science, Bangalore.

4.1 Fabrication of SAW devices on Si using UV lithography process

In general SAW devices are fabricated using photolithographic techniques in electronic industry to obtain IDT pattern either by etching or lift-off techniques. Though both techniques are used in the fabrication of SAW devices, the lift-off process is more suitable for the development of uniform IDT pattern having feature size less than 5 µm, because during the etching process precise control of etching time is difficult for small feature size — inadequate etching time causes un-developed pattern and excessive etching time causes undercut that can be significant enough to wash out the complete IDT structure [63]. Hence, lift-off process is employed in the development of uniform IDT in the proposed SAW devices. The IDT with electrode width of 4 µm is chosen, since dimensions less than 4 µm are not reliable to obtain with UV lithography process and electrode width greater than 4 µm dimensions requires thicker ZnO film difficult to obtain using sputtering process. The basic steps involved in the fabrication of SAW devices on silicon are as follows; layout design, mask preparation, photolithography, and metal deposition over the wafer for lift-off process, ZnO film deposition, photolithography for ZnO pattern, and ZnO wet etching.

4.1.1 Design of SAW devices on silicon

Silicon is commonly used substrate for IC and CMOS fabrication and also well known for low acoustic losses [64]. In this fabrication process *p*-type silicon is considered to minimize the electro-acoustic losses and electromagnetic feed through between IDTs. One-port resonators, two-port resonators and delay lines are fabricated on (100) oriented *p*-type silicon substrate. High resistive (0-100 Ω/cm) *p*-type (100) oriented 2” single side polished silicon wafers of thickness 0.35 mm are procured from University wafers, USA. To prepare ZnO films on silicon substrate, 2" diameter 99.99% ZnO sputtering target with ionic bonded copper backing plate is procured from Vinkarola Instruments, U.S.A. IDT dimensions with desired 50 Ω impedance is designed using equivalent circuit model for synchronous one port resonators, two port resonators with different separations between IDTs, and delay line devices with different delays are designed based on the literature reported by Morgan [3], Nordin [29], and Ramakrishnan [61]. Device dimensions of the fabricated devices are listed in Tables 4.1, 4.2, and 4.3 following the design process discussed in chapter 3.

Table 4.1 Dimensions used for the fabrication of one-port SAW resonators.

Electrode finger width	4 μm
Space between consecutive electrode fingers	4 μm
Pitch (λ/2)	8 μm
Number of finger pairs in IDT structure	40, 45, 55, 60, 65, 75, 85
Aperture	55λ, 60λ, 65λ, 70λ

Table 4.2 Dimensions used for the fabrication of two-port SAW resonators.

Space between consecutive electrode fingers	4 μm
Pitch (λ/2)	8 μm
Number of finger pairs in IDT structure	35, 40, 45, 55, 60, 65, 75, 85
Aperture	55λ, 60λ, 65λ, 70λ
Separation between input and output IDTs	0.5λ, 1.5λ
Separation between IDT and reflector grating	0.25λ, 0.75λ, 1λ, 1.25 λ, 2λ

Table 4.3 Dimensions used for the fabrication of SAW delay line devices.

Space between consecutive electrode fingers	4 μm
Pitch (λ/2)	8 μm
Number of finger pairs in IDT structure	55, 60, 65
Aperture	60λ
Center-to-center separation between IDTs	70λ, 80λ

Some of the important criteria to be considered in the fabrication of SAW devices on silicon are as follows,

i. One-port resonators, two-port resonators, and delay lines SAW devices on silicon substrate with periodically patterned ZnO films are designed with λ=16 μm and h/λ of 0.19 which gives high velocity and high K^2 (Table 3.1). The IDT with ZnO pattern in the spaces are designed for 50 Ω admittance at the corresponding resonance frequency of 317 MHz (VP_{T1})

using equivalent circuit model as described in chapter 3, section 3.5. The IDT dimensions for the fabrication of SAW devices are tabulated in Tables 4.1, 4.2, and 4.3, for IDT metallization ratio of 0.5.

ii. Bond pads are designed according to the dimensions of conventional ground-source-ground (GSG) probes with 100 μm pitch to facilitate characterization of fabricated SAW devices using RF probe station and network analyzer.

iii. Minimum of 2 mm spacing is provided between adjacent devices to ensure the possibility of manual scribing and semi-automatic dicing of processed wafer.

iv. Adequate space at both ends of the device, so that the generated SAW will decay eventually or absorbing materials can be coated at the edge of the device.

v. The devices are organized to fit maximum number of devices in the mask layout.

4.1.2 Fabrication of SAW devices on silicon

The general procedure for fabricating SAW devices and process parameters mentioned in [3], [63], and the processes for the patterning of ZnO film described in [66] are closely followed in this work. Conventionally IDTs are prepared using aluminum electrodes, however Al is prone to react with chemical etchants used in ZnO patterning. Gold is chosen for IDT pattern, since it is not affected by the chemicals used in the process of ZnO patterning. Extreme thin layer of chromium is used as an adhesive between gold and silicon substrate. The metal depositions are carried out using thermal evaporation or DC sputtering. The following fabrication steps are carried out on a 2 inch silicon substrate.

(a) Layout design

The layout of IDT and ZnO patterns are graphically designed using CleWin software. Bi-layered design with standard alignment marks is chosen to accomplish both the IDT and ZnO pattern layouts without any misalignment. Fig. 4.1(a) shows the arrangement of SAW devices over a 2" area with multiple alignment marks. Fig. 4.1(b) displays the one port SAW resonator with GSG contact pad and electrical shield around the device. Fig. 4.1(c) depicts the two port SAW resonator and its magnified view is shown in Fig. 4.1(d). The SAW delay line devices having IDT center-to-center distance of 80λ with free and metallized propagation paths are shown in Fig. 4.1(e).

(b) Mask writing

Direct laser writing can be employed over a photoresist-coated wafer to make IDT patterns with high accuracy. As the devices are to be fabricated on a 2" wafer, direct laser writing consumes a significant amount of time, hence chromium mask plates are prepared using laser writer and the mask plates are used in UV lithography process.

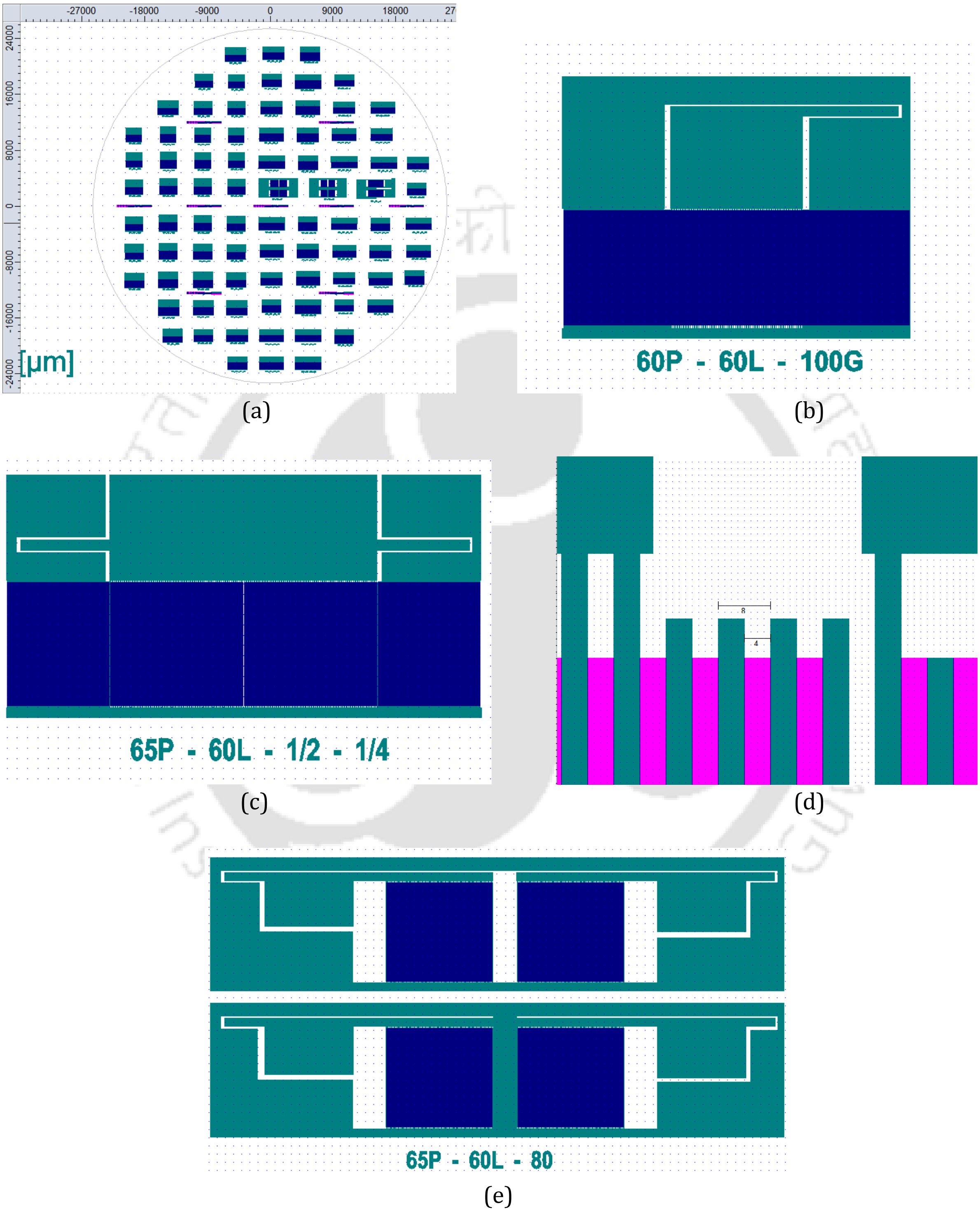

Fig. 4.1. (a) Mask layout using CleWin software, (b) schematic of one port SAW resonator, (c) schematic of and two port SAW resonator, (d) magnified view of device showing the dimensions of IDT, and (e) schematic of the delay line devices with open and metalized propagation paths.

Standard alignment markers are included in the layout to facilitate second layer lithography for patterning the ZnO film. GSG compatible contact pads of 100 µm pitch are designed and incorporated in all the devices for testing. 3” chrome mask plates with 2” active area are prepared using laser writer (Hidelberg Instruments, Germany).

The mask plate with positive photoresist is loaded into the laser writer and the mask plate with desired dimensions are engraved using a standard lens. The laser written chrome mask plates are developed using MF-26A developer (MicroChem, USA). The exposed chromium region is etched using chrome etchant solution. Chrome etchant solution contains, ceric ammonium nitrate $(NH_4)_2Ce(NO_3)_6$ or sulfate $(NH_4)_4Ce(SO_4)_4.2\ H_2O$, with small amounts of HNO_3 [66]. The unwanted photo-resist is removed using acetone, followed by piranha cleaning process for 30 s. An optical images of a portion of the first mask and second mask shown in Fig. 4.2, show that the developed mask has turned out properly with desired dimensions.

(c) Cleaning of wafers

Silicon wafers are cleaned using standard RCA1 and RCA2 cleaning processes followed by 15 s HF dip. Standard RCA1 recipe is used to remove organic contaminants present in silicon wafers. RCA1 recipe is prepared using de-ionized (DI) water, hydrogen peroxide (H_2O_2) and NH_4OH with ratios of 5:1:1, and heated up to 75°C. The wafers are dipped in the recipe for 10 minutes followed by DI cleaning. Further, the wafers are processed with RCA2 cleaning to remove metallic contaminants. RCA2 recipe is prepared using DI water, hydrogen peroxide and hydrochloric acid in the following ratios (H_2O:H_2O_2:HCl = 6:1:1) and heated up to 75°C. The wafers are dipped in the RCA2 solution for 10 minutes followed by HF dip for 30 s to remove the presence of native oxide. Finally, the wafers are placed in DI water and dried using filtered nitrogen gas.

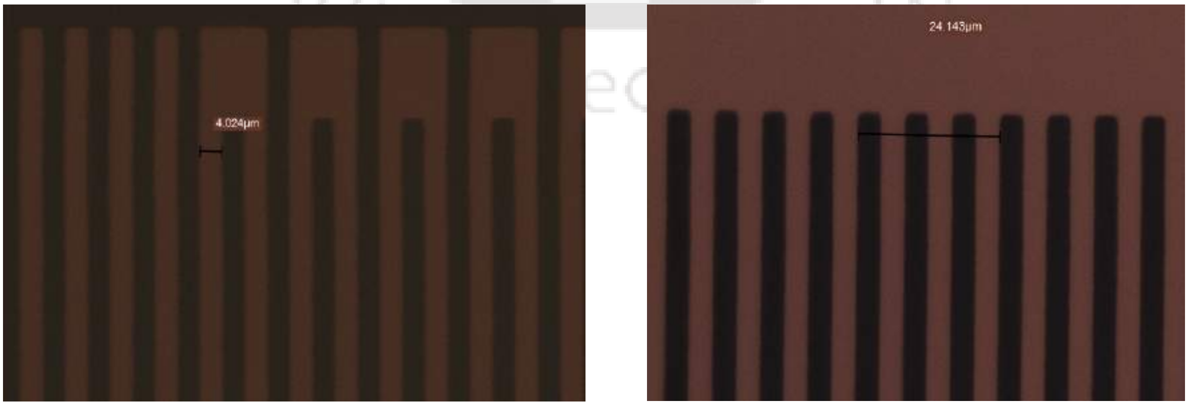

(a) (b)

Fig. 4.2. Optical microscopic images of (a) IDT structure on mask plate 1 and (b) ZnO pattern on mask plate 2.

(d) Oxidation of silicon wafers

In general the dry oxidation process results in high quality oxide film less than 250 nm thick, but in the proposed device the required oxide layer thickness is very large and dry oxidation process is not practical. Using PECVD (Plasma-enhanced chemical vapor deposition) method thicknesses up to 20 μm can be achieved, however the quality of the film is not suitable for acoustic wave propagation [63]. So, we employed wet oxidation process to obtain the desired oxide layer thickness of 2 μm. After 10 hours of process of wet oxidation at 1100°C, we obtained oxide layer of thickness 1.63 μm for the wafers placed at the far side of the chamber and 1.73 μm oxide thickness for silicon wafers placed at the center of the chamber.

(e) Photoresist coating

The wafers are cleaned with acetone and IPA for photoresist coating. The wafers are spin-coated with positive photoresist for the development of IDT pattern. It is ensured that the center of the wafer is exactly aligned with the center of the spin coater to obtain uniform photoresist thickness. AZ 5142 photoresist (AZ Electronic Materials, UK) is dispensed from the bottle and spread all over the wafer. The wafer spinning program starts with 500 rpm for 5 s, followed by 1000 rpm for 5 s and finally 6000 rpm for 40 s, and the ramp rate of 500 rpm/s is used. By this method, the photoresist thickness around 1.2 μm is achieved over the wafer. The major fabrication process steps are shown in Fig. 4.3.

(f) Soft baking

The spun samples with photoresist coating are placed on a hot plate at a temperature of 110°C for 60 s. To avoid wafer getting stuck to the hot plate surface, aluminum foil is placed between wafer and hot plate.

(g) UV exposure

The samples with photoresist coating are placed in mask aligner MJB4 (SUSS MicroTech) with 2 inch substrate chuck. The setup parameters such as wafer thickness, separation between mask plate and wafer, wedge correction, and alignment of substrate are performed manually and UV exposure of 7 s is finalized after three trials.

(h) Sample development

The exposed samples are developed in MF-26A solution, care has been taken to develop IDT structure without over development or under development by constant inspection under microscope. Development time varies sample to sample, due to intermediate cleaning of samples with DI water for inspection under microscope.

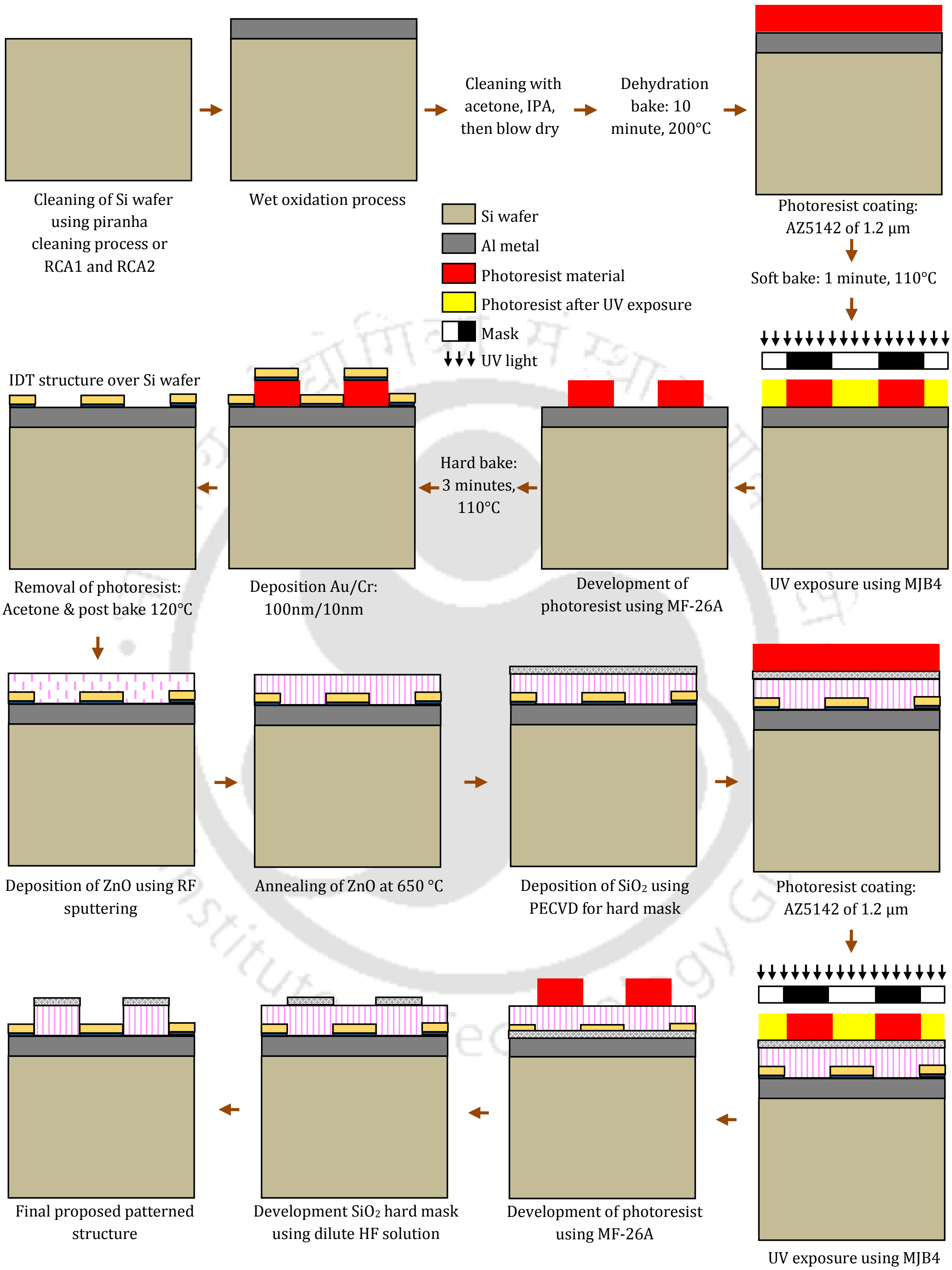

Fig. 4.3. Process flow employed for the fabrication of periodically patterned-ZnO/SiO_2/Si SAW devices.

Fig. 4.4 shows the sample after development. After development the samples are hard baked for 180 s at a temperature of 110°C using hot plate.

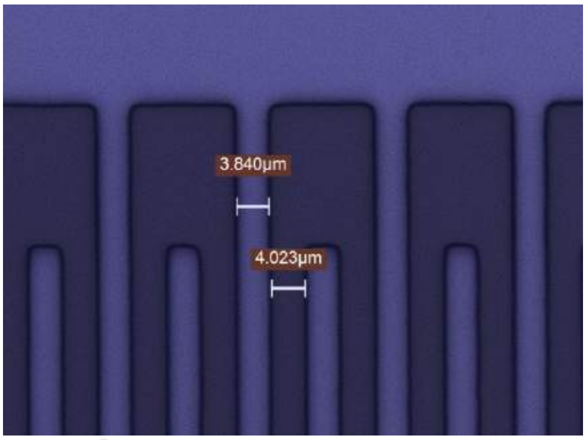

Fig. 4.4. Microscopic view of IDT pattern developed after UV lithography process using MF-26A developer.

(i) Metal deposition

Since aluminum is reactive with the acids used for ZnO patterning, we use gold for IDT structure and chromium to promote the adhesion between gold and silicon. Initially 10 nm thickness of chromium is deposited on silicon substrate before depositing 100 nm gold. The sputtering parameters for gold and chromium metals are listed in Table 4.4.

Table 4.4 RF sputtering conditions of gold and chromium metal deposition.

Metal	Power	Pre deposition	Deposition time
Chromium (Cr) (10 nm)	100 W	600 s	22 s
Gold (Au) (100 nm, 150 nm)	25 W	0 s	300 s, 450 s
Base pressure	5×10^{-6} Torr		
Working pressure	6.4×10^{-3} Torr		
Distance between substrate and target	7.5 cm		
Substrate temperature	Room temperature		

(j) Lift off

After chromium (10 nm) and gold (100 nm) deposition, the samples are placed in petri dish with acetone and the dish is placed in ultra-sonication for 10–15 minutes for lift-off process. The microscopic image of IDT structure after lift-off process is shown in Fig. 4.5.

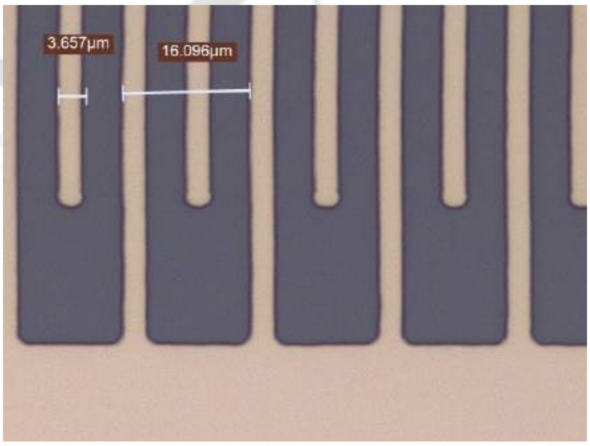

Fig. 4.5. Microscopic image of IDT structure showing electrodes and bus bar, obtained after lift-off process.

(k) ZnO deposition

(002) oriented ZnO films are deposited over the samples using 2 inch commercial sputtering target of 99.99% pure ZnO using

RF sputtering system with argon flow of 20 sccm at IIT Guwahati. A test run is carried out for a duration of 105 minutes with ZnO deposition conditions mentioned in Table 4.5, and a ZnO film thickness of 2.5 μm is obtained, implying a growth rate of 23.81 nm/min. The ZnO thickness that gives high K^2 and high phase velocity is obtained by FE simulations in Chapter 3. Accordingly, ZnO film depositions are carried out for 134 minutes to obtain thickness of 3.2 μm on silicon wafers without oxide layer and for 118 minutes to obtain 2.8 μm for wafers with oxide layer.

Table 4.5 RF sputtering deposition parameters used for ZnO thin films.

Power	45 W
Base pressure	6×10^{-6} Torr
Working pressure	5×10^{-2} Torr
Distance between substrate and target	5 cm
Substrate temperature	250 °C
Pre deposition	600 s

(l) Annealing

After deposition of ZnO film, the samples are annealed at different temperatures to obtain optimum crystalline nature of the film with fine grain structure and minimum defects. Annealing is performed at 400°C, 500°C, 550°C, 600°C, 650°C, and 700°C, and X-ray diffraction (XRD) 2θ scan is performed on the test samples and the result of XRD analysis is plotted in Fig. 4.6(a). The intensity peak observed at 34.4° in the XRD result confirms (002) orientation of ZnO film. In addition, the peak intensity is maximum for annealing temperature of 650°C, therefore,

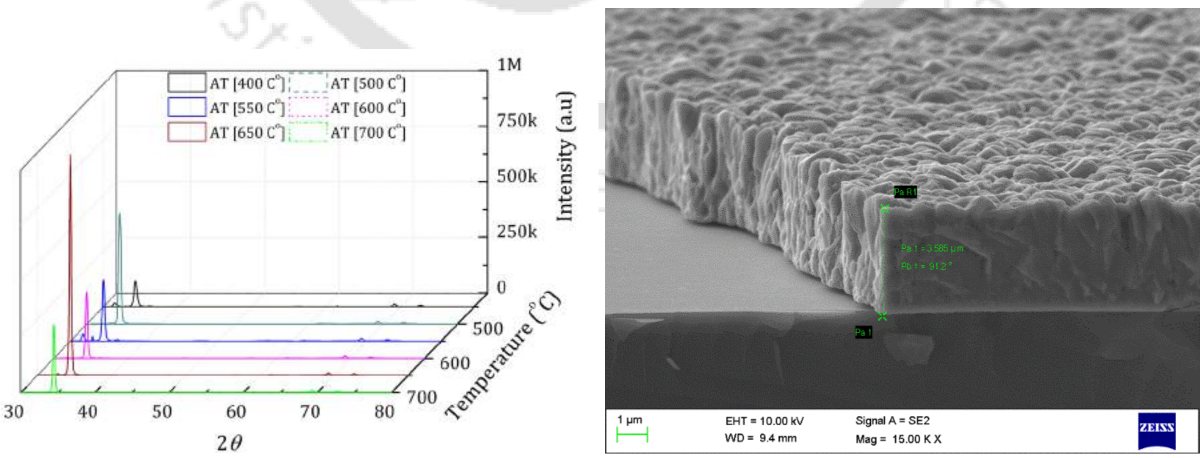

(a) (b)

Fig. 4.6. (a) XRD analysis of ZnO film on silicon substrate annealed at different temperatures and (b) FESEM image of ZnO thin film deposited on silicon substrate without oxide layer after annealing at 650°C.

annealing after deposition of ZnO is carried out at 650°C in the fabrication of proposed devices. The FESEM image of annealed ZnO film is shown in Fig. 4.6(b). Thickness measurements are performed using Dektack profilometer to determine the thickness of deposited ZnO films. The obtained thicknesses are in the range of 3.8–4.3 μm and 3–3.2 μm observed for samples without and with oxide layer respectively. The ZnO film thickness obtained using 2" sputtering target on 2" wafer is highly non-uniform– 4.3 μm at the center and 1.1 μm at the edge of the wafer.

(m) Development of photoresist for ZnO patterning

We carried out several trials on the development of photoresist pattern for ZnO etching. The photoresist patterns developed using positive photoresist (AZ 5214) and negative photoresist (AZ nLof 2020) were found to wash away due to undercut during the etching process that we tried with 10 chemical recipes, including dilute HF and dilute acetic acid. Image reversal technique was also tried, as it includes longer baking time after UV exposure and results into strong adhesion with the surface. Though the developed photoresist pattern withstood for longer duration in comparison with previous two trials, the photoresist pattern washed away before completion of ZnO patterning. The microscopic images of washed out photoresist patterns are shown in Fig. 4.7.

The details of trial runs carried out for ZnO patterning using different types of photoresists are listed in Table 4.6. Finally, we opted for hard mask (HM) of SiO_2 for ZnO patterning in conjunction with convection flow of etchant along the aperture using magnetic stirrer. From the microscopic images we observed that the HM was able to withstand ZnO etchants and the impact of flowing etchant due to strong adhesion property of HM produced by PECVD process.

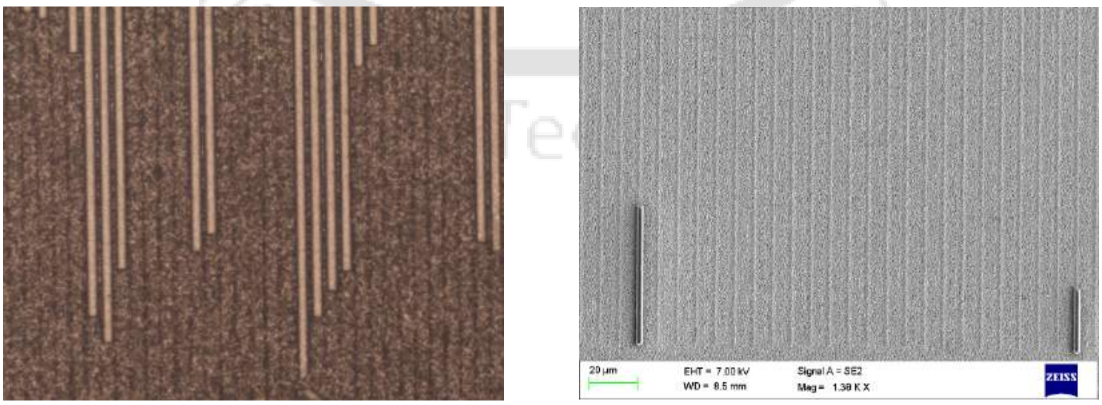

(a) (b)

Fig. 4.7. (a) Microscopic image of photoresist pattern on test sample after ZnO etching process using dilute HF solution and (b) its FESEM image showing undercut as the cause of washing away of photoresist.

The SiO_2 film of 100 nm was deposited using PECVD process with the following deposition parameters

High frequency power: 10 W (Frequency = 13.56 MHz)
Deposition time: 2 minute 40 s
Gases flow: N_2O (710 sccm): SiH_4 (8.5 sccm): N_2 (161 sccm)
Chamber pressure: 1 Torr
Temperature: 350°C.

Table 4.6 Trial runs carried out for ZnO patterning using different types of photoresists.

Photoresist	Chemical recipe	Etching time	Observations and comments
Positive photoresist AZ 5214	1% Hydrofluoric acid and 0.1M acetic acid	320 s	HF attacking chromium underneath the gold
Negative photoresist AZ nLof 2020	1% Hydrofluoric acid and 0.1M acetic acid	180 s	Photoresist is not withstanding
Image reversal process AZ 5214	1% Hydrofluoric acid and 0.1M acetic acid	420 s	Photoresist is not withstanding
SiO_2 Hard Mask [100 nm]	0.2M acetic acid with convectional flow	3 nm/s	Successfully patterned

(n) Development of photoresist pattern for HM

For the development of hard mask, another UV lithography process has been carried out using positive photoresist (AZ 5214) and UV exposure of 7 s, as discussed in Section 4.1.2(g), is used in the development of HM. The exposed samples are developed using MF-26A solution, care has been taken to develop hard mask for ZnO pattern properly by frequent inspection under microscope. After the development of photoresist the samples are hard baked for 180 s at 110°C using hot plate.

(o) Development of SiO_2 hard mask for ZnO etching

After the photoresist development, the samples are placed in BOE solution (buffered oxide etch [NH_4F:HF = 13:1]) for 25 s–30 s to form HM for ZnO etching. The microscopic images of device with patterned structure before and after removal of photoresist are shown in Fig. 4.8. Extreme caution has been taken in the development of hard mask, as the inspection under the microscope provides the dimensions of photoresist pattern only and the underneath SiO_2 dimensions are not visible unless photoresist is removed using acetone and once photoresist is

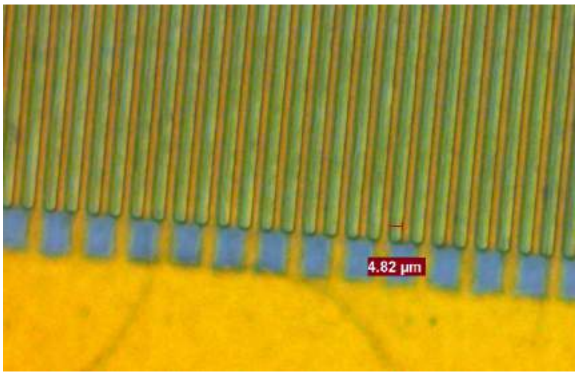

(a)

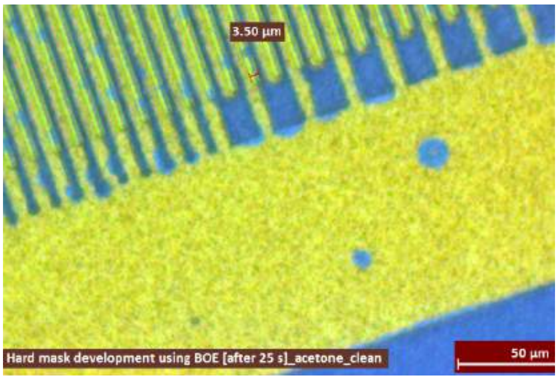

(b)

Fig. 4.8. Microscopic images of the device after the development of HM, (a) before removal of photoresist and (b) after removal of photoresist showing HM.

removed the SiO_2 pattern is unalterable. Therefore we have to rely on etching time estimated in trials to develop HM with desired dimensions.

(p) ZnO Patterning

In general chemical etching of zinc oxide is carried out using acids or weak bases like HNO_3, H_2SO_4, HCl, HF, H_3PO_4, NH_4Cl, and CH_3COOH. In case of strong acids like H_2SO_4 and HCl attack chromium metal and may result in washout of the gold layer. In case of other acids like H_3PO_4 and HNO_3 the ZnO etch rate is very high, so weak acid or weak base like CH_3COOH and NH_4Cl are recommended for ZnO etching [67]. NH_4Cl is widely used chemical for patterning of ZnO which provides high vertical etch rate than lateral etch rate [65]. In this work, due to non-availability of NH_4Cl, we employed various recipes of dilute HF and dilute CH_3COOH for patterning of ZnO [68].

Trial 1: Dilute HF solution

A test sample with 4.5 µm ZnO film on silicon substrate is spin-coated with AZ nLOF 2070 negative photoresist followed by UV lithography process and developed using MF-26A to obtain the patterned structure. A test sample is placed in 1% of aqueous HF solution for ZnO etching. Inspection is carried out with 60 s interval and the process is discontinued at 300 s. The photoresist is washed off during the process, due to the undercut beneath the photoresist pattern as a result of high lateral etch rate of ZnO in 1% HF solution. A fresh solution of 0.04% dilute HF is prepared to reduce the lateral etch rate, however from the test run it is observed that the vertical etch rate is quite low compared to horizontal etch rate which results in washing away of photoresist pattern.

Trial 2: $CH_3COOH:H_3PO_4:H_2O$

A test sample is placed in dilute solution of phosphoric acid and acetic acid in ratios of [1:1:30]. Inspection is carried out after 150 s, from the observation the ZnO film is completely etched away, further we tried another three recipes by diluting the solution in following ratios [1:1:50], [1:1:100], and [1:1:250] but still the ZnO etch rate is very high for the photoresist to withstand.

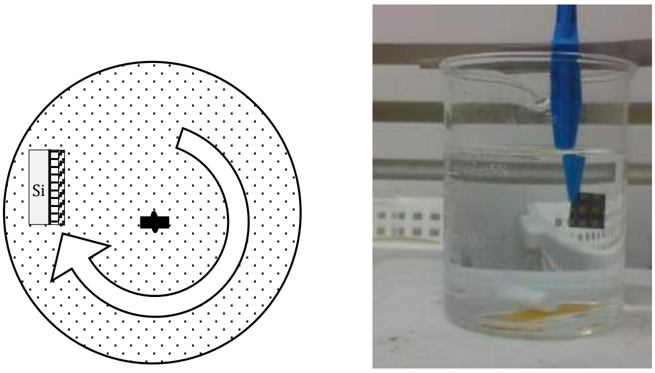

(a) (b)

Fig. 4.9. (a) Illustration of conventional flow of etchant over the device, the cross-section along the aperture is depicted and (b) experimental setup for patterning of ZnO film using magnetic stirrer.

Trial 3: Dilute CH_3COOH

The etch rate of ZnO in acetic acid is very low compared to dilute HF or any other acids. So, we carried out some initial test run using 0.1M acetic acid. A test sample is dipped in 0.1 molar acetic acid solution and regular inspection is made, but in comparison with HF, the photoresist is able to withstand in the acetic acid solution for longer duration.

Trial 4: 0.2M CH_3COOH with mechanical stirring

Based on the initial trials and reported literature [65], to enhance the vertical etch rate of ZnO, etchant solution with convection flow parallel to the aperture of patterned photoresist is organized using mechanical stirring with the help of a magnetic stirrer, as shown in Fig. 4.9. Concentration of acetic acid and flow speed of the solution are varied to obtain anisotropic etching of ZnO films.

Convectional flow with velocity 1.6 m/s is used for ZnO patterning. Convectional flow velocity less than 1.6 m/s results in undercut as observed from SEM images and flow velocity greater than 2 m/s washes away HM. The FESEM image of pattern structure with 98.72 nm SiO_2 hard mask is shown in Fig. 4.10. From the test runs, acetic acid of 0.2 M with 1.6 m/s convectional flow velocity are the optimal conditions for ZnO patterning. The etch rates of ZnO in 0.1 M, 0.2 M, and 0.3 M concentrations of acetic acid are 2.5 nm/s, 4.2 nm/s, and 3.7 nm/s respectively. Various chemical recipes used for patterning are listed in Table 4.7, where PR is photoresist and HM is the SiO_2 hard mask used for

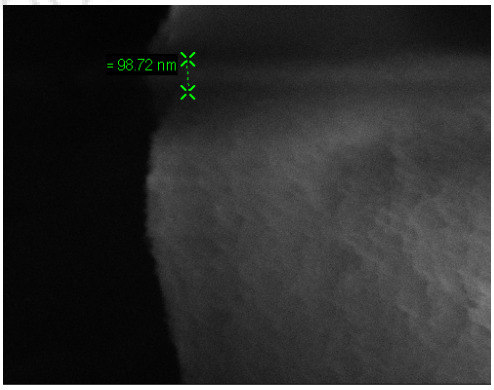

Fig. 4.10. SEM image depicts the SiO_2 hard mask over the ZnO pattern.

patterning. The FESEM images of ZnO pattern obtained using 0.1M, 0.2M, and 0.3M concentration of acetic acids are shown in Fig. 4.11.

Table 4.7 Details of test runs carried out on ZnO patterning.

Test run	Photoresist type	Chemical recipe	Etching time/rate	Observations and comments
1	Positive	BOE [Buffered oxide etchant]	400 s	Large undercut washing away the whole resist pattern
2	Positive	$HF:H_2O$ [1:100]	480 s	Large undercut washing away the whole resist pattern
3	Negative	$HF:H_2O$ [1:250]	320 s	Under cut and ZnO etch rate is very low
4	Positive	$CH_3COOH:H_3PO_4:H_2O$ [1:1:30]	150 s	Both layers are completely etched out–very high etch rate
5	Positive	$CH_3COOH:H_3PO_4:H_2O$ [1:1:50]	120 s	Pattern is washed away
6	Positive	$CH_3COOH:H_3PO_4:H_2O$ [1:1:100]	180 s	Pattern is washed away
7	Positive	$CH_3COOH:H_3PO_4:H_2O$ [1:1:250]	270 s	Pattern is washed away
8	Hard mask	CH_3COOH: H_2O [0.6:100] (with stirring)	2.5 nm/s	Patterned successfully, slight under cut is observed
9	Hard mask	$CH_3COOH:H_2O$ [1.2:100] (with stirring)	4.2 nm/s	Patterned successfully and desired vertical pattern is obtained
10	Hard mask	$CH_3COOH:H_2O$ [1.8:100] (with stirring)	3.7 nm/s	Vertical pattern is obtained but ridges are formed on the pattern

ZnO pattern obtained on actual device using 0.2M acetic acid with convectional flow of 1.6 m/s is shown in Fig. 4.11(d) and slight misalignment in location of ZnO pattern with respect to IDT can be observed.

4.1.3 Notable observations from the fabrication process

Following are some of the notable observations during the device fabrication using UV lithography process

1. Adhesion of chromium/gold electrodes with silicon surface is not satisfactory as IDT structure started peeling off during annealing process. Adhesion of chromium/gold electrodes with SiO_2 surface is found to be more robust.
2. High radial non-uniformity of ZnO thickness is observed using 2” sputtering target on 2” wafer.

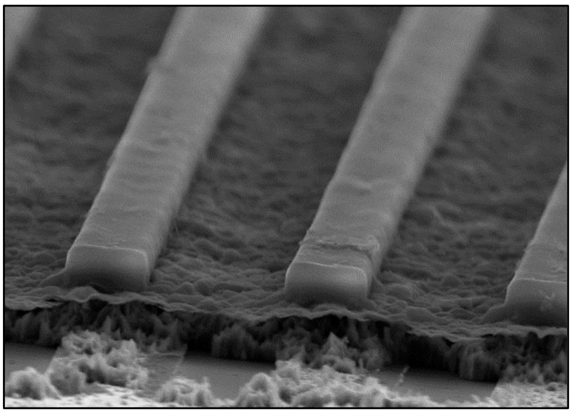

(a) 0.1M acetic acid

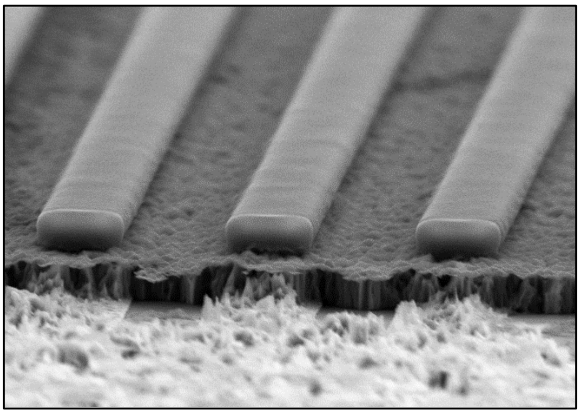

(b) 0.2M acetic acid

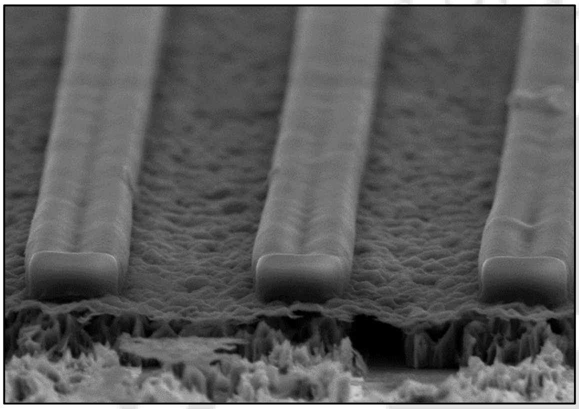

(c) 0.3M acetic acid

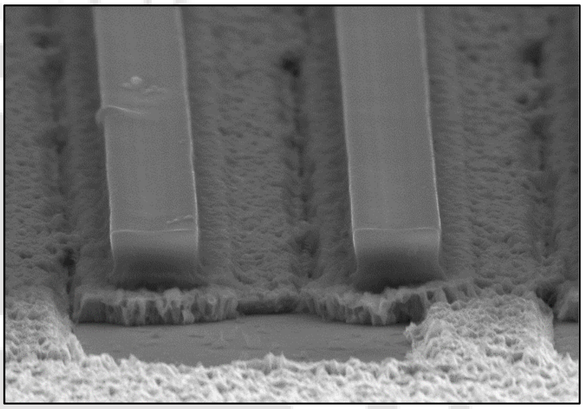

(d) Section of actual device with optimal conditions

Fig. 4.11. FESEM images of patterned ZnO film on test samples using dilute acetic acid of concentration (a) 0.1M, (b) 0.2M, (c) 0.3M. (d) Shows the ZnO pattern obtained on actual device using 0.2M acetic acid with convectional flow of 1.6 m/s.

3. Positive photoresist (AZ 5214) and negative photoresist (AZ nLOF) are unable to withstand the convectional flow of acetic acid etchant during ZnO patterning. Therefore, HM is suitable for ZnO patterning.
4. Since the photoresist on top of HM completely blocks the view of HM due to undercut, we have to rely on etching time estimated in trials to develop HM with desired dimensions.
5. ZnO pattern obtained using 0.2M acetic acid with convectional flow of 1.6 m/s is found to be most appropriate.

4.2 Fabrication of SAW devices on Si using *e*–beam lithography process

In general laser writing and *e*-beam lithography processes are employed for high accuracy and devices with sub-micron dimensions. We made an attempt to fabricate high frequency, greater than 5 GHz, SAW one port and two port resonators on silicon substrate with patterned ZnO films using *e*-beam lithography process. The layout of IDT pattern and ZnO pattern for one port and two port resonators are designed using CleWin software. In this process the mask layout is imported into the software for *e*-beam lithography. The dimensions of the proposed one port and two port SAW resonators to be fabricated are mentioned in Table 4.8. The IDT of wavelength 960 nm and electrode width 200 nm, implying a metallization ration of 0.42, is designed for 50 Ω impedance and ZnO pattern of width 200 nm is considered in the IDT spacing. Metallization ratio of 0.42 is chosen in order to avoid the merging of IDT lines during *e*-beam lithography process, the IDT bus bars are extended to form GSG contact pad for testing via a probe station. Default alignment marks available in the instrument interface software are chosen to facilitate two layer lithography process.

Table 4.8 Dimensions of proposed SAW devices using *e*-beam lithography.

Parameters	One port resonator	Two port resonator
Electrode width	200 nm	200 nm
Aperture	60λ	60λ
Metallization ratio	0.42	0.42
Distance between input and output IDTs	–	λ/2
Distance between IDT and reflector grating	λ/4	λ/4

(a) *Cleaning of wafers*

Silicon samples are cleaned using standard piranha solution followed by 15 s HF dip to remove contaminants present in silicon wafers. Piranha recipe is prepared with 3:1 ratio of H_2SO_4 and H_2O_2. The samples are kept in piranha solution of 30 s and cleaned with DI water and further dipped in dilute HF solution for 15 s to remove the presence of native oxide. Finally, wafers are placed in DI water and dried using nitrogen flush.

(b) Oxidation of silicon wafers

The samples are placed in oxidation furnace to obtain SiO_2 thickness of 300 nm using wet oxidation process. After the oxidation process, the thickness of oxide layer measured using Dektack profilometer is 278 nm.

(c) Photoresist coating

The samples are spin-coated with PMMA, 950 KC_3, a bi-layered positive photoresist, for the development of IDT pattern. The wafer spinning program starts with 500 rpm for 5 s, followed by 1000 rpm for 5 s and finally 6000 rpm for 45 s, and the ramp rate of 500 rpm/s is used. Speed ramp of 500 rpm/s is maintained throughout the spinning processes. By this method, the

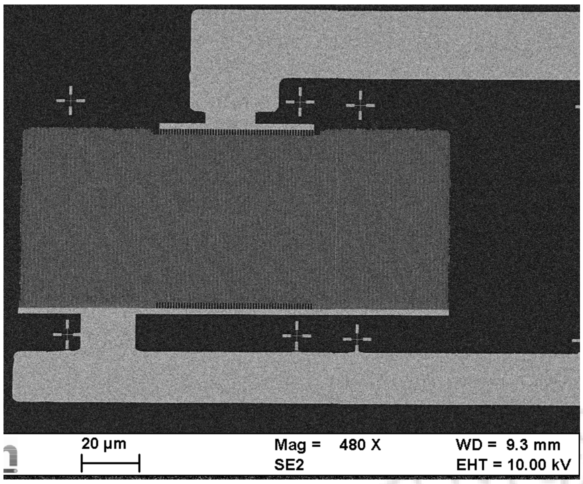

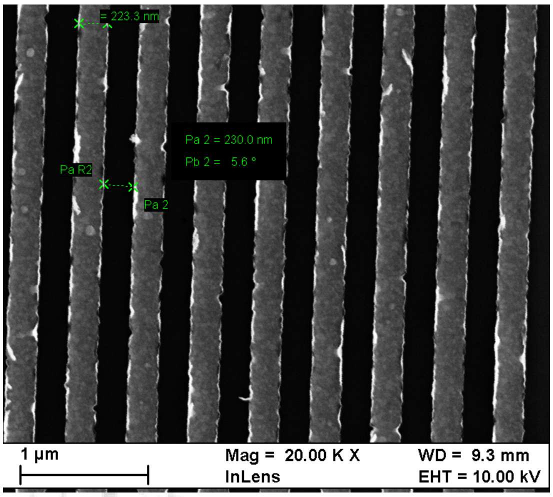

(a) (b)

Fig. 4.12. SEM images of (a) one port SAW resonator and (b) magnified view of IDT structure.

photoresist coating thickness of about 180 nm is achieved over the wafer. The samples with photoresist are pre baked using a hot plate at 180°C temperature of for 120 s.

(d) Lithography

Several trials are conducted to obtain the optimum dosage values of lithography process by observing the photoresist pattern under the microscope and the dosage of 160 μC/cm^2 with beam current of 140 pA is finalized. The samples are developed by dipping in MIBK solution for 60 s and then in IPA solution for 60 s, followed by DI water clean and nitrogen flush. Further metal depositions of chromium and gold of 10 nm and 40 nm thicknesses respectively are carried out using DC sputtering process over the developed photoresist samples. Lift off process is carried out by placing the samples in acetone solution for long duration without ultra-sonication to form IDT pattern. The samples are washed with DI water after ensuring that the lift off process is complete. The FESEM image of developed electrode pattern is shown in Fig. 4.12.

(e) ZnO deposition

A test run of ZnO deposition for 1000 s resulted in ZnO film thickness of 278 nm. Accordingly we carried out deposition for 690 s to get ZnO film thickness of 192 nm as obtained from the simulation results given in Chapter 3. The deposition is carried out at room temperature and the deposition conditions are listed in Table 4.9. Photoresist coating, prebaking and *e*–beam lithography processes for patterning of ZnO film are carried out as discussed above for IDT development. We chose not to perform annealing process on the samples, as the annealing process at 650 °C may damage gold electrodes.

Table 4.9 ZnO deposition conditions for RF sputtering.

Power	50 W
Deposition time	750 s
Base pressure	6×10^{-6} Torr
Working pressure	5×10^{-2} Torr
Distance between substrate and target	7. 5 cm
Substrate temperature	Room temperature

(f) Patterning of ZnO

From the etch rates obtained from the UV lithography samples discussed in previous section, 0.2M acetic acid solution is prepared and the *e*-beam samples are dipped in the solution with 1.6 m/s convectional flow for 54 s to 60 s. SEM images of the fabricated one port SAW resonator and the magnified view of the IDT structure are shown in Fig. 4.13. Further the samples are cleaned with acetone and DI water and then dried using nitrogen flush.

4.3. Summary

The proposed patterned-ZnO SAW devices on silicon substrate are fabricated in order to verify the results of simulations of proposed SAW devices with patterned-ZnO. In this chapter we discussed the fabrication steps of proposed SAW devices on silicon with periodically patterned ZnO films using UV lithography and *e*-beam lithography processes. Important aspects of SAW device fabrication on silicon and silicon with oxide layer are discussed. A large number of resonators and delay line devices are fabricated on a 2" silicon wafer. Several trails are conducted to finalize the photoresist and chemical recipe for the vertical patterning of ZnO film. *E*-beam lithography process is employed in the fabrication of high frequency SAW devices with ZnO pattern and the process parameters used in this research can be employed for bulk manufacturing of proposed SAW devices on silicon substrate.

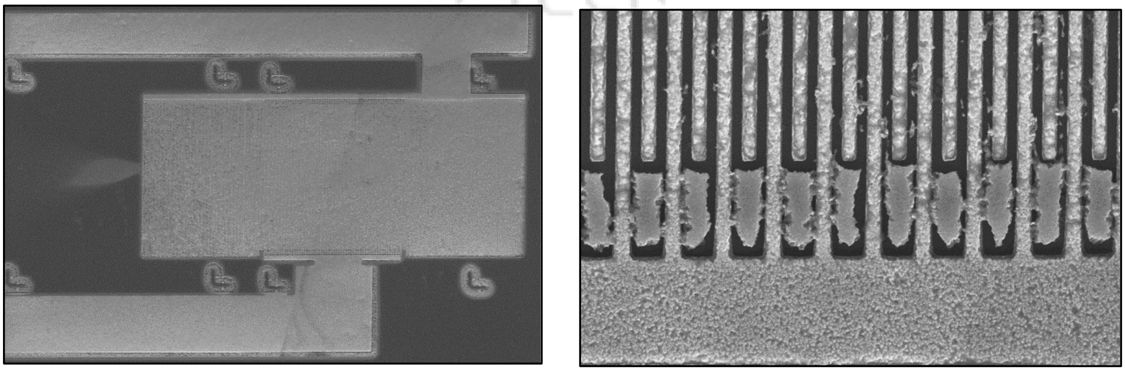

(a) (b)

Fig. 4.13. SEM image of (a) one port SAW resonator and (b) IDT structure with patterned-ZnO.

Chapter 5

Testing of Fabricated Patterned-ZnO/Si SAW Devices

This chapter of the thesis presents the testing of proposed periodically patterned-ZnO/Si SAW devices using network analyzer (Agilent E8361A) and RF probe station (Cascade Microtech Summit 9000). The obtained S-parameters provide the device characteristics like resonance frequency, impedance, and insertion loss. The finite element simulations of patterned-ZnO SAW devices on silicon substrate are once again performed with the dimensions as fabricated and the simulated results are compared with the measured results for validation.

5.1 S parameters of fabricated SAW devices on silicon substrate

The fabrication of proposed SAW devices with periodically patterned ZnO films is described in the previous chapter. The resonance frequencies and insertion loss characteristics of the surface modes generated in the proposed SAW devices are determined from the S parameters obtained using RF probe station and network analyzer. The RF probe of pitch of 100 μm is used for characterization of fabricated SAW devices. The measurement setup for characterization with RF probe station and network analyzer is shown in Fig. 5.1. Initial through open short matched (TOSM) calibration has been carried out using GSG (ground-source-ground) probes with open circuit, short circuit, 50Ω load, and through conditions for a wide range of frequencies from 30 MHz to 6 GHz. We fabricated one-port resonators, two-port resonators and delay lines SAW devices using patterned-ZnO film on silicon substrate without and with 1.73 μm thick oxide layer.

(a) (b)

Fig. 5.1. Experimental setup used for the determination of S parameters of fabricated SAW devices (a) RF probe station with network analyzer and (b) RF probes.

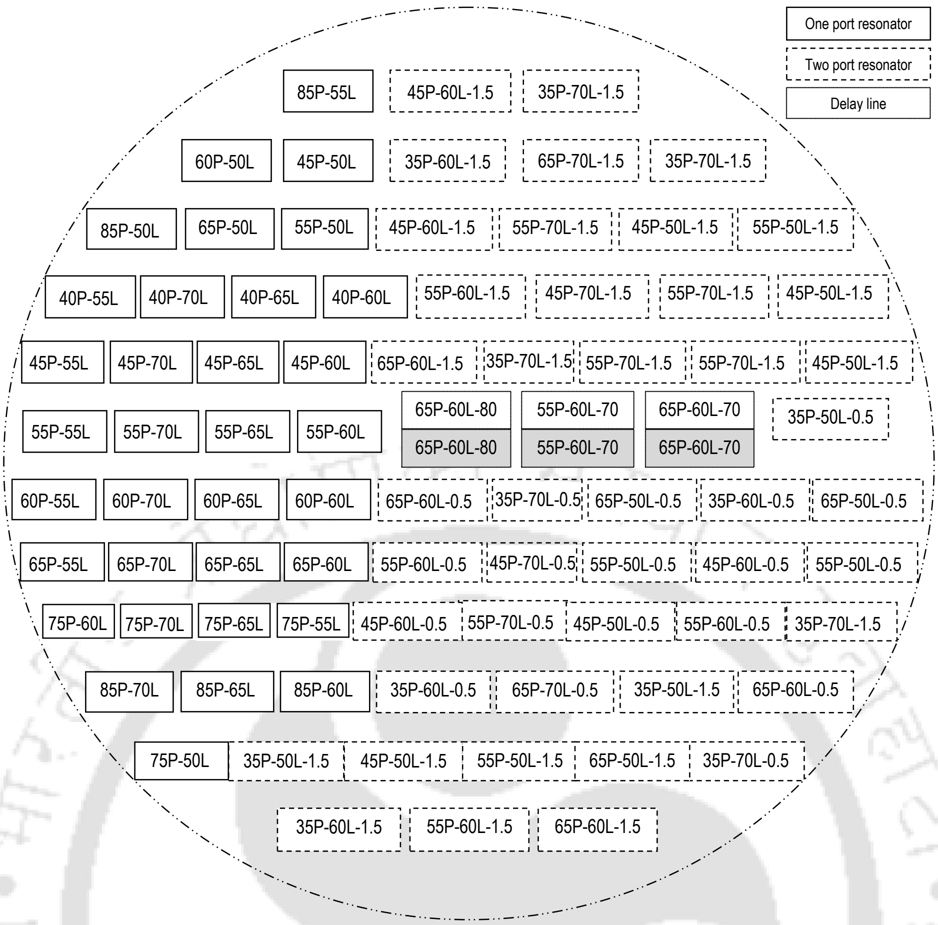

Fig. 5.2. Layout showing the distribution and arrangement of SAW devices on processed 2” wafers. Shaded devices are the delay lines with metalized propagation path.

The distribution of SAW devices fabricated on a complete 2” wafer and labels of every individual SAW device are shown in Fig. 5.2. For a one port SAW resonator the label recites AP-BL, where A is number of finger pairs in IDT and B is aperture length in terms of multiple of wavelength. In case of a two port SAW resonator, AP-BL-L_c is used as device label, where L_c is the distance between IDT and reflector grating in terms of multiple of wavelength. For a delay line SAW device AP-BL-d is used, where d is the center-to-center distance between input and output IDT in terms of multiple of wavelength. E.g. 55P-65L-0.5 defines a two port resonator with 55 finger pairs having an aperture of 65λ and the distance between IDT and reflector grating is 0.5λ. Similarly 65P-60L-80 defines a SAW delay line with IDTs having 65 finger pairs of aperture 60λ and the center-to-center distance between input and output IDTs of 80λ. In Fig. 5.2, the shaded delay lines have metalized propagation path.

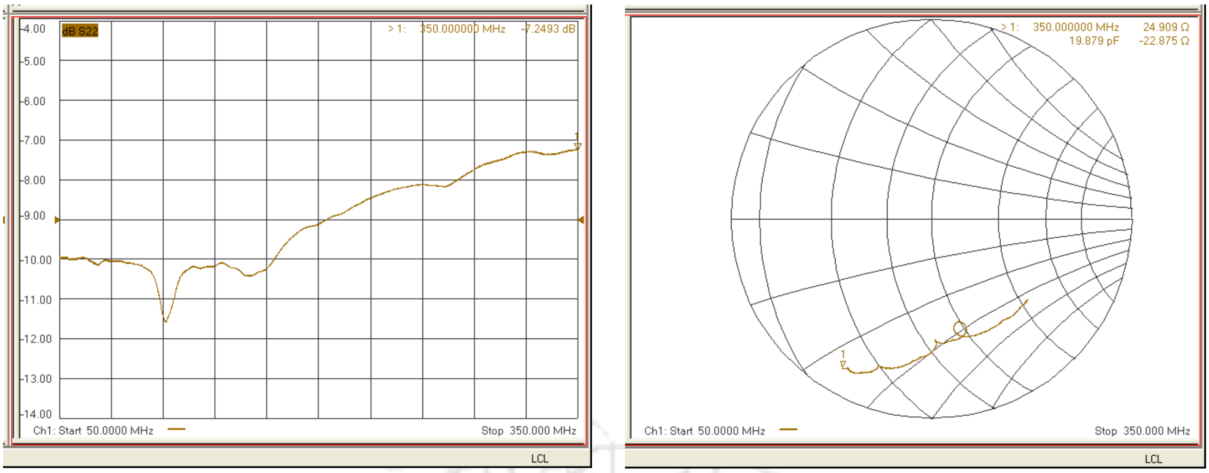

(a) (b)

Fig. 5.3. Characteristics of one port SAW resonator 75P-55L (a) magnitude plot of S11 parameter and (b) Smith chart.

5.2 S parameters of one port SAW resonator

In this section, the S11 characteristics of the fabricated one port SAW resonators with periodically patterned ZnO are presented. After the fabrication processes like annealing and patterning of ZnO film, we tested the devices which appeared to be intact under microscope from several wafers and the measured data of 29 one-port SAW resonators were satisfactory. The measured S11 parameter and smith chart results of a fabricated proposed one port SAW resonator are shown in Fig. 5.3 and we have re-plotted the magnitude and phase characteristics of S11 using the data obtained from network analyzer to provide more details about resonance frequencies as shown in the Fig. 5.4.

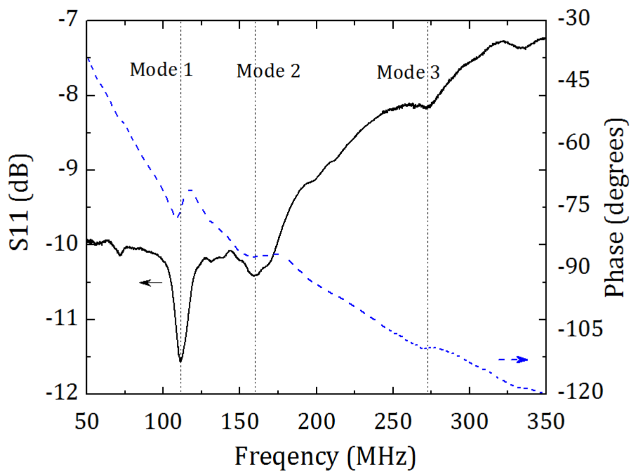

Fig. 5.4. Magnitude and phase plots of S11 parameter measured for 75P-55L SAW one port resonator and the modes are identified by the corresponding localized peaks inmagnitude plot.

The S11 characteristics of one port SAW resonator labeled 75P-55L shows three resonance frequencies with the first resonance frequency at 111.5 MHz with return loss (RL) -11.568 dB, the first higher order mode observed at 159.125 MHz with RL -10.422 dB, and the second higher order mode observed at 275.375 MHz with RL -8.139 dB. The resonance peaks for high order modes are not clearly visible due to the impedance mismatch between the device and the ports of network analyzer and can be seen from the smith chart shown in Fig. 5.3(b). The observed resonance peaks are termed as Mode 1, Mode 2, and Mode 3. Mode 1 exhibits a resonance frequency (f_r) of 111.5 MHz and anti-resonance frequency (f_a) is around 122 MHz. 1 dB bandwidth (BW) of 13.125 MHz at resonance frequency of 111.5 MHz corresponds to a Q of 8.49. Using the resonance and anti-resonance frequencies the effective coupling coefficient K_{eff}^2 of the device can be calculated using [69]

$$K_{eff}^2 = (f_a^2 - f_r^2)/f_a^2 \tag{5.1}$$

The calculated K_{eff}^2 for Mode 1 is 0.16.

5.2.1 Simulation of one port SAW resonator as fabricated

To validate the test result and identify the type of surface modes generated in the structure, FE simulations are performed with dimensions of the device as fabricated. A periodic structure of the fabricated one port SAW resonator device (75P-55L) is considered to study the resonance frequencies. The 2D periodic geometry of the fabricated one port SAW resonator is shown in Fig. 5.5(a). The structure comprises of a silicon substrate with an oxide layer of 1.73 μm and IDT pattern made of gold of thickness 0.11 μm. The dimensions the device observed from FESEM are as follows. ZnO pattern of height 2.5 μm above the 0.7 μm thick ZnO film remnant of etching process and a shift in ZnO pattern having an overlap of around 0.4 μm with the IDT structure. Eigenmode analysis and frequency dependent

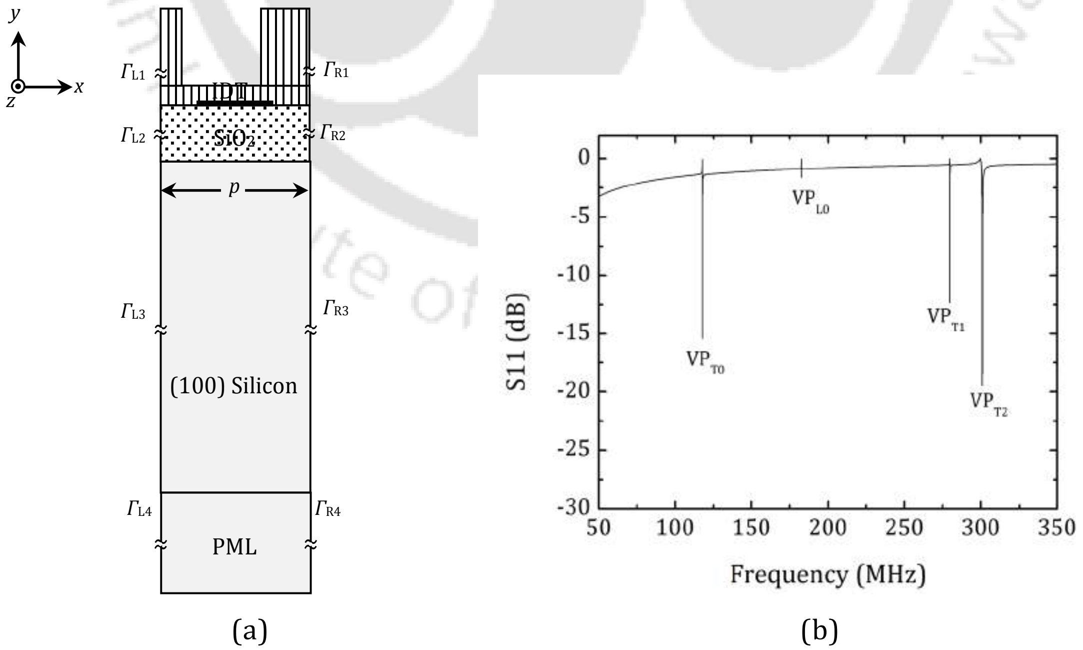

Fig. 5.5. (a) The 2D geometry of fabricated proposed one port SAW resonator with SiO_2 layer and (b) S11 characteristics obtained from FE simulations.

analysis are carried out for a frequency range of 50 MHz to 350 MHz on the 2D periodic structure shown in Fig. 5.5(a) and the simulated S11 characteristics are shown in Fig. 5.5(b).

From Fig. 5.5(b), we observe four surface modes generated in the structure and the types of surface modes are identified from their surface displacement profiles. The observed resonance frequencies are 117.91 MHz (VP_{T0}), 182.6 MHz (VP_{L0}), 279.65 MHz (VP_{T1}), and 297.462 MHz (VP_{T2}). Hence Mode 1, Mode 2, and Mode 3 in Fig. 5.4 correspond to VP_{T0}, VP_{L0}, and VP_{T1} respectively. However an additional mode (VP_{T2}) is observed in the simulated S11 characteristics. The comparison of measured results and simulated results are listed in Table 5.1.

Table 5.1 Comparison of measured results and simulated results of fabricated 75P-55L device.

Surface mode	Resonance frequency (MHz)		Comments
	Measured	Simulated	
VP_{T0}	111.500	117.910	An error of 5.4% is observed.
VP_{L0}	159.125	182.600	An error of 12.8% is observed. The surface mode generated by the longitudinal bulk mode in ZnO is dominant due to the misalignment of patterned structure, which has been observed from the simulation study discussed below.
VP_{T1}	275.375	279.650	An error of 1.5% is observed.
VP_{T2}	Indistinct	297.462	The peak is not distinguishable in the S11 measurement characteristics, due to impedance mismatch.

The error in the practical values and simulated values is due to idealistic nature of simulations having considerations like perfect ZnO pattern, uniform height of ZnO pattern, smooth surface roughness, and materials with negligible losses, whereas in case of practical fabrication the device characteristics are affected by several parameters such as, dimensions of ZnO pattern, position of ZnO pattern, radial non-uniform ZnO height, voids or cracks in ZnO film formed during annealing process, quality of IDT structure, and adhesion between ZnO pattern and surface of the substrate, which are not considered in the simulation.

From the initial simulations discussed in Chapter 3, Section 3.2, the ZnO blocks are located exactly in the middle of IDT spaces, therefore electric field across ZnO blocks is dominant than in-line electric field and it results in only surface modes (VP_T) excited by transverse BAW in ZnO. However in the fabricated devices the shift in ZnO pattern with respect to IDT

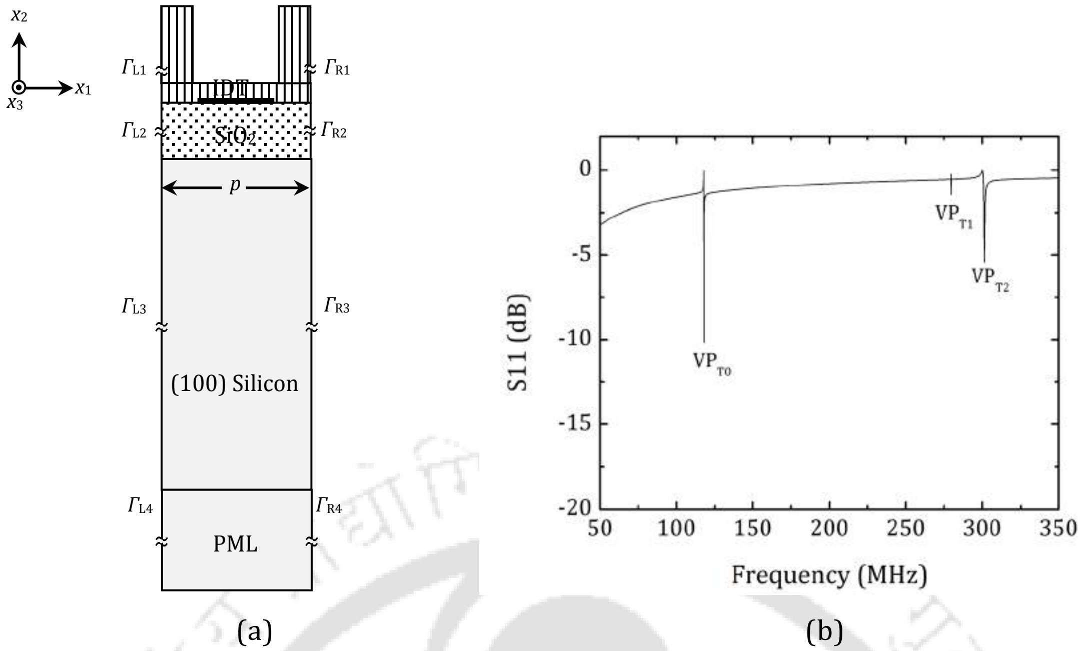

Fig. 5.6. (a) The 2D geometry of fabricated proposed SAW resonator with SiO_2 layer without shift in ZnO pattern (b) S11 characteristics obtained from FE simulations.

has resulted in overlap of ZnO blocks with electrodes causing longitudinal BAW in ZnO blocks due to increased in-line electric field along ZnO block. The longitudinal BAW in ZnO results in generation of surface modes in silicon (VP_L) which is visible in Fig 5.4 and Fig. 5.5.

As an additional verification of generation of VP_{L0} mode, we repeated the simulation of the device shown in Fig. 5.5(a) without the shift in ZnO pattern with respect to IDT and its S11 characteristics show the non-existence of VP_{L0} mode, as shown in Fig. 5.6(b). This confirms the presence of VP_{L0} mode because of misalignment of ZnO blocks with respect to IDT and the detailed simulation study about the misalignment is carried out in the next section.

The resonance frequencies noticeable in S11 magnitude and phase plots of the 29 one port SAW resonators fabricated on various samples are listed in Table 5.1. The resonance peaks not listed are undetectable in S11 characteristics due to the impedance mismatch and partly due to the uncertainties in the fabrication process steps especially during annealing process.

Table 5.2 Measured S11 parameters of fabricated one port SAW resonators.

Device	VP_{T0} (MHz)	Return loss, RL (dB)
Sample 1: ZnO-Pattern/1.73 µm SiO_2/Si		
65P-55L	109.719	-3.09
65P-65L	108.969	-3.49
65P-70L	110.094	-4.08
75P-55L	111.500	-11.57
75P-65L	109.906	-9.14
75P-70L	109.344	-8.20
85P-60L	110.469	-3.27
85P-70L	110.094	-3.60
Sample 2: ZnO-Pattern/1.73 µm SiO_2/Si		
40P-65L	108.969	-6.10
40P-70L	109.063	-2.00
45P-55L	109.156	-2.55
45P-65L	109.063	-5.59
45P-70L	109.531	-2.40
55P-55L	108.969	-2.71
55P-65L	109.063	-4.91
55P-70L	108.875	-3.04
60P-50L	108.781	-2.54
65P-50L	109.344	-5.77
65P-55L	109.156	2.95
65P-60L	110.094	-5.47
65P-70L	109.344	-2.94
85P-50L	109.531	-2.76
85P-50L	110.375	-9.04
85P-60L	111.219	-4.92
85P-60L	113.094	-8.49
85P-65L	113.188	-9.67

The devices 55P-50L, 65P-65L, 75P-50L, 75P-60L are not listed as the resonance peaks are not visible due damaged structure.

5.3 S parameters of two port SAW resonator fabricated on silicon substrate

The measured S-parameter characteristics of a two port SAW resonator fabricated on silicon substrate without oxide layer are shown in Fig. 5.7. In the S12 characteristics, we can identify four resonance modes at the zero crossings in the phase plots. Mode 1 at 92.93 MHz with an insertion loss (IL) of -26.25 dB, Mode 2 at 136.034 MHz with IL -30.94 dB, Mode 3 at 285.12 MHz with IL -29.72 dB, and Mode 4 at 318.61 MHz with IL -31.43 dB.

Table 5.3 Resonance and anti-resonance frequencies for surface modes and corresponding effective coupling coefficients (K_{eff}^2) using S21 characteristics of 65P-60L-0.5 two port SAW resonator.

Surface mode	Resonance (MHz)	Anti-resonance (MHz)	K_{eff}^2
VP_{T0}	092.93	108.247	0.26
VP_{L0}	136.034	184.128	0.45
VP_{T1}	284.769	309.172	0.15
VP_{T2}	318.610	335.000	0.09

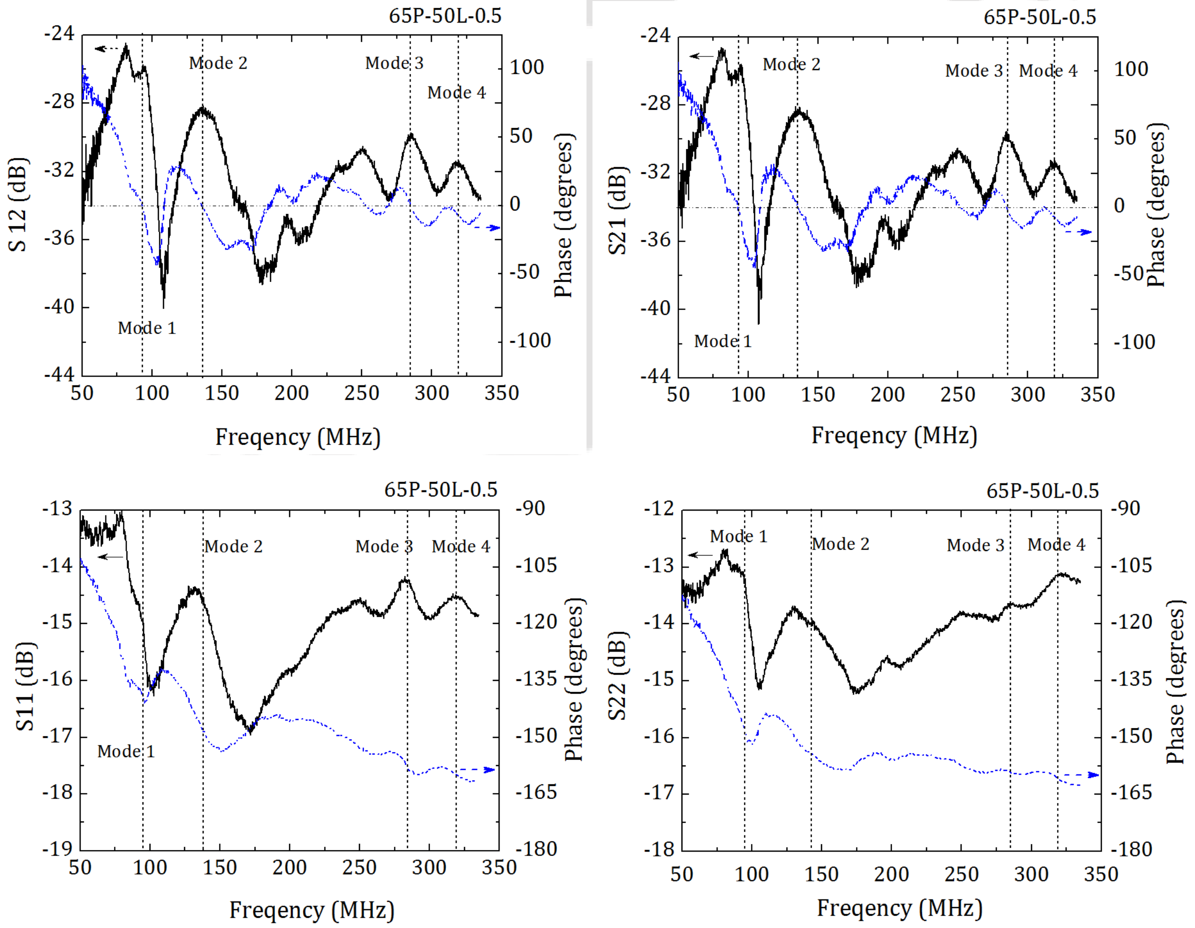

Fig. 5.7. Magnitude and phase plots of measured S parameters of a fabricated two port SAW resonator labeled 65P-60L-0.5 on plain silicon wafer without an oxide layer. The resonance modes are identified by the zero crossings in the phase plots of S12.

Using the resonance and anti-resonance frequencies observed from S21 characteristics, effective coupling coefficient K_{eff}^2 for all surface modes generated in the structure are calculated and mentioned in Table 5.3.

5.3.1 Simulation of two port SAW resonator on silicon substrate as fabricated

Since the simulation of a two port SAW resonator with reflector gratings is practically time demanding and requires high computational resources, a periodic section of fabricated device with periodic boundary conditions is simulated using the dimensions measured on fabricated two port SAW resonator by FESEM. Frequency dependent finite element simulations are carried out with the dimensions as fabricated, so that the measured S parameters of two port resonator are verified as well as the modes generated in device are identified. A periodic section of fabricated one port SAW resonator is considered for the FE simulations and the 2D geometry is shown in Fig. 5.8(a). The geometry of one period section of fabricated device comprises of silicon substrate of half wavelength width (8 µm), IDT pattern made of gold of thickness 0.11 µm, ZnO pattern of height 3.4 µm above the 0.7 µm thick ZnO film remnant of etching process and a shift in ZnO pattern having an overlap of around 0.4 µm with the IDT structure and frequency dependent analysis is carried for a frequency range of 50MHz to 350MHz. The S11 characteristics of simulated structure is shown in Fig. 5.8(b). From the results we observed four surface modes generated in the structure at frequencies 91.003 MHz (VP_{T0}), 187.788 MHz (VP_{L0}), 264.957 MHz (VP_{T1}), and 320.63 MHz (VP_{T2}). The type of surface modes generated in the structure are determined

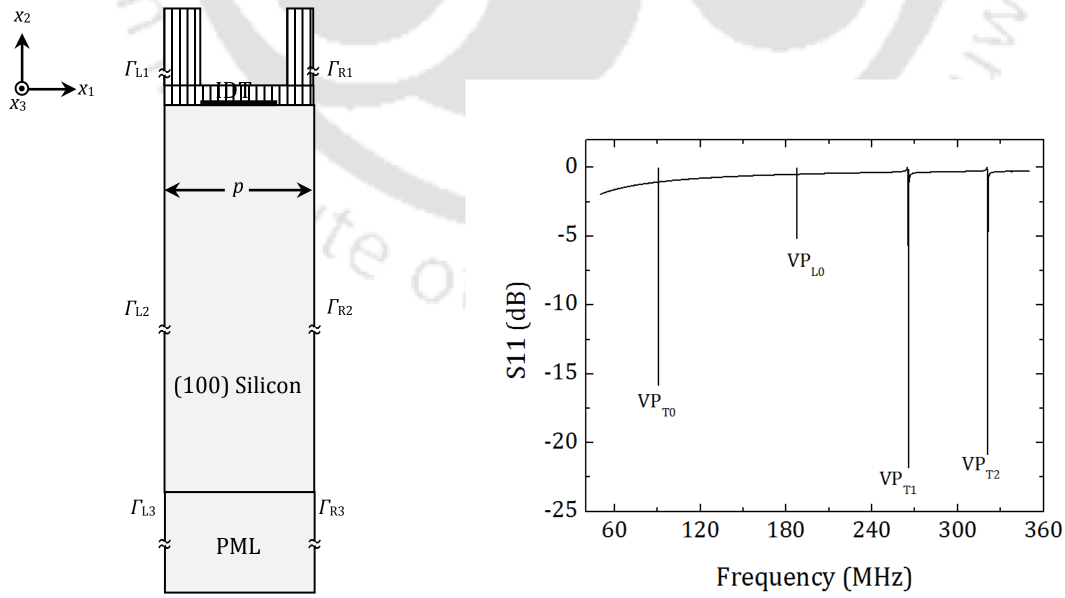

(a) (b)

Fig. 5.8. (a) The 2D geometry of fabricated proposed SAW resonator on silicon substrate with ZnO pattern shift of 0.5 µm (b) S11 characteristics obtained from FE simulations.

from the displacement profiles and the comparison of fabricated results and simulated results are listed in Table 5.4.

Table 5.4 Comparison of measured S11 results and simulated results for 65P-60L-0.5 two port SAW resonator.

Surface mode	Experimental (MHz)	Simulated (MHz)	Comments
VP_{T0}	092.930	091.030	An error of 2% is observed
VP_{L0}	136.034	187.788	An error of 27% is observed
VP_{T1}	284.769	264.957	An error of 7% is observed
VP_{T2}	318.610	320.630	An error of 0.6% is observed

From the above table the experimental results are in good agreement with the simulation results for VP_T modes with maximum error of 7% and the possible reasons for deviation are disconnections in some electrodes, non-uniform etching of ZnO pattern due to the difference in flow rates of etchant in the groove structure, non-uniformity in ZnO height along the aperture, variations in ZnO pattern, shape of ZnO block, and also the adhesion between ZnO pattern and silicon substrate. An error of 27% is observed for VP_{L0} mode. The quality of ZnO deposition deteriorates for film thicknesses greater than 1 µm and significantly affects the velocity of longitudinal BAW rather than transverse BAW which is predominately dependent on the dimensions of the structures. Therefore, resonance frequency of VP_{L0} mode which is generated by longitudinal BAW in ZnO blocks of 4.3 µm height has significantly deviated.

5.3.2 S parameters of two port SAW resonator fabricated on silicon substrate with oxide layer

The measured S parameter characteristics of a two port SAW resonator 45P-50L-0.5 fabricated on silicon substrate with 1.73 µm oxide layer are shown in Fig. 5.9. The magnitude and phase plots of S parameters re-plotted in Fig. 5.10 indicate the resonance modes generated in the device.

We identify the resonance modes from the zero crossings observed in phase plot of the S12 characteristics of 45P-50L-0.5; Mode 1 at 106.063 MHz with IL -22.73 dB, Mode 2 at 145.344 MHz with IL -23.77 dB, Mode 3 at 288.22 MHz with IL -25.47 dB, Mode 4 at 320.84 MHz with IL -24.74 dB. As observed from the results of simulations of one port and two port SAW resonators, Mode 1, Mode 2, Mode 3 and Mode 4 correspond to VP_{T0}, VP_{L0}, VP_{T1}, and VP_{T2} respectively. The series and parallel resonance frequencies of surface modes generated in the structure can be obtained from the phase plots (Fig. 5.10) of the fabricated two port

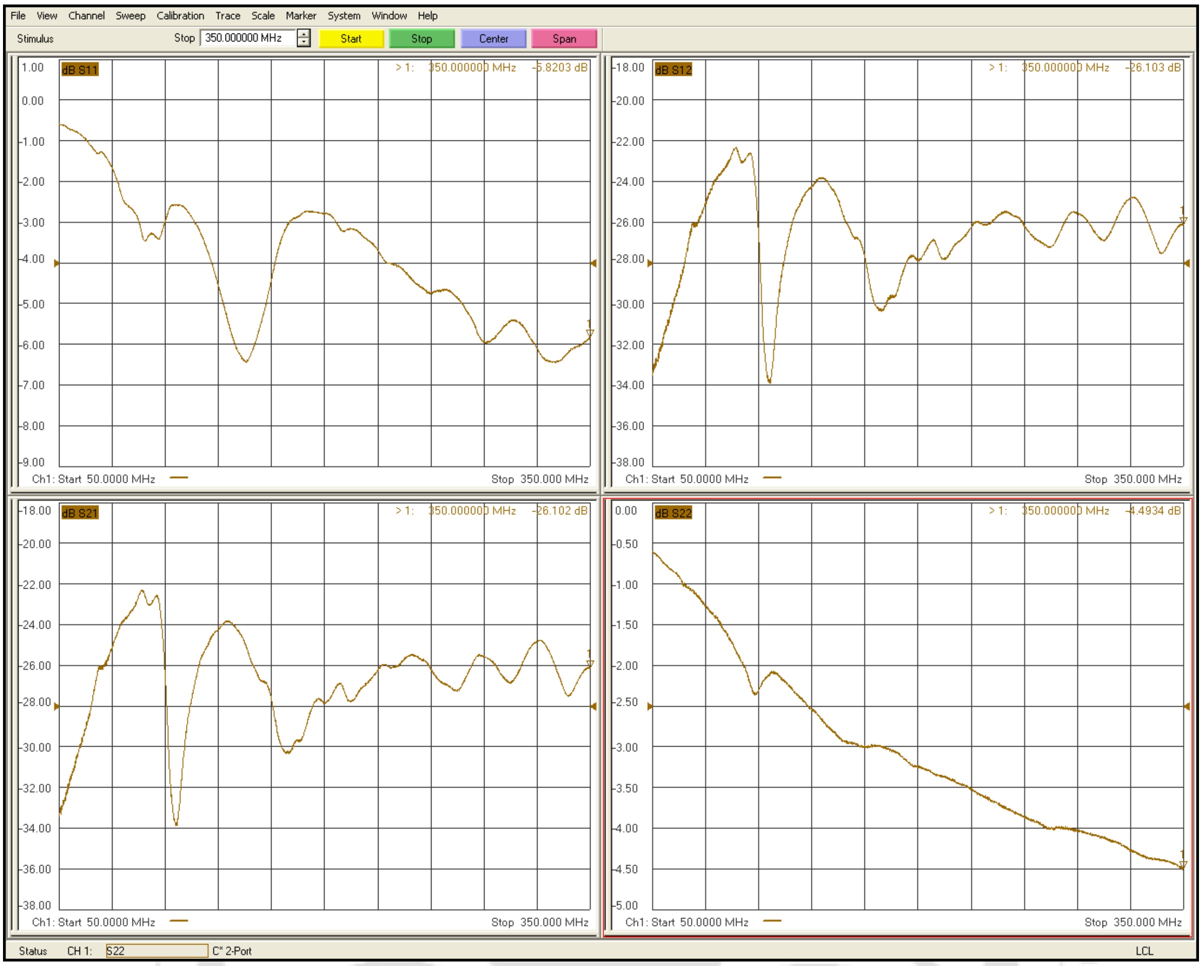

Fig. 5.9. The snapshot of measured S parameter characteristics of a two port SAW resonator labeled 45P-50L-0.5 fabricated on silicon wafer with 1.73 µm thick oxide film.

SAW resonator 45P-50L-0.5. The resonance and anti-resonance frequencies with effective coupling coefficient values of all the modes are listed in Table 5.5. From the simulations discussed in Chapter 3, the surface modes generated by the longitudinal bulk wave in ZnO pattern are undetectable but in practical results the VP_{L0} mode is significant due to the misalignment of ZnO pattern with respect to IDT structure, as verified in the case of devices discussed in Sections 5.2 and 5.3.1.

Table 5.5 Resonance and anti-resonance frequencies for surface modes and corresponding effective coupling coefficient values of two port SAW resonator 45P-50L-0.5 fabricated on silicon substrate with oxide layer.

Surface mode	Resonance (MHz)	Anti-resonance (MHz)	K_{eff}^2
VP_{T0}	106.063	114.500	0.140
VP_{L0}	151.531	179.563	0.287
VP_{T1}	287.188	305.000	0.110
VP_{T2}	321.969	337.344	0.089

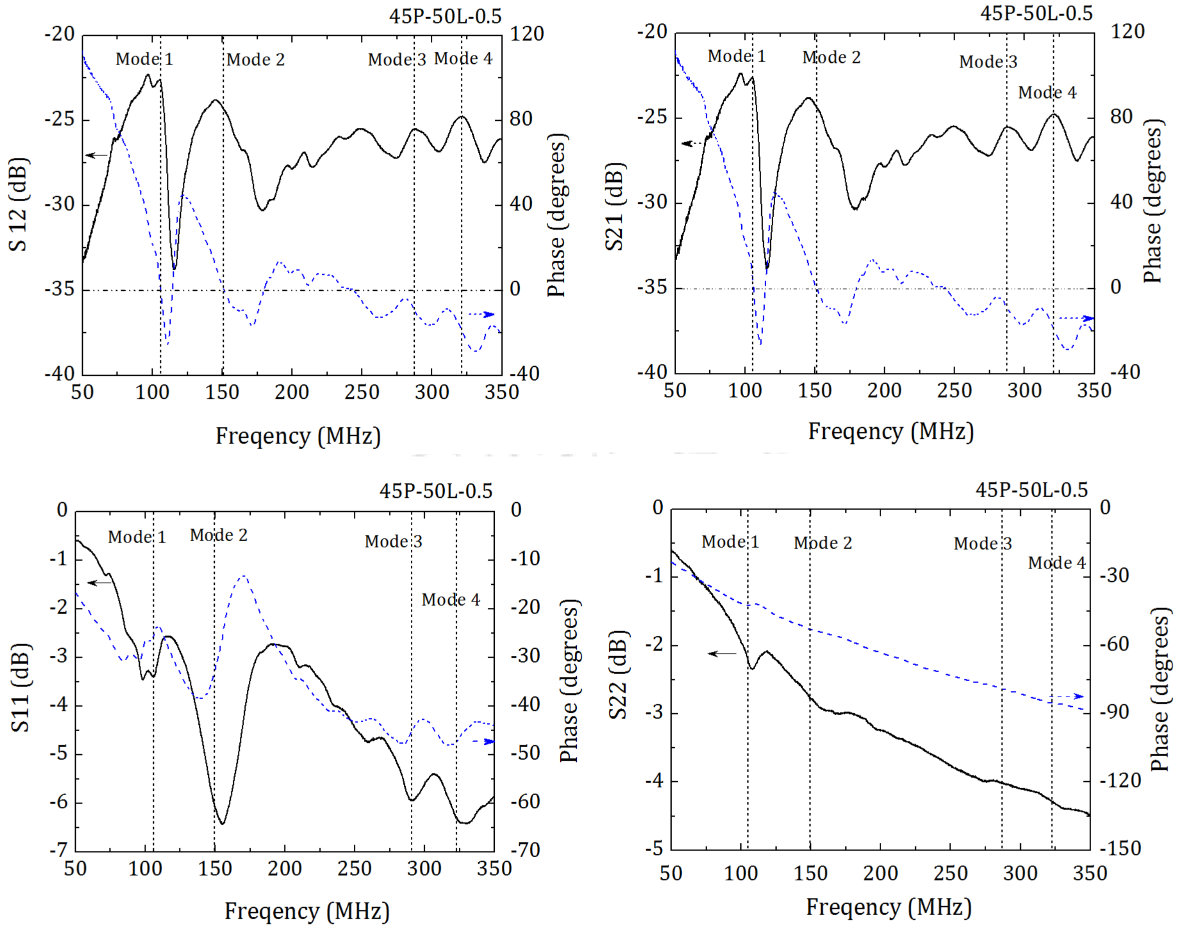

Fig. 5.10. Magnitude and phase plots of S11, S12, S22, and S21 characteristics of fabricated two port SAW resonator labeled 45P-50L-0.5 having an oxide layer of 1.73 μm. The resonance modes are identified by the zero crossings in S12 phase plot.

From the characteristics, Mode 1 exhibits a low insertion loss compared with the other three modes, the reason being the device impedance at mode 1 is closer to 50 Ω source impedance whereas the impedance mismatch is greater at other modes resulting in small peak magnitudes [71]. The simulated S11 parameter after adding compensation network for impedance matching is obtained for one representative case in the following section.

5.3.3 Compensation network to match impedance

The measured S11 parameters of 45P-50L-0.5 labeled two port SAW resonator fabricated on silicon substrate with oxide layer is considered as a representative case for studying the S11 parameter after adding a compensation network to match the device impedance with the source impedance at the designed resonance frequency. From the data generated by the network analyzer for S11 parameter of 45P-50L-0.5 device without matching network, VP_{T1}

mode is observed at 292.25 MHz with RL -5.937 dB and phase -47.7°. Following steps are performed to obtain the S11 characteristics with matched network:

Step 1: Conversion of polar data to complex data.

RL -5.937 dB and phase −47.7° values at 292.25 MHz are converted to the polar form as 0.51∠−47.27° and the complex form as **I** = 0.346−*j*0.3745.

Step 2: Calculation of input impedance of the device using the formula

Z = 50((1+**I**)/(1−**I**)), where **I** is the calculated complex data obtained in step 1.

Therefore **Z** = 69.86−*j*66.213.

Step 3: Calculation of *L* and *C* for the matching network

The values of *L* and *C* of the matching network for **Z** calculated in step 2 to obtain effective impedance of 50 Ω are 32.34 nH and 8.473 pF respectively with capacitor in series and inductor in parallel connection with the device.

Step 4: Calculation of S11 using the following formula

S11=20log|(**Z**−50)/(**Z**+50)|

The obtained S11 characteristics after addition of matching circuit are shown in Fig. 5.11. The plot shows that devices with matching network exhibit low return loss at the designed frequency 292.25 MHz. If dry etching process was used instead of wet etching, the experimental results would have been closer to the simulated results.

The summary of measured S parameter characteristics of 26 two port SAW resonators fabricated on various samples without oxide layer as well as with oxide layer are listed in Table 5.6. The table comprises of details of resonance frequencies and insertion loss parameters of the surface modes generated in the structure.

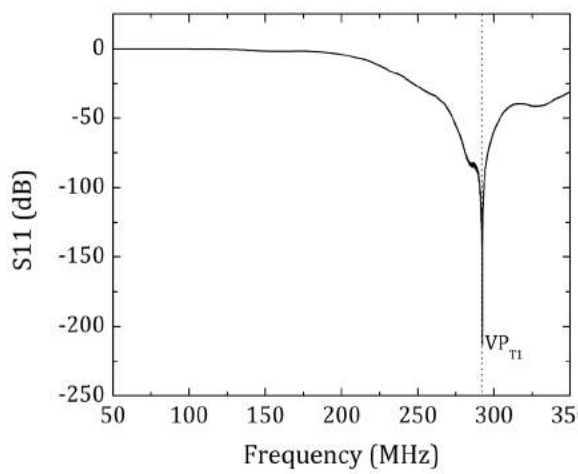

Fig. 5.11. The S11 characteristics of 45P-50L-0.5 SAW device with matching network.

Table 5.6 Measured S 12 parameters of fabricated two port SAW resonators.

Device	VP_{T0} (MHz)	IL (dB)	VP_{L0} (MHz)	IL (dB)	VP_{T1} (MHz)	IL (dB)	VP_{T2} (MHz)	IL (dB)
Sample 1: Patterned-ZnO/1.73μm-SiO_2/Si								
45P-50L-0.5	106.06	-22.73	151.53	-24.39	288.22	-24.47	320.84	-24.74
55P-50L-1.5	113.75	-19.22	149.97	-17.60	291.03	-19.26	320.66	-19.92
65P-50L-0.75	113.38	-18.59	145.63	-17.39	288.41	-19.19	321.13	-19.82
65P-60L-1.5	103.62	-22.66	139.34	-22.28	290.28	-25.34	320.19	-25.88
Sample 2: Patterned-ZnO/1.73μm-SiO_2/Si								
45P-50L-1.5	112.06	-26.41	143.91	-21.54	288.03	-24.78	–	–
45P-60L-0.5	110.38	-20.49	144.00	-18.44	288.5	-19.07	–	–
55P-50L-1.5	112.16	-25.68	143.06	-23.47	289.34	-24.03	–	–
65P-50L-1.5	108.03	-27.46	147.28	-26.63	289.53	-29.32	–	–
35P-70L-0.5	109.25	-31.92	147.59	-30.44	287.75	-32.03	320.28	-32.59
45P-60L-0.5	110.84	-31.51	148.16	-31.38	292.62	-33.74	321.59	-34.65
45P-70L-0.5	113.47	-32.95	148.91	-32.35	291.5	-35.65	321.87	-36.65
55P-60L-0.5	109.06	-31.72	146.75	-31.63	287.84	-34.9	320.66	-36.04
55P-70L-0.5	113.56	-37.97	144.31	-37.82	286.53	-41.36	322.16	-42.32
65P-60L-0.5	092.09	-33.09	143.37	-33.13	290.19	-37.02	322.16	-39.18
Sample 3: Patterned-ZnO/Si								
35P-60L-0.5	093.99	-28.67	141.73	-30.89	282.99	-30.8	317.37	-32.10
55P-50L-1.5	092.92	-27.25	137.81	-29.21	288.33	-31.24	318.79	-31.6
55P-60L-1.5	092.75	-26.14	136.92	-28.01	288.15	-29.54	318.08	-30.09
55P-70L-0.5	–	–	142.59	-29.59	288.00	-30.88	318.40	-33.67
65P-50L-0.5	092.93	-26.25	136.21	-28.30	285.12	-29.72	318.61	-31.43
65P-60L-0.5	094.53	-25.78	145.83	-24.73	288.68	-25.93	318.97	-28.74

Devices 35P-50L-1.5, 35P-60L-1.5, and 55P-60 L-1.5 in sample 1 and devices 65P-60L-0.5, 65P-70L-0.5 in sample 3, are damaged and not listed. The calculated Q factor for various modes generated in the fabricated SAW devices are tabulated in Table 5.7.

Table 5.7 Measured Q factor for various surface modes generated in the fabricated two port SAW resonators.

Device	VP_{T0} BW (MHz)	*Q* VP_{T0}	VP_{L0} BW (MHz)	*Q* VP_{L0}	VP_{T1} BW (MHz)	*Q* VP_{T1}	VP_{T2} BW (MHz)	*Q* VP_{T2}
Patterned-ZnO/1.73μm-SiO₂/Si								
45P-50L-0.5	8.34	12.7	27.93	5.42	18.84	15.3	16.03	20.01
55P-50L-1.5	9.2	12.3	36.23	4.13	–	–	–	–
65P-50L-0.75	10.24	11.1	41.24	3.63	–	–	–	–
65P-60L-1.5	10.78	9.6	46.16	3.38	19.41	14.9	18.56	17.20
Patterned-ZnO/Si								
35P-60L-0.5	12.64	8.5	23.33	4.6	10.5	26.9	14.78	21.46
55P-50L-1.5	14.96	6.21	43.29	3.2	12.29	23.5	15.50	20.57
55P-60L-1.5	15.55	6	44.18	3.0	13.72	21.0	16.39	19.41
55P-70L-0.5	–	–	46.85	3.0	10.14	28.3	13.95	22.81
65P-50L-0.5	16.20	5.83	16.4	8.3	8.56	33.3	14.4	22.10
65P-60L-0.5	10.86	8.7	–	–	16.03	18.0	–	–

Devices 35P-50L-1.5, 35P-60L-1.5, and 55P-60 L-1.5 in sample 1 and devices 65P-60L-0.5, 65P-70L-0.5 in sample 3, are damaged and not listed. 45P-50L-1.5, 55P-50L-1.5, 65P-50L-1.5, 35P-70L-0.5, 45P-60L-0.5, 45P-70L-0.5, 55P-60L-0.5, 55P-70L-0.5 devices on Sample 2 exhibit small peaks in order to calculate the Q factor.

5.4 The study of effect of misalignment of patterned ZnO structure

In order to study the effect of misalignment of ZnO pattern and width of ZnO pattern on the device characteristics, FE simulations are performed on a periodic section of proposed SAW device and eigenmode analysis with parametric sweep of position of ZnO pattern as well as width of ZnO pattern.

We carried out a frequency dependent analysis on the periodic structure shown in Fig. 5.12, without misalignment *i.e.* the ZnO pattern is located in the middle of spaces of IDT. We performed frequency dependent analysis on the proposed structure to study the effect of misalignment of ZnO pattern on SAW characteristics. Fig. 5.12(a) shows the cross-sectional view of a section of one port SAW resonator. In general, ± 0.5 μm shift is expected during lithography process and the maximum possible misalignment of proposed ZnO pattern structure is 6 μm. We carried out eigenmode analysis and the change in resonance

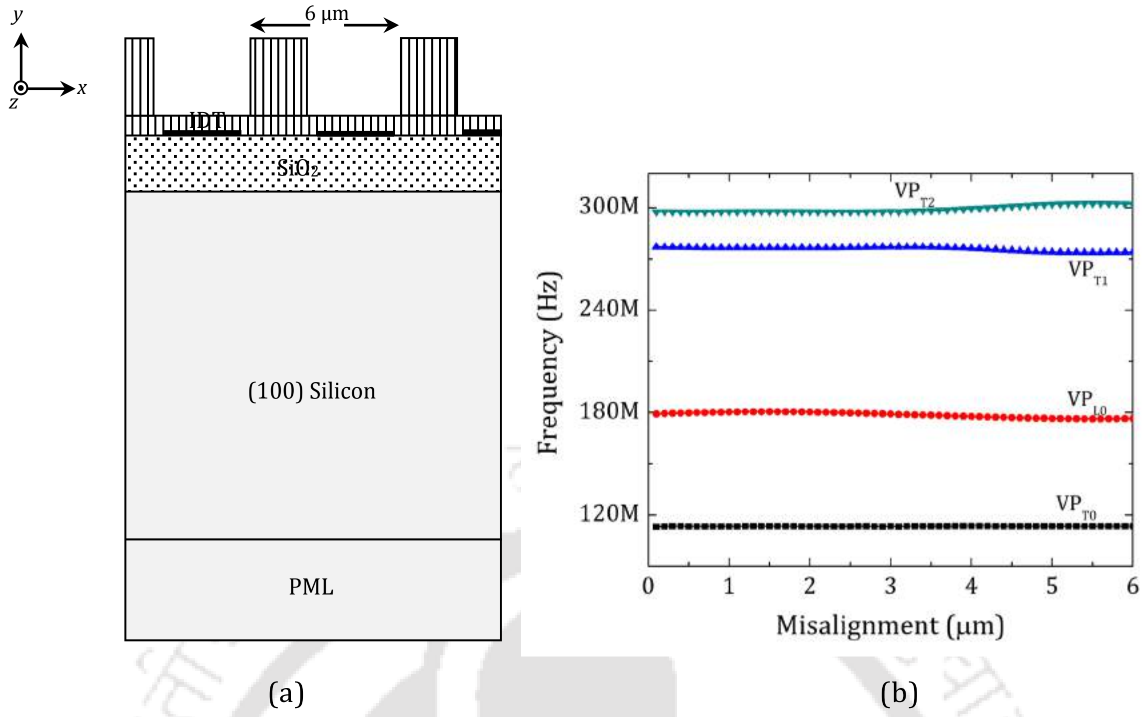

Fig. 5.12. (a) Cross sectional view of a section one port SAW resonator and (b) frequency characteristics with respect to misalignment shift of ZnO pattern.

frequencies of surface modes generated in the structure with respect to the misalignment of ZnO pattern are plotted in Fig. 5.12(b).

From the results we observe a maximum shift in frequency of around 0.4 MHz per 0.1 µm misalignment for VP_{T2} mode. From the experimental results we have observed four resonance peaks of surface modes generated by both longitudinal and transverse bulk waves in ZnO pattern, whereas from the simulation results of proposed structure without

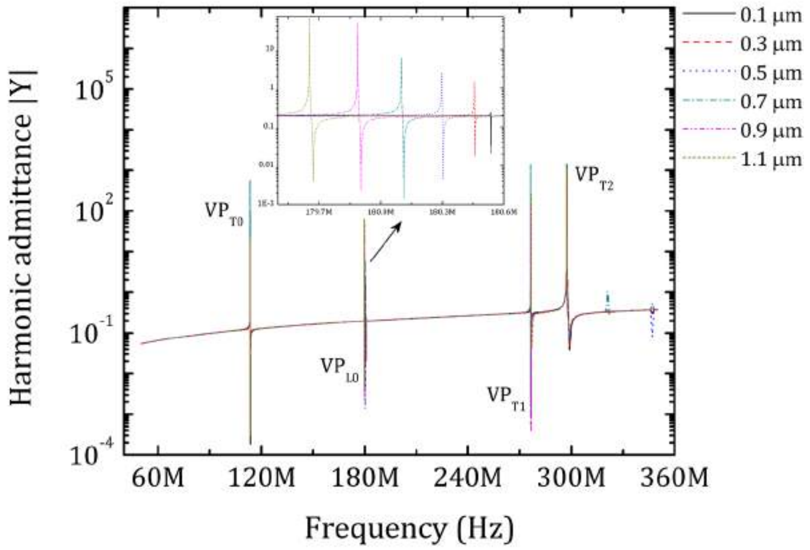

Fig. 5.13. Admittance characteristics of proposed structure at different values of misalignment.

misalignment the surface modes generated by longitudinal waves are insignificant. The reason behind the significance of VP_{L0} mode is due to the shift of ZnO pattern, which leads to increased in-line electric field along the ZnO block results in strong perturbation of longitudinal modes in the structure that couples acoustically to silicon substrate to generated VP_{L0} mode.

To validate the above statement, we perform frequency dependent analysis on the structure by shifting the ZnO pattern along *x* and the admittance characteristics of the device with different misalignment values of ZnO pattern are shown in Fig. 5.13. In this analysis, we consider dimensions of fabricated device with ZnO pattern located in the spaces of IDT and with step size of 0.2 μm shift along *x*. From the magnified window around VP_{L0} mode in Fig. 5.13, we observe gradual increase in the magnitude of VP_{L0} mode, as the ZnO pattern starts overlapping the electrode increasing the in-line electric field along ZnO blocks. This confirms the generation of VP_{L0} mode due to misalignment of ZnO pattern with respect to IDT.

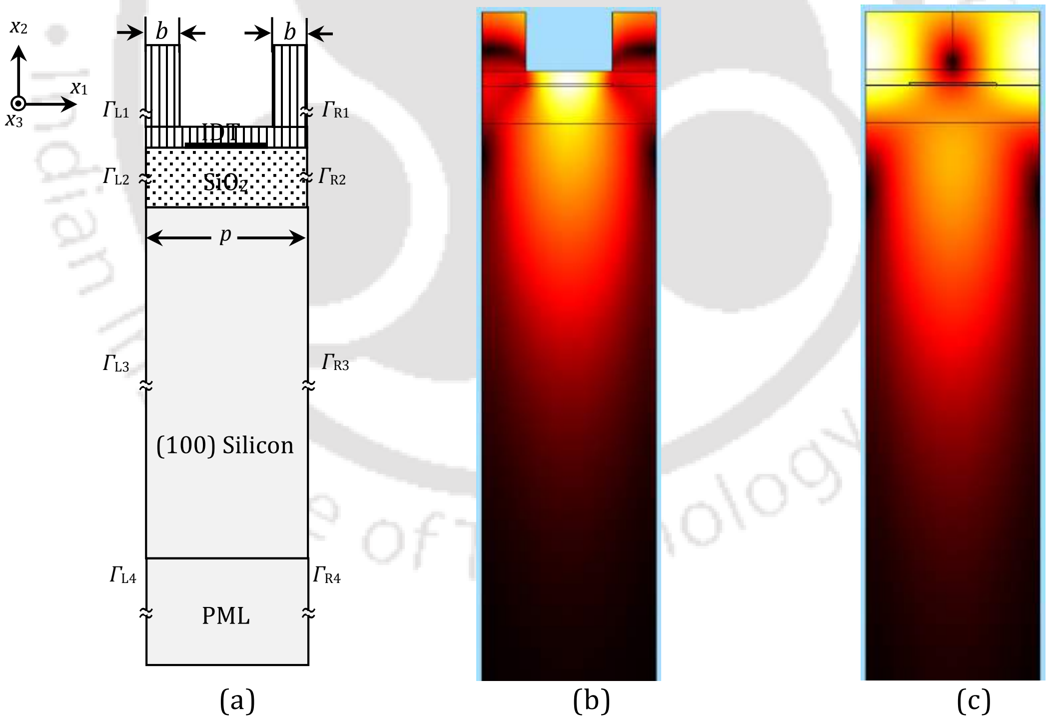

Fig. 5.14. (a) The 2D geometry used for parametric sweep of ZnO width, *y*-displacement profile of surface modes generated in the structure at (b) $2b/\lambda = 0.25$, and (c) $2b/\lambda = 0.5$.

5.5 The study of effect of width of patterned ZnO structure

The uncertainties in the dimensions of HM during development and in ZnO etching process result into width variation of ZnO blocks. The 2D simulation of width variation in ZnO pattern is carried out using periodic geometric structure shown in Fig. 5.14 (a). Parametric sweep in eigenmode analysis is carried out to obtain the frequency dispersion characteristics of surface modes generated in the structure with respect to the width ($2b$) of ZnO block. The y-displacement profiles of surface modes generated in the structure at $2b/\lambda$ = 0.25 and 0.5 are shown in Fig. 5.14 (b) and (c) respectively, and the dispersion characteristics are shown in Fig. 5.15. VP_T modes are significantly affected than VP_L modes by variation in ZnO width and the maximum frequency shift of around 5 MHz per 0.1 μm variation in ZnO width is observed for VP_{T2} mode. Fig. 5.15, we can observe that the frequency increase abruptly at $2b/\lambda$ =0.5 which is equivalent to continuous film and the structure behaves as a conventional thin film SAW resonator.

From the study of effect of misalignment in ZnO pattern and width variation of ZnO pattern, we observe that the shift in resonance frequency with respect to misalignment of patterned structure is negligible, as the operating frequency of the device depends on the width and height of ZnO blocks rather than positioning of ZnO pattern. The fact can also be verified using standard formulas for the transverse and longitudinal bulk modes generated in the ZnO pattern.

The frequency of the first bulk transverse mode is given by the formula [70]

$$f_{T0} = 0.162\,\frac{a}{h^2}\sqrt{\frac{\mu}{\rho}} = 0.162\,\frac{a}{h^2}\sqrt{\frac{E}{\rho}\frac{1}{2(1+\mu)}} = 0.162\,\frac{a}{h^2}\sqrt{\frac{c_{44}}{\rho}} \tag{5.1}$$

where a is width and h is height of ZnO block, E is Young's modulus, μ shear modulus, and ρ the density of ZnO.

The frequency of higher order transverse bulk modes is given by

$$f_{Tn} = 2.81\left[n-\frac{1}{2}\right]^2 f_{T0} \tag{5.2}$$

where n in an integer, n = 1, 2, 3….

The frequency of bulk longitudinal modes is given by

$$f_L = \frac{m}{4h}\sqrt{\frac{E}{\rho}\frac{1-\mu}{(1+\mu)(1-2\mu)}} = \frac{m}{4h}\sqrt{\frac{c_{11}}{\rho}} \tag{5.3}$$

where h is height of ZnO pattern, ρ density of ZnO, E is Young's modulus, μ is shear modulus, and integer m = 1, 3, 5…

From (5.1) and (5.3) the frequency of transverse BAW is proportional to width of ZnO whereas frequency of longitudinal BAW is independent of ZnO width, hence VP_T modes are significantly affected by width of ZnO block.

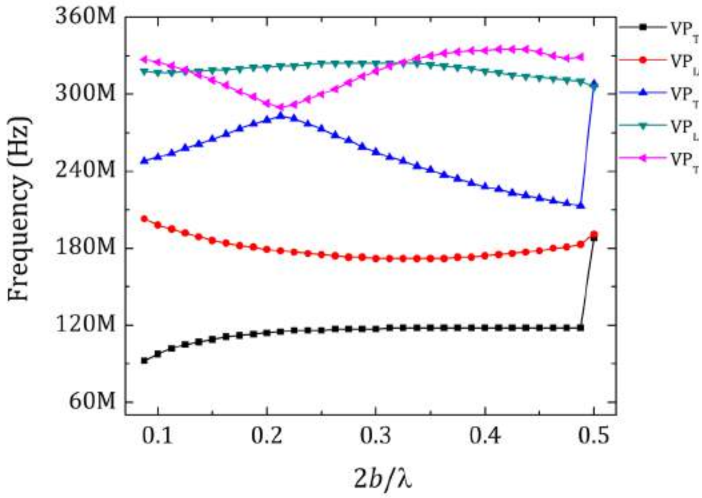

Fig. 5.15. Frequency variation with respect to base width of ZnO pattern on the proposed structure.

5.6 Calculation of K^2 using delay line configurations

In the previous chapters a significant emphasis is made on coupling coefficient and phase velocity and in order to calculate K^2 of proposed structure, we have fabricated several SAW delay lines with free surface propagation path and metalized propagation path and K^2 is calculated using

$$K^2 = \left(\frac{v_f - v_m}{v_f}\right)$$

where v_f and v_m are the free surface velocity and metalized surface velocity, respectively.

The S21 parameters of free and metalized surface delay lines fabricated on silicon substrate without oxide layer are shown in Fig. 5.16. From the S21 characteristics of free surface delay

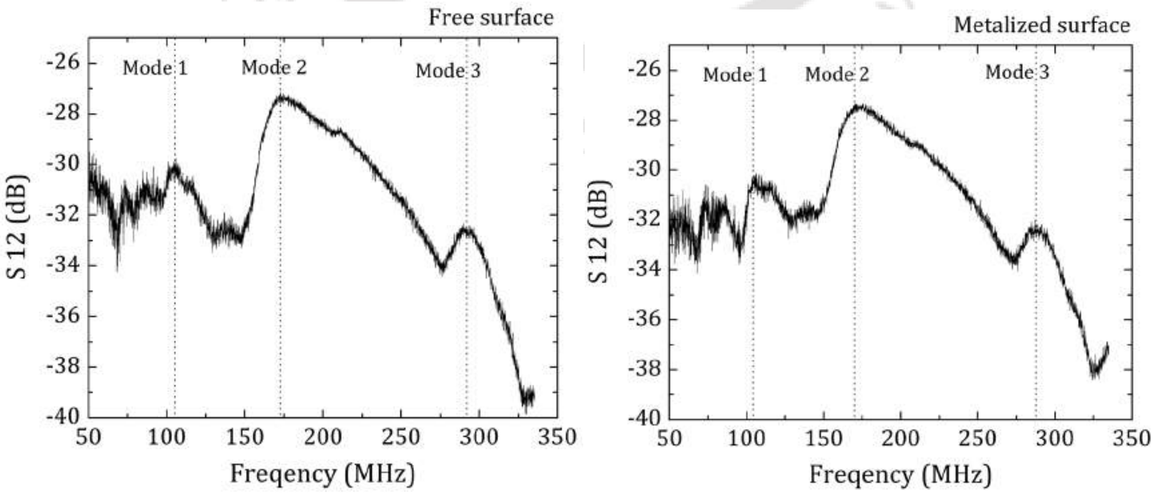

(a) (b)

Fig. 5.16. S21 characteristics of (a) free surface delay line and (b) metalized surface delay line.

line, we observe three resonance frequencies with Mode 1 at 107.8 MHz with IL -29.79 dB, Mode 2 at 174.24 MHz with IL -27.11 dB, and Mode 3 is observed around 293.67 MHz with IL -32 dB. From the S21 characteristics of delay line with metalized propagation path, Mode 1 is observed at 105.486 MHz with IL -30.2 dB, Mode 2 at 172.72 MHz with IL -27.81 dB, and Mode 3 is observed around 286.47 MHz with IL -32.4 dB. Using the S21 characteristics of delay line devices the calculated K^2 for Mode 1 is 4.29%, for Mode 2 is 1.74%, and for Mode 3 is 4.9%. From the previous simulations, Mode 1, Mode 2, and Mode 3 correspond to VP_{T0}, VP_{L0}, and VP_{T1} respectively. The obtained K^2 values are greater than K^2 of conventional thin film SAW devices. However it is less than the simulated K^2 values, because as observed from the FESEM analysis the ZnO structure is not a complete ZnO pattern and obtained structure is having a remnant film thickness in the range of 0.5–1 μm with a patterned ZnO structure with height in range of 3.3–3.8 μm. FE simulations are performed on a periodic structure of IDT with dimensions as fabricated and calculated the K^2 using free and metalized surface boundary conditions and the K^2 value of 3.85% for VP_{T0}, 4% for VP_{L0}, and 5.6% for VP_{T1}, which are in good agreement with practically obtained value.

5.7 S parameters of SAW devices fabricated through *e*-beam lithography process

5.7.1 One port SAW resonators

The S11 parameters and smith chart of a proposed SAW one port resonator fabricated using *e*-beam lithography process are shown in Fig. 5.17(a). The fabricated one port SAW resonator consists of 65 finger pairs with an aperture length of 60 wavelengths, IDT wavelength of 960 nm, electrode width 200 nm, ZnO pattern width of 200 nm, and metallization ratio of 0.42. We have re-plotted the characteristics to provide more detail and is shown in the Fig. 5.17(b). The S11 characteristics shows five resonance frequencies with first resonance frequency at 1.186 GHz with RL -0.46 dB, first higher order mode at 1.5003 GHz with RL -0.58 dB, second higher order mode observed at 2.12 GHz with RL -0.5 dB, third higher order mode at 4.4976 GHz with RL -0.54 dB, and fourth higher order mode at 4.9978 GHz with RL -0.63 dB. The return loss of all the resonance peaks are small due to the impedance mismatch. The samples are not annealed because of small electrode dimensions and commonly un-annealed ZnO has significant oxide defects that causes high insertion losses. The surface modes observed in the measured results are identified through FE simulations.

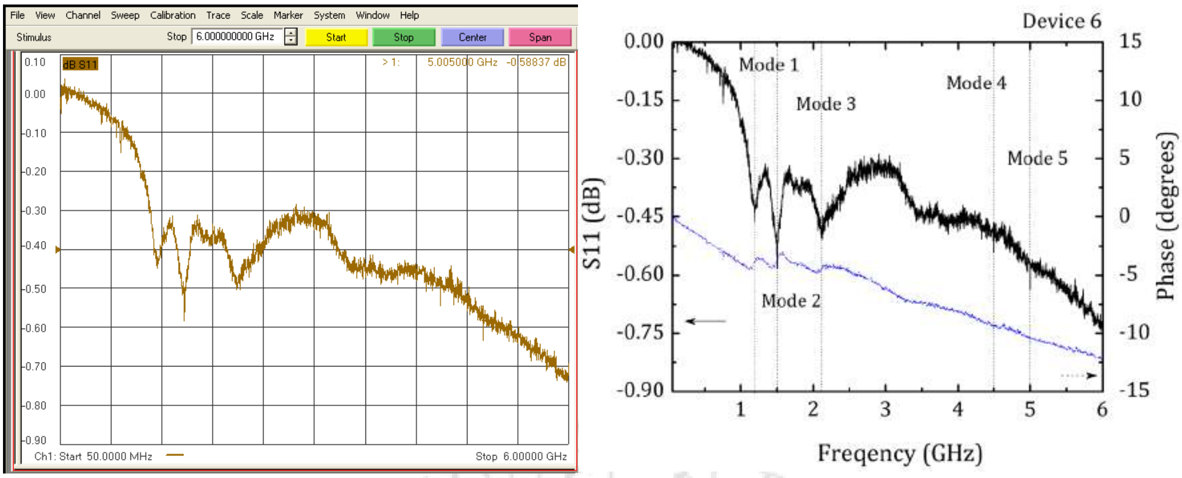

(a) (b)

Fig. 5.17. (a) Magnitude of S11 parameter obtained from network analyzer and (b) S11 characteristics showing magnitude and phase parameters plotted from the exported data.

5.7.2 Simulation of fabricated SAW device using e-beam lithography process

2D periodic structure of the one port SAW resonator as fabricated is shown in Fig. 5.18. The structure comprises of a silicon substrate with an oxide layer of 278 nm, IDT pattern made of chromium/gold of thickness 10 nm/60 nm and ZnO pattern of width 160 nm and height of 220 nm is located on the IDT structure. During fabrication we are unable to obtain a ZnO patterned structure in the spaces of IDT, due to the limitation of the equipment we carried out the second lithography using the same IDT pattern on the sample. Annealing process is avoided for the samples with sub-micro dimensions, since the gold electrodes can't endure the annealing process, as observed in the fabrication process of SAW devices using UV lithography process. We performed eigenmode analysis on the 2D structure shown in Fig. 5.18, and compared the simulation results with the test results and presented in Table 5.8. From comparison of experimental and simulated results, VP surface modes generated by the longitudinal BAW excited in ZnO block exhibit an error around 20%. Since, the longitudinal BAW modes are significantly affected by the quality of ZnO pattern than the transverse BAW, whereas transverse BAW's are predominately depends on the dimensions of the structures.

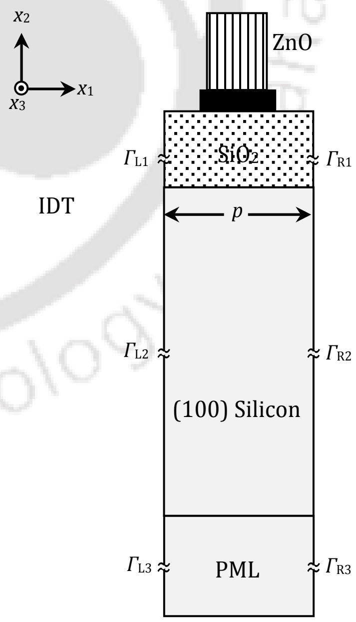

Fig. 5.18. The 2D geometry of fabricated proposed SAW resonator on silicon substrate with 278nm thick oxide layer using *e*-beam lithography.

Table 5.8 Comparison of tested and simulated results of e-beam SAW one port resonator device

Surface mode	Experimental (GHz)	Simulated (GHz)	Comments
VP_{T0}	1.181	0.935	Significant variation between fabricated and simulated is due to the un–annealed ZnO film, since the device characteristics are predominantly depends on the quality of ZnO film. In case of pattern structure the device operating frequency depends on the dimension of ZnO pattern.
VP_{L0}	1.502	1.951	
VP_{T1}	2.125	2.290	
VP_{L1}	4.499	4.840	
VP_{T2}	4.998	5.144	

The fact can be substantiate from equations (5.1) and (5.3). The resonance frequencies of BAWs generated in the ZnO pattern depends on the Young's modulus and Poisson's ratio, whereas the elastic constants are effected by annealing temperature and sputtering deposition conditions. Specifically the Young's modulus (E) of ZnO is greatly affected by annealing, with increase of temperature from room temperature to 800°C, the E increases from 129 GPa – 449 GPa and also the crystalline nature of the film increases substantially, which can be observed from the XRD results of ZnO films deposited at room temperature, shown in Fig. 5.19. From the XRD results, the annealed film shows high crystalline nature compared to un-annealed ZnO film. The S11 parameters of other fabricated devices are tabulated in Table 5.9.

Table 5.9 S11 parameters of surface modes generated in one port SAW resonators fabricated using *e*-beam lithography.

S. No	VP_{T0} (GHz)	RL (dB)	VP_{L0} (GHz)	RL (dB)	VP_{T1} (GHz)	RL (dB)	VP_{L1} (GHz)	RL (dB)	VP_{T2} (GHz)	RL (dB)
Sample: ZnO-Pattern/200-nm-SiO_2/Si										
3	1.186	-0.44	1.503	-0.62	2.127	-0.49	4.499	-0.54	4.997	-0.64
4	1.181	-0.37	1.502	-0.54	2.123	-0.45	4.499	-0.46	4.998	-0.56
5	1.184	-0.43	1.502	-0.58	2.125	-0.48	4.498	-0.50	4.998	-0.60
6	1.186	-0.46	1.500	-0.58	2.123	-0.50	4.498	-0.54	4.998	-0.63
7	1.181	-0.45	1.502	-0.55	2.123	-0.50	-	-	-	-
8	1.186	-0.33	1.502	-0.46	2.125	-0.43	4.497	-0.47	4.998	-0.55
9	1.186	-0.34	1.502	-0.45	2.116	-0.45	4.497	-0.47	4.998	-0.57
10	1.186	-0.29	1.502	-0.41	2.1251	-0.41	-	-	-	-

Device 2 the input port exhibits high impedance around 500 Ω and device 1 is not in condition to take the measurement. For devices 7 and 10 higher order modes are not clearly visible.

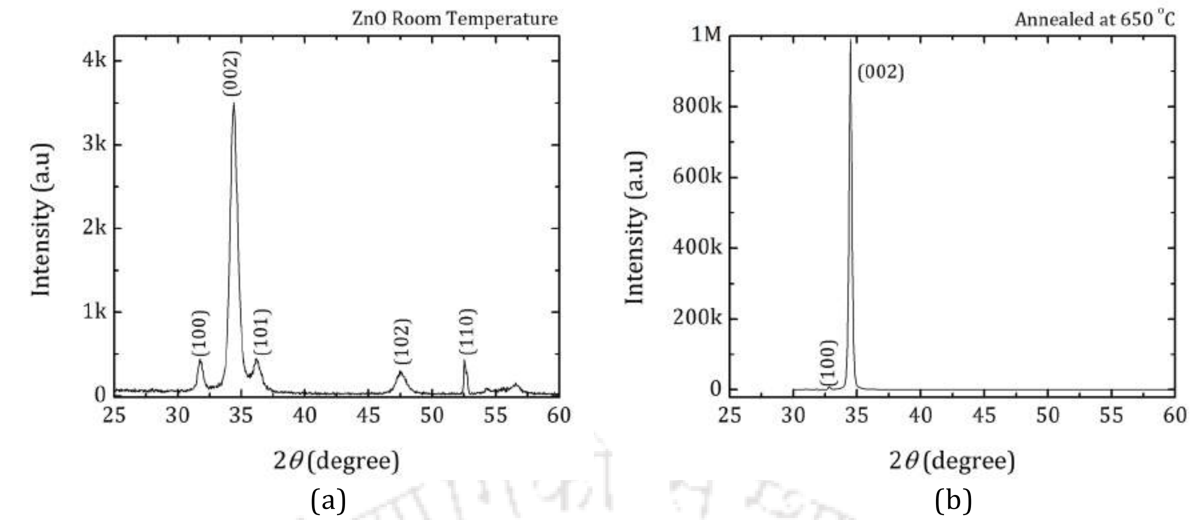

Fig. 5.19. (a) The XRD pattern of ZnO film deposited at room temperature and (b) XRD pattern of ZnO sample annealed at 650 °C.

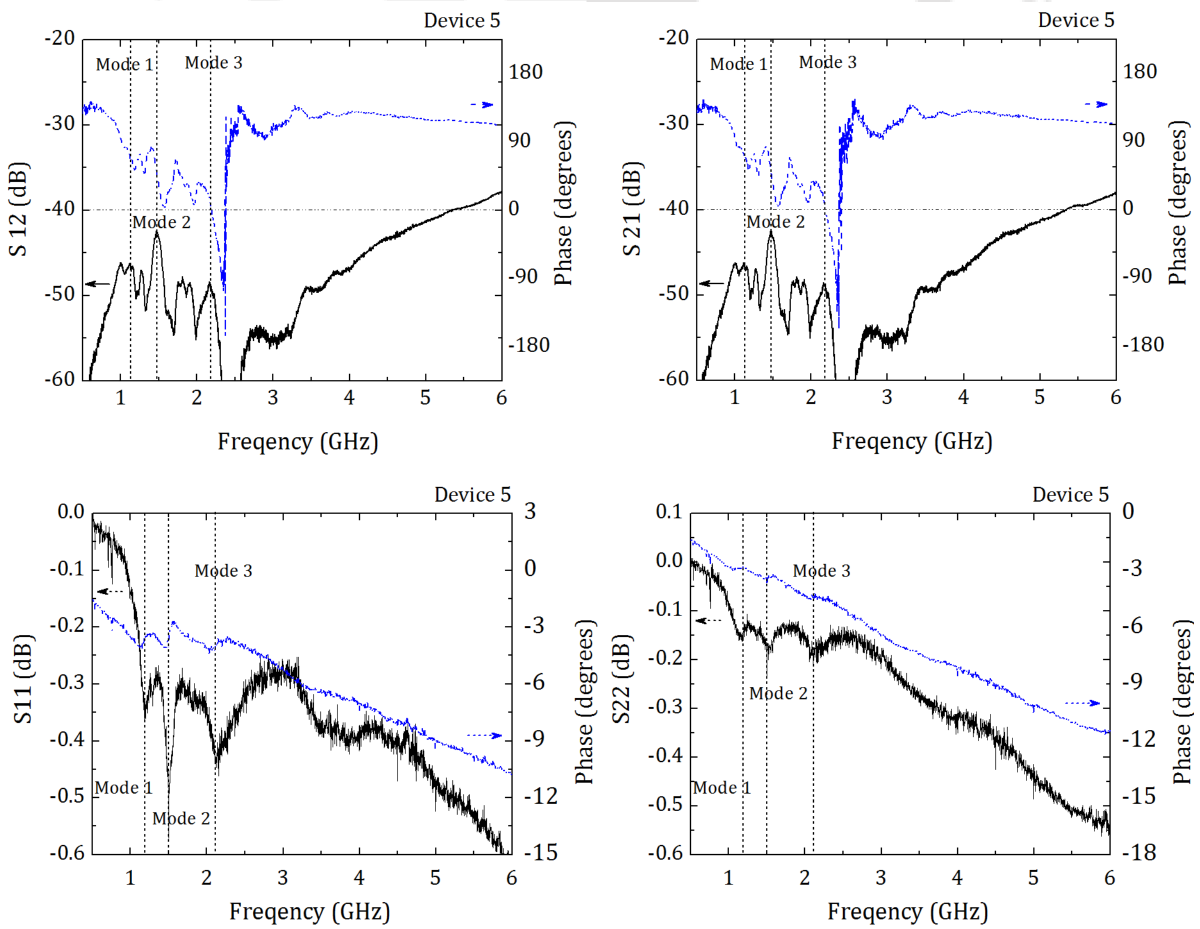

Fig. 5.20. Magnitudes of S11, S12, S22, and phase plots of S12 characteristics of a fabricated two port SAW resonator having 65 pairs of electrode and 60 wavelength aperture length on silicon substrate with 200 nm oxide layer. The modes are identified by the corresponding localized peaks in S11, S22 characteristics and phase zero crossing of S12, S21.

5.7.3 Two port SAW resonators

The S parameters of a two port SAW resonator fabricated on sample with 278 nm oxide layer are shown in Fig. 5.20. From the S12 characteristics, mode 1 at 1.15633 GHz with an insertion loss (IL) of -46.55 dB, mode 2 at 1.47428 GHz with a IL of -42.51 dB, mode 3 at 2.16039 GHz with a IL of -48.51 dB, and higher order modes mode 4 and mode 5 are not visible from the S12 characteristics. Modes 1, 2, and 3 correspond to VP_{T0}, VP_{L0}, and VP_{T1} respectively.

Using S12 characteristics and 3 dB band from VP_{L0} the device Q is calculated using

$Q = f_0$/3dB BW, 3 dB band width is calculated as 0.119 GHz and f_0 of 1.47428 GHz, and obtained Q is equal to 12. The S12 parameters of other fabricated two port devices are tabulated in Table 5.10.

Table 5.10 Measured S12 parameters of fabricated two port SAW resonators using *e*-beam lithography.

S. No	VP_{T0} (GHz)	IL (dB)	VP_{L0} (GHz)	IL (dB)	VP_{T1} (GHz)	IL (dB)	VP_{L0} 3 dB bandwidth (GHz)	Q VP_{L0}	VP_{T1} 3 dB bandwidth (GHz)	Q VP_{T1}
Sample: ZnO-Pattern/200 nm SiO_2/Si										
1	1.188	-46.81	1.474	-40.11	2.166	-48.14	0.113	13.00	0.186	11.65
2	-	-	1.472	-51.12	2.129	-55.12	0.1488	09.89	0.258	08.25
3	-	-	1.472	-47.26	2.153	-52.11	0.119	12.37	0.156	13.80
4	1.099	-44.22	1.476	-40.65	2.162	-46.83	0.117	12.60	0.139	15.55
5	1.156	-46.55	1.474	-42.51	2.160	-48.51	0.110	13.43	0.190	11.37
6	0.976	-32.93	1.463	-35.51	2.164	-42.79	0.115	12.69	0.297	07.27
7	1.002	-44.89	1.469	-42.06	2.166	-47.90	0.108	13.62	0.305	07.10
8	1.000	-45.00	1.471	-43.88	2.175	-51.76	0.121	12.61	0.202	10.70
9	1.002	-53.74	1.485	-53.86	1.961	-56.10	0.099	15.00	-	-
10	-	-	1.472	-59.91	-	-	0.102	14.49	-	-

For device 2 and 3 mode VP_{T0} is not visible and for devices 9 and 10 the output port is damaged significantly and resulting in high insertion loss.

5.8 Summary

This chapter details the testing of the fabricated proposed SAW device using UV lithography process and *e*-beam lithography process. The device characteristics are obtained using RF probe station cascaded to a network analyzer. After the initial calibration testing is carried out over a wide range frequency range of 50 MHz to 350 MHz. A large number of devices are tested and the characteristics of 29 devices are tabulated. One port SAW resonators, device labeled 75P-55L, from S11 characteristics we observed three resonant peaks. Mode

1 is observed at 111.5 MHz with RL -11.568 dB with a Q factor of 8.49 and effective coupling coefficient 0.16. FE simulation is carried out with dimensions as fabricated and compared with the measured results, the error between measured result and simulated result is around 5% for VP_T modes. The modes generated in the structure are identified from the displacement profiles of simulation result.

From the measured S parameters of two port SAW resonator labeled 65P-50L-0.5 on silicon substrate, four resonant peaks are observed, Mode 1 at 92.93 MHz with an IL of -26.25 dB, Mode 2 at 136.034 MHz with an IL of -30.94 dB, Mode 3 at 285.12MHz with an IL of -29.72 dB, and Mode 4 at 318.61 MHz with an IL of -31.43 dB and respective K_{eff}^2 are calculated based on resonance and anti-resonance frequencies. FE simulation is performed with dimensions of two port resonator as fabricated and the deviation between experimental and simulation results of fabricated devices is less than 7% and the Mode 1, Mode 2, Mode 3 and Mode 4 are correspond to VP_{T0}, VP_{L0}, VP_{T1}, and VP_{T2} surface modes. From the simulations discussed in Chapter 3, the surface modes generated by the longitudinal bulk wave in ZnO pattern are undetectable but in practical results the VP_{L0} mode is significant due to the misalignment of ZnO pattern with respect to IDT structure. An error of 27% is observed for VP_{L0} mode, since the quality of ZnO deposition deteriorates for film thicknesses greater than 1 μm and significantly affects the velocity of longitudinal BAW rather than transverse BAW which is predominately dependent on the dimensions of the structures. Therefore, resonance frequency of VP_{L0} mode which is generated by longitudinal BAW in ZnO blocks of 4.3 μm height has significantly deviated. If dry etching process was used instead of wet etching, the experimental results would have been closer to the simulated results.

For a two port SAW resonator labeled 45P-60L-0.5 fabricated on silicon substrate with an oxide layer of 1.73 μm thickness through UV lithography process, we observed four resonance frequencies from S12 characteristics and a maximum operating frequency of 322.16 GHz with an insertion loss of 39.18 dB is observed and exhibited by VP_{T2} mode, which is validated through FE simulations. Device labeled with 45P-50L-0.75 on sample 1, exhibits a best performance in terms of both insertion loss and maximum operating frequency. It exhibits a maximum operating frequency of 321.13 MHz with an insertion loss of -19.82 dB. From the K_{eff}^2 values, device on silicon substrate exhibits slightly higher values compared to device on silicon substrate with oxide layer.

Further FE simulations are carried out to study the effect of misalignment of ZnO pattern and dimensions of ZnO pattern and observed that the VP_{L0} mode will be dominant as the

ZnO pattern shifts over the electrode. Based on the simulation results of ZnO base width variation and misalignment of ZnO pattern, the operating frequency of device predominantly on dimensions of ZnO pattern and the dominant nature of VP_{L0} depends on the position of ZnO pattern.

Delay line SAW devices with free and metalized propagation path are fabricated and tested in order to obtain the K^2 values of modes generated in the structure. The calculated K^2 for VP_{T0} is 4.29%, VP_{L0} exhibits a K^2 value of 1.74%, and for VP_{T1} is 4.9% and the simulated K^2 values of 3.85% for VP_{T0}, 4% for VP_{L0}, and 5.6% for VP_{T1} are calculated.

10 one port resonators and 10 two port resonators are fabricated using *e*-beam lithography process are tested over a frequency range of 50 MHz to 6 GHz. High frequency of operation around 4.998 GHz is observed by Mode 4 which is VP_{T2} surface mode. From the S12 characteristics of two port SAW resonators, device 9 and mode VP_{L0} exhibits an operating frequency of 1.4854 GHz with an insertion of loss of -53.86 dB and a Q factor 15. Device 6 exhibits a best performance of operating frequency 1.46316 GHz with an insertion loss of -35.51 dB and a Q factor of 12.69. Significant error is observed between measured results and simulated results, due to un-annealed ZnO film.

Chapter 6

Edge Reflection Surface Acoustic Wave Devices on Silicon

ER type SAW devices on silicon, the second major contribution of this research work, which offer substantially small device area, since the device area on a silicon chip is crucial and minimizing the area of the SAW device would be of high priority in monolithic integration. This chapter presents the development of two types of edge reflection (ER) type SAW devices on silicon substrate using ZnO thin films and using periodically patterned-ZnO films. The simulations of the proposed ER type SAW devices on silicon are carried out using COMSOL Multiphysics and the fabrication design parameters are extracted using device dispersion characteristics and equivalent circuit model. Fabrication and testing of the proposed edge reflection type SAW devices on silicon validates the practicability of the devices. In order to demonstrate an application of the proposed devices, we realized coupled resonator filters and ladder filters using ER type SAW resonators on silicon substrate for RF signal processing applications.

In general, (002) *c*-axis oriented ZnO films have the ability to generate Rayleigh and Love waves depending on the relative orientation of IDT [33], [49]. Shear horizontal type surface acoustic waves (SH-SAW) such as (Love wave, BGS wave) exhibit an exciting property of complete reflection at free edges without mode conversion [72], [73]. Using the edge reflection property of SH-SAW and the Love wave generation capability of ZnO film, we realized ER type SAW devices on silicon using ZnO films and periodically patterned-ZnO films on silicon substrate having free edges at the end of the device. In ER type SAW devices, micro-machined vertical groove patterns are developed in silicon substrate to accomplish the total reflection of Love waves generated in ZnO film at the free edges formed by the grooves, transduction of Love wave is carried out using an IDT.

From the chapter 3, we notice that the patterning of ZnO thin films on the SAW devices results in the generation of surface mode with unique quality high K^2 and high phase velocity. Therefore, we carried out similar FE simulations on ER type SAW devices with patterned-ZnO film and obtain the dispersion characteristics of SH-SAW generated by the periodically patterned-ZnO film. The effect of IDTs made of heavy metals like gold and palladium on the device characteristics are studied using FE simulations. ER type SAW devices with patterned-ZnO film are fabricated using the dispersion characteristics obtained from FEM simulations and equivalent circuit model.

6.1 Introduction

A conventional one port SAW resonator on piezoelectric substrate comprises of an IDT for the transduction of surface waves, located between a pair of reflector gratings consisting of a large number of electrode fingers to accomplish the confinement of the SAW forming a resonance cavity as shown in Fig. 6.1(a) [3]. The surface waves are generated on the both sides of the IDT and are reflected at each and every metallic strip of the reflector grating. The wave propagates through the grating structure up to an effective distance known as penetration depth L_p at which the wave is effectively reflected and the gap between IDT and reflector grating is denoted by L_g. Due to the λ/2 pitch of grating structure the reflected waves add in phase to form standing wave pattern between the reflector gratings. In general, the surface waves are reflected from a free surface perpendicular to the direction of propagation and the characteristics of reflected wave depends on the type of SAW and phase at the instant of incident. In case of Ryleigh SAW, the incident wave on a free surface undergoes mode conversion to BAW, the energy of BAW depends on the phase of Rayleigh wave at the instant of impact. In case of SH-type SAW like BGS and Love wave, the wave is efficiently reflected from the free surface without any mode conversion and depending on the phase at the instant of impact, the reflected wave can add in phase with the transmitted SAW to form a standing wave pattern. Using the property of total reflection Suzuki *et al.* [72], reported the realization of resonators on a piezoelectric substrate with free parallel edges. Further, Kadota *et al.* [73] reported several edge reflection type SAW devices fabricated on single crystal piezoelectric substrates like 41° *Y–X* lithium niobate, 64° *Y–X* lithium niobate, and 128° *Y–X* lithium tantalate.

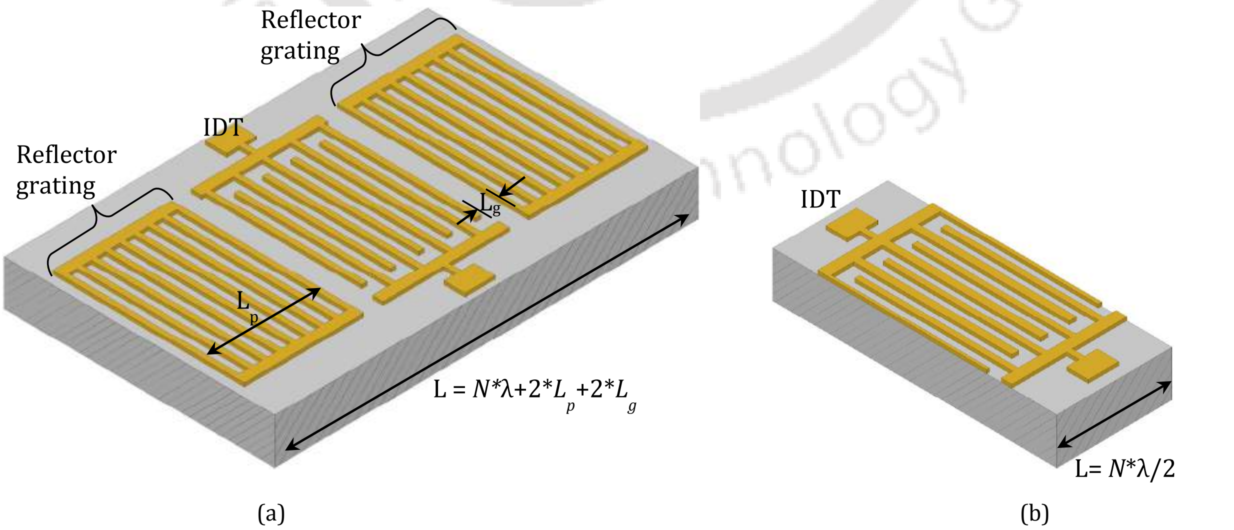

Fig. 6.1. 3D schematics of (a) conventional one port SAW resonator with reflector gratings and (b) edge reflection type SAW resonator with edge electrodes.

Fig. 6.1(b) shows the 3D schematic of an edge reflection type SAW resonator on piezoelectric substrate, which comprises of an IDT placed between a pair of parallel free edges of the piezoelectric substrate. Applying an electric signal to IDT results in generation of SH-SAW that propagate orthogonal to the aperture length and at the free edges the wave is reflected back without mode conversion adding in phase to the incoming SH-SAW to form standing wave pattern between the parallel edges. The surface wave confinement in ER type SAW devices is accomplished by the parallel edges rather than reflector gratings with a large number of electrode fingers, hence reducing the size of the device appreciably. In an ER type SAW device, the wavelength of SAW is λ, the overall length of device must be an integral multiple of λ, for the constructive interference between the generated wave and the reflected wave from the edges to form standing wave pattern [73]. IDT positioned between the parallel edges of the substrate comprises of set of electrodes fingers with width λ/4 and another set of electrodes with width λ/8 located at the free edges of the substrate, whereas λ/4 electrodes are arranged between the two λ/8 electrodes with λ/4 spacing between consecutive electrodes.

Using the one port SAW resonator configuration several edge reflection type SAW devices such as longitudinally coupled resonator filter (LCR), transversely coupled resonator filter (TCR) and various configurations of ladder filters can be realized using ER type one port SAW resonator with free edges for signal processing applications.

6.2 Love wave based SAW devices on silicon using ZnO films

As we already discussed in chapter 2, that (002) oriented ZnO can support both Rayleigh and Love waves depending on the relative orientation of IDT. There have been several reports on Love wave based ZnO thin film SAW devices on various substrates like quartz, lithium tantalate, and silicon. In Table 6.1 few selected literature on Love waves generated in ZnO thin films for various applications are listed. In 2000, Kalantar *et al.* [51], reported the transduction of love wave on silicon substrate with an oxide layer. Further, the study of SAW filters developed using love waves generated in the ZnO/SiO_2/Si structure was also reported in [52]. Kadota *et al*. [10] and [74] reported quartz substrate based SAW devices with ZnO overlay for SAW filters applications with narrow band and low loss characteristics, utilizing the shear horizontal leaky SAW generated in the structure. In 2006 Krishnamurthy et al. [33], reported the design and fabrication of high frequency Love wave based SAW device on silicon for bio-sensing applications and also reported the generation of Love waves in the ZnO film with change in orientation of IDT structure. Utilizing the ZnO film property of supporting both Rayleigh and Love waves, Moreira *et al.* [11] reported the generation of both Rayleigh and Love modes in ZnO/AT-Quartz structure and identified the type of surface wave using liquid drop test.

Table 6.1 List of selected reports on Love wave based ZnO thin film SAW devices.

SI. No	Layered structure	Application	Reference and year
1.	ZnO/ SiO_2/Si	Love wave transducer	Kalantar *et al.* [50] 2000
2.	ZnO/ SiO_2/Si	Love mode SAW filters	Kalantar *et al.* [51] 2001
3.	ZnO/Quartz	Low loss IF SAW filters	Kadota *et al.* [10] 2003
4.	ZnO/SiO_2/Si	Love waves for high frequency sensors	Krishnamurthy *et al.* [33] 2006
5.	ZnO/Quartz	SH-Leaky SAW based narrow band SAW filters	Kadota *et al.* [74] 2008
6.	ZnO/Quartz	Identification of Love waves in layered ZnO/Quartz SAW devices.	Moreira *et al.* [11] 2008

6.3 Proposed edge reflection (ER) type SAW devices on silicon using ZnO films

Utilizing the total reflection property of Love wave at free edges and the generation of Love wave in ZnO films, we propose an ER type SAW device on silicon, as shown in Fig. 6.2. The proposed ER type SAW device comprises of a silicon substrate with an optional oxide layer and a ZnO film in conjunction with IDT for the transduction of Love waves. The total reflection of Love wave is accomplished by the free edges formed after dicing the silicon substrate having length in multiples of λ/2, in order to obtain the free surface edges to aid in constructive interference and forming standing wave pattern, as shown in Fig. 6.2(a). Since, the operation of device substantially depends on the length of the device and the fabrication process comprises of dicing or cutting of silicon substrate makes the fabrication difficult for high frequency devices difficult. As it requires extreme precision in creating edges with accuracy and also inappropriate for bulk manufacturing. To circumvent the cumbersome dicing process, we employed micro machined vertical grooves patterns in silicon substrate developed by either RIE or DRIE process, the schematic of proposed structure with micro machined vertical grooves is shown in Fig. 6.2(b).

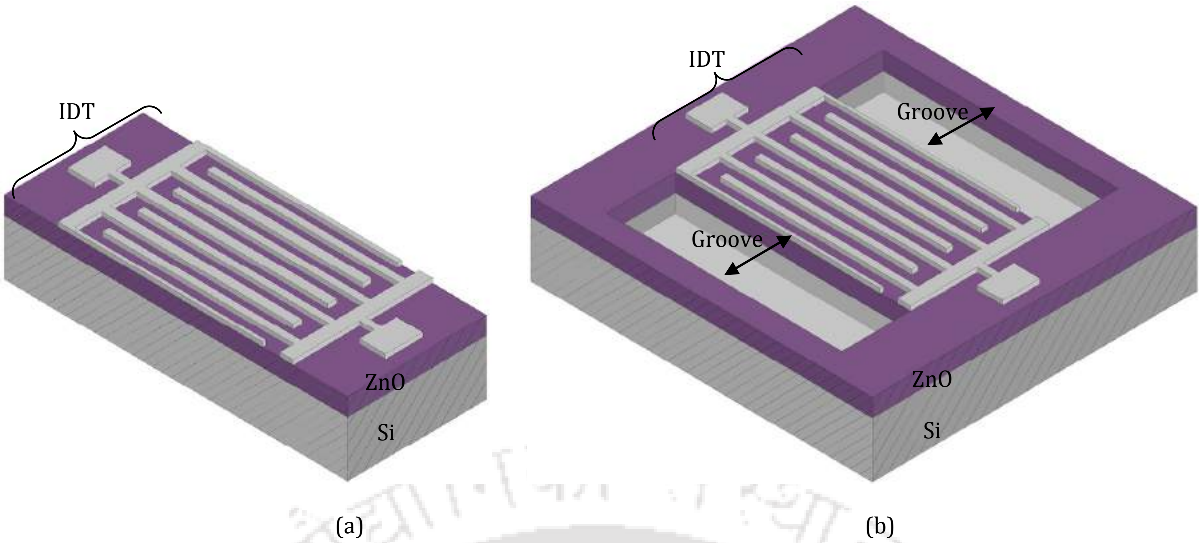

Fig. 6.2. (a) Schematic of proposed ER type SAW resonator using a diced section of silicon substrate and (b) schematic of proposed ER type SAW resonator developed using micro machined vertical grooves for bulk manufacturing.

The device comprises of a silicon substrate with piezoelectric film with an IDT on top of it, located between two vertical grooves developed in silicon with $\lambda/8$ electrodes of IDT positioned at the edges formed by the grooves. Love waves generated along the ZnO film by applying sinusoidal input with its resonant frequency, propagate perpendicular to the aperture of IDT and totally reflected at the free edges to add in phase with the generated wave forming standing wave pattern between the two parallel edges of the substrate. The characteristics of proposed device are obtained using 3D FE simulations, as the wave propagation is in the transverse plane it is necessary to carry out the 3D simulations.

6.4 Finite element simulations of ER type SAW devices on silicon

In general, a one port ER type SAW resonator comprises of an IDT having plurality of electrode fingers of width $\lambda/4$ arranged between a pair of $\lambda/8$ electrodes located at the edge of the device having length of $N*\lambda$. It requires a high computational resources and consumes time, as similar to the simulation methodology of conventional layered SAW resonator on silicon as described in Chapter 2 Section 2.5, we carried out the FE simulations using COMSOL Multiphysics using one wavelength of proposed ER type SAW resonator. This section of the chapter presents the 3D simulations of the proposed ER type SAW resonator on silicon with ZnO film and dispersion characteristics of possible ZnO/Si layered configurations.

6.4.1 Simulation methodology

The structure of one-port SAW resonator with proposed structure is shown in Fig. 6.2, which comprises of a silicon substrate with IDT patterned over the surface and arranged between the parallel edges formed by the micro machined vertical grooves, and ZnO is deposited over the IDT for transduction of Love waves. In general the IDT consists of 100-150 pairs of electrode fingers when designed for 50Ω impedance. Simulation of complete structure with 100-150 pairs of electrodes and large aperture length is practically difficult, time consuming and requires high end computational system. So, we have considered only one wavelength of device with two edge electrodes of λ/8 and one λ/4 electrode positioned in the middle as shown in the Fig. 6.3(b). Instead of periodic boundary conditions, free boundary conditions are applied to the edge boundaries and continuity periodic boundary conditions are applied to the boundaries along the aperture assuming infinitely long aperture with operating frequency independent of aperture length of simulated structure. Uniform IDT with metallization ratio of 0.5 is considered over the (100) oriented silicon substrate and ZnO is deposited over the IDT structure, as depicted in Fig. 6.3(b). The meshed one wavelength ER type SAW resonator is shown in Fig. 6.3(c). The (002) oriented ZnO with *c*-axis along the sagittal plane is chosen due its maximum electromechanical

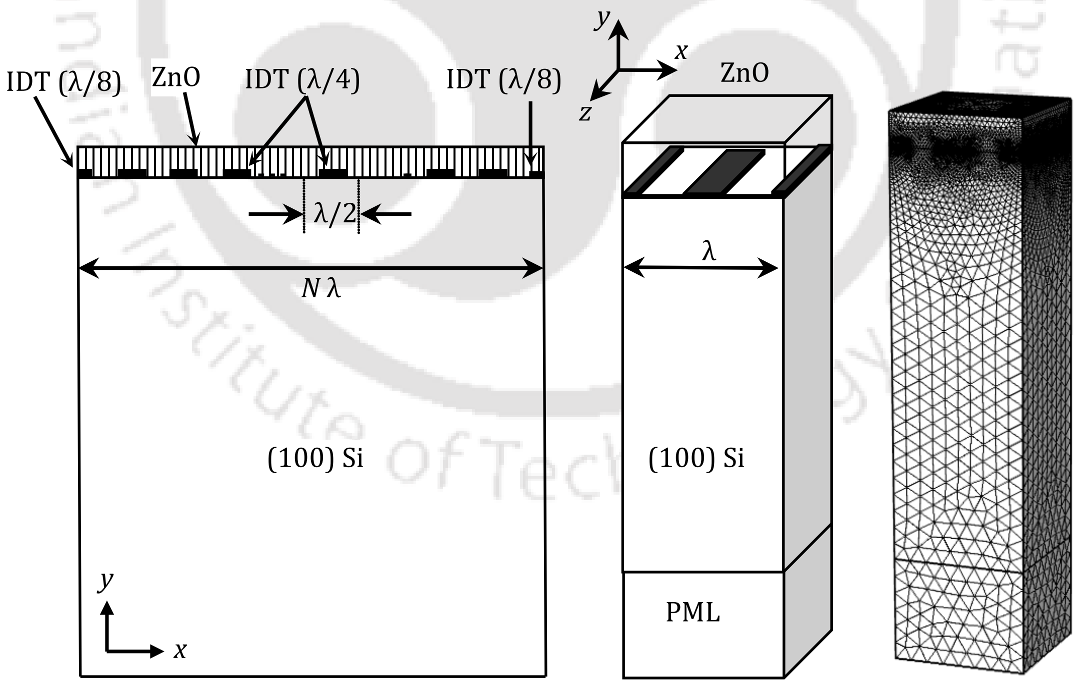

(a) (b) (c)

Fig. 6.3. (a) Cross sectional view of the proposed ER type SAW device and (b) 3D geometry with periodic boundaries along aperture used to obtain phase velocity and coupling coefficient dispersion characteristics as well as admittance characteristics, and (c) meshed ER type SAW resonator of 1λ.

Note: IDT position is varied according to the device configuration.

coupling along *c*-axis [49]. Perfectly matched layer (PML) is considered at the bottom of the silicon substrate as an absorbing boundary to eliminate the unwanted reflections from bottom surface and fixed boundary condition is applied to the bottom surface of PML. We assume center electrode of width 2 µm, edge electrode width of 1 µm having 100 nm thickness with pitch 4 µm and the material properties of ZnO, silicon, and aluminum used in the simulation are adapted from [22], [35] and are given in Appendix A. An input potential of 1V is assumed for the edge electrode and ground boundary conditions are applied to middle electrode in order to obtain admittance characteristics of the proposed ER type SAW device.

In the simulations, the effect of mechanical properties of aluminum and silicon are taken into account. From Eigen mode analysis, the frequency of generated surface mode is obtained and its phase velocity (v) is calculated using $v = f\lambda$, where λ is the wavelength of IDT. 3D simulations are carried out to obtain the dispersion curves of transversely polarized surface modes generated in the structure. The electromechanical coupling coefficient (K^2) of the proposed structure is calculated using

$$K^2 = 200 * \left(\frac{v_f - v_m}{v_f}\right) \% \tag{6.1}$$

where v_f and v_m are the SAW phase velocities obtained when the interface boundary between ZnO and silicon containing IDT is electrically free and shorted, respectively.

6.4.2 Results of ER type one port ZnO/Si SAW resonator;

Eigenmode analysis is performed on the 3D model shown in Fig. 6.3(b) to obtain the phase velocity and K^2dispersion characteristics of all possible ZnO/Si configurations. Free surface velocity dispersion characteristics of the Love modes generated in the ZnO/Si structure with respect to ZnO film thickness are shown in Fig. 6.4. Within one wavelength thickness of ZnO, three Love modes are observed. First higher order Love mode (L_1) is generated at h/λ= 0.325 with a phase velocity of 5330 m/s and second higher order Love mode (L_2) generated at h/λ= 0.65 with a phase velocity of 5326 m/s. From the

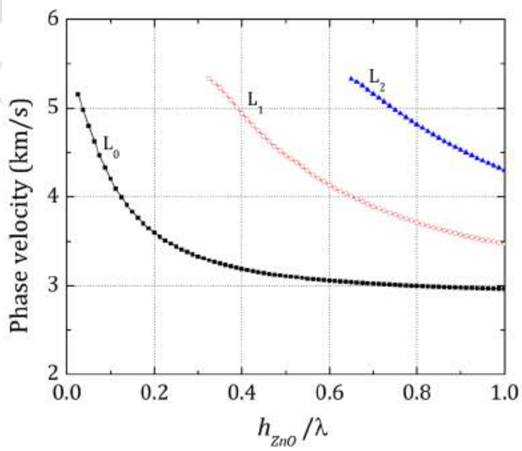

Fig. 6.4. Phase velocity dispersion characteristics of Love modes generated in the ZnO/Si structure.

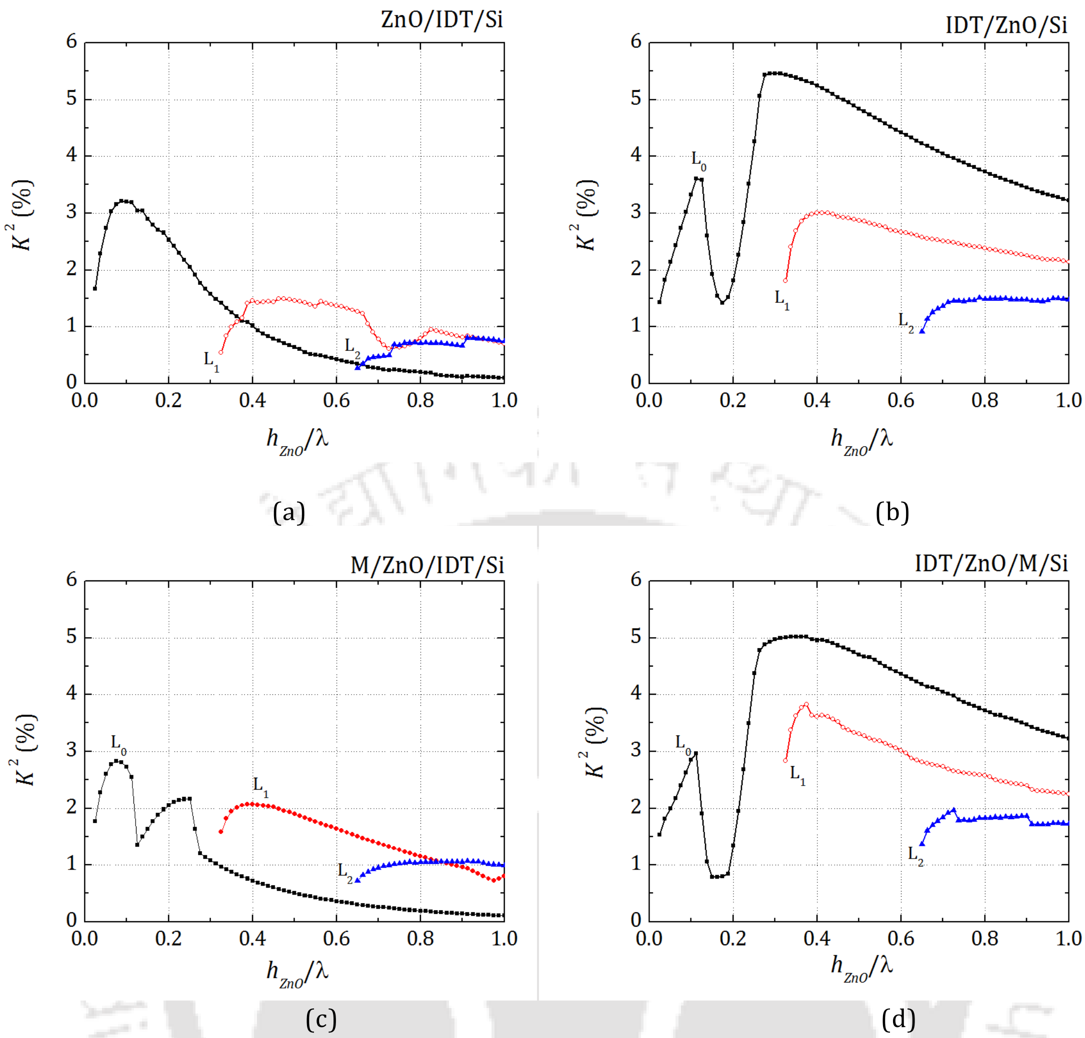

Fig. 6.5. The coupling coefficient characteristics of various Love modes generated in all possible configurations of ZnO/Si structure.

characteristics, the velocity of Love waves phase velocity with increase in ZnO film thickness and tends to reach the velocity of Love wave in the bulk ZnO (2507 m/s) [3]. The K^2 dispersion characteristics of all four configurations are shown in Fig. 6.5 (a, b, c, and d).

From K^2 characteristics of configuration ZnO/IDT/Si, L_0 exhibits a relative maximum K^2 value of 3.2% at h/λ= 0.1 with phase velocity of 4327 m/s and the L_1 and L_2 exhibit low K2 values and also generated at higher thicknesses of ZnO. In configuration IDT/ZnO/Si, L_0 exhibits a relative maximum K^2 value of 5.45% at h/λ= 0.275 with phase velocity of 3378 m/s. From all four configurations it is observed that the L_0 exhibits relative maximum K^2 values compared to L_1 and L_2 surface modes. L_0 exhibits a K^2 value of 2.8% at h/λ= 0.07 and 5% at h/λ= 0.32 for configurations M/ZnO/IDT/Si and IDT/ZnO/M/Si respectively. The obtained phase velocity and K^2 values are in good agreement with reported Love wave base

ZnO/Si structure [44]. The notable observations from the dispersion characteristics of K^2 and phase velocity are listed in Table 6.2.

Table 6.2 Notable observations from the phase velocity and K^2 dispersion characteristics of all four possible configurations.

Configuration	Mode	h/λ	Phase velocity (m/s)	K^2 (%)
IDT/ZnO/Si	L_0	0.275	3378	5.50
	L_0	0.113	4092	3.60
	L_1	0.375	5086	3.30
IDT/ZnO/M/Si	L_0	0.388	3202	5.06
	L_0	0.100	4203	3.00
	L_1	0.388	3196	3.80
ZnO/IDT/Si	L_0	0.100	4203	3.34
	L_1	0.425	4808	1.70
M/ZnO/IDT/Si	L_0	0.075	3701	2.80
	L_1	0.388	5013	2.00

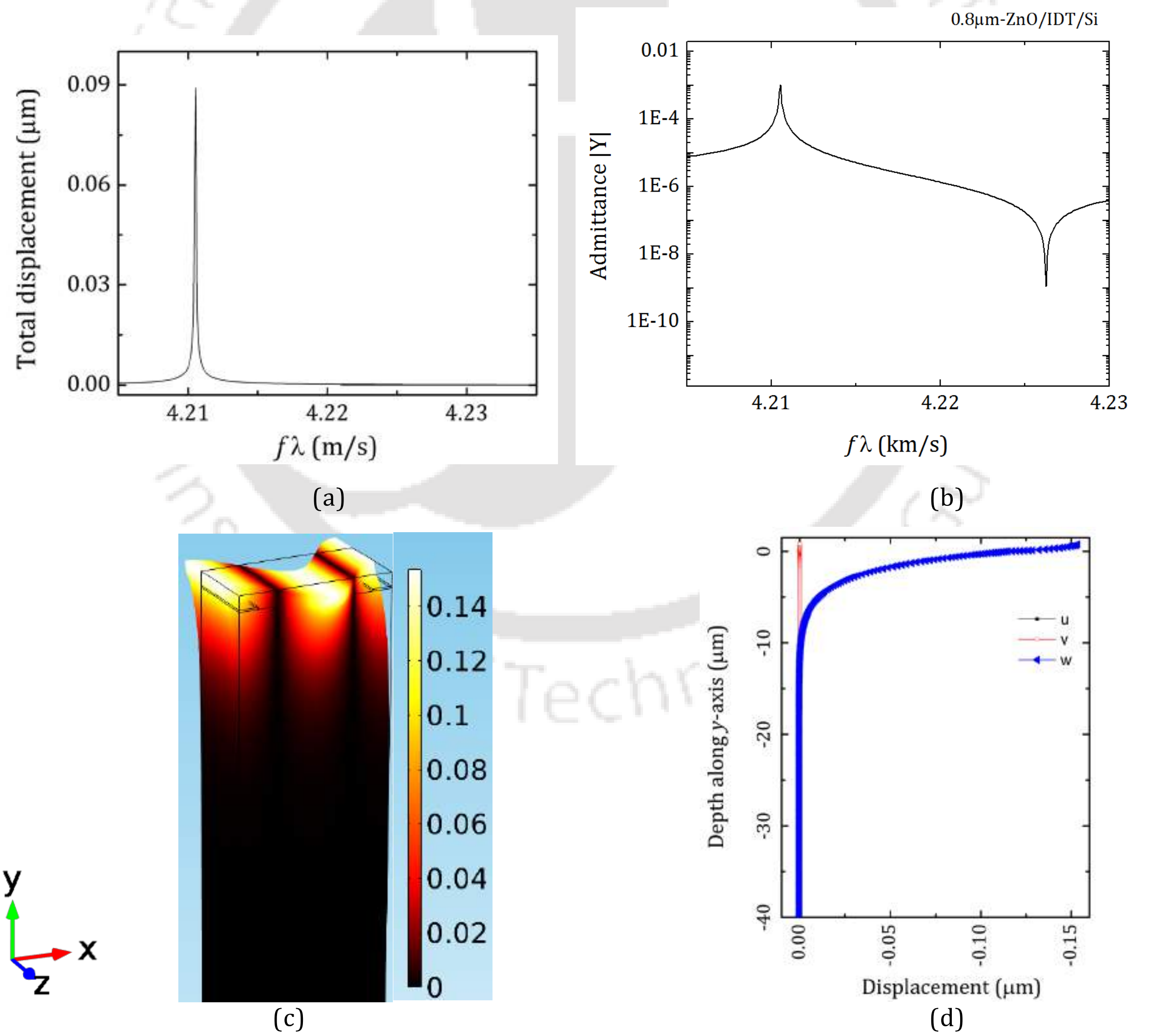

Fig. 6.6. Characteristics of L_0 mode generated in the 0.8μm-ZnO/IDT/Si structure at h/λ of 0.10. (a) Total displacement, (b) admittance, (c) surface displacement profiles and (d) particle

However, all configuration exhibit tradeoff between phase velocity and K^2 values. Further frequency dependent analysis is carried out on configurations IDT/ZnO/Si and ZnO/IDT/Si, since they exhibit high coupling coefficient and high phase velocity respectively, to obtain the admittance and displacement characteristics of L_0 generated in the structure. The HA plot and displacement profile of L_0 generated in the proposed structure ZnO/IDT/Si configuration at h_{ZnO}/λ= 0.1 are shown in Fig. 6.6 and the displacement and HA characteristics of IDT/ZnO/Si configuration are shown in Fig. 6.7.

The surface displacement profile along with the particle displacement profile along the depth (y-axis) shows the generation of Love mode in the ZnO film as well as the reflections from the free edges resulting in formation of standing wave pattern. Configuration ZnO/IDT/Si exhibits phase velocity of 4211 m/s and bandwidth of 1.9 MHz which is

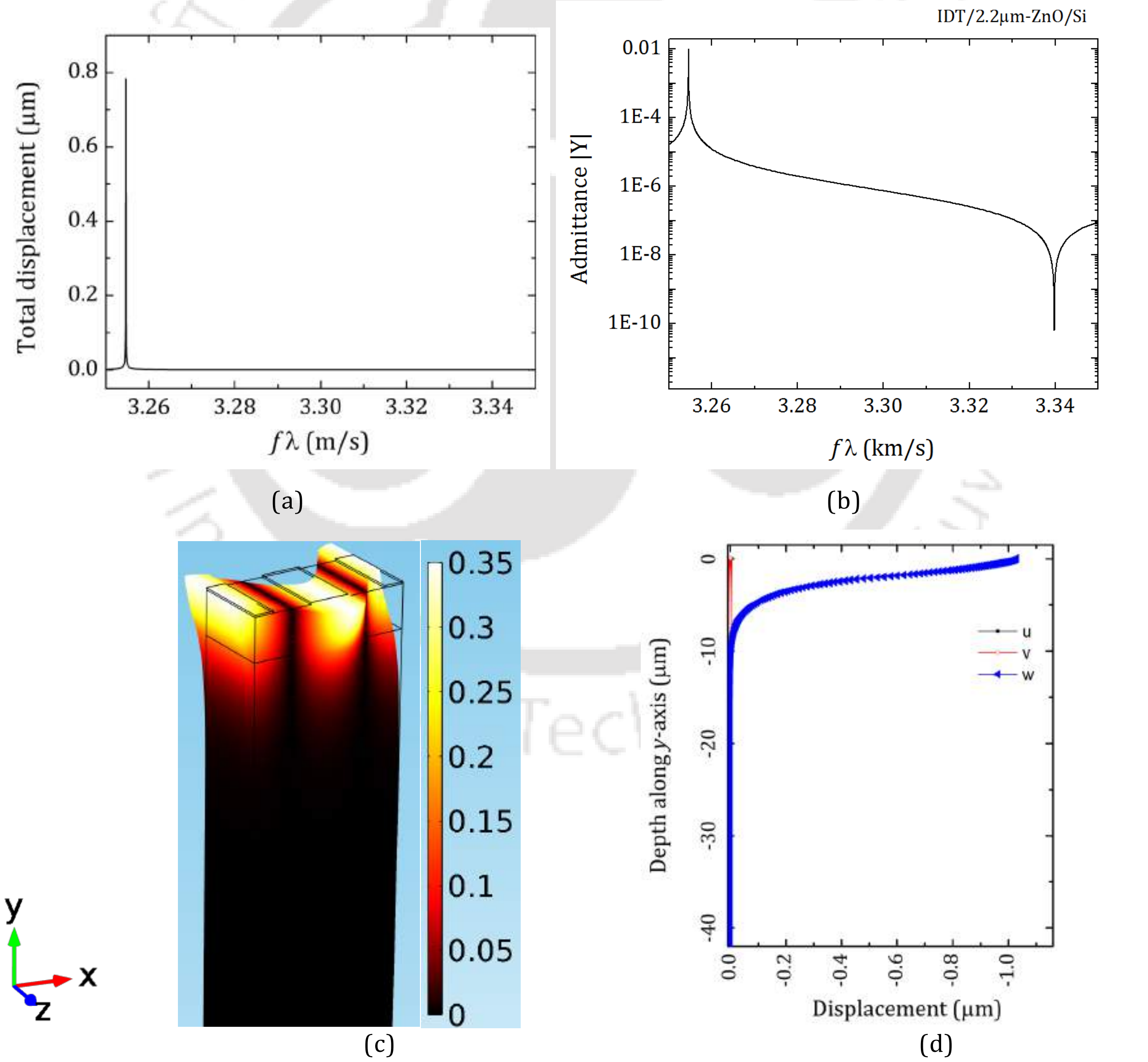

Fig. 6.7. Characteristics of L_0 mode generated in the IDT/2.2μm-ZnO/Si structure at h/λ of 0.275 (a) Total displacement, (b) admittance, (c) surface displacement profiles and (d) particle displacement

calculated from the series and parallel resonant frequency obtained from the admittance characteristics. The maximum total displacement of 0.09 μm is observed at the edges.

Fig. 6.7, shows the admittance characteristics and displacement profile of IDT/ZnO/Si configured SAW one port resonator. Phase velocity of 3254.6 m/s and bandwidth of 10.65 MHz is obtained from the admittance plot and a maximum displacement of 0.795 μm. From the obtained results we can justify that the bandwidth of conventional thin film SAW device is proportional to coupling coefficient and IDT position on the top of the device exhibits greater displacements than IDT at the ZnO-Si interface. Both configurations, ZnO/IDT/Si and IDT/ZnO/Si configurations shows good coupling coefficient and phase velocity that can be integrated with silicon based circuitry. Visser [64] reported that the K^2 characteristics of a devices can be improved considerable by considering buffer layers between the piezoelectric thin film and silicon substrate.

6.5 Effect of buffer layers in ER type SAW devices on silicon

From the above section, we noticed that the configurations ZnO/IDT/Si and IDT/ZnO/Si exhibit good coupling coefficient for the fabrication of ER type devices to integrate with silicon based circuitry. The K^2 characteristics of a devices can be improved considerable using buffer layers between the piezoelectric layer and substrate. Visser [31] [64], pointed

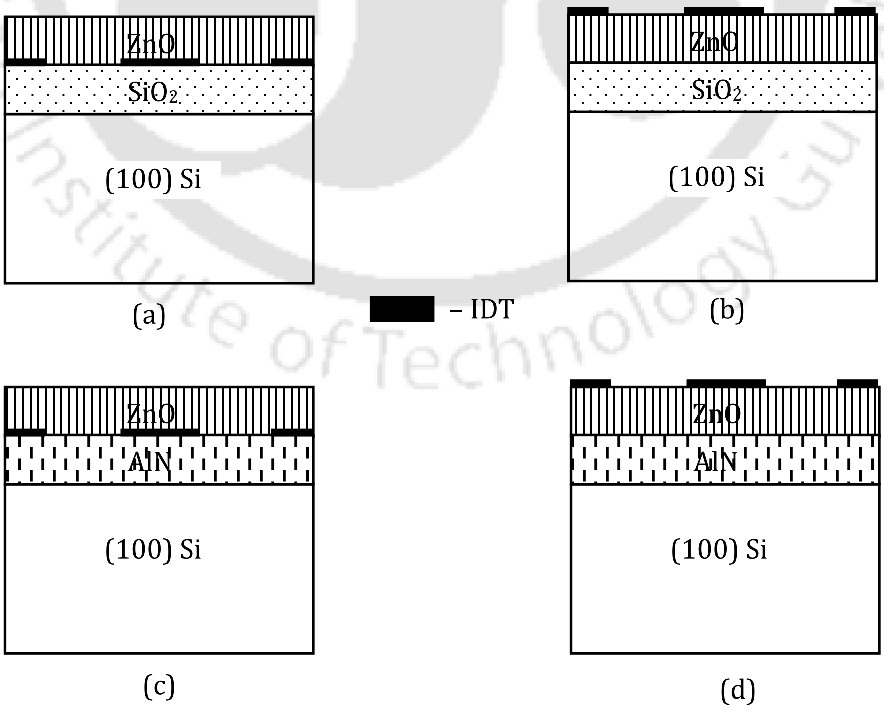

Fig. 6.8. Cross sectional view of one periodic section of the proposed ER type SAW device with buffer layers. (a) ZnO/IDT/SiO_2/Si, (b) IDT/ZnO/SiO_2/Si, (c) ZnO/IDT/AlN/Si, and (d) IDT/ZnO/AlN/Si.

out that the coupling coefficient can be increased appreciable by the inclusion of SiO_2 film between the ZnO film and silicon substrate as well as aid in the promotion of quality of ZnO film [61]. The effect of buffer layers (SiO_2 and AlN) on the dispersion characteristics of proposed ER type devices are studied using FE simulations. We performed eigenmode analysis to obtain the velocity and K^2 dispersion characteristics and frequency dependent analysis for bandwidth characteristics. A periodic section of proposed ER type SAW devices with buffer layers on silicon substrate are shown in Fig. 6.8. FE simulations are performed to obtain the SAW characteristics using the similar geometry (Fig. 6.3) with a buffer layer of SiO_2 or AlN sandwiched between ZnO film and silicon. Periodic boundary conditions are applied to the surface along the aperture and *free* boundary conditions are given to the surfaces in the direction of propagation.

6.5.1. Effect of SiO_2 buffer layer on ZnO/Si structure

Eigenmode analysis is carried out on the structures (Fig. 6.8(a) and (b)) to obtain the phase velocity and K^2 dispersion curves of both configurations. Initially, parametric sweep of SiO_2 film thickness is carried out constant ZnO film thickness of 0.8 µm and 2.4 µm for configurations having IDT below ZnO film and IDT on top of ZnO film respectively.

Configuration: ZnO/IDT/SiO_2/Si

Fig. 6.9 shows the phase velocity and K^2 dispersion characteristics of ZnO/IDT/SiO_2/Si structure. Fig. 6.9(a) and (b) shows the dispersion characteristics with respect to SiO_2 film thickness. With increase in the thickness of SiO_2, the phase velocity of surface modes generated in the structure tends to reach the surface wave velocity of bulk SiO_2 and the coupling coefficient characteristics show a constant reduction of with increase in SiO_2 thickness. From the characteristic curves we notice that, after $h/\lambda = 0.25$ the phase velocity and coupling coefficient of the L_0 mode is non-dispersive in nature with respect to SiO_2 film thickness. To find the optimal thickness of ZnO, we considered a constant 2 µm thickness of SiO_2 and performed eigenmode analysis with parametric sweep of ZnO film thickness and the obtained dispersion characteristics are shown in Fig. 6.9(c) and (d). The calculated K^2 values of the generated modes are tabulated in Table 6.3.

Configuration: IDT/ZnO/ SiO_2/Si

The K^2 dispersion characteristics of IDT/ZnO/SiO_2/Si structure are shown in Fig. 6.10. Initially the effect of SiO_2 is studied by varying its thickness up to h/λ =1, and further, the parametric sweep with ZnO film thickness is carried out to find the optimal ZnO thickness

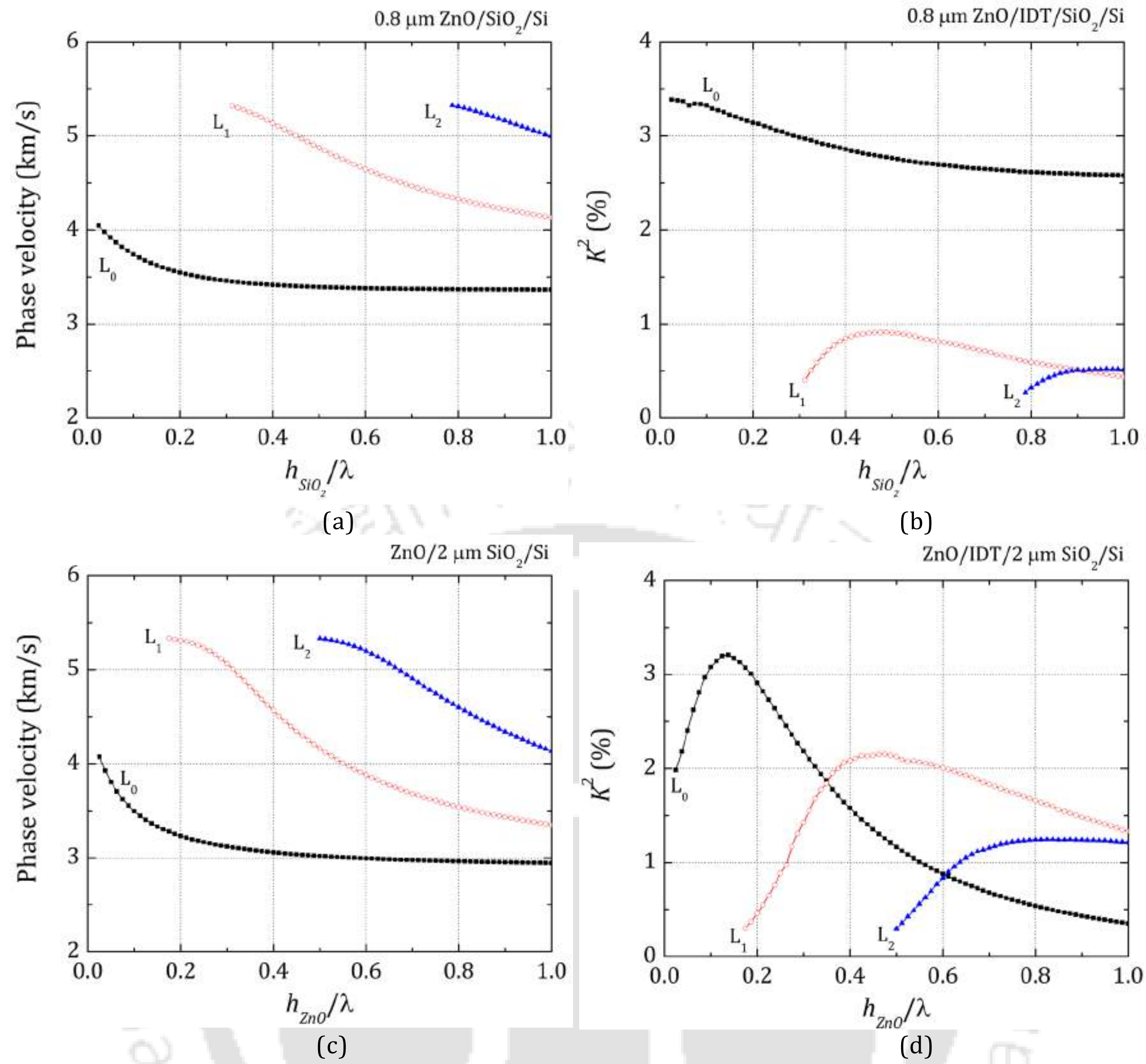

Fig. 6.9. Dispersion characteristics of Love modes generated in the $ZnO/IDT/SiO_2/Si$ structure.

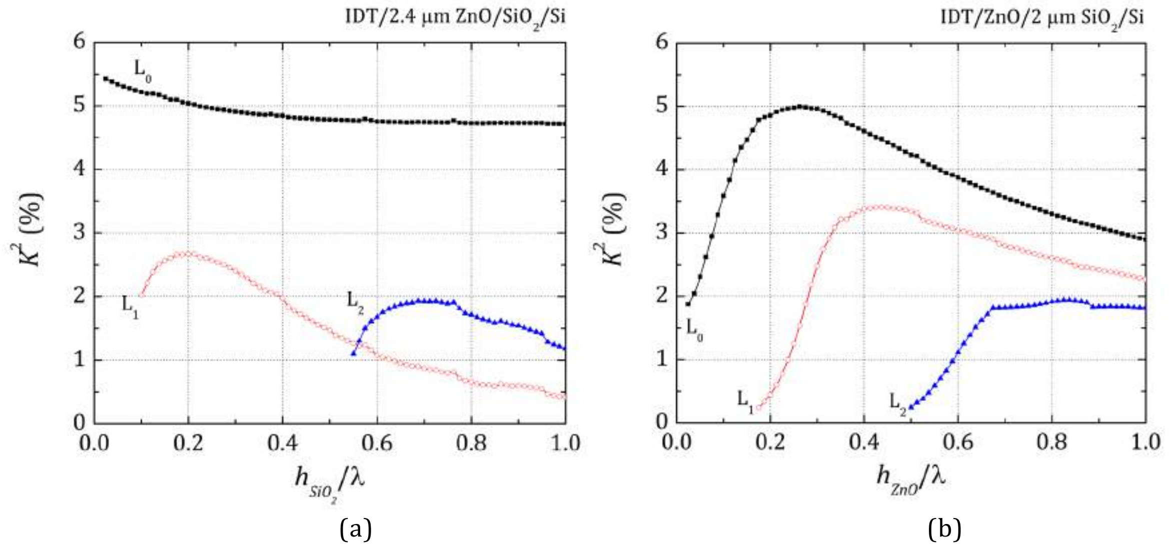

Fig. 6.10. K^2 dispersion characteristics of Love modes generated in the $IDT/ZnO/SiO_2/Si$ structure, (a) with respect to SiO_2 film thickness, constant ZnO thickness and (b) with respect to ZnO film thickness, constant SiO_2 film thickness.

for fabrication. Fig. 6.10(b) shows the K^2 dispersion characteristics with respect to ZnO film thickness. The relative maximum K^2 is exhibited by L_0 at h/λ =0.265. From the K^2 values of both configurations, it is noted that the configuration with IDT on top of ZnO film exhibits better K^2 values, however it requires large thickness of ZnO compared to ZnO/IDT/ SiO_2/Si configurations. The notable observations of SiO_2 buffer layer in both the configurations, such as relative maximum K^2 and generation of higher order modes are listed in Table 6.3.

Table. 6.3 Notable observations of ZnO/IDT/SiO_2/Si and IDT/ZnO/SiO_2/Si configurations with constant oxide thickness of 2 μm.

Mode	h/λ of ZnO film	Phase velocity (m/s)	Relative maximum K^2 (%)
Configuration: ZnO/IDT/2 μm SiO_2/Si			
L_0	0.138	3365	3.20
L_1	0.475	4249	2.15
L_2	0.675	4989	1.10
Configuration: IDT/ZnO/2 μm SiO_2/Si			
L_0	0.263	3152	5.00
L_1	0.450	4345	4.00
L_2	0.838	4495	2.00

6.5.2 Effect of AlN buffer layer on ZnO/Si structure

Eigenmode analysis is carried out on the structures (Fig.6.8 (c) and (d)) to obtain the phase velocity and K^2 dispersion curves of both configurations. Initially, parametric sweep of AlN film thickness with constant ZnO film thickness of 0.8 μm and 2.4 μm for IDT below ZnO and IDT on top of ZnO structures respectively is carried out, at which both configurations shows relative maximum coupling coefficient having an IDT wavelength of 8 μm. The dispersion characteristics of ZnO/IDT/AlN/Si configuration is shown in Fig. 6.11(a) and (b) are the phase velocity and K^2 characteristics obtained with a constant ZnO film thickness and parametric sweep of AlN film thickness.

Configuration: ZnO/IDT/AlN/Si

From Fig. 6.11(a) and (b), we observed only one Love wave generated in 0.8μm-ZnO/AlN/Si structure. Because of large difference in acoustic impedance values of ZnO and AlN, the generated wave is confined to ZnO film. We observed that the velocity and K^2 are constant beyond h/λ = 0.5 with a relative maximum K^2 value of 7.5% with phase velocity of 4875 m/s. Further, we consider AlN thickness of 4 μm in the structure and ZnO film thickness

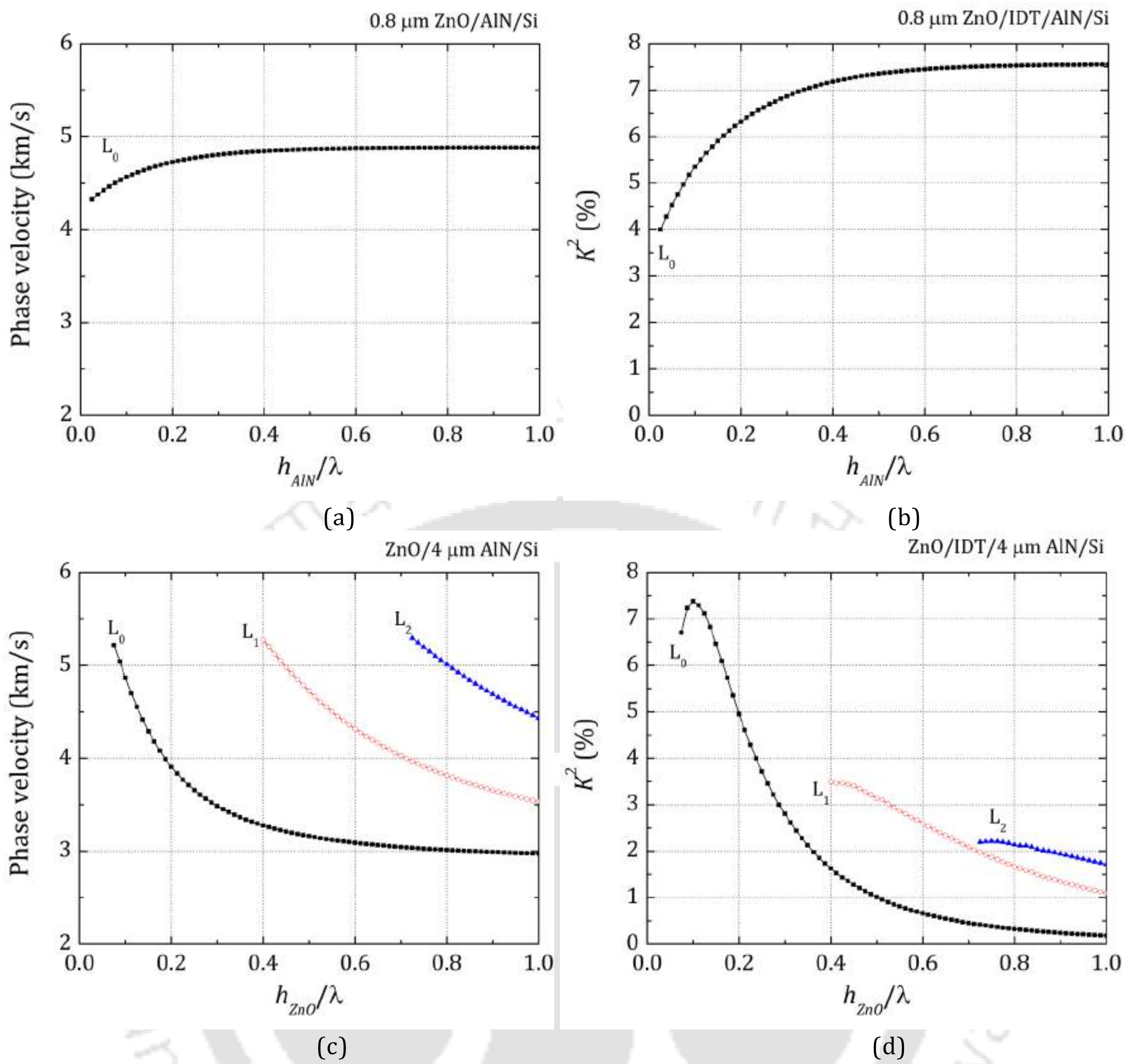

Fig. 6.11. Phase velocity and K^2 dispersion characteristics of Love modes generated in the IDT/ZnO/AlN/Si structure. (a) and (b) with respect to AlN thickness, constant ZnO film thickness, (c) and (d) with respect to ZnO thickness, constant AlN film thickness.

parametric sweep is carried out and results are shown in Fig. 6.11(c) and (d). We observe three modes generated in the structure and the calculated values are tabulated in Table 6.4.

IDT/ZnO/ AlN/Si:

The dispersion characteristics of structure with IDT on top of ZnO film is shown in Fig. 6.12. Similar to previous analysis, initial parametric simulations are carried with a constant ZnO thickness and further ZnO film parametric sweep is carried out with a constant AlN film thickness. The phase velocity and K^2 values suitable for fabrication at respective thicknesses of ZnO are tabulated in Table 6.4. We observed that the velocity and K^2 are constant beyond h/λ = 0.5 with a relative maximum K^2 value of 6.8% with phase velocity of 3484 m/s. From Fig. 6.12(c) and (d), L_0 exhibits high K^2 value compared with other modes in the structure.

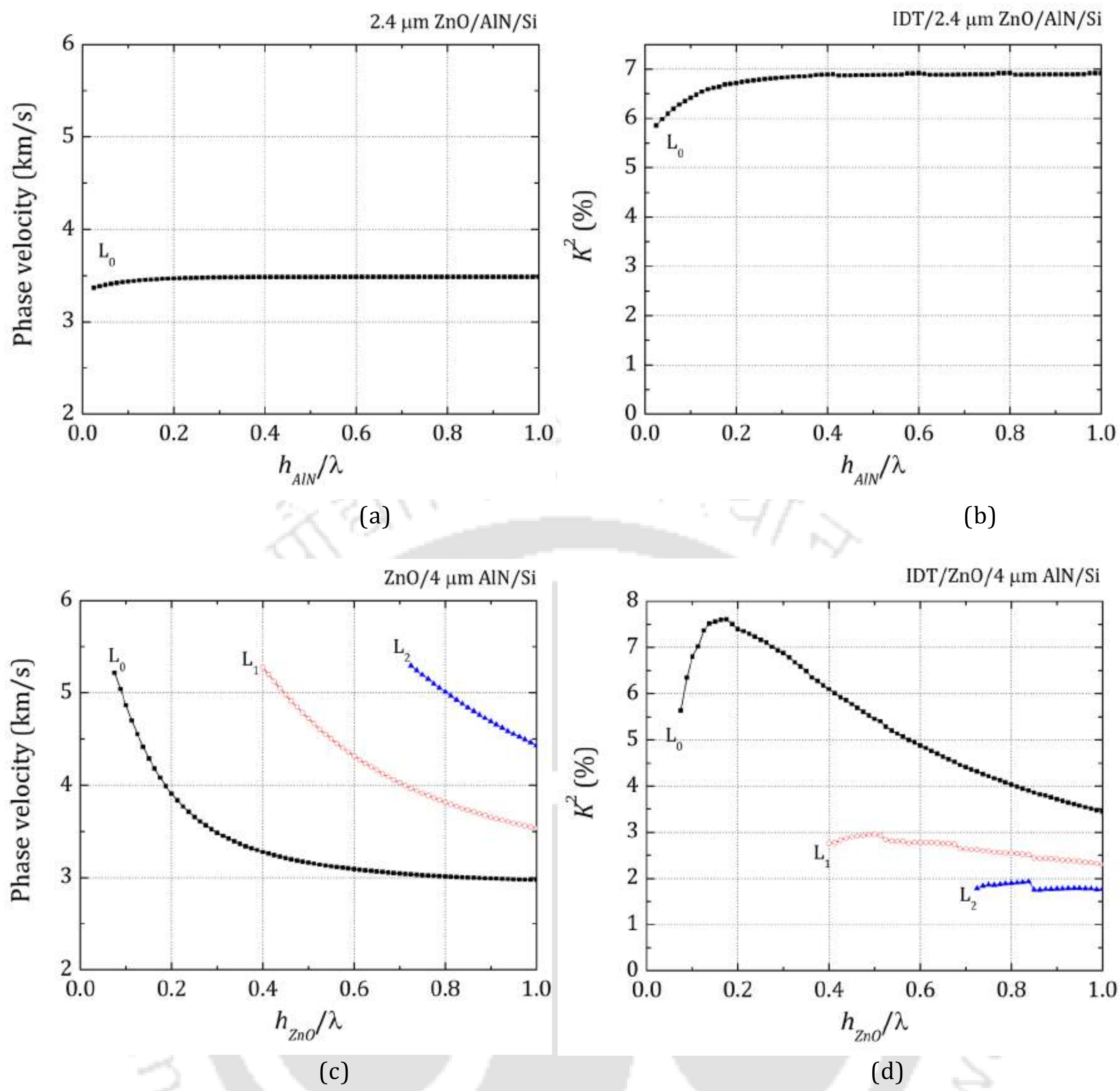

Fig. 6.12. Phase velocity and K^2 dispersion curves of Love modes generated in the IDT/ZnO/AlN/Si structure. (a) and (b) dispersion charactersitics with respect to AlN, a fixed ZnO film thickness, (c) and (d) with respect to ZnO thickness, fixed AlN film thickness.

Table. 6.4 Notable observations of ZnO/IDT/AlN/Si and IDT/ZnO/AlN/Si configurations with constant oxide thickness of 4 μm.

Mode	h/λ of ZnO film	Phase velocity (m/s)	Relative maximum K^2 (%)
Configuration: ZnO/IDT/4 μm AlN/Si			
L_0	0.100	4864	7.40
L_1	0.400	5277	3.50
L_2	0.750	5243	2.21
Configuration: IDT/ZnO/4 μm AlN/Si			
L_0	0.138	4416	7.50
L_1	0.500	4722	2.95
L_2	0.800	5055	1.90

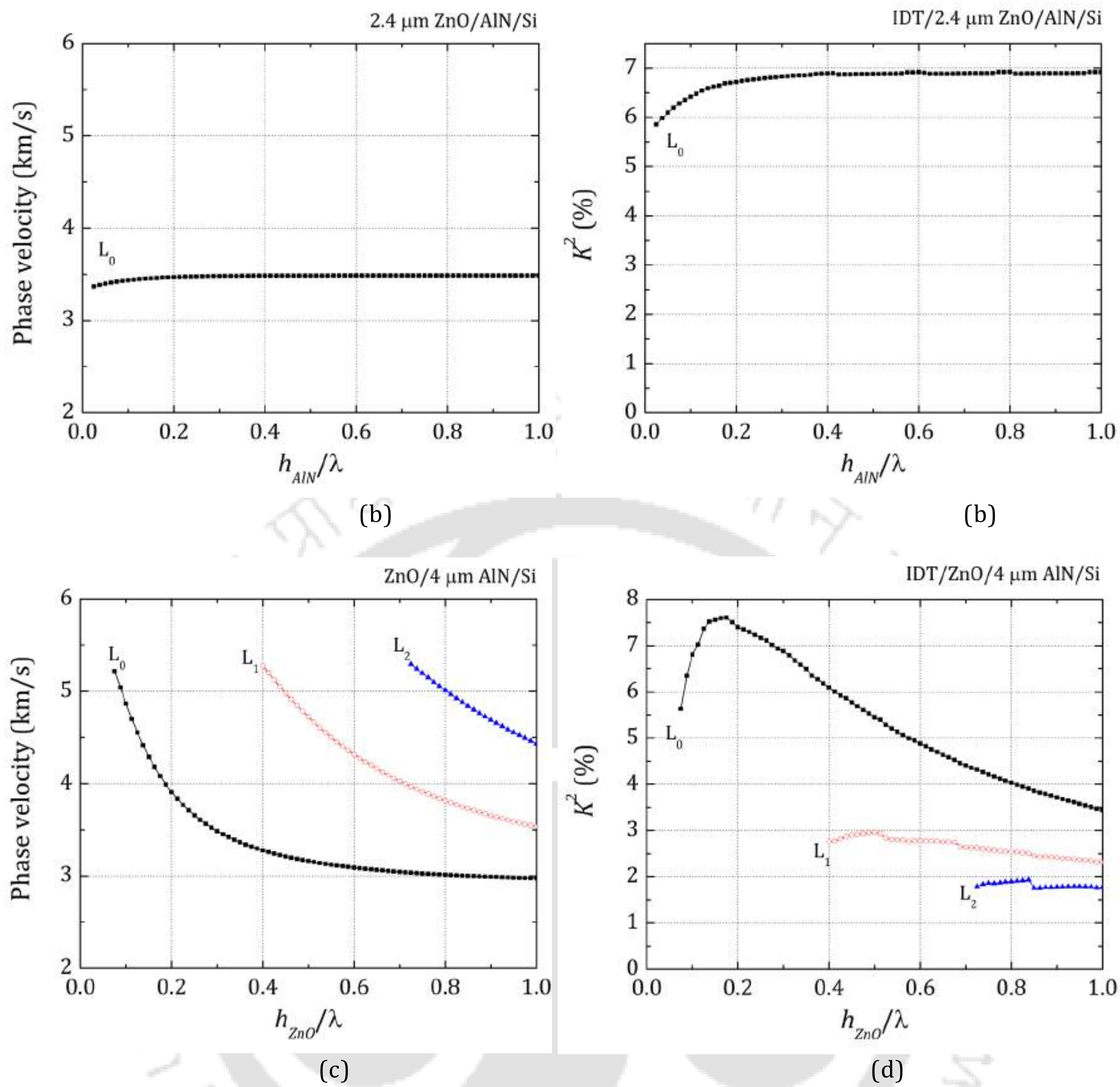

Fig. 6.12. Phase velocity and K^2 dispersion curves of Love modes generated in the IDT/ZnO/AlN/Si structure.

From this study, we noticed that the phase velocity and K^2 values of the configuration depends on the position of IDT and thickness of ZnO film rather than the thickness of AlN buffer layer. As, AlN is a piezoelectric material and exhibit high acoustic velocity than ZnO it promotes the acoustic wave confinement to ZnO film and also improves the K^2 values significantly.

6.5.3 Frequency dependent analysis

We performed frequency dependent analysis on all four configurations discussed above to study the effect of IDT position and buffer layers on the bandwidth of proposed ER type SAW devices on silicon. A potential of 1V is applied to the center electrode and ground electrical boundary conditions are applied to edge electrodes to obtain the admittance

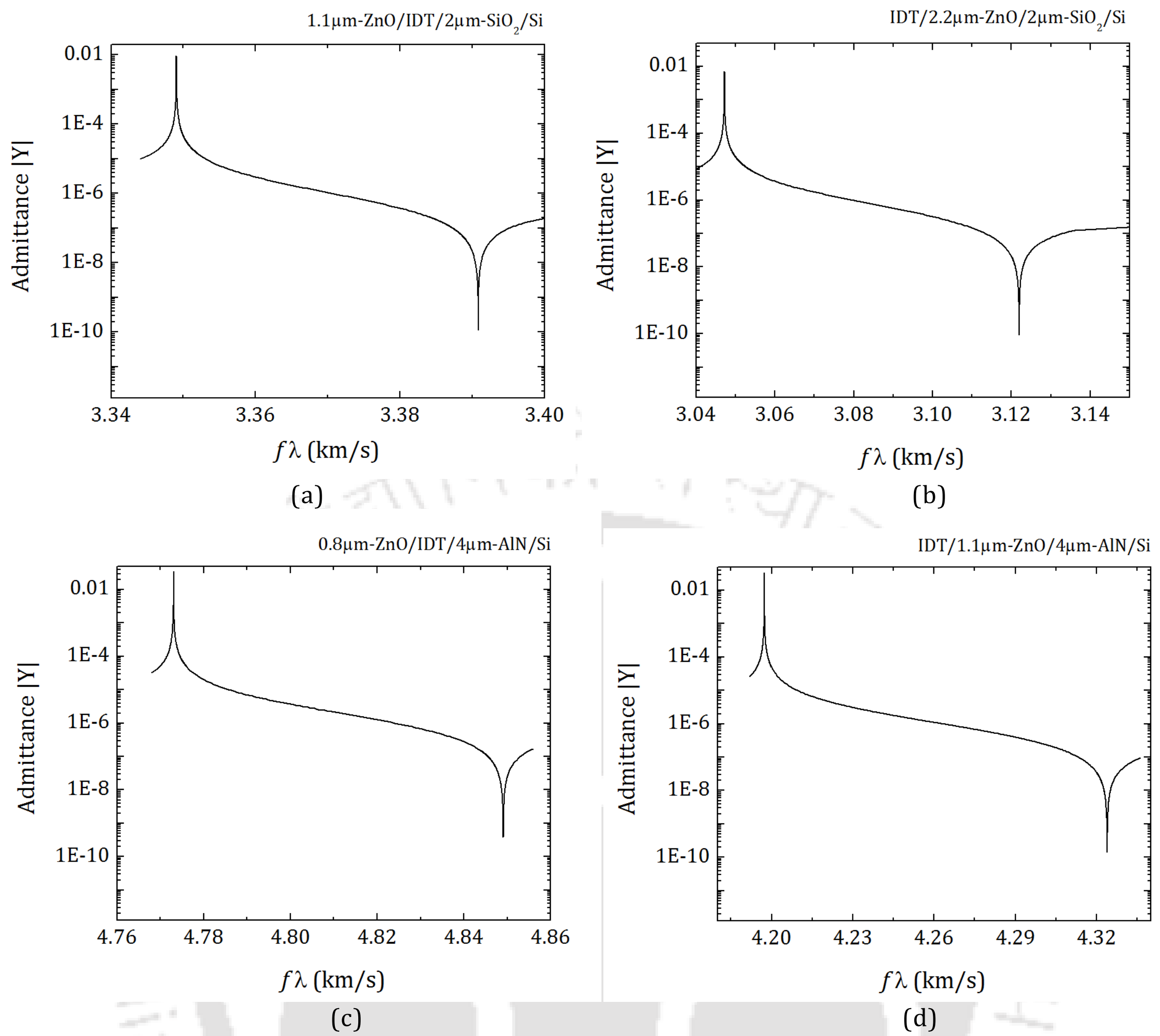

Fig. 6.13. Admittance characteristics of various configurations (a) 1.1μm-ZnO/IDT/2μm-SiO_2/Si, (b) IDT/2.2μm-ZnO/2μm-SiO_2/Si, (c) 0.8μm-ZnO/IDT/4μm-AlN/Si, and (d) IDT/1.1μm-ZnO/4μm-AlN/Si.

characteristics of ER type SAW resonator with buffer layers. The obtained admittance characteristics are show in Fig. 6.13.

Table. 6.5 Phase velocity, series resonance, parallel resonance, total displacement, and bandwidth of ER type SAW devices with buffer layers.

Configuration	Series resonance (f_s) (MHz)	Parallel resonance (f_r) (MHz)	Bandwidth (MHz)	Maximum displacement (μm)
IDT/ZnO/Si	406.825	417.475	10.65	0.795
ZnO/IDT/Si	526.375	528.280	1.905	0.320
IDT/ZnO/SiO_2/Si	380.905	390.245	9.340	0.590
ZnO/IDT/SiO_2/Si	418.632	423.850	5.218	0.785
IDT/ZnO/AlN/Si	524.670	540.485	15.81	1.870
ZnO/IDT/AlN/Si	596.635	606.640	10.00	0.785

The calculated phase velocity, bandwidths and maximum displacement of all configurations are tabulated and compared with configurations without buffer layers in Table 6.5.

6.5.4 Observations

The results and observations from the FE simulations of ER type SAW devices on silicon using ZnO film with all possible configurations and the effect of buffer layers are summarized as follows:

1. The dispersion characteristics show high coupling coefficient values in structures having IDT on top of ZnO compared with IDT below ZnO.
2. The frequency dependent analysis shows the generation of Love wave in ZnO with substantial displacement in z-direction.
3. The results shows that the inclusion of AlN buffer layer will improve the coupling coefficient significantly compared with SiO_2 layer and also aid in confining the surface wave in ZnO film.
4. Configurations IDT/ZnO/Si and IDT/ZnO/SiO_2/Si exhibit high coupling coefficient at higher thicknesses of ZnO (h/λ>0.25), whereas configurations with IDT underneath ZnO exhibit acceptable coupling coefficient at small thickness of ZnO (h/λ<0.15).
5. ZnO/IDT/Si and ZnO/IDT/SiO_2/Si exhibit low bandwidth, suitable for resonator applications.
6. The Love waves generated in the thin film ER type SAW devices also exhibit the tradeoff between the coupling coefficient and phase velocity.
7. The maximum surface wave velocity is exhibited by the first higher order surface wave in ZnO/Si and ZnO/SiO_2/Si configurations are almost equal to the shear bulk velocity of the silicon substrate.
8. All the surface modes generated in the structure with AlN buffer layers exhibit maximum surface wave velocity almost equal to the shear bulk velocity of AlN, because of the large thickness of AlN and high surface velocity, the effect of silicon substrate is insignificant on the surface waves generated in the structure.
9. In ZnO/Si and ZnO/SiO_2/Si configurations the coupling coefficient is extensively depends in the position of IDT and in case of ZnO/AlN/Si structure the position of IDT has negligible effect on K^2.
10. IDT/ZnO/AlN/Si configuration exhibit high coupling coefficient and high bandwidth, suitable for ladder filter applications that can be integrated with silicon circuitry.
11. The optimal thicknesses and configurations suitable for fabrication are tabulated in Table 6.6.

Table 6.6. Optimal parameters of ZnO and buffer layers suitable for fabrication.

Mode	h/λ of ZnO film	Phase velocity (m/s)	Relative maximum K^2 (%)
Configuration: ZnO/IDT/Si			
L_0	0.100	4203	3.20
L_1	0.325	5330	0.45
Configuration: IDT/ZnO/ Si			
L_0	0.275	3378	5.45
L_1	0.325	5322	1.80
Configuration: ZnO/IDT/2 µm SiO_2/Si			
L_0	0.138	3365	3.20
L_0	0.025	4073	2.00
L_1	0.175	5061	0.30
L_1	0.425	4450	2.13
L_2	0.500	5332	0.29
L_2	0.737	4783	1.20
Configuration: IDT/ZnO/ 2 µm SiO_2/Si			
L_0	0.262	3152	5.00
L_0	0.025	4068	1.87
L_1	0.175	5332	0.24
L_1	0.400	4564	3.40
L_2	0.500	5328	0.24
L_2	0.800	4597	1.90
Configuration: ZnO/IDT/4 µm AlN/Si			
L_0	0.100	4864	7.40
L_0	0.075	5216	6.70
L_1	0.400	5277	3.50
L_2	0.725	5292	2.19
Configuration: IDT/ZnO/4 µm AlN/Si			
L_0	0.138	4416	7.50
L_0	0.075	5210	5.63
L_1	0.400	5272	2.76
L_2	0.725	5286	1.78

6.6 ER type SAW device on silicon using periodically patterned-ZnO film

In chapter 3, we discussed that a bulk wave incident at a periodic structure can undergo mode conversion into a surface wave that can be longitudinal polarized or transversely polarized surface wave depending on the type incident bulk mode. Using this phenomenon of generation of transversely polarized surface waves at periodic structure, we proposed an edge reflection type SAW devices on silicon using periodically patterned ZnO film as shown in Fig. 6.14. The proposed device comprised of a silicon substrate with an optional oxide layer and a periodically patterned ZnO film disposed in the spaces of an IDT for the transduction of Love waves. The edge reflection of Love wave is accomplished by developing vertical grooves in silicon substrate to obtain the free surface edges as shown in Fig. 6.14.

An electric signal applied to IDT results in the generation of electric field across the periodically patterned-ZnO exciting bulk acoustic waves in individual pattern, and the bulk waves in periodically patterned ZnO couple acoustically to silicon substrate resulting in the generation of transversely polarized surface acoustic wave along the silicon substrate.

In general, a one port ER type SAW resonator comprises of an IDT, which is having plurality of electrode fingers of λ/4 for the generation of surface acoustic wave and a pair of λ/8 electrodes at the edge of substrate to accomplish total reflection of generated Love wave

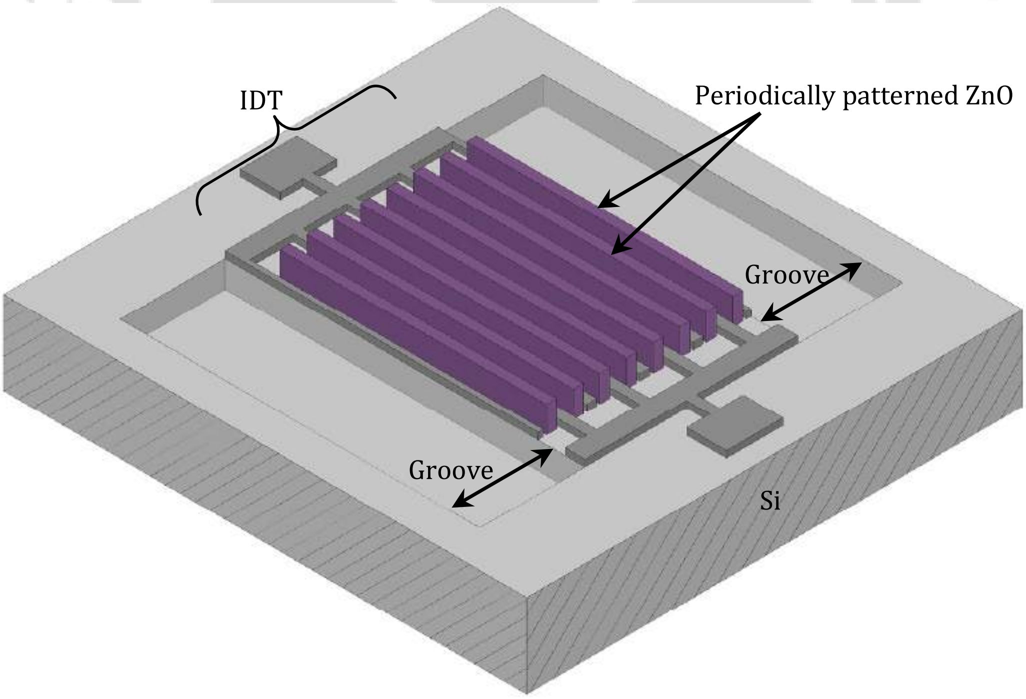

Fig. 6.14. Proposed ER type SAW resonator on silicon substrate using periodically patterned ZnO film and vertically etched grooves for total reflection of generated Love waves.

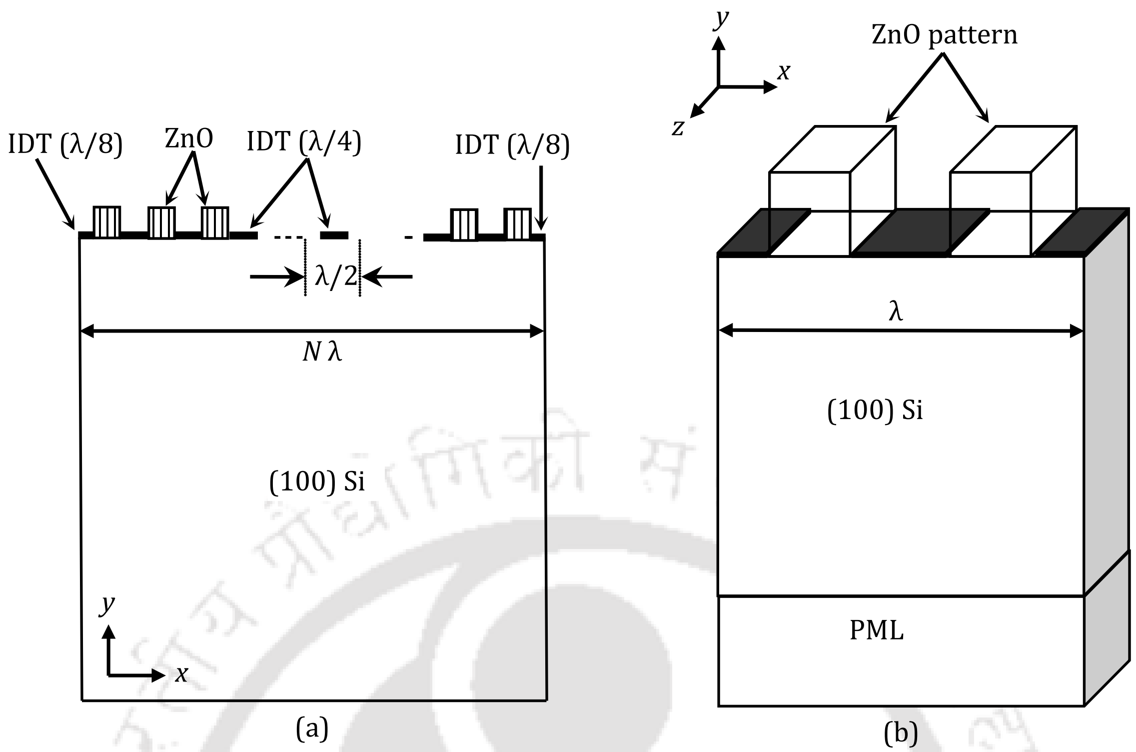

Fig. 6.15. (a) Cross sectional view of the proposed ER type SAW device with periodically patterned-ZnO on silicon and (b) 3D geometry with periodic boundaries along aperture used to obtain phase velocity and coupling coefficient dispersion characteristics as well as admittance characteristics.

and form standing wave pattern. The simulations of conventional layered SAW resonator on silicon using FEM are described in Chapter 2 Section 2.5. This section of the chapter presents 3D simulation of proposed ER type SAW resonator on silicon using periodically patterned-ZnO film using COMSOL Multiphysics.

6.6.1 Simulation methodology

The structure of one-port SAW resonator with proposed structure is shown in Fig. 6.15, it consists of a silicon substrate with IDT patterned over the surface and ZnO is deposited over the IDT. In general the IDT consists of 100-150 pairs of electrode fingers when designed for 50 Ω impedance at resonant frequency. Simulation of complete structure with 100 pairs of electrodes and large aperture length is practically difficult, time consuming and required high end computational system. So, we have considered only one wavelength of device with two edge electrodes of λ/8 and one λ/4 electrode in the middle as shown in the Fig. 6.15(b). Instead of periodic boundary conditions, free boundary conditions are applied to the edge boundaries and continuity periodic boundary conditions are applied to boundaries along the aperture assuming infinitely long aperture and to be noted the operating frequency is independent of aperture length of simulated structure.

Uniform IDT with metallization ratio of 0.5 is considered over the (100) oriented silicon substrate and patterned-ZnO is disposed in the spaces of the IDT structure, as depicted in Fig. 6.15(b). The (002) oriented ZnO with *c*-axis along the sagittal plane is chosen due its maximum electromechanical coupling along *c*-axis [46]. Perfectly matched layer (PML) is considered at the bottom of the silicon substrate as an absorbing boundary to eliminate the unwanted reflections from bottom surface and fixed boundary condition is applied to the bottom surface of PML. We assume middle electrode width of 2 μm, edge electrode width of 1 μm and 100 nm thickness with pitch 4 μm and the material properties of ZnO, silicon, and aluminum used in the simulation are adapted from [39] and are given in Appendix A. Initially eigenmode analysis is carried out to obtain phase velocity and coupling coefficient dispersion curves and further frequency dependent analysis carried out by applying an input potential of 1V is assumed for the edge electrode and ground boundary conditions are applied to middle electrode in order to obtain admittance characteristics of the proposed ER type SAW resonator on silicon.

6.6.2 Results of ER SAW one-port resonator with patterned-ZnO

The phase velocity and coupling coefficient dispersion characteristics of surface modes generated in the structure are shown in Fig. 6.16. From the dispersion characteristics we observed only one surface mode excited in the structure. The displacement profile and the admittance characteristics of generated surface wave is shown in Fig. 6.17.

The reason behind the generation of one surface wave is, that (002) oriented ZnO exhibits zero shear coupling coefficient along the *c*-axis, which has been clearly discussed in chapter 3. From the displacement profiles we observed that the generation of Love wave is due to

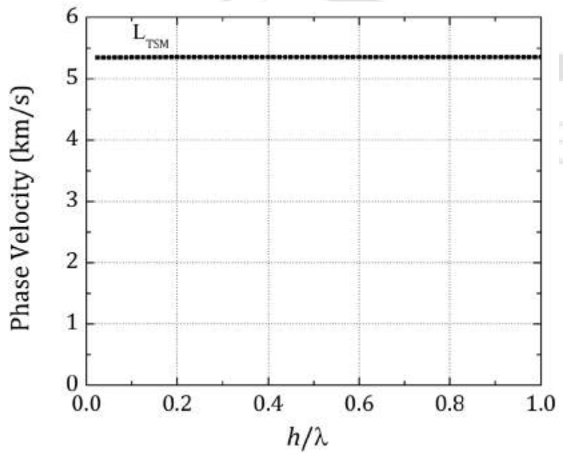

(a)

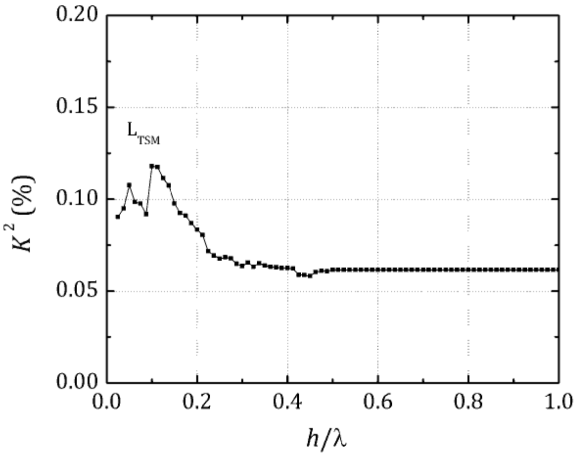

(b)

Fig. 6.16. Phase velocity dispersion characteristics of Love wave generated in the patterned-ZnO/IDT/Si structure.

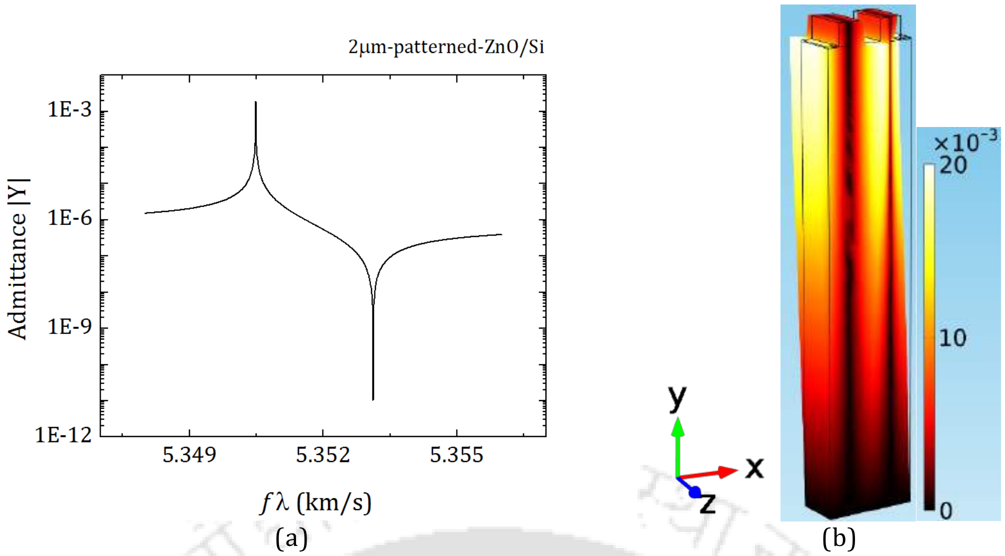

Fig. 6.17. (a) Admittance characteristics of Love wave generated in the patterned-ZnO/IDT/Si structure and (b) the displacement profile of generated surface mode at resonance frequency.

the conversion of thickness shear mode (TSM) excited in ZnO pattern. In case of thickness shear mode based devices, the frequency of operation depends on the thickness of the film of piezoelectric material between two electrodes whereas in case of proposed structure the frequency of operation depends on both height and width of ZnO pattern.

From Fig. 6.17, we observed that the proposed ER type SAW resonator with 2 μm patterned-ZnO exhibits resonance frequency of 668.875 MHz with a maximum total displacement of 0.3 μm and a very narrow band width of 0.329 MHz, from the displacement profile we observed that the displacement distribution is along the substrate depth also validates for low coupling coefficient.

This can be overcome by using heavy metals or buffer layers to guide the generated surface wave. Kadota *et al.* [73] reported that use of heavy metals like tungsten (W), gold (Au), tantalum (Ta) results in concentration of surface energy within 1λ depth and also heavy metals increases the reflection coefficient of the IDT. Based on the literature reported by Kadota, we performed eigenmode analysis on the proposed structure to study the effect of heavy metal on surface displacement profile and operating frequency.

6.6.3 Effect of heavy metals on SAW characteristics

To study the effect of heavy metals on characteristics of surface waves generated by the mode conversion of TSM modes excited in ZnO pattern, we performed frequency dependent analysis to obtain the admittance plot and displacement profiles. In this study we selected various heavy metals like gold (Au), tungsten (W), palladium (Pd), and copper (Cu) for IDT

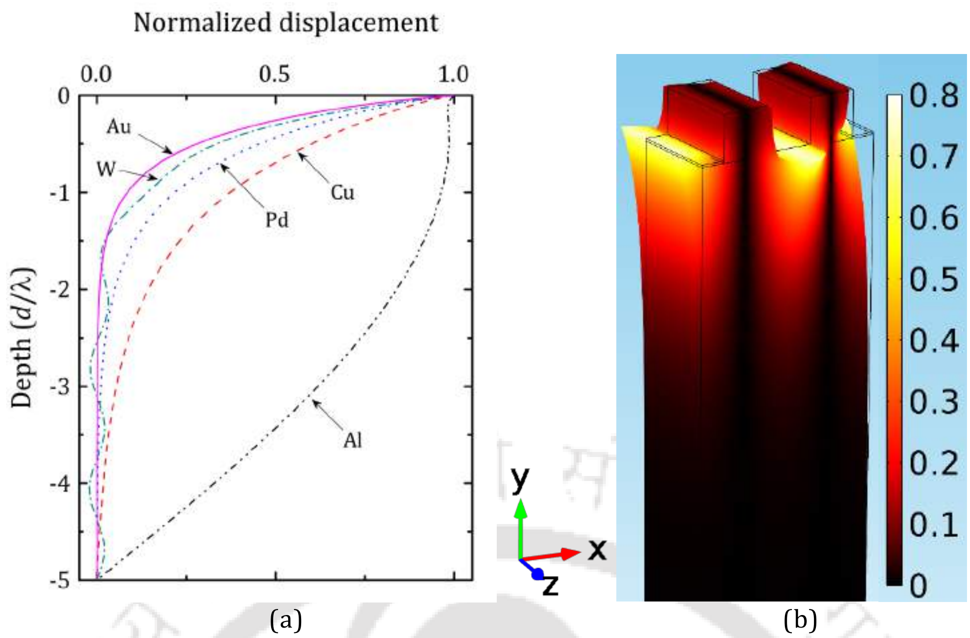

Fig. 6.18. (a) Displacement distribution of SH-SAW generated in silicon with IDT of various metals and (b) the displacement profile of generated surface mode in silicon with gold electrodes.

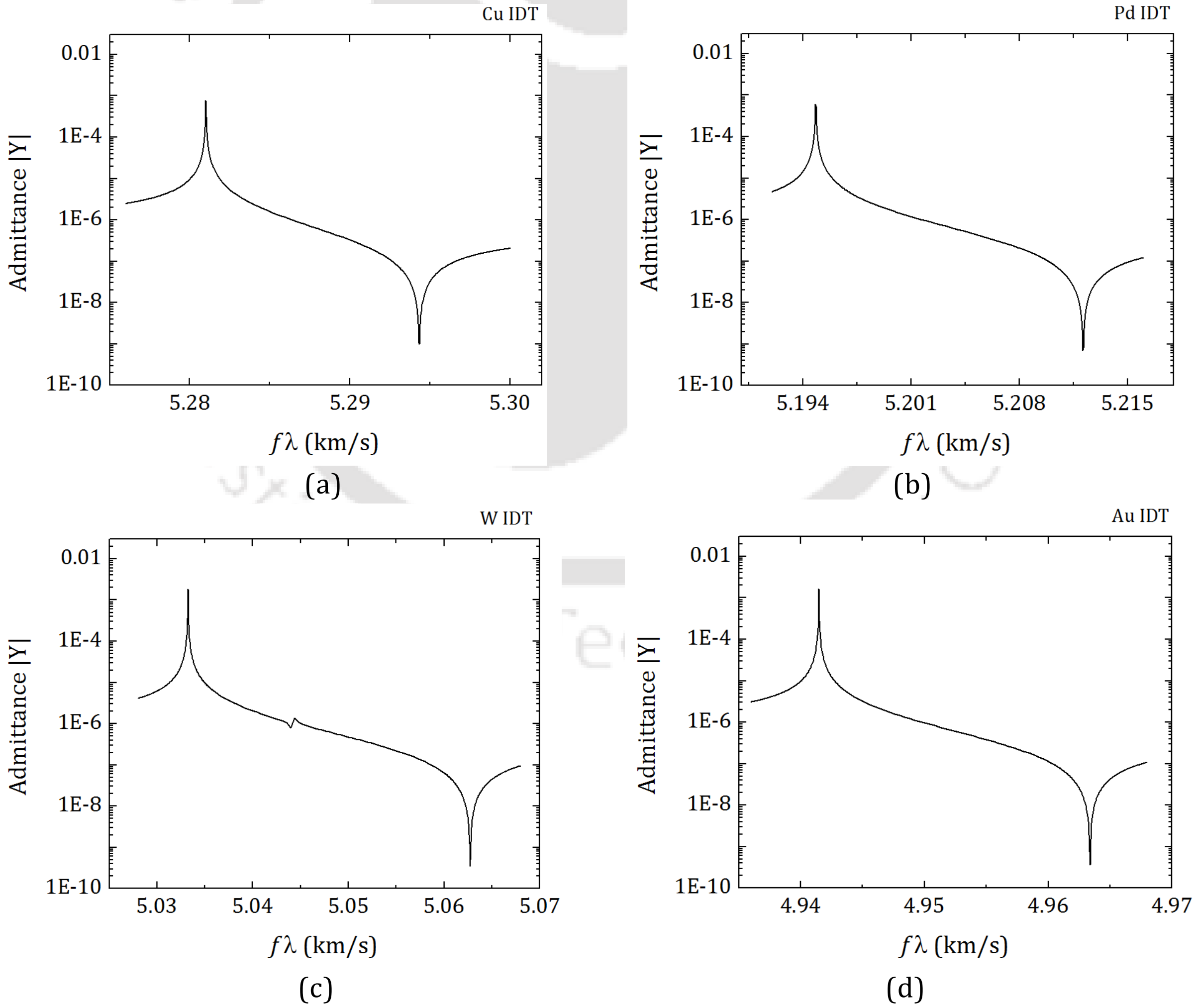

Fig. 6.19. Admittance characteristics of Love mode generated in the ER type 2μm-patterned-ZnO/Si SAW resonator with (a) copper IDT, (b) palladium IDT, (c) tungsten IDT and (d) gold IDT.

structure with an electrode thickness of 0.1 μm and one wavelength of resonator structure with λ/8 electrodes at the edges. The displacement distribution of surface wave in silicon with various metal electrodes and displacement profile of simulated structure with gold electrodes are shown in Fig. 6.18 and the obtained admittance characteristics with 8 μm are shown in Fig. 6.19 and details are tabulated in Table 6.7. From the characteristics we observed that, the band width is increased with heavy metals as well as the coupling coefficient. Since the coupling coefficient is proportional to band width of device.

Table 6.7 Admittance characteristics of surface wave in silicon with IDT of various metals.

Metal	Series resonance f_r (MHz)	Parallel resonance f_p (MHz)	Band width (MHz)
Al	668.811	669.140	0.329
Cu	660.125	661.795	1.670
Pd	649.350	651.515	2.165
W	629.155	632.840	3.685
Au	617.685	620.425	2.740

6.6.4 Effect of buffer layers in ER type patterned-ZnO/Si structure on SAW characteristics

The K^2 characteristics of a proposed SAW device can be improved considerable using buffer layers between the piezoelectric layer and substrate as Visser [31], pointed out that the coupling coefficient can be increased appreciable by the inclusion of SiO_2 film between the ZnO film and silicon substrate as well as aid in the promotion of quality of ZnO film [61]. In case of proposed patterned structure AlN is not suitable for Love wave propagation, due to the condition the Love wave can generate in thin films having acoustic velocity less than the acoustic velocity of the substrate, whereas AlN has high acoustic velocity than silicon substrate. In this study, SiO_2 buffer layer is chosen due its lower acoustic velocity than silicon and also compatible with CMOS integration process. We performed eigenmode analysis on the proposed structure with SiO_2 film and its thickness as parametric sweep having constant ZnO thickness. The obtained dispersion characteristics are show in Fig. 6.20.

The phase velocity characteristics shows that the increase in SiO_2 thickness the resultant velocity of generated Love wave tends to reach the surface wave velocity of bulk SiO_2. A relative maximum coupling coefficient of 2.52% is observed at 1.8 μm SiO_2 thickness with phase velocity of 4786 m/s. A frequency dependent analysis is carried out to study the SAW displacement profile and bandwidth characteristics. 1V electric potential is applied to the central electrode and ground electrical boundary condition is applied to edge electrodes.

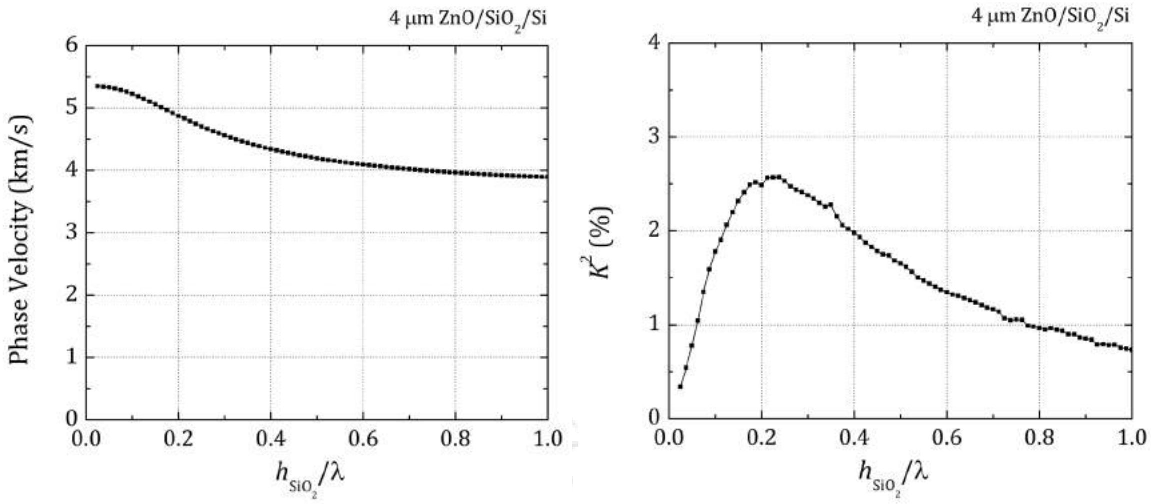

(a) (b)

Fig. 6.20. Phase velocity dispersion characteristics of Love wave generated in the 4μm-patterned-ZnO/IDT/SiO_2/Si structure.

Fig. 6.21, shows the admittance characteristics and displacement profile of the generated Love mode due to the mode conversion of TSM in ZnO pattern. From the characteristics of proposed structure with buffer layer, we observed the operating frequency of 585.525 MHz with bandwidth of 1.67 MHz and maximum displacement of 0.45 μm at the edges and center of the device. By the inclusion of oxide layer the bandwidth of the resonator is increased by 5 times as well as coupling coefficient is improved to 2%.

6.6.5 Observations

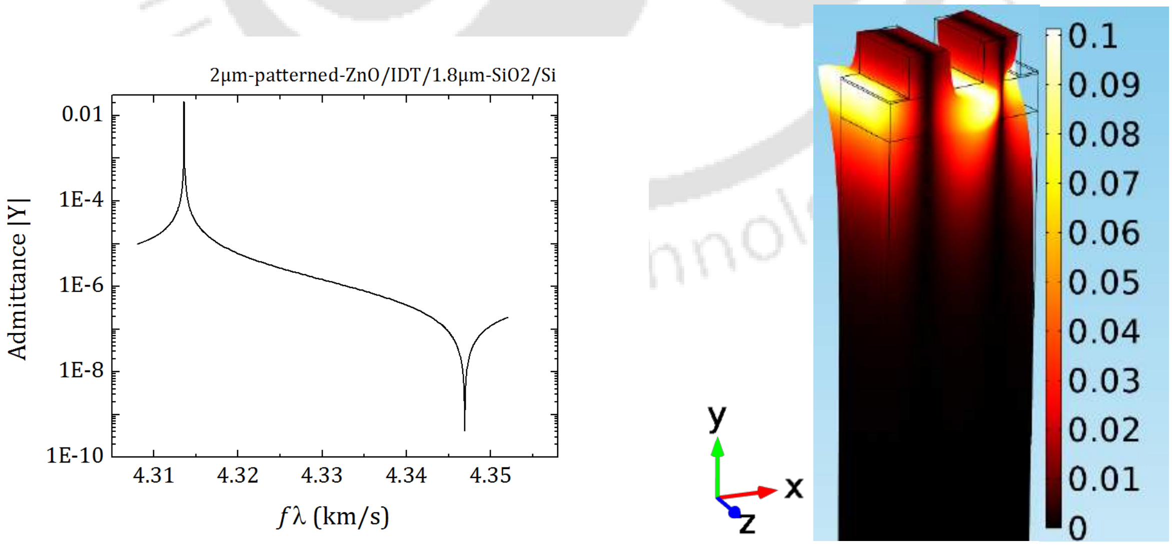

(a) (b)

Fig. 6.21. (a) Admittance characteristics of Love mode generated in the 2μm-patterned-ZnO/IDT/1.8μm-SiO_2/Si structure and (b) displacement profile of Love mode generated by TSM mode excited in ZnO pattern.

The results and observations from the FE simulations of ER type SAW resonators on silicon using patterned-ZnO film with all possible configurations and the effect of buffer layers are summarized as follows:

1. The dispersion characteristics shows a constant high phase velocity with respect to ZnO height. The device exhibit low coupling coefficient due to distribution of energy of the generated SH-SAW.
2. Use of heavy metals like gold, tungsten, and platinum, in the IDT design results in the confinement of surface wave within 1λ depth in to substrate and can also improves the coupling coefficient appreciable.
3. The FE simulation results of proposed structure with oxide buffer layer shows the improvement in coupling coefficient significantly compared with pattern-ZnO/Si. Also provides better wave guiding.
4. The phase velocity characteristic depends on the substrate and buffer layer, whereas in case of proposed device (chapter 3) phase velocity predominantly depends on the ZnO pattern and type of bulk mode generated in it.

6.7 Applications of ER type SAW resonator

In general, SAW device are commercially renowned for band pass filters that provides high stability, low acoustic losses, and operates without any external power supply. Various band pass filters like transversely coupled resonator (TCR) filters, longitudinal coupled resonator (LCR) filters, dart filters, impedance element filters, and ladder filters are under wide usage in communication industry [3]. Commonly, filters are realized on the piezoelectric substrate having IDT structure and reflector gratings. Kadota *et al.* [10] reported the development of band pass filters using edge reflection type SAW device on piezoelectric substrates.

Similarly, using the proposed edge reflection type SAW resonators, we design, fabricate and tested the LCR, TCR and ladder filters to prove their commercial fabrication viability. The details of these three types of filter configuration are as follows

6.7.1. Longitudinally coupled resonator filter (LCR)

The 3D schematic of LCR filters using edge reflection type IDT's are shown in Fig. 6.22(a). The device comprises of a pair IDT's arranged adjacent along the direction of propagation. The λ/8 electrodes are located at the free edges of silicon substrate having ZnO film that supports the generation of Love wave. In a LCR filter operation is based on the coupling of symmetric and asymmetric modes generated in the structure and forms a pass band region

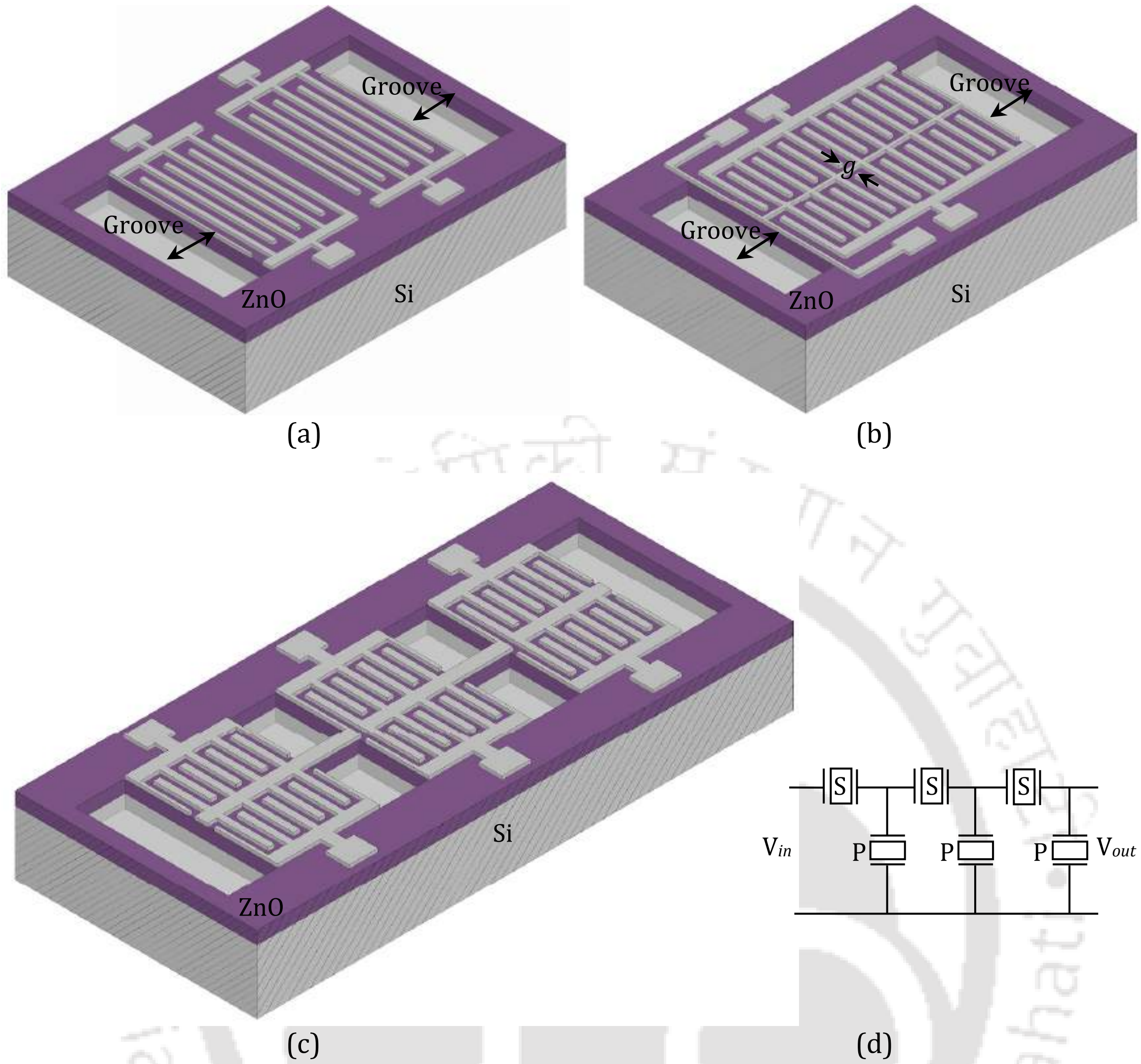

Fig. 6.22. Schematics of resonator filter configurations using ER type SAW resonators, (a) two port resonator filter, (b) longitudinal coupled resonator filter, (c) ladder filter, and (d) block diagram of arrangement of series (S) and parallel (P) resonators in a typical ladder filter.

between resonance and anti-resonance. The device configuration and functionality is similar to two port resonator that offers low losses devices at GHz frequencies, as shown in Fig. 6.22(a). In LCR filter, two longitudinal modes (symmetrical and asymmetrical modes) are coupled to form pass band region. [3] and [10]

6.7.2 Transversely coupled resonator filter (TCR)

TCR filter works on the concepts resonance and guiding of wave to realize a band pass filter. In general, TCR filters exhibits extremely small bandwidth typically around 0.1% and also provides good stop-band rejection ratio compared to LCR filters. The device consists of two resonators located physically close together in a columnar manner, and IDTs of both resonators having a common bus bar, as shown in Fig. 6.22(b). A wave generated in one

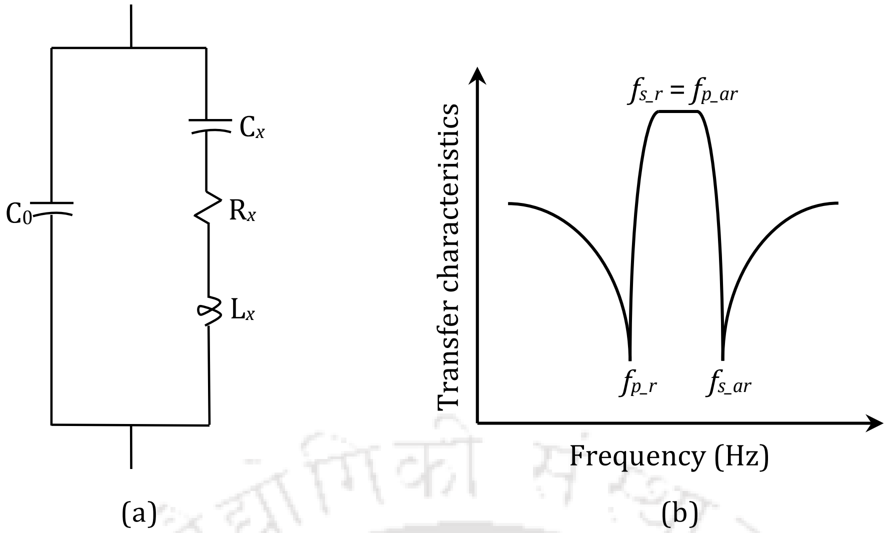

Fig. 6.23. (a) Equivalent circuit of IDT and (b) typical characteristics of an L-section.

resonator couples to the other resonator to form symmetric and asymmetric modes. The aperture W of transducers are made quite small to ensure proper coupling, typical values of W are in range of 3-6 wavelengths and the gap g is also small. The modes in the two devices couple transversely to form symmetrical and asymmetrical modes in the combined device and operate as a band pass filter with exceptionally narrow bandwidth of 0.1%, low insertion loss and excellent stop band rejection. The mode velocities of symmetric and asymmetric modes are similar to those of one port resonator and typically higher order modes are either absent or weakly coupled.

6.7.3 Ladder filters

Ladder filters are common type of band pass filters used for RF filtering in mobile phones with typical center frequencies in range of 1GHz to 2GHz. 3D schematic of an L-section ladder filter is illustrated in Fig. 6.22(c) and structure is depicted in Fig. 6.22(d). The basic L section of a ladder filter consists of a series one port resonator (S) and a shunt one port resonator (P) connected between the terminals of S and ground. The equivalent circuit modes of an IDT is shown in Fig. 6.23(a) and the resonance (f_r) and anti-resonances (f_{ar}) frequencies can be modeled by [73]

$$f_r = \frac{1}{2\pi}\sqrt{\frac{1}{LC_x}}$$

$$f_{ar} = \frac{1}{2\pi}\sqrt{\frac{1}{LC_x} + \frac{1}{LC_0}}$$

In an L-section, let us consider f_{s_r} and f_{s_ar} are the resonance and anti-resonance frequencies of series resonator (S), and f_{s_r} and f_{s_ar} be the resonance and anti-resonance frequencies of parallel resonator (P). The typical transfer characteristics of an L-section is shown in Fig. 6.23(b) and to achieve the band pass characteristics the resonators designed in such a way that $f_{s\_r} = f_{p\_ar}$ and resonance and anti-resonance frequencies of parallel and series resonators respectively, from the edges of the pass band. In the pass band region the L-section behaves as a two capacitor network with parallel resistances and the filter selectivity performance can be improved by adding multiple stages of L-section. The input and output ports of a ladder can be terminated by series or parallel resonators based on the application. The bandwidth and attenuation parameters depends on the static capacitances of the resonators and capacitance ratios of series and parallel resonators.

6.8 Design of ER type SAW devices on silicon using equivalent circuit model

The ER type SAW devices on silicon are designed using equivalent circuit model for the fabrication process. In design of ER type SAW device the dimensions of IDT for 50 Ω impedance are calculated using the phase velocity and K^2 dispersion characteristics. The equivalent circuit modes is discussed clearly in Chapter 2, same formulas are employed in this design. Due to fabrication limitations we opted for ZnO/IDT/Si configuration with and without oxide film. Similarly patterned-ZnO/IDT/Si configured ER type SAW devices with an optional oxide layer is designed using the methodology formulated in Chapter 3. One port resonators, two port resonators, transversely coupled resonator (TCR) filters, and ladder filters using ZnO films and periodically patterned ZnO-films with and without oxide buffer layer are designed and the calculated IDT dimensions are tabulated below.

Table 6.8 Calculated IDT dimensions of ER type SAW devices on silicon using equivalent circuit model.

Device	Aperture length (*W*)	Number of finger pairs (*N*)
ZnO film/IDT/Si		
One port resonator	40λ, 50λ, 60 λ	95, 85, 78
Two port resonator	50λ	85, 30, 10
TCR filter	3λ, 4λ, 5λ, 6λ	347, 300, 269, 245
Ladder filter	50λ	85
Pattern-ZnO/IDT/Si		
One port resonator	40λ, 50λ, 60 λ	104, 93, 85
Two port resonator	50λ	93, 30, 10
TCR filter	3λ, 4λ, 5λ, 6λ	380, 329, 294, 268
Ladder filter	50λ	93

6.9 Summary

In this chapter, the theory and operation of edge reflection type SAW resonators and their realization on silicon substrate using vertically patterned grooves and ZnO films is studied. Simulations are carried out on all possible layered configurations to obtain velocity and K^2 dispersion characteristics with respect to ZnO thickness. ZnO *c*-axis is oriented transverse to the direction of SAW propagation. The simulation results validate the generation of Love wave with substantial displacement along the transverse direction. However, the proposed device with ZnO film needs tradeoff between phase velocity and K^2. Configurations IDT/ZnO/Si and ZnO/IDT/Si show encouraging phase velocity with acceptable coupling coefficient for realizing on silicon substrate. However, the proposed device with ZnO film needs tradeoff between phase velocity and K^2.

To improve K^2 and velocity dispersion characteristics we employed SiO_2 and AlN buffer layers. Eigenmode analysis is performed to obtain the phase velocity and K^2 dispersion characteristics for configurations ZnO/IDT/Si and IDT/ZnO/Si with buffer layer sandwiched between ZnO film and silicon substrate. Configurations IDT/ZnO/Si and IDT/ZnO/SiO_2/Si exhibit high K^2 (greater than 5%) but at higher thicknesses of ZnO ($h/\lambda>0.25$), whereas configurations ZnO/IDT/Si and ZnO/IDT/SiO_2/Si exhibit acceptable K^2 (between 2% and 5%) at small thickness of ZnO ($h/\lambda<0.15$).

Further, we employed aluminum nitride (AlN) as the buffer layer and the dispersion characteristics are obtain from eigenmode analysis. The results show that the inclusion of AlN buffer layer in place of SiO_2 layer improves K^2 by 35% and velocity by 6% for h_{AlN}/λ up to 0.2 and no noticeable improvement is observed for higher thickness of AlN.

To overcome the tradeoff exhibited by the thin films, based on the reported literature and the study in Chapter 3, we employed periodically patterned ZnO for the generation of Love waves in silicon substrate. The results of finite element simulations of ER type patterned-ZnO SAW device show the generation of thickness shear mode in the ZnO pattern which is mode converted into transverse surface wave on silicon substrate. As compared with ZnO film ER type SAW device, the phase velocity is increased slightly but K^2 has reduced drastically to 0.1%. The main reason for low K^2 is found to be significant radiation of SAW into the bulk of silicon. The use of heavy metals for the IDT structure such as gold, palladium, tungsten and platinum has shown confinement of energy near to the surface and improvement in K^2.

We employed SiO_2 buffer layer to improve the K^2 characteristics of the patterned-ZnO ER type SAW device, as the buffer layer confines the wave to the surface and results in low acoustic losses. The results of finite element simulations show the improvement in K^2 value to 2.3% and slight reduction in phase velocity. In the proposed structure, AlN is not suitable for buffer layer, since the acoustic velocity of AlN is greater than the silicon substrate, AlN/Si structure does not support Love wave.

The proposed ER type SAW devices on silicon using ZnO films and periodically patterned films are fabricated using the design parameters obtained from dispersion characteristics and equivalent circuit model.

Chapter 7

Fabrication of Edge Reflection Type SAW Devices on Silicon

This chapter presents the fabrication process of edge reflection type SAW devices on silicon using ZnO film and patterned-ZnO film. In order to validate the practicability and bulk manufacturing of proposed devices, we fabricated one port resonators, two port resonators, transverse coupled filters, and ladder filters using UV lithography process.

7.1 Fabrication of edge reflection type SAW devices on silicon

The conventional edge reflection type SAW devices are predominantly fabricated on piezoelectric substrate using photolithographic patterning techniques used in the semiconductor industry [1]. In the fabrication of edge reflection type devices, the length of the device is very crucial in forming standing wave pattern between the free edges that are obtained by dicing the piezoelectric substrate. In general IDTs are patterned using aluminum (Al) thin metal film deposited on the surface of the piezoelectric substrate using thermal evaporation or RF sputtering and IDTs are patterned using UV lithography followed by developing stage where the unwanted Al is removed by etching process. In the proposed edge reflection (ER) type SAW devices on silicon, the IDTs are fabricated on silicon substrate with free edges formed by developing vertical grooves in silicon using deep reactive ion etching (DRIE) process. ZnO films are disposed over the patterned IDT structure using RF sputtering and using UV lithography process disposed ZnO is chemically etched to obtain periodically patterned ZnO and opening the contact pads for characterization.

7.1.1. Design of edge reflection type SAW devices

The one-port resonators, two port resonator filters, transversely coupled resonator filters, and ladder filters are fabricated on (100) oriented *p*-type silicon substrate, since it exhibits low acoustic losses. *p*-type silicon is considered to avoid unwanted losses like electro-acoustic losses and electromagnetic feed through. High resistive (0-100 Ω/cm) 2” single side polished silicon wafers of thickness 0.35 mm and diced quarter pieces of 4 inch single side polished p-type (100) oriented silicon wafers with thickness 0.5 mm and resistivity (1-10 Ω/cm) are employed in the fabrication process. Some of the important criteria to be considered in the fabrication of ER type SAW devices on silicon are as follows

i. The IDTs are designed for 50 Ω impedance at resonance frequencies of 275 MHz and 320 MHz for ER type devices with ZnO films and patterned-ZnO film respectively.

ii. Bond pads are designed to match RF probe station requirements, with ground source ground contact pads.
iii. Devices are acoustically isolated using 250 µm - 400 µm wide grooves in silicon obtained using deep ion reactive etching (DRIE) process.
iv. Groove depth of 80 µm is considered to ensure the reflection of generated Love wave without mode conversion.
v. The devices are organized to fit maximum number of devices in the mask layout.
vi. The distance between two parallel edges must be an integral multiple of λ or $\lambda/2$.

7.1.2 Fabrication process

The fabrication procedure of the edge reflection type SAW devices on piezoelectric substrates mentioned in [10] is closely followed in this work.

(a) Layout design

The layout of IDT, groove dimensions and ZnO patterns are graphically designed using CleWin software. Three layered design with standard alignment marks is chosen to accomplish the IDT, groove and ZnO pattern layouts without any misalignment. The mask plates are prepared according to the process employed in Chapter 4, Section 4.12(b). The unwanted photo-resist is removed using acetone, followed by piranha cleaning process for 30 s. Microscopic images of IDT mask plate and the magnified view of IDT structure are shown in Fig. 7.1. The major fabrication process steps of three possible processes are shown in Fig. 7.2, Fig. 7.3, and Fig. 7.4 respectively.

(b) *Cleaning of wafers*

Silicon samples are cleaned using standard piranha cleaning followed by 15 seconds HF dip. Piranha recipe is prepared with 3:1 ratios of H_2SO_4 and H_2O_2 to remove contaminants present in silicon wafers. The samples are dipped HF solution for 30 s to remove the presence of native oxide. Finally, wafers are cleaned with DI water and dried using filtered nitrogen gas.

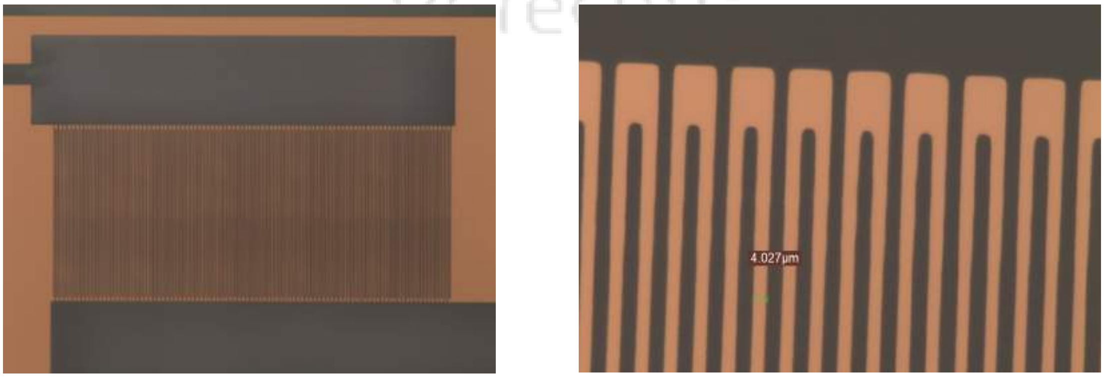

(a) (b)

Fig. 7.1. (a) Optical microscopic images of IDT structure on mask plate and (b) magnified view of IDT.

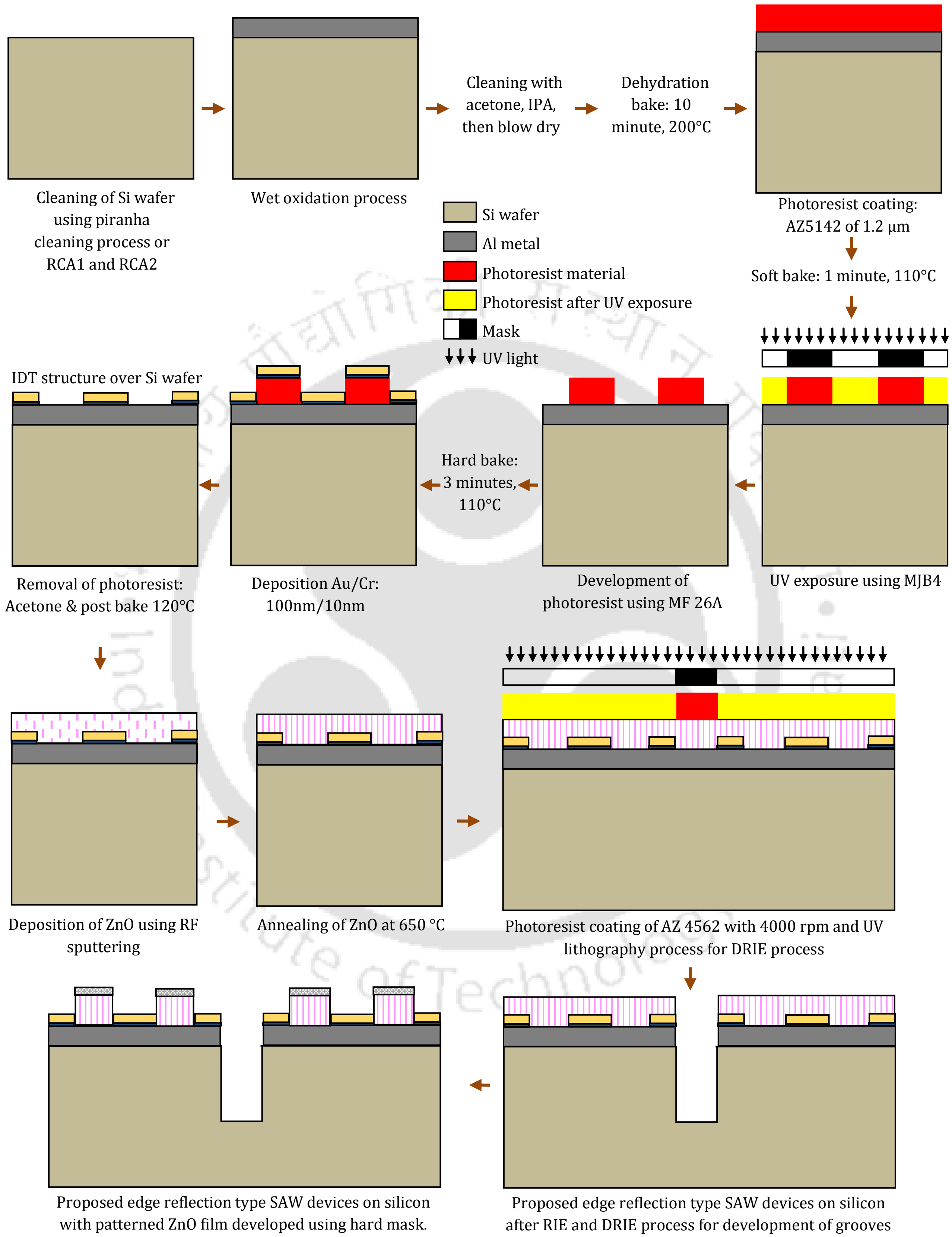

Fig. 7.2. Fabrication Process flow of ER type SAW devices on silicon with grooves developed at the last.

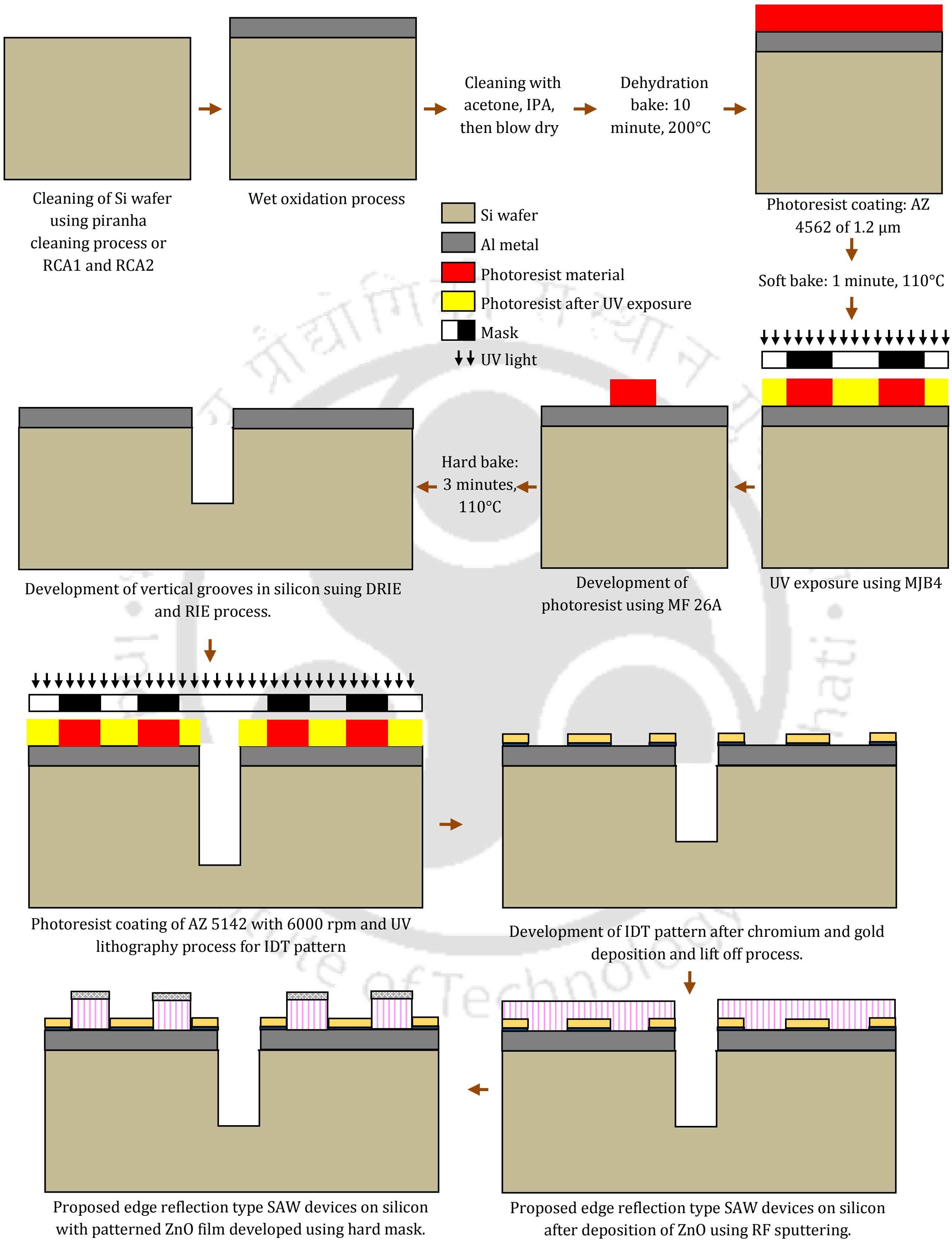

Fig. 7.3. Fabrication Process flow of ER type SAW devices on silicon with grooves developed first IDT.

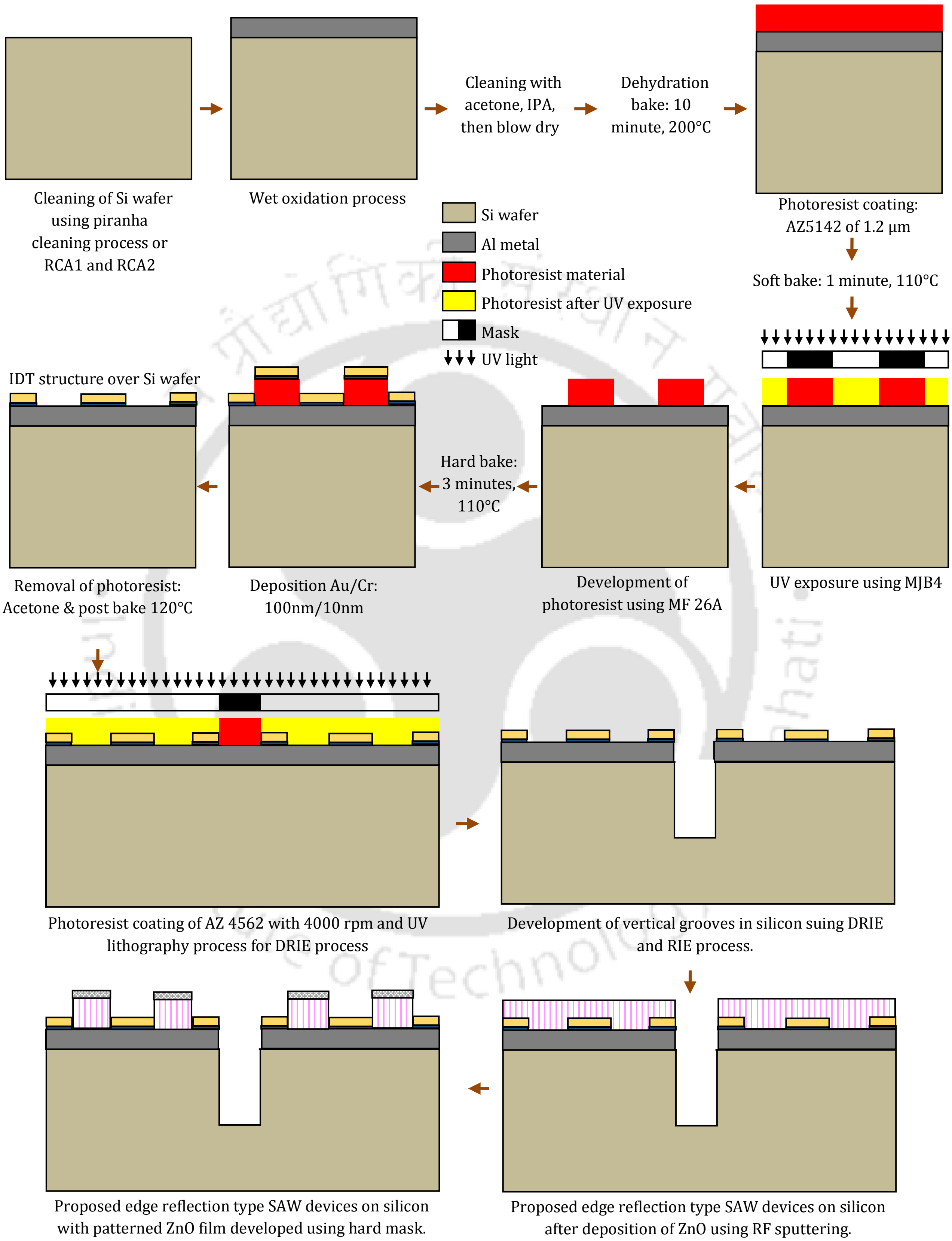

Fig. 7.4. Fabrication Process flow of ER type SAW devices on silicon with grooves developed after IDT.

(c) Oxidation of silicon wafers

2 µm thick oxide layers are obtained on silicon samples through wet oxidation process of duration 11 hr at 1100°C, we obtained oxide layer thicknesses of 2.06 µm on silicon wafers. We propose three possible fabrication processes for ZnO/IDT/Si structured edge reflection type SAW devices. Fig. 7.2 shows, the efficient process for the development of ER type SAW devices on silicon. However due to the limited fabrication facilities, we opted for the fabrication process flow detailed in Fig. 7.3, where vertical grooves are developed using UV lithography process followed by DRIE process. Due to the presence of oxide layer, initially RIE process is employed for oxide removal and followed by DRIE process for silicon substrate. The microscopic image of developed grooves in silicon are shown in Fig. 7.5(a). Lithography process is carried out for the IDT pattern, but due to the presence of grooves, the obtained photoresist coating is not uniform due to the edges, as shown in Fig. 7.5(b). Further, the deposition of chromium and gold metals are carried out using RF sputtering and followed by lift process. The microscopic images of obtained IDT

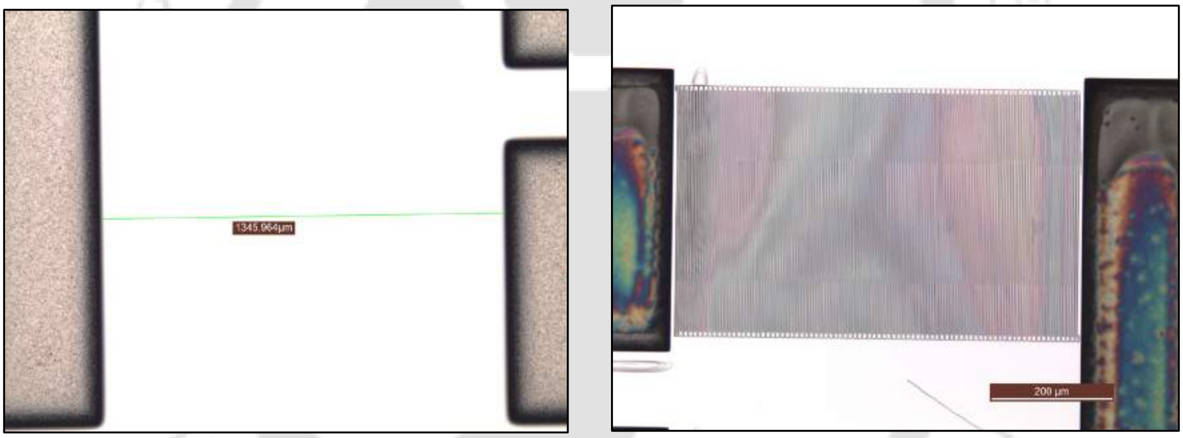

(a) (b)

Fig. 7.5. Microscopic images of vertical grooves developed in silicon substrate and (b) developed IDT photoresist pattern developed using MF-26A solution.

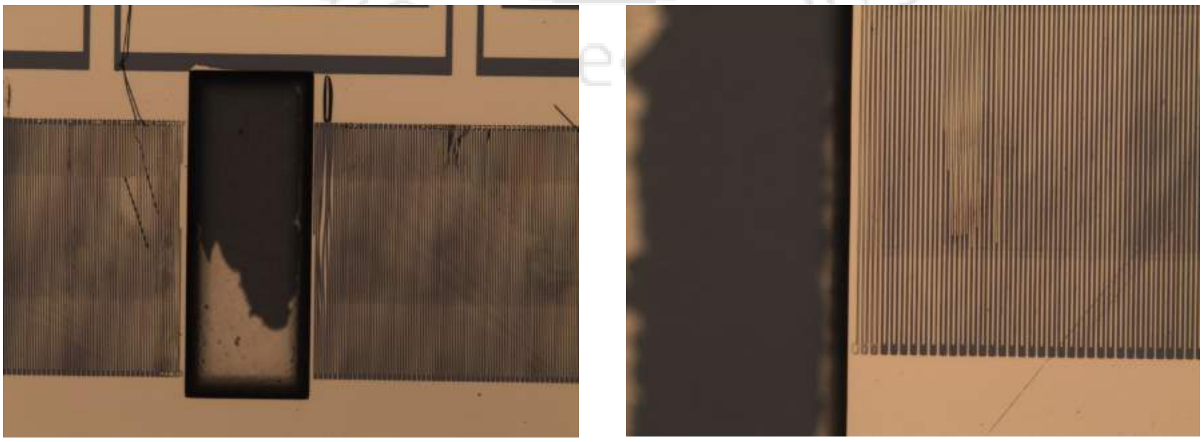

Fig. 7.6. Microscopic images of developed IDT structure after the development of mircomachined grooves.

structure are shown in Fig. 7.6. From the microscopic images of IDT structure, we conclude that the fabrication process is not suitable for the fabrication of ER type SAW devices due to the uneven development of photoresist causes improper IDT structure.

As the first process is limited by fabrication facility and second process is practically not possible, we opted for third process (Fig. 7.4) where the development of vertical groove process is carried out after the development of IDT structure. Finally, ZnO is deposited using RF sputtering. The detailed fabrication process steps are as follows.

(d) Photoresist coating

The wafers are spin-coated with positive photoresist for the development of IDT pattern and then placed inside the spin coater. It is ensured that the center of the wafer is exactly aligned with the spin coater. AZ 5142 photoresist (AZ Electronic Materials, UK) is dispensed from the bottle and spread all over the wafer. The wafer spinning program starts with 500 rpm for 5 s, followed by 1000 rpm for 5 s and finally 6000 rpm for 40 s, and the ramp rate of 500 rpm/s is used. By this method, the photoresist thickness around 1.2 µm is achieved over the wafer.

The spun samples with photoresist coating are placed on a hot plate at a temperature of 110°C for 60 s. To avoid wafer getting stuck to the hotplate surface, aluminum foil is placed between wafer and hot plate.

(e) UV exposure for IDT structure

The sample with photoresist coating is placed in MJB4 (SUSS MicroTech) with 2" substrate chuck. The setup parameters such as wedge correction and alignment of substrate are performed manually and exposure is carried out with an optimized UV dosage of 7 seconds. The exposed samples are developed using MF 26A solution, care has been taken to develop IDT

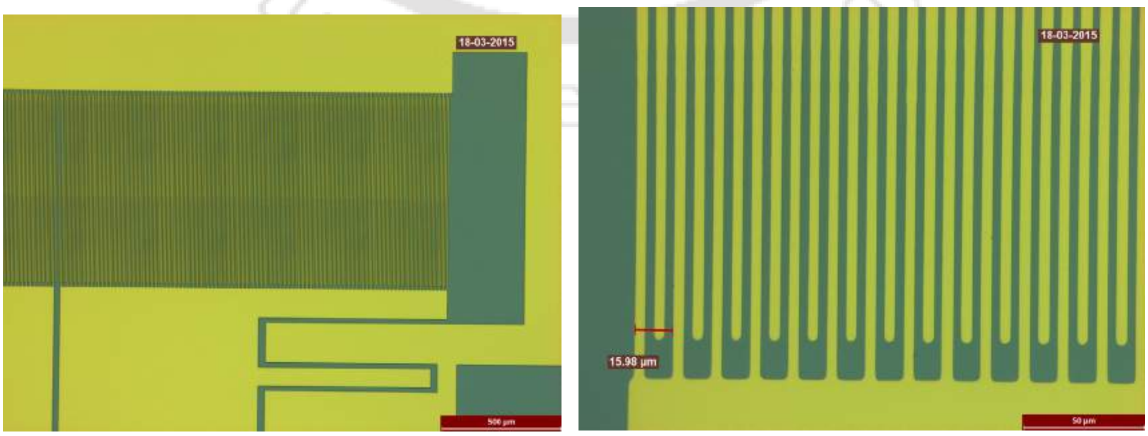

(a) (b)

Fig. 7.7. (a) Developed IDT structure of a two port resonator and (b) magnified view of IDT structure.

structure without over development or under development by constant inspection under microscope. Further, chromium (10 nm) and gold (100 nm) thickness are deposited using RF sputtering process, and the complete sputtering parameters are mentioned in Chapter 4, Section 4.1.2(*i*). After metallization the samples are kept in acetone for lift off process followed with DI water rinse and dried using nitrogen flush. The microscopic image of obtained IDT structure is shown in Fig. 7.7.

(f) Photoresist coating for DRIE process

The wafers are spin coated with positive photoresist for the development of vertical grooves in silicon pattern. The samples are placed inside the spin coater. It is ensured that the center of the wafer is exactly aligned with the spin coater. AZ 4562 photoresist (AZ electronic chemicals) is dispensed from the bottle and spread all over the wafer. The wafer spinning program starts with 500 rpm for 5 s, followed by 1000 rpm for 5 s and finally 4000 rpm for 40 s, and the ramp rate of 500 rpm/s is used. By this method, the photoresist thickness around 5 μm is achieved over the wafer.

(g) UV exposure for DRIE process

Before UV exposure, the samples with photoresist coating are placed on a hot plate at a temperature of 110°C for 60 s. The setup parameters such as wedge correction and alignment of substrate are performed manually and exposure is carried out with an UV dosage of 14 s finalized after a few trials. The exposed samples are developed using MF 26A solution for 75-80 s, followed by post baking process at 110°C for 180 s. The microscopic image of obtained groove pattern is shown in Fig. 7.8(a) shows the developed groove pattern with some uncovered metal region. In general, metals are not allowed in the DRIE or RIE process due to contamination issues. So, to overcome this problem, we kept sample in gold etchant (KI:Iodine:DI = 4:1:40) and

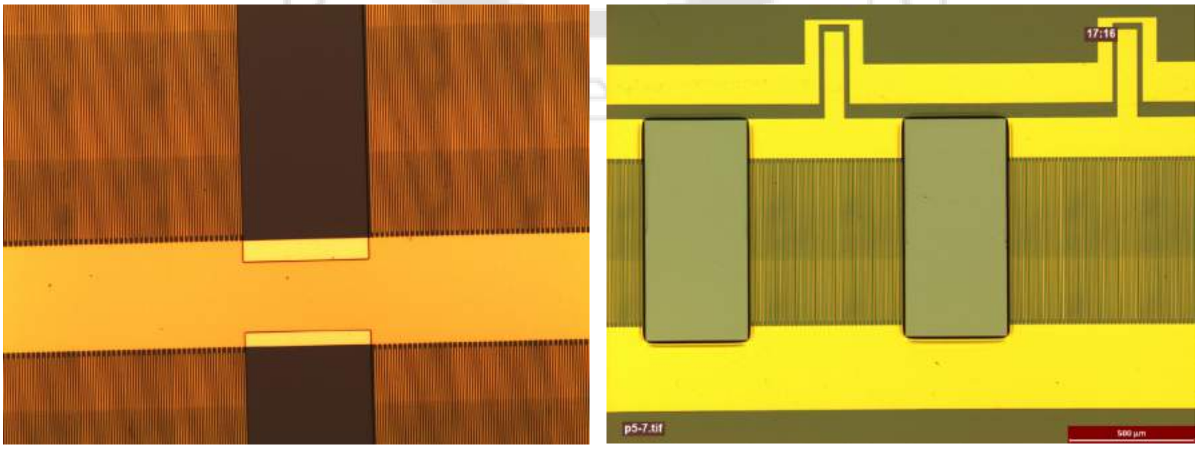

(a) (b)

Fig. 7.8. (a) Developed groove structure and (b) removal of unwanted metallic regions.

further in chromium etchant to remove the uncovered gold and chromium metal portions. Fig. 7.8(b) shows the removal of unwanted metallic portions of IDT bus bars.

(h) RIE process

Before DRIE process, the oxide layer has been etched using RIE process. The parameters of the RIE process are as follows

RF power: 50 W

Chamber pressure: 5 mTorr

Temperature: 0°C

Recipe: CHF_3-40

Etching Time: 11 minutes

(i) DRIE process

DRIE process is carried out to obtain 80 μm deep vertical grooves in silicon to aid in total reflection of generated surface waves. The etching parameters of the DRIE process are as follows

RF power: 75 W

Chamber pressure: 20 mTorr

Temperature: 30°C

Recipe: SF_6: C_4F_8: O_2 = 250:150:10 sccm

Etching Time: 14 minutes

The microscopic images of the device after the RIE and DRIE processes are shown in Fig. 7.9(a) and (b), respectively.

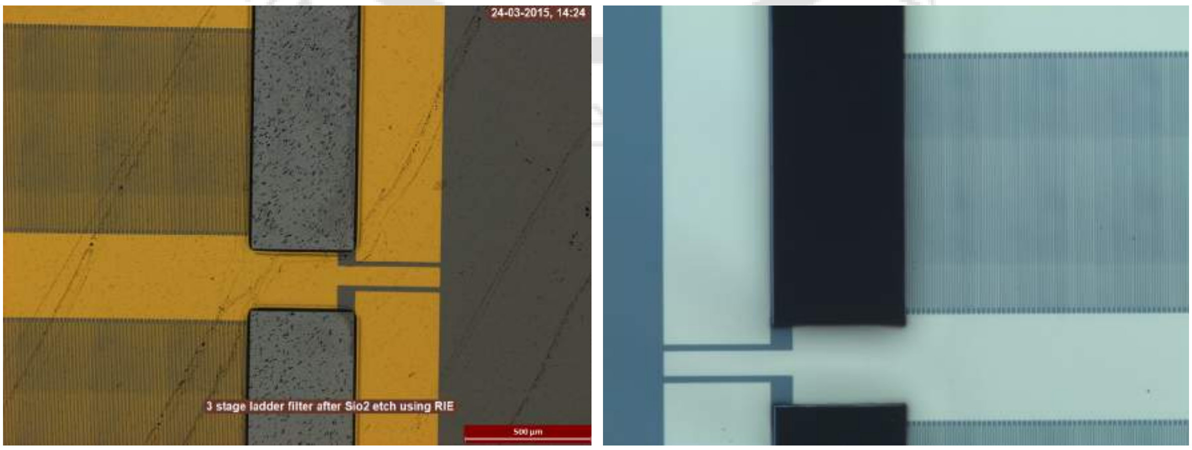

(a) (b)

Fig. 7.9. (a) Microscopic image of ER device after RIE process (b) ER type device after DRIE process showing the vertically developed groove.

(j) ZnO deposition

According to trail run of ZnO deposition at room temperature carried out at IISc, Bangalore, we obtained 278 nm thick ZnO film for 1000 s deposition implying a growth rate of 16.68 nm/minute. Accordingly we carried out ZnO deposition for 59 mins to obtain 1 µm thickness of ZnO film. The deposition is carried out at room temperature with RF power of 50 W in argon environment with vacuum parameters similar to Table 4.5 in Chapter 4, Section 4.12 (*k*). The samples are annealed at temperature of 650°C finalized after XRD analysis as mention in Chapter 4, Section 4.12 (*l*). Etching of ZnO is carried out according to the ZnO etching process discussed in Chapter 4, Section 4.1.2.

7.2 Summary

In this chapter we discuss the three possible fabrication processes to obtain the edge reflection type SAW devices on silicon substrate with ZnO thin films and periodically patterned ZnO films using UV lithography processes. A large number of one port resonators, two port resonators, transversely coupled resonators and ladder filters fabricated over an entire 2" silicon wafer.

Chapter 8

Testing of Fabricated ER type SAW Devices on Silicon

This chapter presents testing of proposed edge reflection type SAW devices on silicon substrate using ZnO films and using periodically patterned ZnO films. Network analyzer (Agilent E8361A) and RF probe station (Cascade Microtech Summit 9000) are used to obtain the S parameters that reveal the device characteristics like resonance frequency, impedance and insertion loss characteristics. Identical device structure as fabricated is simulated using finite element method and the results are compared with the test results.

The fabrication process of proposed ER type SAW devices with ZnO films and periodically patterned ZnO films are described in the previous chapter. The resonance frequency and insertion loss characteristics of the proposed ER type SAW devices are determined from S11 and S12 or S21 parameters obtained using the testing setup discussed in Chapter 5, having RF probe station connected to network analyzer with a RF probe of pitch 100 μm. Initial calibration has been carried out using GSG (ground-source-ground) probes with open circuit, short circuit, matched and through electrical conditions for a wide range of frequencies from 30 MHz to 350 MHz.

The distribution of ER type SAW devices fabricated over a complete wafer with label of every individual SAW device is shown in Fig. 8.1. All the devices other than filters are labeled as A-B, where A is number of finger pairs and B is aperture length in terms of multiple of wavelength. In case of ladder filters, P-A-B is used for device with patterned-ZnO film and C-A-B label is used for device with ZnO film. Label A-B-Pi indicates a π section ladder filter.

8.1 S parameters of ER type ZnO/Si one port SAW resonator

In this section the S parameters characteristics of the fabricated one port SAW resonators with ZnO/IDT/Si configuration are elaborated. Out of several trials in the fabrication of edge reflection type SAW devices with ZnO film, a few one-port resonators fabricated on silicon and substrate with 2.062 μm oxide film are in good condition for measurement as most of the devices are damaged during annealing process.

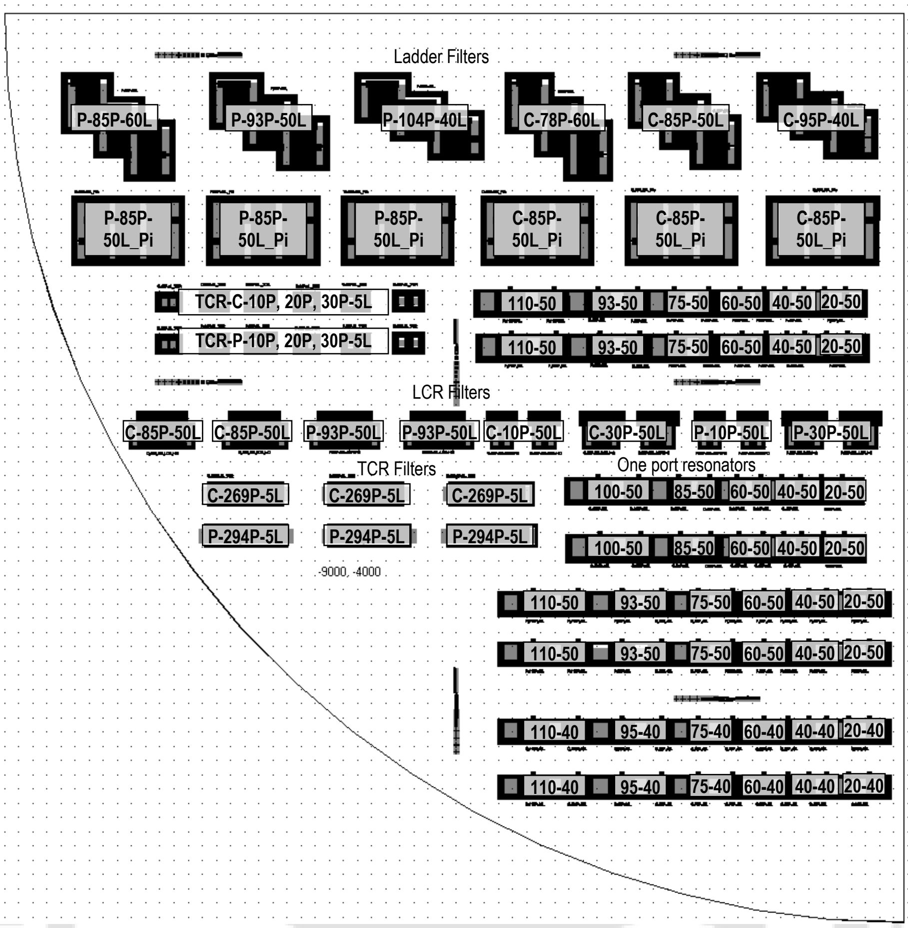

Fig. 8.1. Layout showing the distribution and arrangement of proposed ER type SAW devices on the mask plate and on silicon wafers.

The typical S11 parameters of a fabricated proposed SAW one port resonator are shown in Fig. 8.2(a). We have re-plotted the S11 characteristics as shown in the Fig. 8.2(b) for clarity.

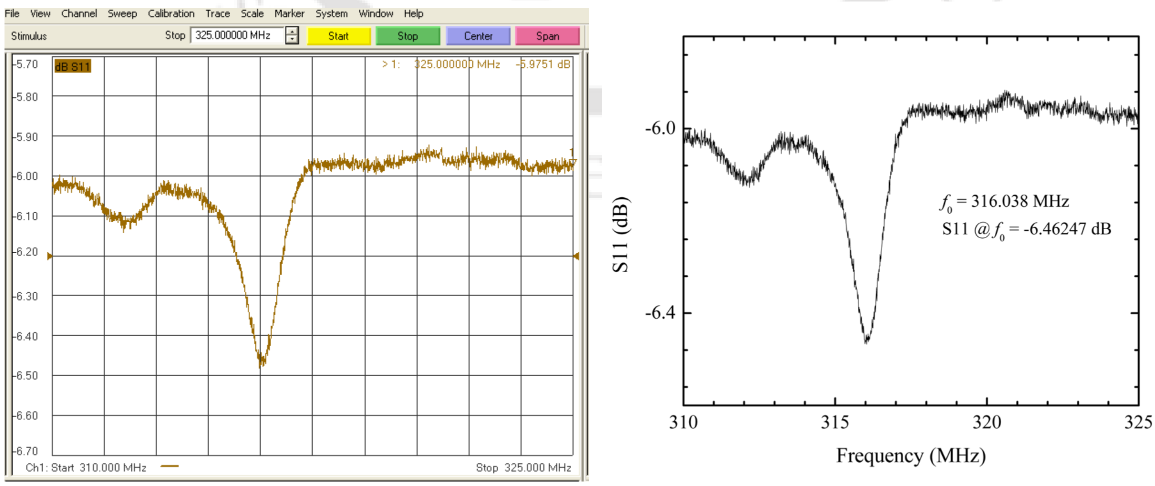

(a) (b)

Fig. 8.2. (a) Magnitude of S11 parameter of a one port ER type SAW resonator 100P-50L and (b) re-plotted S11 characteristics with labels.

In the S11 characteristics of tested one port SAW resonators labeled 85P-50L, 60P-50L, 100P-50L, the resonance peaks are not observable as their input port impedances are too low. S11 characteristics of one port SAW resonator labeled 100P-50L show a resonance frequency at 316.038 MHz with RL of -6.47 dB. However the devices were designed to operate at 270 MHz. The impedance mismatch is the most common reason for the deviations in the S parameters of the devices. Therefore we tested a one port SAW resonator using a compensation network for matching impedance. A representative case given in following section shows how the correct device characteristics can be obtained with the addition of compensation network.

8.1.1 Testing of ER type one port SAW resonator using compensation network

As discussed above the characteristics of the device labeled 100P-50L are once again obtained after addition of a compensation network for impedance matching. Using the network analyzer the impedance value of the device obtained without compensation network is 18+*j*2.335 Ω. Accordingly the values of the components of compensation network to give 50 Ω impedance are calculated as a series inductor of 11.86 nH and a parallel capacitor of 18.90 pF. After connecting the matching circuit, the measured S11 parameters are shown in Fig. 8.3. From the characteristics the resonance peak is observed at 261.727 MHz with RL -37.19 dB, and 3dB bandwidth of 0.525 MHz noted using the data obtained from the network analyzer. Using the resonance frequency and 3dB bandwidth the calculated Q is 498.5.

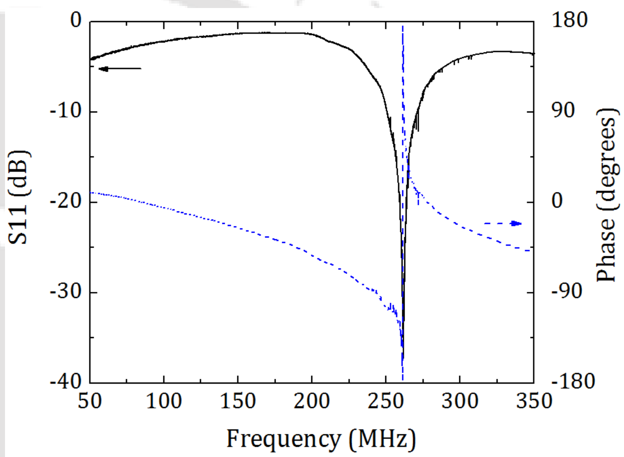

Fig. 8.3. Measured S11 parameters showing the magnitude and phase plots of 100P-50L one port ER type SAW resonator with compensation network indicating resonance frequency of about 260 MHz.

8.1.2 FE simulation of ER type ZnO/Si one port SAW resonator

In the simulation of ER type ZnO/Si one port SAW resonator, we considered the device length of one wavelength with dimensions as observed under FESEM and obtained the resonance frequencies of the device. The 3D geometry of the ER type one port SAW resonator for FE simulation is shown in Fig. 8.4(a). The dimension measured under FESEM are as follows, λ of 16 μm, electrode of width 4 μm and thickness 0.11 μm, and ZnO film

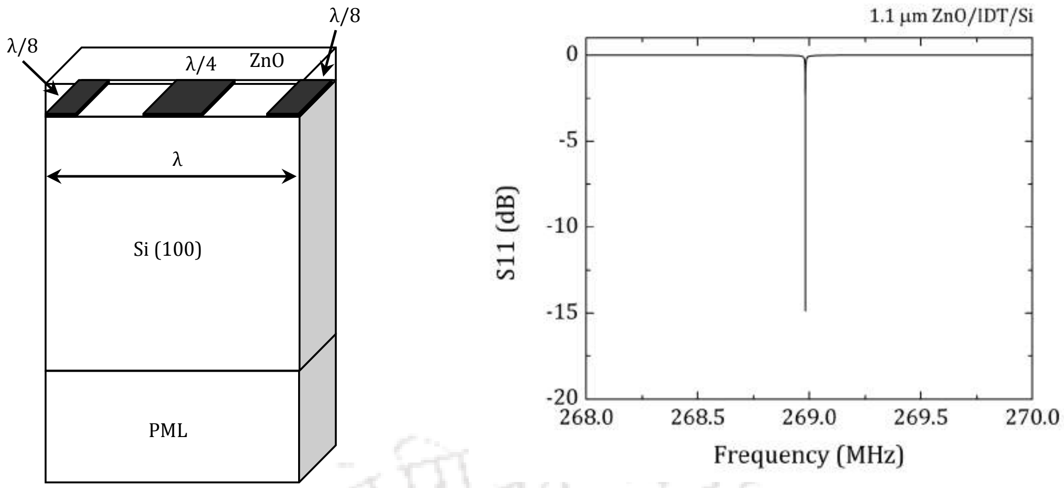

(a) (b)

Fig. 8.4. (a) One wavelength of ER type one port SAW device with periodic boundaries along the aperture and (b) S11 characteristics showing resonance frequency at about 269 MHz.

thickness of around 1.1 μm observed after RF sputtering and annealing processes. We performed eigenmode and frequency dependent analysis on the 3D geometry, so that the measured S11 parameters can be verified. The simulated S11 characteristics given in Fig. 8.4(b) show resonance peak at 268.978 MHz, and the error between the measured result and simulated result is 2.7%.

8.2 S parameters of ER type ZnO/Si two port SAW devices

Out of the fabricated two port SAW resonators and filters mentioned in Section 6.8, the measured S parameters of working devices are listed in Table 8.1.

Table 8.1 Measured S12 parameters of fabricated two port ER SAW resonator filters with ZnO film.

Device	f_0 (MHz)	IL (dB)	BW (MHz)	Q
Sample 1: ZnO-film /2μm-SiO₂/Si (Two port resonators, TCR filters and Ladder filters)				
85P-50L	168.400	-16.93	46.69	3.3
63P-50L-LCR	169.906	-15.71	51.19	3.32
63P-50L-LCR	167.844	-15.66	51.09	3.28
269P-5L-TCR	168.781	-10.56	37.5	4.5
269P-5L-TCR	168.031	-13.33	26.81	6.26
269P-5L-TCR	167.938	-10.55	36.375	4.62
78P-60L-Ladder	156.313	-28.22	37.125	4.21
Sample 2: ZnO-film/Si (Two port resonators and TCR filters)				
One port resonators, transverse coupled filters and ladder filters fabricated on silicon substrate are damaged after annealing process and the contact pads peeled away during RF probing.				

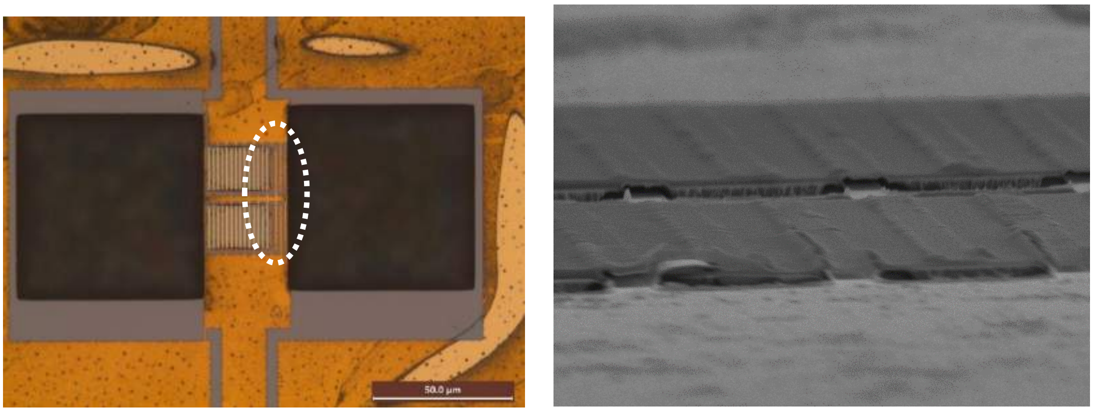

(a) (b)

Fig. 8.5. (a) Microscopic image of TCR filter after fabrication showing the washed away ZnO film at the edges and (b) FESEM image showing steps formed in ZnO film due to the presence of IDT underneath.

During the etching process the edges of ZnO film in sample 1 washed away due to the non-uniform photoresist caused by the vertical grooves made in silicon substrate by DRIE process which had to be carried out before ZnO deposition in order to avoid zinc contamination. In addition the presence of IDT under the ZnO film caused steps in ZnO film. The microscopic and FESEM images of a TCR filter after device fabrication are shown in Fig. 8.5.

8.3 S parameters of ER type SAW devices with patterned-ZnO

The proposed ER type SAW devices with patterned-ZnO as mentioned in Section 6.8 have been fabricated and the measured S parameters of the devices are listed in Table 8.2.

Table 8.2 Measured S12 parameters of fabricated two port ER SAW resonators using patterned-ZnO film.

Device	f_0 (MHz)	IL (dB)	f_1 (MHz)	IL (dB)	f_2 (MHz)	IL (dB)	f_3 (MHz)	IL (dB)
Sample 1: ZnO-Pattern/2μm-SiO₂/Si								
269P-5L-TCR	105.41	-18.84	209.28	-29.34	285.87	-28.05	319.44	-28.53
269P-5L-TCR	105.55	-33.33	209.56	-43.57	285.03	-39.69	319.25	-40.04
Sample 2: ZnO-Pattern/Si								
269P-5L-TCR	95.937	-24.66	208.72	-32.27	287.28	-31.74	-	-
269P-5L-TCR	93.125	-25.78	199.72	-34.99	287.65	-34.35	324.97	-36.29
269P-5L-TCR	89.46	-17.48	204.41	-25.96	285.68	-26.3	319.94	-27.35

Most of the devices except TCR filters are not in condition to test as the edges of patterned-ZnO structure washed away due to the non-uniform photoresist.

From the simulation results in Section 6.6.2, a resonance peak at 317 MHz caused by the TSM excited in (100) oriented ZnO pattern is expected. From the measured S parameter characteristics, we observe multiple resonance peaks instead of one resonance peak at 317 MHz. Subsequent XRD analysis revealed the ZnO orientation as (002) instead of desired (100) which is difficult to obtain. It confirms that the modes observed in Table 8.2 are in fact vertically polarized surface modes generated by (002) patterned-ZnO film, as discussed in Section 5.2.

8.4 Summary

This chapter describes the testing carried out on the fabricated proposed ER type SAW devices using UV lithography process. The device characteristics are determined using RF probe station cascaded to a network analyzer. The testing is carried out in the frequency range of 50 MHz to 350 MHz for SAW devices having IDT wavelength of 16 μm. A few devices have been found in proper condition for testing.

ER type one port SAW resonator exhibits a resonance frequency of 261.727 MHz after adding compensation network for impedance matching and the error between the experimental result and simulated result is 2.7%.

Since, ZnO is deposited after IDT has been fabricated, relative ZnO orientation is unpredictable and test results have deviated from the simulated results. An attempt has been made to fabricate TCR and ladder filters with fabrication restrictions where the vertical grooves in silicon had to be made using DRIE prior to ZnO deposition, which resulted in significant deviations in the device structure.

Chapter 9

Conclusion and Recommendations

9.1 Conclusion

The research work has two major contributions, viz. the development of high performance SAW devices on silicon substrate using patterned-ZnO film and the realization of compact edge reflection (ER) type SAW devices on silicon using ZnO film and patterned ZnO film. The device comprises of a silicon substrate with IDT structure on which ZnO film is deposited and patterned in such a way that ZnO is retained in the spaces of IDT resulting in a periodic structure of ZnO. The bulk waves excited in each block of ZnO pattern are acoustically coupled to silicon substrate to launch surface waves propagating along the silicon surface. As the SAW propagation is in silicon which has higher acoustic velocity and higher acoustic impedance for transverse BAW than ZnO, the proposed SAW devices exhibit high frequency of operation and high coupling coefficient compared with conventional ZnO thin film SAW devices on silicon.

Transduction of SAW in silicon by the mode conversion of BAW excited in periodically patterned-ZnO is investigated using finite element simulations. First higher order surface wave generated by transverse BAW in ZnO exhibits unique property of high phase velocity 5272 m/s with high coupling coefficient value of 6.4% at h/λ = 0.19. Inclusion AlN buffer layer has found to increase the velocity and K^2.

Large number of SAW devices based on the proposed configurations have been fabricated on silicon substrate. The deviation between experimental and simulation results of VP_T modes generated in the fabricated devices is less than 7%. From the simulations discussed in Chapter 3, the surface modes generated by the longitudinal bulk wave in ZnO pattern are undetectable but in practical results the VP_{L0} mode is significant due to the misalignment of ZnO pattern with respect to IDT structure. In addition, the quality of ZnO film deteriorates for deposition thicknesses greater than 1 µm and significantly affects the velocity of longitudinal BAW (generating VP_L) rather than transverse BAW (generating VP_T) which is predominately dependent on the dimensions of the structures.

The second major contribution of this research work is the development of extremely compact SAW devices of edge reflection (ER) type on silicon using ZnO film. The device comprises of the IDT structure located on a resonant plinth of silicon formed between a pair of parallel grooves in silicon substrate, covered with ZnO overlay for the transduction of Love waves.

Various configurations of proposed ER type SAW resonator are simulated and the results show that the two configurations, IDT/ZnO/Si and ZnO/IDT/Si, exhibit excellent characteristics and are easy to fabricate. Inclusion of AlN buffer layer is beneficial as it is found to increase the velocity and K^2 values.

The simulation results with patterned-ZnO film show the generation of shear horizontal SAW in silicon substrate instead of Love wave decreasing K^2 because of significant acoustic radiation into the bulk of silicon. Therefore SiO_2 buffer layer is necessary with patterned-ZnO in ER type SAW devices. The proposed ER type SAW devices on silicon using ZnO film and pattern-ZnO are fabricated and tested. Since, ZnO is deposited after IDT has been fabricated, relative ZnO orientation is unpredictable and test results have deviated from the simulated results.

9.2 Recommendations for future work

The devices proposed in the present work offer potential for integrating SAW devices in silicon ICs and are suitable for lab on chip, sensing, signal processing, communication and space applications. The proposed patterned-ZnO structure has shown little dependency on the quality of ZnO and is suitable for mass production. The ER type SAW devices can be extremely small and are commercially viable for monolithic integration with circuits on silicon.

This research work can be extended in the following directions

- Development of non-dispersive SAW devices on silicon substrate using SiO_2 and appropriate piezoelectric material for periodic patterned structure is suggested.
- The dispersion study of surface modes generated in the devices made on piezoelectric substrates may be carried out.
- Edge reflection type SAW devices may be fabricated on semiconductor substrates other than silicon.
- High frequency ER type SAW devices can be realized using high acoustic velocity substrates like sapphire and diamond.
- Ladder filter configurations may be realized on silicon to integrate with CMOS circuitry for RF commercial applications.
- Using (100) oriented patterned-ZnO films non-dispersive ER type SAW devices can be realized using the mode conversion of thickness shear mode excited in ZnO block.
- (110) Oriented silicon can be used for the fabrication of low cost ER type SAW devices with patterned and thin films of ZnO.

Material Constants of ZnO, AlN, SiO_2, and Si

The material constants of zinc oxide, aluminium nitride, silicon di-oxide, and silicon are adapted from [22], [35], and [38].

A.1 Material constants of zinc oxide (ZnO)

Density (ρ) = 5676 kg/m^3

$$\text{Stiffness, } C^E = \begin{pmatrix} 21 & 12.1 & 12.5 & 0 & 0 & 0 \\ 12.1 & 21 & 12.5 & 0 & 0 & 0 \\ 12.5 & 12.5 & 21.1 & 0 & 0 & 0 \\ 0 & 0 & 0 & 4.25 & 0 & 0 \\ 0 & 0 & 0 & 0 & 4.25 & 0 \\ 0 & 0 & 0 & 0 & 0 & 4.45 \end{pmatrix} \times 10^{10}\,\mathrm{N/m^2}$$

$$\text{Piezoelectric constant}, e = \begin{pmatrix} 0.0 & 0.0 & -0.61 & 0.0 & -0.59 & 0.0 \\ 0.0 & 0.0 & 0.0 & 0.0 & 0.0 & 0.0 \\ 0.0 & 0.0 & 1.14 & 0.0 & 0.0 & 0.0 \end{pmatrix} \mathrm{C/m^2}$$

$$\text{Permittivity}, e = \begin{pmatrix} 8.34 & 0 & 0 \\ 0 & 8.34 & 0 \\ 0 & 0 & 8.84 \end{pmatrix}$$

A.2 Material constants of aluminium nitride (AlN)

Density (ρ) = 3260 kg/m^3

$$\text{Stiffness, } C^E = \begin{pmatrix} 34.5 & 12.5 & 12 & 0 & 0 & 0 \\ 12.5 & 34.5 & 12 & 0 & 0 & 0 \\ 12 & 12 & 39.5 & 0 & 0 & 0 \\ 0 & 0 & 0 & 11.8 & 0 & 0 \\ 0 & 0 & 0 & 0 & 11.8 & 0 \\ 0 & 0 & 0 & 0 & 0 & 11 \end{pmatrix} \times 10^{10}\,\mathrm{N/m^2}$$

$$\text{Piezoelectric constant}, e = \begin{pmatrix} 0.0 & 0.0 & -0.58 & 0.0 & -0.59 & 0.0 \\ 0.0 & 0.0 & 0.0 & 0.0 & 0.0 & 0.0 \\ 0.0 & 0.0 & 1.55 & 0.0 & 0.0 & 0.0 \end{pmatrix} \mathrm{C/m^2}$$

$$\text{Permittivity}, \boldsymbol{\varepsilon} = \begin{pmatrix} 9.03 & 0 & 0 \\ 0 & 9.03 & 0 \\ 0 & 0 & 10.7 \end{pmatrix}$$

A.3 Material constants of silicon di-oxide (SiO_2)

Density (ρ) = 2210 kg/m^3

$$\text{Stiffness, } C^E = \begin{pmatrix} 7.85 & 1.61 & 1.61 & 0 & 0 & 0 \\ 1.61 & 7.85 & 1.61 & 0 & 0 & 0 \\ 1.61 & 1.61 & 7.85 & 0 & 0 & 0 \\ 0 & 0 & 0 & 3.12 & 0 & 0 \\ 0 & 0 & 0 & 0 & 3.12 & 0 \\ 0 & 0 & 0 & 0 & 0 & 3.12 \end{pmatrix} \times 10^{10}\,\text{N/m}^2$$

$$\text{Permittivity}, \boldsymbol{\varepsilon} = \begin{pmatrix} 3.75 & 0 & 0 \\ 0 & 3.75 & 0 \\ 0 & 0 & 3.75 \end{pmatrix}$$

A.4 Material constants of Silicon (Si)

Density (ρ) = 2330 kg/m^3

$$\text{Stiffness, } C^E = \begin{pmatrix} 16.56 & 6.39 & 6.39 & 0 & 0 & 0 \\ 6.39 & 16.56 & 6.39 & 0 & 0 & 0 \\ 6.39 & 6.39 & 16.56 & 0 & 0 & 0 \\ 0 & 0 & 0 & 7.95 & 0 & 0 \\ 0 & 0 & 0 & 0 & 7.95 & 0 \\ 0 & 0 & 0 & 0 & 0 & 7.95 \end{pmatrix} \times 10^{10}\,\text{N/m}^2$$

$$\text{Permittivity}, \boldsymbol{\varepsilon} = \begin{pmatrix} 11.8 & 0 & 0 \\ 0 & 11.8 & 0 \\ 0 & 0 & 11.8 \end{pmatrix}$$

B. Absorbing Boundary Conditions

In order to avoid acoustic reflections from the boundaries or edges of the SAW substrate, absorbing boundary conditions are applied in the simulations. The influence of wave reflections from boundaries can be reduced by assuming critical damping along the boundaries [46]. This can be achieved by employing suitable values for Rayleigh damping coefficients in the COMSOL Multiphysics software [46]. In Rayleigh damping model, the Rayleigh damping matrix **Z** is a linear combination of mass matrix and stiffness matrix as given below

$$\xi = A_{dM}\, M + B_{dk}\, k$$

where the mass proportional damping parameter (A_{dM}) and stiffness proportional damping parameter (B_{dk}) are damping coefficients and they are related to damping ratio (ξ) as

$$\xi = \frac{A_{dM} + B_{dk}\omega^2}{2\omega}$$

Absorbing boundary can be achieved by assuming critical damping, $\xi = 1$ and $A_{dm} = 0$ then $B_{dk} = 1/\pi f$.

Bibliography

[1] J. W. Gardner, V. K. Varadan, and O. O. Awadelkarim, *Microsensors, MEMS and Smart Devices*, John Wiley & sons, Inc., New York, 2002.

[2] C. C. W. Ruppel and T. A. Fjeldly, *Advances in Surface Acoustic Wave Technology, Systems and Applications*, vol. 1, World scientific, 2000.

[3] D. P. Morgan, *Surface Acoustic Wave Filters with Applications to Electronic Communications and Signal Processing*, Elsevier, 2007.

[4] Oldrich Novotny, *Seismic Surface Waves*, Lecture notes, Salvador, Bahia, 1999.

[5] M. Thompson, *Surface-Launched Acoustic Wave Sensors: Chemical Sensing and Thin Film Characterization*. John Wiley & Sons, 1997.

[6] R. M. White, "Surface elastic waves", *Proc. of IEEE*, vol. 58, no. 8, Aug. 1970.

[7] A. N. Darinskii, M. Weihnacht, and H. Schmidt, "Mutual conversion of bulk and surface acoustic waves in gratings of finite length on half infinite substrates. I. FE analysis of surface wave," *Ultrasonics* 53(5), 998–1003, 2013.

[8] V. Plessky, "3rd type FBARs", *Proc. IEEE Ultrasonics Symposium*, pp. 239–242, July 2013.

[9] Y. Suzuki, H. Shimizu, M. Takeuchi, K. Nakamura, and A. Yamada, "Some study on SAW resonators and multiple-mode filters," *Proc. IEEE Ultrasonics Symposium*, pp. 297–302, 1976.

[10] M. Kadota et al., "Very small IF resonator filters using reflection of shear horizontal wave at free edges of substrate," *IEEE Transactions on Ultrasonics, Ferroelectronics, and Frequency Control*, vol. 49, no. 9, pp. 1269–1278, Sep. 2002.

[11] F. Moreira, M. E. Hakiki, O. Elmazria, F. Sarry, L. L. Brizoual, and P. Alnot, "Theoretical and experimental identification of love wave frequency peaks in layered Structure ZnO/quartz SAW device," *IEEE Sensors Journal*, vol. 8, no. 8, Aug. 2008.

[12] J. H. Hines, D. C. Malocha, K. B. Sundaram, K. J. Casey, and K. R. Lee, "Deposition parameters studies and surface acoustic wave characterization of PECVD silicon nitride films on lithium niobate", *IEEE Transactions on Ultrasonics, Ferroelectronics, and Frequency Control*, vol. 42, no. 3, May 1995.

[13] K. Yamanouchi, H. Satoh, T. Meguro, and Y. Wagatusma, "High temperature stable GHz range low loss wide band transducers and filters using SiO_2/$LiNbO_3$, $LiTaO_3$", *IEEE Transactions on Ultrasonics, Ferroelectronics, and Frequency Control*, vol. 42, no. 3, May 1995.

[14] S. J. Ippolito, K. K. Zadeh, A. Trinchi, W. Wlodarski, and M. Tobar, "Layered SAW nitrogen dioxide sensor based on a ZnO/36^o YX $LiTaO_3$ structure with WO_3 selective layer," *Proc. Frequency Control Symposium*, pp. 931–934, May 2003.

[15] A. Z. Sadek, W. Wlodarski, K. K. Zadech, Y. Li, W. Yu, X. Li, and X. Yu, "A ZnO nanorod based 64^o YX $LiNbO_3$ surface acoustic wave CO sensor," *Sensors, 2006. 5th IEEE Conference*, pp. 691–694, 2006.

[16] D. Phan and G. Chung, "High sensitivity SAW UV sensor by using third harmonic based ZnO/Si structure", *IEEE Sensors Conference*, pp. 525-527, 2010.

[17] D. A. Powell, K. K. Zadeh, S. Ippolito, and W. Wlodarski, "A layered SAW device based on ZnO/LiTaO3 for liquid media sensing applications," *IEEE Ultrasonics Symposium*, vol. 1, pp. 493–496, 2002.

[18] M. Kadota and H. Kando, "IF SAW filters without love waves spurious consisting of ZnO film and specific cut angle quartz substrate", *Proc. IEEE Frequency Control Symposium*, pp. 888–892, 2003.

[19] Y. Nakai, T. Nakao, K. Nishiyama, and M. Kadota, "Surface acoustic wave duplexer composed of SiO2 film with convex and concave Cu-electrodes/LiNbO3 structure", *Proc. IEEE Ultrasonics Symposium*, pp. 1580–1583, 2008.

[20] G. Kino and R. S. Wagers, "Theory of interdigital couplers on nonpiezoelectric substrates," *Journal of Applied Physics*, vol. 44, no. 4, 1973.

[21] F. S. Hickernell, "Zinc-oxide thin-film surface wave transducers," *Proc. of The IEEE*, vol. 64, no. 5, May 1976.

[22] H. Nakahata, A. Hachigo, K. Higaki, S. Fujii, S. I. Shikata, and Naoji, "Theoretical study on SAW characteristics of layered structures including a diamond layer," *IEEE Transactions on Ultrasonics, Ferroelectrics, and Frequency Control*, vol. 42, no. 2, May 1995.

[23] Ali B. A. D, A. Ahmed, C. Popov, U. Schmid, and N. P. Kherani, "Aluminium nitride/nano-diamond structures for high-frequency surface acoustic wave nano-transducers," *Micro & Nano Letters*, 2012, vol. 7, issue. 10, pp. 1030–1032.

[24] J. H. Visser, M. J. Vellekoop, A. Venema, E. Van der drift, P. J. M. Rek, A. J. Rek, A. J. Nederlof, and M. S. Nieuwenhuizen, "Surface acoustic wave filters ZnO-SiO_2-Si layered structures," *Proc. IEEE Ultrasonics*, vol. 1, Issue Date: 3–6, pp. 195–200, Oct. 1989.

[25] M. J. Vellekoop, G. W. Lubking, and A. Venema, "Acoustic wave based monolithic microsensors," *Proc. IEEE Ultrasonics Symposium*, pp. 565–574, 1994.

[26] O. Tigli and M. E. Zaghloul, "Design and fabrication of novel a SAW bio/chemical sensor in CMOS," *IEEE Sensors*, pp. 137–140, 2005.

[27] O. Tigli and M. E. Zaghloul, "A novel SAW device in CMOS: Design, modeling and fabrication," *IEEE Sensors Journal*, vol.7, no. 2, Feb. 2007.

[28] O. Tigli, L. Bivona, P. Berg, and M. E. Zaghloul, "Fabrication and characterization of a surface acoustic wave biosensor in CMOS technology for cancer biomarker detection, *IEEE Transactions on Biomedical Circuits and Systems*, vol. 4, no. 1, Feb. 2010.

[29] A. N. Nordin and M. E. Zaghloul, "Modeling and fabrication of CMOS surface acoustic wave resonators," *IEEE Transactions on Microwave Theory and Techniques*, vol. 55, no. 5, May 2007.

[30] F. Sidek, A. N. Nordin, and M. E. Zaghloul, "Development of an RF-CMOS surface acoustic wave (SAW) Resonator", *Circuits and Systems (MWSCAS 2010), 53rd IEEE International Midwest Symposium*, pp. 1–4, Aug. 2011.

[31] J. H. Visser, "Surface acoustic wave filters in ZnO-SiO_2-Si layered structures," PhD thesis dissertation, 1989.

[32] K. Uehara, C. Yang, S. Kim, S. Kameda, H. Nakase, and K. Tsubouchi, "Fabrication of 5-GHz-Band SAW Filter with Atomically-Flat-Surface AlN on Sapphire," *Proc. IEEE Ultrasonics Symposium*, vol. 1, pp. 203–206, 2004.

[33] S. Krishnamoorthy and A. A. Iliadis, "Development of high frequency ZnO/SiO_2/Si love mode surface acoustic wave devices," *Solid-State-Electronics*, vol. 50, pp. 1113–1118, 2006.

[34] T. Pastureaud, M. Solal, B. Biasse, B. Aspar, J. Briot, W. Daniau, W. Steichen, R. Lardat, V. Laude, A. Laens, J. Friedt, and S. Ballandras, "High-Frequency Surface Acoustic Waves Excited on Thin-Oriented $LiNbO_3$ Single-Crystal Layers Transferred onto Silicon," *IEEE Transactions on Ultrasonics, Ferroelectronics, and Frequency Control*, vol. 54, no. 4, Apr. 2007.

[35] Laurent. L. Brizoual, O. Elmazria, S. Zhgoon, A. Soussou, F. Sarry, and M. D. Djouadi, "AlN/ZnO/Diamond waveguiding layer acoustic wave structure: Theoretical and experimental results," *IEEE Transactions on Ultrasonics, Ferroelectrics, and Frequency Control*, vol. 57, no. 8, Aug. 2010.

[36] V. I. Anisimkin and N. V. Voronova, "Acoustic properties of the film/plate layered structure", *IEEE Transactions on Ultrasonics, Ferroelectrics, and Frequency Control*, vol. 58, no. 3, Mar. 2011.

[37] D. Phan and G. Chung, "High sensitivity SAW UV sensor by using third harmonic based ZnO/Si structure", *Proc. IEEE Sensors Conference*, pp. 525–527, 2010.

[38] D. Royer and E. Dieulesaint, *Elastic waves in solids I Free and Guided Propagation*. Berlin: Springer-Verlag, 2000.

[39] A. Arnau (Ed.), *Piezoelectric Transducers and Applications*. New York: Springer–Verlag, 2004.

[40] D. S. Ballantine, R. M. White, S. I. Martin, A. I. Ricco, E. T. Zellers, G. C. Frye, and H. Wohltjen, *Acoustic Waves Sensors theory, design, and physico–chemical Applications*. New York: Academic Press, 1997.

[41] W.R. Smith, H. M. Gerard, J.H. Collins, T.M. Reeder, and H.J.Shaw, "Analysis of interdigital surface wave transducers by use of an equivalent circuit model," *IEEE Transactions on Microwave Theory and Techniques*, vol. 17, pp. 856–864, 1969.

[42] Ken-ya Hashimoto, *Surface Acoustic Wave Devices in Telecommunications*, springer, 2000.

[43] *COMSOL Multiphysics Version 3.4 Documentation*, COMSOL AB, Stockholm, Sweden, 2007.

[44] R. Lerch, "Simulation of piezoelectric devices by two-and-three-dimensional finite elements," *IEEE Transactions on Ultrasonics, Ferroelectrics, and Frequency Control*, vol. 37, pp. 233–247, 1990.

[45] S. Rahman, M. Kataoka, C. H. W. Barnes, and H. P. Langtangen, "Numerical investigation of a piezoelectric surface acoustic wave interaction with a one-dimensional channel," *Physical Review B*, vol. 74, p. 035308, 2006.

[46] M. Z. Atashbar, B. J. Bazuin, M. Simpeh, and S. Krishnamurthy, "3D FE simulation of H_2 SAW gas sensor," *Sensors and Actuators B*, vol. 111, pp. 213–218, 2005.

[47] D. H. Wu and H. H. Chen, "Application of Taguchi robust design method to SAW mass sensing device," *IEEE Transactions on Ultrasonics, Ferroelectrics, and Frequency Control*, vol. 52, pp. 2403–2410, 2005.

[48] S. J. Ippolitto, K. Kalantar-Zadeh, D. A. Powell, and W. Wloderski, "A 3-Dimensional Finite Element Approach for Simulating Acoustic Wave Propagation in Layered SAW devices," in *proc. IEEE Ultrasonics Symposium*, pp. 303 – 306, 2003.

[49] H. Morkoç and Ü. Özgür, "*Zinc Oxide: Fundamentals, Materials and Device Technology*," Germany, Wiley-VCH, 2009.

[50] K. Kalantar-zadeh, W. Wlodrski, A. Holland, and G. Reeves, "A ZnO/SiO_2/Si love mode transducer," *Proc. Optoelectronic and Microelectronic Materials and Devices IEEE Conference*, pp. 367–370, 2000.

[51] K. Kalantar-zadeh, W. Wlodrski, and K. Galatis, "Love mode surface acoustic wave filters," *IEEE Electronics Letters*, vol. 37, no. 12, pp. 802–803, Jun 2001.

[52] H. D. Gao and S.Y. Zhang, "Influence of material parameters on acoustic wave propagation modes in ZnO/Si bi-layered structures," *IEEE Transaction on Ultarasonics, Ferroelectrics, and Frequency Control*, vol. 52, no. 12, Dec. 2005.

[53] R. Ro, R. Lee, Y. F. Chiang, and C. C. Sung, “Surface acoustic wave reflection characteristics of electrodes in ZnO/diamond structure”, *Proc. IEEE Ultrasonics Symposium*, pp.936– 939, Sep. 2009.

[54] S. Wu, Z. Lin, R. Ro, and M. Lee, “Rayleigh and shear horizontal surface acoustic properties of (100) ZnO films on silicon,” *IEEE Transactions on Ultrasonics, Ferroelectrics, and Frequency Control*, vol. 57, no. 5, May 2010.

[55] Ken-ya Hashimoto, *Surface Acoustic Wave Devices in Telecommunications*, springer, 2000.

[56] M. E. Hakiki, O. Elmazria, and P. Alnot, “Theoretical investigation of surface acoustic wave in the new, three-layered structure: ZnO/ AlN/ Diamond,” *IEEE Transactions on Ultrason. Ferroelectr. Freq. Control.*, vol. 54, no. 3, pp. 676–681, March 2007.

[57] G. Zhang, “Nanostructure-enhanced surface acoustic wave’s biosensor and its computational modeling,” *Journal of Sensors*, vol. 2009, pp. 1–11, 2009.

[58] N. Ramakrishnan, A. K. Namdeo, H. B. Nemade, and R. P. Palathinkal, “Simplified model for FEM simulation of SAW delay line sensor,” *Journal of Procedia Engineering*, vol. 41, pp. 1022–1027, 2012.

[59] M. I. Rocha-Gaso, R. F.Fernandez-Diaz, A. Arnau-Vives, C. March-Iborra, “Mass sensitivity evaluation of love wave sensor using 3D finite element method,” *Proc. Frequency Control Symposium*, pp. 228–231, 2010.

[60] P. E. Lagasse, I. M. Mason, and E. A. Ash, “Acoustic surface waveguides-Analysis and assessment,” *IEEE Transactions on Microwave Theory and Techniques*, vol. MTT–21, no. 4, pp. 225–236, April 1973.

[61] Shih W-C, Wu M-S, Shimizu M, and Shiosaki T, “The effect of an SiO_2 buffer layer on the SAW properties of ZnO/SiO2/GaAs structure,” *IEEE Transactions on Ultrasonics, Ferroelectrics, and Frequency Control*, vol. 40, no. 6, May 1993.

[62] A. Venema and R. F. Humphryes, “Equivalent circuit for a SAW IDT in multi-layer media with an electrically conductive silicon substrate,” *Proc. IEEE Ultrasonics Symposium*, pp. 637–641, 1977.

[63] Marc J. Madou, *Fundamentals of micro fabrication and nanotechnology*, Volume II, CRC Press, 2012.

[64] B. A. Auld, *Acoustic fields and waves in solids*, Melbourne, Florida: Charles Krieger; 1991.

[65] J. W. Kwon and E. S. Kim, “Fine ZnO patterning with controlled sidewall-etch front slope,” *Journal of Microelectromechanical Systems*, vol. 14, no. 3, pp. 603–609, 2005.

[66] P. Walker and W. H. Tarn, *CRC Handbook of Metal Etchants*. Florida: CRC Press, 1991, p. 28.

[67] T. Zhang, L. Sun, D. Han, Y. Wang, and R. Han, "Surface uniform wet etching of ZnO films and influence of oxygen annealing on etching properties," *Proc. IEEE NEMS Conference*, pp. 626–629, Feb 2009.

[68] B. Seo, S. Lee, J. H. Seo, J. Jeon, and H. Choe, "Study of the wet etch behavior of a Zinc-oxide semiconductor in acid solutions," *Journal of Korean Physical Society*, vol. 53, no. 1, pp. 402–405, July 2008.

[69] *IEEE Standard on Piezoelectricity*, ANSI/IEEE Standard 176, 1987.

[70] J. KrautKramer and H. KrautKramer, *Ultrasonic testing of materials*, Springer-Verlag, 4th edition, 1990.

[71] V. Teppati, A. Ferrero, and M. Sayed, *Modern RF and Microwave Measurement Techniques*, Cambridge University Press, 2013.

[72] Y. Suzuki, H. Shimizu, M. Takeuchi, K. Nakamura, and A. Yamada, "Some study on SAW resonators and multiple-mode filters," *Proc. IEEE Ultrasonics Symposium*, pp. 297–302, 1976.

[73] M. Kadota, T. Yoneda, K. Fujimoto, T. Nakao, and E. Takata, "Small-sized resonator IF filter using shear horizontal wave on heavy metal film/quartz substrate," *Proc. IEEE International Frequency Control Symposium*, pp. 50–53, 2002.

[74] M. Kadota, T. Nakao, T. Murata, and K. Matsuda, "Surface acoustic wave filter in high frequency range with narrow bandwidth and excellent temperature property," *Proc. IEEE Ultrasonics Symposium*, pp. 1584–1587, 2008.

[75] A. Springer, F. Hollerweger, R. Weigel, S. Berek, W. Euile, C. C. W. Ruppel, and M. Guglielmi, "Design and performance of a SAW ladder-type filter at 3.15 GHz using SAW mass-production technology," *IEEE Transactions on Microwave Theory and Techniques,* vol. 47, no. 12, Dec. 1999.

[76] S. M. Sze, Physics of Semiconductor Devices, 2nd edition, 2000.

List of Publications

Patents

1. Sai Krishna Santosh G and Harshal B. Nemade, “Edge reflection type surface acoustic wave device on silicon substrate,” Indian patent application no. 633/KOL/2015, journal no. 28/2015.
2. **Edge reflection type ladder filters on silicon** *is ready for submission.*

Journal and conference

1. Sai Krishna Santosh G and Harshal B. Nemade, "Investigation of properties of surface acoustic waves generated by periodically patterned ZnO on silicon substrate," *Ultrasonics*, Elsevier, vol. 59, pp. 40–44, May 2015.

2. Sai Krishna Santosh G and Harshal B. Nemade, “High frequency SAW devices on silicon using ZnO nanopillars,” *International Conference on Advance Nanomaterials and Nanotechnology (ICANN)*, December 8-11, 2015.

Sai Krishna Santosh G, Harshal B. Nemade, "Effect of buffer layers on the surface acoustic wave characteristics generated by periodically patterned ZnO on silicon substrate," (manuscript submitted) *Ultrasonics*, Elsevier.

Sai Krishna Santosh G, Harshal B. Nemade, “Edge Reflection Type SAW Resonators on Silicon Substrate Using ZnO Thin Films,” submitted to UFC 2017.